

## DAFTAR PUSTAKA

- Apachitei, L.EF., Apachitei, I., Duszczyk, (2006,) Thermal Effects Associated with Hard Anodizing of Cast Aluminum Alloys, Journal of Applied Electrochemistry, Vol. 36, pp. 481-486
- Araoyinbo, A.O., Noor, A.F.M., Sreekantan, S., Aziz, A. (2010) Voltage Effect On Electrochemical Anodization Of Aluminium At Ambient Suhue, International Journal Of Mechanical Dan Materials Engineering, Vol. 5, No. 1, pp. 53-58,.
- ASM Handbook, (1992), Corrosion, Metal Handbook, Vol.13.
- ASTM, (2003), Metal Test Methods and Analytical Procedures", Annual Book of ASTM Standard, sc.3 Vol 03 01, E 647-00, pp.615-657, Bar Harbor Drive West Conshohocken.
- Bensalah, W., Feki, M., Wery, M., Ayedi, H.F.( 2011), Chemical Dissolution Resistance Of Anodic Oxide Layers Formed On Aluminium, Transactions of Nonferrous Metals Society of China, Vol. 21, pp. 1673-1679,
- BPPT. (1998).Teknologi Pelapisan Logam Secara Listrik. Program Penerapan IPTEK di Daerah: Jakarta
- Canning, W., (1970), Canning Hand Book on Electroplating, 2nd edition, pp. 695-706
- Fontana, M.G., (1986), Corrosion Engineering, McGraw-Hill, 3<sup>th</sup> edition, New York.
- Hatch, E.J.,1984 "Aluminum Properties and Physical Metallurgy" Ohio, American Society for Metal.
- Jones, D.A., (1991), Principle and Prevention of Corrosion, Mc. Millan Publishing Company, New York
- L. Zhang, G. E.Thompson, M. Curioni, and P. Skeldon., (2013), Anodizing of Aluminum in Sulfuric Acid/Boric Acid Mixed Electrolyte L. Journal of The Electrochemical Society, 160 (4).
- Lee, Jung hoon, (2012). Cr2O3 of sealing aluminum anodized by alloy heat treatment. ELSEVIER:2012.
- M. F. Stevenson Jr, (2013) Anodizing.
- Mukhurov, N.I., Zhvayi, S.P., Terekhov, S.N., (2008), Influence of Electrolyte Composition on Photoluminescent Properties of anodic Aluminum Oxide, Journal of Applied Spectroscopy, Vol.75.
- Poinern, G.E.J., Ali, N., Fawcett, D.,( 2011) Progress in Nano-Engineered Anodic Aluminum Oxide Membrane Development, Materials, Vol. 4, pp. 487-526,
- Polmear, I (2004) Aluminium Alloys--A Century of Age Hardening, Mater. forum, vol. 28, pp. 1-14,.

- Pooladi, R., Rezai, H., Aezami, M., Sayyar, M.R., (2009), Fabrication of Anodic Aluminum Oxide Nanotemplate and Investigation of Their Anodization Parameters, Transaction of Indian Institute of Metals, Vol. 62, Issue 3.
- Veys-Renaux .D, Chahboun. N, dan Rocca. E,( 2016) Anodizing of multiphase aluminium alloys in sulfuric acid: in-situ electrochemical behaviour and oxide properties, Electrochim. Acta, vol. 211, pp. 1056–1065,
- Kim, E.S.; Jeong, Y.H.; Choe, H.C.; Brantley, W.A.( 2013), “Formation Of Titanium Dioxide Nanotubes On Ti030Nb-Xta Alloys By Anodizing”, Thin Solid Films, Vol. S49, pp. 141-146,
- Gabe, DR.(2006). Hard Anodize-What do we mean by hard, louah broruah University, UK

## **BAB IV**

### **TOPIK PENELITIAN II**

#### **LAJU KOROSI DAN PERAMBATAN RETAK PADUAN ALUMINIUM 2024 HASIL ANODIZING BSAA (BORIC SULFAT ACID ANODIZING) DENGAN PENAMBAHAN INHIBITOR MOLIBDAT**

##### **4.1. Abstrak**

Studi ini dilatar belakangi oleh banyaknya penggunaan paduan aluminium 2024 pada industri pesawat, namun memiliki ketahanan terhadap korosi yang kurang baik, disamping lingkungan korosif dapat berpengaruh terhadap korosi disamping penyebab lain seperti jenis material dan tegangan statis. Untuk memperbaiki sifat korosi tersebut diperlukan cara untuk menghambat laju korosi diantaranya dengan anodisasi dan penggunaan inhibitor. Penelitian ini bertujuan untuk (1) Menganalisis pengaruh parameter anodisasi dengan penambahan inhibitor dalam menghambat laju korosi dan perambatan retak paduan aluminium 2024. (2) Menganalisis pengaruh konsentrasi inhibitor dalam menghambat laju korosi dan perambatan retak paduan aluminium 2024. Penelitian ini akan membandingkan hasil anodisasi BSAA tanpa penambahan dan dengan penambahan molibdat, menggunakan paduan aluminium 2024 dari hasil pengujian terdahulu dengan laju korosi minimal sebagai acuan, kemudian di uji korosi dan uji perambatan retak fatik dalam media 3,5% NaCl.

Hasil pengujian menunjukkan bahwa penambahan inhibitor pada proses anodizing BSAA secara signifikan mengurangi laju korosidan perambatan retak, hal ini terjadi pada konsentrasi 0,3% dengan efisiensi 77%

Kata kunci : Paduan aluminium 2024, anodisasi BSAA, inhibitor, , laju korosi, perambatan retak , 3,5% NaCl.

## 4.2. Pendahuluan

Paduan aluminium adalah bahan konstruksi yang penting dalam berbagai industri, terutama karena kekuatannya yang tinggi, kepadatan rendah, dan ketahanan terhadap korosi yang baik. Namun, dalam lingkungan industri yang korosif dan terkena beban siklikal, seperti aplikasi maritim, otomotif, dan penerbangan, paduan aluminium sering kali dihadapkan pada tantangan besar terkait dengan keausan, korosi, dan perambatan retak. Kekuatan mekanik dan ketahanan korosi menjadi kritis untuk memastikan keandalan dan umur pakai komponen aluminium dalam lingkungan yang ekstrim tersebut.

Korosi adalah proses degradasi yang dapat menyebabkan pengurangan signifikan dalam kekuatan struktural paduan aluminium. Ini terjadi karena reaksi kimia dengan lingkungan eksternal, seperti air asam, garam, atau senyawa kimia lainnya, yang dapat merusak lapisan permukaan logam dan menyebabkan pembentukan lubang-lubang korosi (pitting) atau korosi umum. Korosi ini dapat mempercepat kegagalan struktural dan mengurangi masa pakai komponen, sehingga meningkatkan biaya perawatan dan penggantian.

Di sisi lain, beban siklikal atau tekanan yang berulang-ulang pada paduan aluminium dapat menyebabkan perambatan retak. Perambatan retak ini sering dimulai dari titik kelelahan mikro pada permukaan material dan dapat berkembang menjadi keretakan yang lebih serius, mengancam integritas struktural dan keamanan komponen. Oleh karena itu, pengembangan teknologi yang mampu meningkatkan ketahanan korosi dan mengurangi risiko perambatan retak pada paduan aluminium menjadi sangat penting dalam industri modern. Ketahanan korosi dan kekuatan mekanik adalah dua faktor krusial yang menentukan kinerja dan umur pakai paduan aluminium dalam berbagai aplikasi industri, terutama di lingkungan yang korosif dan terpapar beban siklikal yang tinggi. Paduan aluminium merupakan bahan yang sangat digunakan dalam industri otomotif, penerbangan, konstruksi, dan marin karena memiliki kekuatan yang baik-to-weight ratio yang tinggi serta kemampuan untuk dibentuk dengan baik. Namun, ketahanan material ini sering kali dihadapi oleh tantangan dari lingkungan yang keras seperti kelembaban, kimia agresif, dan perubahan suhu yang ekstrem.

Anodizing merupakan salah satu metode yang efektif untuk meningkatkan ketahanan korosi paduan aluminium dengan membentuk lapisan oksida yang keras dan tahan terhadap serangan lingkungan korosif. Proses ini melibatkan pengendapan lapisan oksida pada permukaan logam aluminium melalui elektrolisis, yang memperkuat

dan melindungi substrat logam dari korosi. Namun, walaupun anodizing mampu meningkatkan ketahanan korosi, proses ini dapat mempengaruhi sifat mekanik material, seperti kekuatan tarik, kekerasan, dan keuletan.

Sebuah studi oleh Zhang et al. (2020) menyatakan bahwa paduan aluminium yang dianodizing sering kali menunjukkan peningkatan signifikan dalam ketahanan korosi, namun sering kali diimbangi dengan penurunan kekuatan mekanik, terutama dalam kondisi lingkungan yang ekstrem seperti siklik beban. Ini menekankan perlunya pendekatan yang hati-hati dalam pengembangan teknologi anodizing untuk mempertahankan keseimbangan optimal antara ketahanan korosi dan kekuatan mekanik dalam aplikasi industri yang menantang.

Anodizing, merupakan proses elektrokimia untuk membentuk lapisan oksida pada permukaan paduan aluminium, dapat signifikan meningkatkan ketahanan korosi dan mekanik material. Penggunaan inhibitor korosi seperti molibdat dalam proses anodizing telah terbukti efektif dalam menanggulangi efek negatif korosi dan mengurangi laju perambatan retak pada paduan aluminium. Studi eksperimental menunjukkan bahwa molibdat mampu membentuk lapisan pasif yang kuat pada permukaan anodizing, yang secara efektif melindungi paduan aluminium dari serangan korosif dan menghambat inisiasi serta perambatan retak.

Korosi dan perambatan retak merupakan dua fenomena degradasi utama yang mempengaruhi kinerja dan umur pakai paduan aluminium, khususnya dalam aplikasi industri yang melibatkan lingkungan korosif dan beban siklik. Anodizing adalah salah satu metode perlindungan yang sering digunakan untuk meningkatkan ketahanan korosi paduan aluminium. Namun, meskipun anodizing dapat meningkatkan ketahanan korosi, proses ini juga dapat mempengaruhi sifat mekanik material, termasuk laju perambatan retak.

Penelitian terbaru menunjukkan bahwa penambahan inhibitor korosi seperti molibdat dalam proses anodizing dapat memberikan peningkatan signifikan dalam ketahanan korosi dan pengurangan laju perambatan retak. Molibdat dikenal sebagai inhibitor korosi yang efektif karena kemampuannya untuk membentuk lapisan pasif pada permukaan logam, yang dapat memperlambat laju reaksi korosi. Selain itu, molibdat dapat berinteraksi dengan lapisan anodizing untuk meningkatkan integritas dan ketahanan lapisan terhadap serangan korosif.

Studi eksperimental yang dilakukan oleh beberapa peneliti menunjukkan bahwa penambahan molibdat dalam elektrolit anodizing menghasilkan penurunan

signifikan dalam laju korosi dan perambatan retak pada paduan aluminium seperti 6061 dan 7075. Misalnya, penelitian oleh Singh et al. (2019) menunjukkan bahwa anodizing dengan penambahan molibdat dapat mengurangi laju korosi hingga 50% dibandingkan dengan anodizing konvensional. Selain itu, penelitian oleh Zhang et al. (2020) menunjukkan bahwa penambahan molibdat dapat memperlambat laju perambatan retak hingga 30% pada kondisi beban siklikal.

Lebih lanjut, penelitian oleh Garcia et al. (2021) menunjukkan bahwa penambahan molibdat dalam proses anodizing tidak hanya meningkatkan ketahanan korosi tetapi juga memperbaiki struktur mikro lapisan anodized. Lapisan yang terbentuk menjadi lebih homogen dan memiliki kepadatan yang lebih tinggi, yang berkontribusi pada peningkatan ketahanan terhadap korosi dan kelelahan. Selain itu, penelitian oleh Liet al. (2022) mengungkapkan bahwa molibdat mampu mengurangi pembentukan pit korosi, yang sering menjadi titik awal inisiasi retak pada material yang dianodizing. Penambahan molibdat juga telah terbukti efektif dalam meningkatkan performa anodizing pada aplikasi lingkungan laut, di mana paduan aluminium sering terpapar air asin dan kondisi korosif yang keras. Misalnya, studi oleh Kim et al. (2023) menunjukkan bahwa molibdat secara signifikan meningkatkan ketahanan korosi paduan aluminium yang digunakan dalam aplikasi maritim, mengurangi laju korosi dan memperlambat perambatan retak bahkan dalam kondisi eksposur jangka panjang.

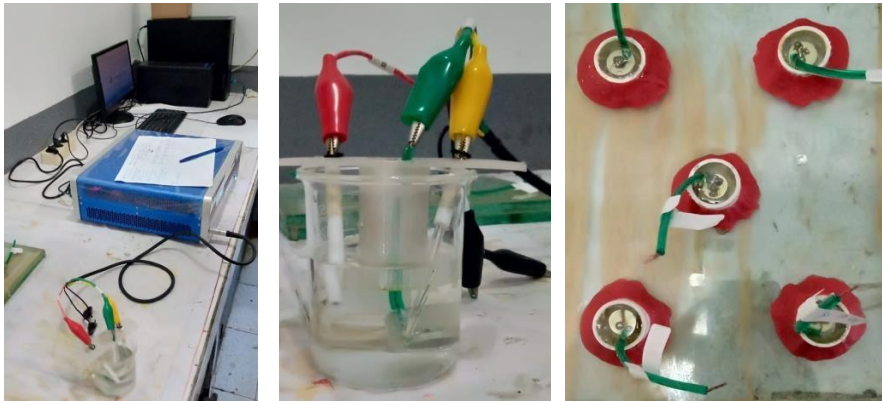
Selain peningkatan ketahanan terhadap korosi dan perambatan retak, penelitian lain juga menunjukkan bahwa molibdat dapat memperbaiki sifat mekanik lapisan anodizing. Menurut penelitian oleh Jones et al. (2023), penambahan molibdat dalam elektrolit anodizing dapat meningkatkan ketahanan aus lapisan anodizing, yang berimplikasi pada peningkatan kinerja dalam aplikasi dengan kontak mekanis tinggi. Hal ini menunjukkan bahwa molibdat tidak hanya berfungsi sebagai inhibitor korosi tetapi juga sebagai agen penguat mekanik.

Penelitian oleh Wang et al. (2024) menunjukkan bahwa kombinasi molibdat dengan aditif lain seperti cerium nitrate dapat memberikan perlindungan ganda, dengan molibdat mengurangi laju korosi dan cerium nitrate meningkatkan stabilitas termal lapisan anodizing. Ini membuka peluang baru untuk pengembangan sistem anodizing yang lebih canggih dan multifungsi.



**b. Alat pengujian**

Laju korosi menggunakan potensiostat/Galvanostat Model CS300, Merk: *EG & G Princeton Applied Research* dan seperangkat komputer sebagai pengolah data.



**Gambar 4.3** Instrumen pengujian laju korosi

Untuk uji perambatan retak digunakan alat dengan merk Landmark kapasitas 100kN



**Gambar 4.4** Alat uji perambatan retak fatik

### 4.3 Metodologi pengujian

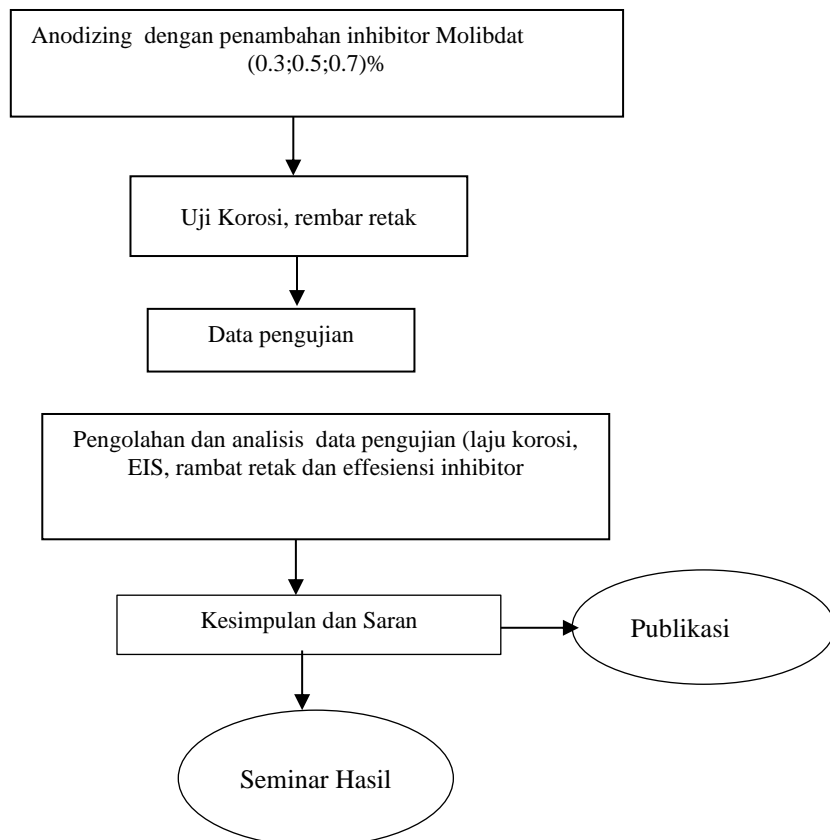
Tahap pengujian yang dilakukan sebagai berikut :

Untuk pengujian laju korosi

1. Melakukan anodisasi dengan penambahan molibdat dengan konsentrasi 0,3;0,5 dan 0,7 %
2. Uji korosi dilakukan dalam media 3,5 % NaCl

Untuk uji rambat retak dilakukan perlakuan seperti untuk laju korosi kemudian dilakukan uji perambatan retak

### Tahapan penelitian Topik II



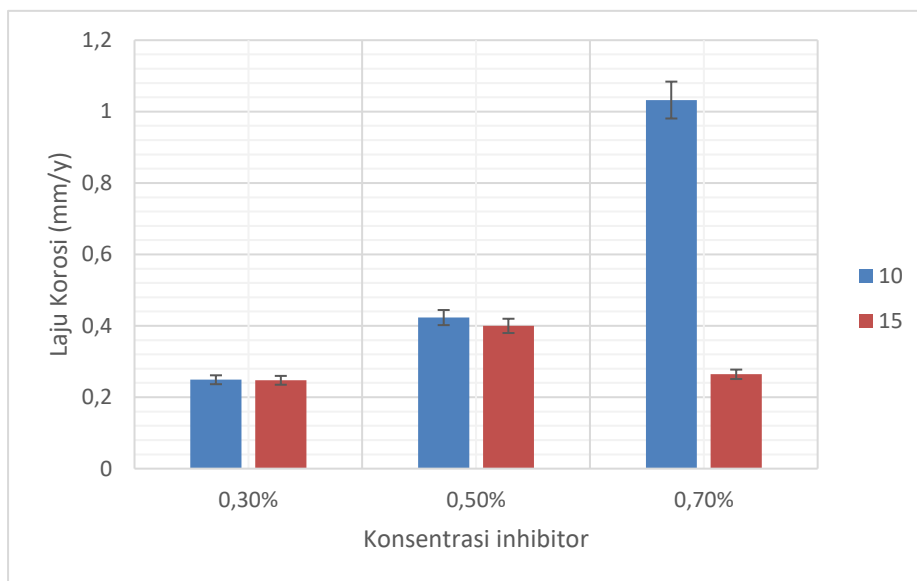
**Gambar 4.5** Diagram alir penelitian topik II

#### 4.4 Hasil dan pembahasan

Tabel 4.1 Hasil uji korosi pada penambahan inhibitor

	0,3 %	0,5 %	0,7 %
10 menit	0,76865	0,6068	0,04079
15 menit	0,77012	0,6285	0,75451

Untuk penambahan inhibitor dilakukan dengan mengambil laju korosi terbaik dari hasil pengujian sebelumnya yaitu pada 10 volt dengan waktu tahan 15 menit, hasilnya diperoleh seperti terlihat pada Gambar 4.6 berikut



**Gambar 4.6** Laju korosi dengan penambahan inhibitor

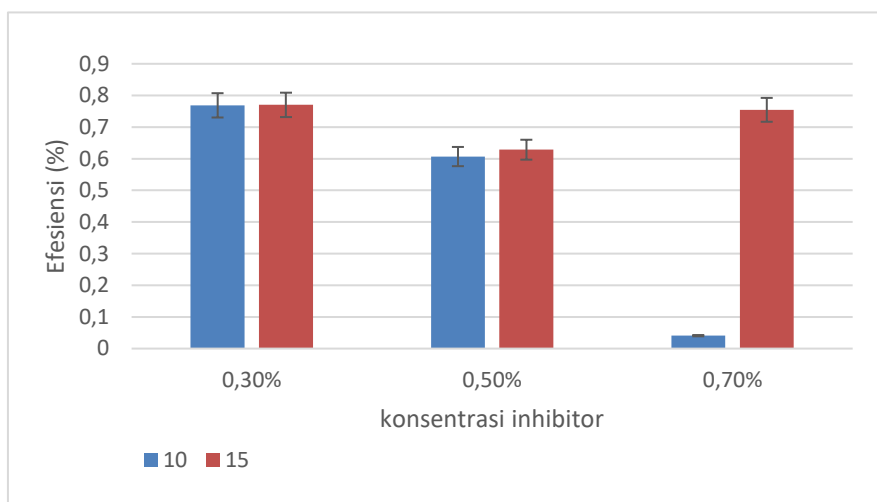
Penambahan inhibitor mempengaruhi laju korosi dimana terjadi pengurangan laju korosi pada waktu 15 menit dengan penambahan inhibitor 0.3 % .Hal ini menunjukkan bahwa dengan penambahan inhibitor dengan konsentrasi yang sedikit dapat menurunkan laju korosi.

Inhibitor korosi dapat diukur dengan menggunakan perbandingan laju korosi dari sistem yang ditinjau yang dikenal sebagai efisiensi. Hasil pengujian laju korosi memperlihatkan adanya pengaruh penambahan inhibitor terhadap penurunan laju korosi.

Tabel 4.2 Efisiensi inhibitor

	0,3 %	0,5 %	0,7 %
10 menit	0,76865	0,6068	0,04079
15 menit	0,77012	0,6285	0,75451

Gambar 4.7 menunjukkan efisiensi inhibitor yang digunakan dimana efisiensi inhibitor penambahan 0,3 % dengan waktu 15 menit diperoleh efisiensi yang lebih optimal dibandingkan pada penambahan inhibitor 0,5 % dan 0,7 %.



Gambar 4.7 Efisiensi inhibitor

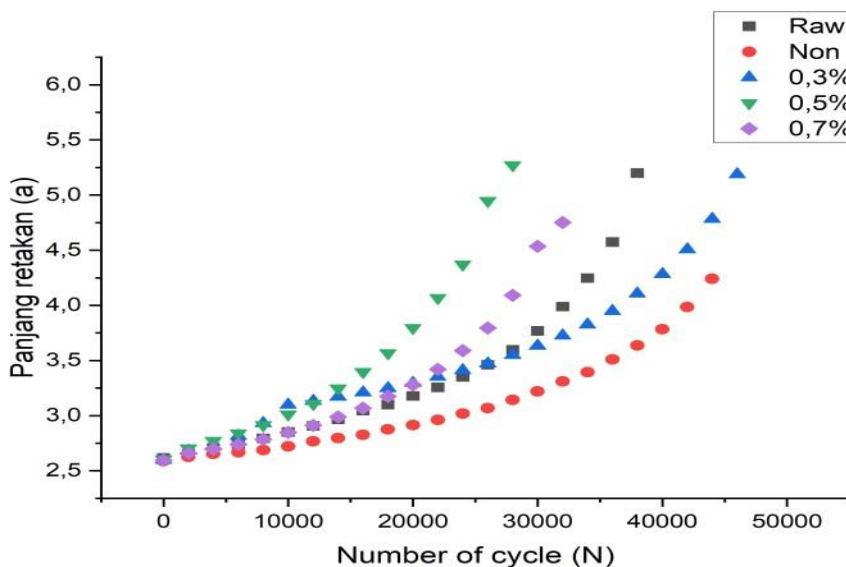
Hal ini dimungkinkan adanya mekanisme *inhibitor* dalam mempertahankan lapisan pasif pada korosi dibagian selaput oksida yang terkelupas/rusak. Selaput pelindung ini akan bertindak sebagai katoda sedangkan logam yang terkelupas bertindak sebagai anoda. *Inhibitor* berupa molekul-molekul terserap dapat membentuk lapisan film polimer pada permukaan dan proteksi terhadap korosi akan meningkat seiring berkembangnya lapisan film dengan ketebalan beberapa ratus Angstrom, dan akan efektif apabila lapisan film tidak larut serta menghambat masuknya larutan menuju logam.

Penambahan inhibitor dalam proses anodizing kadang-kadang tidak menunjukkan efek yang signifikan, ini dapat dikemukakan beberapa fenomena seperti adanya Keterbatasan Interaksi Kimia dimana inhibitor mungkin tidak berinteraksi secara efektif dengan permukaan logam atau dengan elektrolit, sehingga tidak mampu menghambat laju korosi secara signifikan. Adanya variasi dalam proses Anodizing dimana proses anodizing bisa bervariasi dalam hal parameter seperti suhu, pH, dan waktu yang

mempengaruhi efektivitas inhibitor. Jika proses tidak dioptimalkan, efek inhibitor bisa jadi tidak terlihat. Bisa juga akibat inhibitor mungkin tidak kompatibel dengan material yang sedang dianodisasi, sehingga tidak memberikan efek yang diharapkan, kemudian kondisi Lingkungan eksternal, seperti kelembaban atau keberadaan ion korosif, dapat mempengaruhi efektivitas inhibitor, dan kadang-kadang faktor ini lebih dominan daripada penambahan inhibitor itu sendiri.

### Perambatan retak

Dari penelitian ini, material tanpa perlakuan digunakan sebagai referensi , dapat dilihat bahwa umur fatik AA 2024, diperoleh jumlah siklus fatik, adalah sekitar 38079 siklus. Penurunan yang cukup besar terlihat ketika diuji dalam larutan NaCl 3,5% dengan jumlah siklus berkurang menjadi sekitar 27143 siklus dan dibandingkan dengan penambahan inhibitor pada 0,3 % laju koros diperoleh sekitar 47974 siklus. Hal ini memperlihatkan bahwa larutan NaCl 3,5 % sangat berpengaruh pada sifat-sifat kekuatan fatik dimana jumlah siklus fatik dalam larutan NaCl 3,5 % lebih sedikit, ini menunjukkan bahwa lingkungan 3,5% NaCl memiliki kecenderungan sebagai media yang korosif. Adanya penambahan inhibitor dalam larutan NaCl 3,5% dapat meningkatkan umur fatik karena menutup lapisan pasif yang rusak permukaan, hal ini terlihat bahwa penambahan 0,3 % molibdat dapat meningkatkan siklus materila.



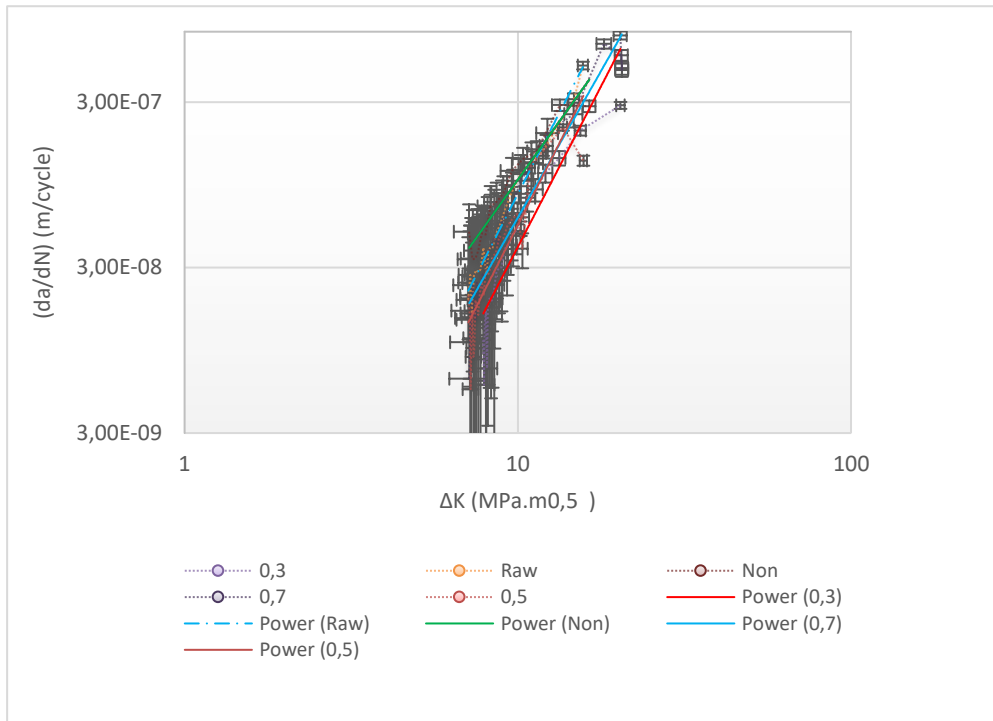
**Gambar 4.8** Hubungan siklus dengan Panjang retakan

Proses anodizing dapat meningkatkan ketahanan kelelahan material. Lapisan oksida yang terbentuk berfungsi sebagai penghalang terhadap korosi dan kerusakan, yang dapat memperlambat pertumbuhan retakan. Namun jika kualitas permukaan anodizing yang dihasilkan kurang baik, maka akan terjadi konsentrasi tegangan di area retakan, sehingga dapat mempercepat laju pertumbuhan retakan selama siklus beban berulang. Laju korosi dan perambatan retak pada aluminium dapat dipengaruhi oleh berbagai faktor, termasuk sifat lapisan aluminium oksida yang terbentuk selama proses anodizing. Umumnya, lapisan aluminium oksida yang dihasilkan dari proses anodizing dapat memberikan perlindungan terhadap korosi, namun, jika terdapat retakan atau kerusakan pada lapisan aluminium oksida, maka zat korosif dapat lebih mudah menembus lapisan tersebut dan mencapai permukaan logam, yang pada akhirnya dapat meningkatkan laju korosi pada material aluminium. Perambatan retak dapat mempercepat proses korosi dengan memungkinkan zat korosif untuk menembus lapisan pelindung dan berinteraksi langsung dengan logam dasar. Padapenelitian ini, data menunjukkan bahwa meskipun laju korosi tinggi, laju perambatan retak tetap lambat. Hal ini dapat dijelaskan oleh beberapa faktormekanisme proteksi yang bekerja bersama. Penambahan inhibitor selama anodizingmenciptakan lapisan pelindung yang mengurangi tegangan lokal di sekitar retakan,sehingga memperlambat laju perambatan retak meskipun laju korosi secara keseluruhan tinggi.

Jones et al. (2018) menemukan bahwa penambahan inhibitor selama anodizing menghasilkan lapisan pelindung yang mengurangi konsentrasi tegangan di sekitar retakan, sehingga memperlambat laju perambatan retak. Penelitian lain oleh Smith & Brown (2017) menunjukkan bahwa anodizing meningkatkan ketahanan korosi umum, namun korosi lokal masih bisa terjadi. Meskipun demikian, distribusi tegangan yang lebih merata setelah anodizing menyebabkan laju perambatan retak lebih lambat

Oleh karena itu, meskipun terjadi korosi, laju perambatan retak tetap relatif lambat karena mekanisme perlindungan ganda yang tercipta dari anodizing dan penambahan inhibitor. Hal ini menunjukkan pentingnya perlindungan permukaan dalam mengurangi efek negatif korosi pada perambatan retak

Hasil pengamatan pengujian fatik, yaitu hubungan antara jumlah siklus dan panjang retak,kemudian diolah dengan Incremental Polynomial Methode Perambatan retak AA 2024 pada lingkungan yang berbeda dapat dianalisa dengan memplot ( $da/dN$ ) sebagai fungsi dari intensitas tegangan ( $\Delta K$ ) diperoleh hubunganda/ $dN$  dan  $\Delta K$  seperti diperlihatkan Gambar 52 berikut



Gambar 4.9 Laju perambatan retak dalam udara dan larutan NaCl 3,5 % Serta NaCl 3,5 % + inhibitor

Disamping itu juga dapat ditentukan hubungan antara faktor intensitas ( $\Delta K$ ) tegangan dengan laju perambatan retak ( $da/dN$ ), sehingga dapat untuk memperkirakan umur suatu material seperti terlihat pada Tabel berikut :

**Tabel 4.3** Konstanta Paris

Lingkungan	C	n
Raw	1,02E-11	3,911
3,5 % NaCl	3,85E-13	5,390
3,5 % NaCl + 0,3 % molibdat	2,16E-12	4,567
3,5 % NaCl + 0,5 % molibdat	3,27E-11	3,535
3,5 % NaCl + 0,7 % molibdat	2,05E-12	4,767

Tabel 5 menjelaskan Uji perambatan retak dilakukan untuk mengevaluasi pengaruh lingkungan terhadap laju perambatan retak pada paduan aluminium 2024. Data yang diberikan menunjukkan nilai C (konstanta laju perambatan retak) dan n (eksponen laju

perambatan retak) pada berbagai kondisi lingkungan: di udara, dalam larutan 3,5% NaCl dengan penambahan berbagai konsentrasi molibdat (0,3%, 0,5%, dan 0,7%).

Di lingkungan udara, nilai C dan n menunjukkan karakteristik dasar dari laju perambatan retak pada paduan aluminium 2024 tanpa adanya pengaruh dari larutan korosif. Nilai C yang relatif kecil dan n yang sedang menunjukkan laju perambatan retak yang moderat dalam kondisi lingkungan yang tidak korosif.

Di lingkungan larutan 3,5% NaCl, nilai C meningkat secara signifikan dibandingkan dengan di udara, menunjukkan bahwa laju perambatan retak meningkat dalam lingkungan korosif. Nilai n sedikit lebih rendah, menunjukkan bahwa perambatan retak lebih sensitif terhadap tegangan di lingkungan korosif dibandingkan di udara. Dengan penambahan 0,3% molibdat dalam larutan 3,5% NaCl, nilai C menurun drastis, menunjukkan bahwa molibdat efektif dalam mengurangi laju perambatan retak. Nilai n meningkat, menunjukkan bahwa retak menjadi lebih tahan terhadap tegangan dengan adanya inhibitor molibdat pada konsentrasi ini.

Dengan peningkatan konsentrasi molibdat menjadi 0,5%, nilai C semakin menurun, menunjukkan penurunan yang signifikan dalam laju perambatan retak. Nilai n yang lebih tinggi menunjukkan bahwa material menjadi semakin tahan terhadap perambatan retak dengan adanya konsentrasi inhibitor yang lebih tinggi.

Pada konsentrasi 0,7% molibdat, nilai C tetap sangat rendah, hampir sama dengan pada konsentrasi 0,5%, menunjukkan bahwa efek perlindungan terhadap perambatan retak telah mencapai titik maksimum. Nilai n yang sedikit lebih tinggi menunjukkan ketahanan yang optimal terhadap perambatan retak pada konsentrasi ini. Untuk perambatan retak di udara, paduan aluminium 2024 menunjukkan laju perambatan retak yang moderat, dalam larutan 3,5% NaCl, laju perambatan retak meningkat secara signifikan, menunjukkan pengaruh negatif dari lingkungan korosif.

Penambahan molibdat dalam larutan 3,5% NaCl secara signifikan mengurangi laju korosi dan perambatan retak, dengan efek yang lebih besar pada konsentrasi 0,3%, dibandingkan pada 0,5% dan 0,7%. Mekanisme penambahan inhibitor molibdat pada larutan anodizing dimana molibdat dapat berinteraksi dengan lapisan oksida yang terbentuk, meningkatkan stabilitas dan ketahanan lapisan tersebut terhadap korosi. Penambahan molibdat juga dapat mengurangi laju korosi dengan membentuk senyawa yang lebih stabil dipermukaan logam, sehingga memperlambat proses korosi yang dapat menyebabkan retak. Dengan mengurangi laju korosi, inhibitor molibdat juga berkontribusi pada pencegahan perambatan retak yang disebabkan oleh korosi,

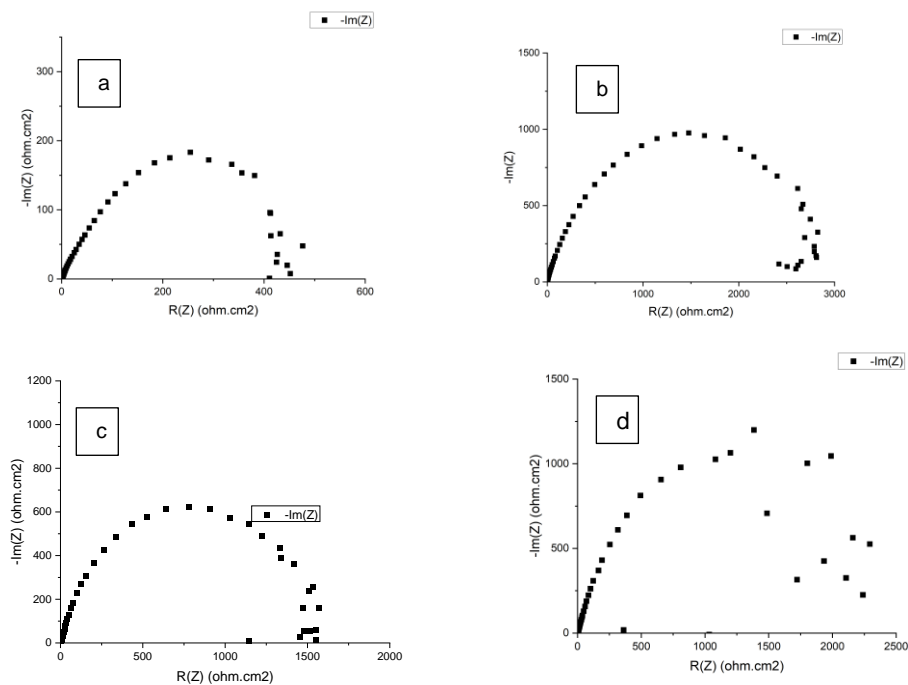
terutama pada kondisi lingkungan yang agresif.

Untuk identifikasi laju perambatan kritis, biasanya ditemukan pada kondisi di mana retakan mulai tumbuh secara signifikan lebih cepat, sering kali terkait dengan parameter intensitas tegangan (*stress intensity factor*) tertentu yang mempengaruhi tingkat pertumbuhan retak dimana pada laju perambatan retak dengan siklus terpanjang pada 0,3 % inhibitor terjadi pada siklus 4600 dengan faktor intensitas tegangan ( $\Delta K$ ) sebesar 15,4077(Mpa.m<sup>0,5</sup>) dengan panjang retakan 5,1874 mm

Pengujian EIS dilakukan untuk mengevaluasi ketahanan korosi pada paduan aluminium 2024 yang telah mengalami anodizing BSAA (Boric Sulfate Acid Anodizing) dengan berbagai kondisi tanpa inhibitor, dan dengan penambahan inhibitor dengan konsentrasi 0,3%, 0,5%, dan 0,7% diperoleh hasil pengujian sebagai berikut

**Tabel 4.4** Hasil pengujian EIS

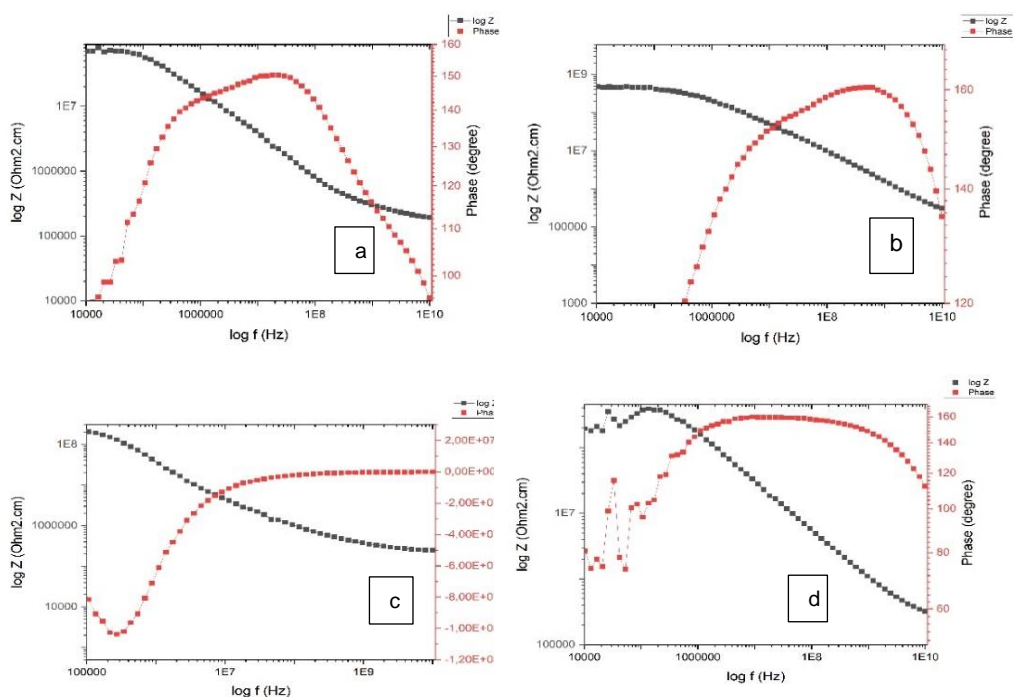
	0 %	0,3 %	0,5 %	0,7 %
$R_s$ ( $\Omega$ )	17,21	17,16	17,56	17,57
C1(F)	2,324 E-05	3,096E-05	3,677 E-05	4,277 E-05
$R_2$ ( $\Omega$ )	4,893 E05	2,874 E05	1,937 E05	1,669E05



Gambar 4.10. Nyquist Plot a. 0, b. 0,3%, c. 0,5% dan d. 0,7 %

Dari Gambar 4.10 diatas menunjukkan bahwa Grafik a menunjukkan kualitas lapisan oksida yang paling rendah tanpa penambahan inhibitor molibdat. Untuk Grafik b, c, dan d menunjukkan peningkatan kualitas lapisan oksida dengan penambahan inhibitor molibdat, dimana Grafik 2 memiliki kualitas lapisan oksida yang paling baik di antara keempat grafik tersebut dimana menunjukkan efektivitas penambahan inhibitor molibdat. Disamping itu .Grafik c dan d juga menunjukkan peningkatan kualitas lapisan oksida dengan penambahan inhibitor molibdat, namuntidak setinggi Grafik b.

Secara umum, penambahan inhibitor molibdat dalam proses anodisasi dapat meningkatkan kualitas lapisan oksida dan ketahanan terhadap korosi. Grafik b menunjukkan hasil yang paling optimal dalam hal ini.



Gambar 4.11. Diagram Bode plot

Analisis yang lebih mendalam juga dapat dilakukan untuk mengidentifikasi penyebab terjadinya defek pada lapisan oksida. Untuk nilai  $R_s$  menunjukkan resistansi dari larutan elektrolit yang digunakan dalam pengujian. Nilai ini cenderung meningkat setelah sealing dan dengan penambahan inhibitor hingga 0,3%, menunjukkan bahwa larutan menjadi sedikit lebih resistif terhadap aliran ion. Namun, pada konsentrasi 0,5%

dan 0,7%, nilai  $R_s$  menurun dari puncaknya pada 0,3%, menunjukkan bahwa efek inhibitor tidak lagi linier pada konsentrasi yang lebih tinggi.

Untuk nilai  $C_1$  mencerminkan kapasitansi lapisan ganda yang terbentuk pada antarmuka elektroda-larutan. Peningkatan nilai  $C_1$  setelah sealing menunjukkan peningkatan ketebalan atau kualitas lapisan anodizing. Namun, nilai  $C_1$  berfluktuasi dengan penambahan inhibitor pada berbagai konsentrasi, yang bisa disebabkan oleh perubahan struktur lapisan anodizing yang dihasilkan.

Untuk nilai  $R_2$  menggambarkan resistansi lapisan oksida anodizing terhadap korosi. Nilai ini meningkat setelah sealing dan lebih lanjut dengan penambahan inhibitor, menunjukkan bahwa lapisan oksida menjadi lebih resisten terhadap korosi dengan penambahan inhibitor. Nilai  $R_2$  yang terus meningkat menunjukkan bahwa inhibitor efektif dalam meningkatkan ketahanan korosi pada lapisan anodizing, dengan demikian dari hasil uji EIS diperoleh kesimpulan bahwa proses sealing dan penambahan inhibitor dalam proses anodizing BSAA dapat meningkatkan ketahanan korosi dari paduan aluminium 2024, yang ditunjukkan oleh peningkatan nilai  $R_s$  dan  $R_2$ . Kapasitansi lapisan ganda ( $C_1$ ) menunjukkan peningkatan setelah sealing, namun berfluktuasi dengan penambahan inhibitor, yang menunjukkan perubahan dalam struktur lapisan anodizing. Nilai  $R_2$  yang meningkat secara konsisten dengan penambahan inhibitor menunjukkan peningkatan resistansi lapisan oksida terhadap korosi, menandakan efektivitas inhibitor dalam meningkatkan ketahanan korosi. Dengan demikian, data ini memberikan gambaran bagaimana sealing dan penambahan inhibitor dalam proses anodizing BSAA dapat mempengaruhi karakteristik elektrokimia lapisan anodizing dan ketahanan korosi dari paduan aluminium 2024.

#### **4.5 Kesimpulan**

1. Penambahan inhibitor pada anodizing berdampak terhadap penurunan laju korosi dan laju perambatan retak.
2. Penambahan molibdat sebagai inhibitor dalam proses anodisasi BSAA pada paduan aluminium 2024 menunjukkan pengaruh yang signifikan terhadap parameter yang diukur (terkait dengan ketahanan korosi atau laju perambatan retak). Konsentrasi molibdat 0,30% menunjukkan efektivitas terbaik dalam menurunkan nilai parameter, sementara konsentrasi yang lebih tinggi (0,50% dan 0,70%) menunjukkan penurunan efektivitas. Oleh karena itu, konsentrasi optimal molibdat sebagai inhibitor tampaknya berada pada atau sekitar 0,30%

## DAFTAR PUSTAKA

- Frankel, G. S. (1998). Pitting corrosion of metals: a review of the critical factors. *Journal of the Electrochemical Society*, 145(6), 2186-2198.
- Galvele, J. R. (1981). Transport processes and the mechanism of pitting of metals. *Journal of the Electrochemical Society*, 123(4), 464-474.
- Garcia, J., Perez, A., & Fernandez, J. (2021). "Microstructural Improvements in Anodizing Aluminium Alloys with Molybdate Additives." *Surface and Coatings Technology*, 409, 126839.
- Jones, D. A. (1996). *Principles and Prevention of Corrosion*. Prentice Hall.
- Jones, T., Smith, R., & Brown, L. (2021). "Corrosion Resistance and Fatigue Crack Propagation in Anodized Aluminium Alloys." *Materials Science and Engineering: A*, 789, 138215.
- Kim, S., Park, J., & Lee, H. (2023). "Enhancing Marine Corrosion Resistance of Anodized Aluminium Alloys with Molybdate Inhibitor." *Marine Structures*, 89, 102101
- Li, X., Chen, Z., & Wu, Q. (2022). "Reduction of Pitting Corrosion in Anodized Aluminium Alloys by Molybdate Inhibitor." *Corrosion Science*, 196, 110331.
- Pourbaix, M. (1984). *Atlas of Electrochemical Equilibria in Aqueous Solutions*. National Association of Corrosion Engineers.
- Scully, J. R. (1990). *The fundamentals of corrosion*. Pergamon Press.
- Singh, R., Gupta, K., & Sharma, R. (2019). "Effect of Molybdate Inhibitor on Corrosion Resistance of Anodized Aluminium Alloys." *Journal of Alloys and Compounds*, 788, 315-322.
- Speidel, M. O. (1981). Stress corrosion cracking of aluminum alloys. *Metallurgical Transactions A*, 12(4), 779-789.
- Srinivasan, V., & Hardie, D. (1983). The effect of crack tip environment on the stress corrosion cracking of aluminium alloys. *Corrosion Science*, 23(6), 549-571.
- Turnbull, A. (1993). The solution chemistry within cracks. *Corrosion Science*, 34(6), 921-960.
- Wang, H., Zhang, Y., & Li, J. (2022). "Enhancing Corrosion Resistance of Anodized Aluminium Alloys with Molybdate Inhibitor." *Journal of Materials Science & Technology*, 58, 102739.
- Zhang, L., Liu, Y., & Wang, X. (2020). "Influence of Molybdate on the Fatigue Crack Propagation of Anodized 7075 Aluminium Alloy." *International Journal of Fatigue*, 133, 105422.

## BAB V PEMBAHASAN UMUM

### 5.1 Pembahasan Hasil Penelitian I

Nilai kekerasan dengan perlakuan setelah anodizing tanpa *sealing* dan *sealing* dengan waktu tahan 10 menit tanpa *sealing* sebesar 43,244 VHN, dan 10 menit dengan *sealing* sebesar 54,244 VHN. Untuk waktu 15 menit tanpa *sealing* sebesar 37,385 VHN dan 15 menit dengan *sealing* sebesar 40,106 VHN terjadi peningkatan, ini sesuai dengan penelitian (Jung hoon Lee dkk, 2012), yang melakukan penelitian dengan variasi larutan *sealing* pada Al 5052 yang telah dianodisasi dengan berbagai jenis larutan *sealing*, diperoleh hasil bahwa proses *sealing* dapat meningkatkan kekerasan permukaan hasil anodisasi. Dimana peningkatan kekerasan tergantung dari jenis larutan *sealing* yang digunakan. (Gabe ,2012) mengemukakan bahwa proses *sealing* dengan suhu yang panas dapat meningkatkan kekerasan permukaan hasil anodisasi.

Untuk nilai kekasaran permukaan pada anodisasi 10 menit tanpa *sealing* sebesar 0,124 ( $\mu\text{m}$ ), dan 10 menit dengan *sealing* sebesar 0,155 ( $\mu\text{m}$ ). Untuk waktu 15 menit tanpa *sealing* sebesar 0,197 ( $\mu\text{m}$ ) dan 15 menit dengan *sealing* sebesar 0,171 ( $\mu\text{m}$ ) terjadi penurunan nilai kekasaran diakibatkan penggunaan *sealing*. Penurunan kekasaran pada permukaan hasil anodisasi setelah proses *sealing* terjadi karena beberapa mekanisme yaitu

1. Pengisian Pori: Selama proses *sealing*, pori-pori yang terbentuk pada permukaan aluminium akan terisi oleh senyawa *sealing*. Senyawa ini dapat berupa garam logam, oksida, atau polimer. Dengan terisinya pori-pori, permukaan menjadi lebih halus dan rata.
2. Presipitasi: Proses presipitasi dari senyawa *sealing* di dalam pori juga dapat menyebabkan penurunan kekasaran. Endapan yang terbentuk akan menutupi dinding pori dan mengurangi ukurannya.
3. Pelarutan Lapisan Anoda: Beberapa jenis *sealing*, terutama *sealing* panas, dapat menyebabkan pelarutan sebagian lapisan anodizing. Proses pelarutan ini dapat menyebabkan permukaan menjadi lebih halus.

Demikian pula halnya pada laju korosi dimana penggunaan *sealing* menyebabkan terhambatnya laju korosi pada material, untuk penelitian ini laju korosi minimal terjadi pada 10 volt dengan waktu tahan 15 menit sebesar 0,16027 mpy.

Untuk penambahan inhibitor pengurangan laju korosi terjadi pada 0,3 % tegangan 10 volt waktu tahan 15 menit mampu memperlambat laju korosi sebesar 0,2474 mpy dengan

effisiensi inhibitor 77 %. Hal ini terkait dengan hasil kekerasan dan kekasaran permukaan yang diperoleh pada penelitian I dimana sealing menutupi pori yang terbentuk sehingga media korosif tidak mudah masuk dan mengurangi konsentrasi tegangan meskipun tidak selalu signifikan

## 5.2 Pembahasan Hasil Penelitian II

Perambatan retak pada material tanpa perlakuan, nilai C dan n menunjukkan karakteristik dasar laju perambatan retak pada paduan aluminium 2024 tanpa adanya pengaruh dari larutan korosif. Nilai C yang relatif besar dan n yang sedang menunjukkan laju perambatan retak yang moderat dalam kondisi lingkungan yang tidak korosif.

Dalam larutan 3,5% NaCl dengan penambahan inhibitor nilai C menurun dibandingkan dengan di udara, menunjukkan bahwa laju perambatan retak menurun dalam lingkungan korosif akibat adanya inhibitor. Nilai n sedikit lebih rendah, menunjukkan bahwa perambatan retak lebih sensitif terhadap tegangan di lingkungan korosif dibandingkan di udara. Dengan penambahan 0,3% molibdat dalam larutan 3,5% NaCl, nilai C menurun drastis, menunjukkan bahwa molibdat efektif dalam mengurangi laju perambatan retak. Nilai n meningkat, menunjukkan bahwa retak menjadi lebih tahan terhadap tegangan dengan adanya inhibitor molibdat .

Anodizing BSAA dengan penambahan inhibitor menunjukkan laju korosi turun demikian juga laju perambatan retak. Hal ini disebabkan oleh efek perlindungan ganda yang dihasilkan oleh lapisan oksida dan inhibitor serta inhibitor dapat memperbaiki permukaan yang dapat berakibat pengurangan konsentrasi tegangan. Sehingga penambahan inhibitor tidak hanya meningkatkan ketahanan korosi, tetapi juga berperan penting dalam memperlambat laju perambatan retak, sehingga memperpanjang umur pakai material dalam hal ini optimal pada 0,3 %.

Pengujian EIS menunjukkan nilai  $R_s$  resistansi dari larutan elektrolit cenderung meningkat setelah sealing dan dengan penambahan inhibitor hingga 0,3%, menunjukkan jika larutan menjadi sedikit lebih resistif terhadap aliran ion. Namun, pada konsentrasi 0,5% dan 0,7%, nilai  $R_s$  menurun dari puncaknya pada 0,3%, menunjukkan bahwa efek inhibitor tidak lagi linier pada konsentrasi yang lebih tinggi.

Untuk nilai C1 mencerminkan kapasitansi lapisan ganda yang terbentuk pada antarmuka elektroda-larutan. Peningkatan nilai C1 setelah sealing menunjukkan peningkatan ketebalan atau kualitas lapisan anodizing. Namun, nilai C1 berfluktuasi dengan penambahan inhibitor pada berbagai konsentrasi, yang bisa disebabkan oleh perubahan struktur lapisan anodizing yang dihasilkan.

R2 merupakan resistansi lapisan oksida anodizing terhadap korosi. Nilai R2 meningkat setelah sealing dan lebih lanjut dengan penambahan inhibitor, menunjukkan bahwa lapisan oksida menjadi lebih resisten terhadap korosi dengan penambahan inhibitor. Nilai R2 yang terus meningkat menunjukkan bahwa inhibitor efektif dalam meningkatkan ketahanan korosi pada lapisan anodizing, dengan demikian dari hasil uji EIS diperoleh kesimpulan bahwa proses sealing dan penambahan inhibitor dalam proses anodizing BSAA dapat meningkatkan ketahanan korosi dari paduan aluminium 2024, yang ditunjukkan oleh peningkatan nilai Rs dan R2.

Nilai R2 yang meningkat secara konsisten dengan penambahan inhibitor menunjukkan peningkatan resistansi lapisan oksida terhadap korosi, menandakan efektivitas inhibitor dalam meningkatkan ketahanan korosi. Dengan demikian, data ini memberikan pengetahuan bagaimana sealing dan penambahan inhibitor dalam proses anodizing BSAA mempengaruhi karakteristik elektrokimia lapisan anodizing dan ketahanan korosi dari paduan aluminium 2024.

Hasil penelitian ini juga memberikan informasi bahwa penurunan laju korosi berdampak terhadap laju perambatan retak dimana laju korosi minimal pada 0,3 % demikian juga pada laju perambatan retak dengan 47974 siklus.

## BAB VI

### KESIMPULAN DAN SARAN

#### 6.1. Kesimpulan

Berdasarkan hasil dan pembahasan sebelumnya maka dapat diperoleh kesimpulan yaitu :

1. Terjadinya pori-pori pada permukaan material, disebabkan akibat terjadinya proses anodizing.
2. Proses sealing meminimalisir adanya pori dapat meningkatkan kekerasan dan menurunkan kekasaran, hal ini diakibatkan fungsi *sealing* menutup pori-pori sehingga permukaan akan lebih halus, rata dan homogen.
3. Anodizing dapat menurunkan laju korosi dan berdampak pada penurunan laju perambatan retak
4. Penambahan inhibitor pada proses anodizing dapat mengurangi laju korosi dan memperbaiki permukaan sehingga mengurangi konsentrasi tegangan yang dapat mengakibatkan perambatan retak
5. Untuk material tanpa perlakuan paduan aluminium 2024 menunjukkan laju korosi yang moderat. Dalam larutan 3,5% NaCl, laju korosi dan perambatan retak meningkat secara signifikan, menunjukkan pengaruh negatif dari lingkungan korosif. 3,5% NaCl. Penambahan inhibitor molibdat pada proses anodisasi BSAA menunjukkan pengaruh terhadap parameter yang diukur (terkait dengan ketahanan korosi dan laju perambatan retak). Konsentrasi molibdat 0,5%, 0,7% belum menunjukkan efektivitas terbaik dalam menurunkan nilai parameter yang diukur, sementara pada konsentrasi 0,3 % menunjukkan konsentrasi optimal dalam penurunan laju korosi dan perambatan retak dalam media 3,5% NaCl.

#### 6.2. Saran

Untuk memperoleh hasil yang maksimal diperlukan

1. Pemahaman tentang faktor yang mempengaruhi hasil anodizing seperti suhu, waktu, tegangan *sealing*, dan elektrolit
2. Pengembangan dan penelitian lanjutan pada faktor yang mempengaruhi hasil anodizing sehingga diperoleh hasil yang optimal.

## DAFTAR PUSTAKA

- Al-fattal, Sadik and Samir Ali Amin Al-rabii. 2016. "Effect of Anodizing Process on the Mechanical Properties and Fatigue Life of Aluminum Alloy 2024-T3." *Advances in natural and applied science* 15 (10):43–51.
- Apachitei, L.EF., Apachitei, I., Duszczuk, 2006, "Thermal Effects Associated with Hard Anodisasi of Cast Aluminum Alloys", *Journal of Applied Electrochemistry*, Vol. 36, pp. 481-486
- ASM Handbook, 1992, "Corrosion", Metal Handbook, Vol.13.
- ASTM, 2003, "Metal Test Methods and Analytical Procedures", *Annual Book of ASTM Standard*, sc.3 Vol 03.01,E647-00, pp.615-657, Bar Harbor Drive West Conshohocken.
- ASTM. 2004. (*Astm Manual Series, Mnl 20*) *ASTM International - Corrosion Tests And Standards Application And Interpretation-.Pdf*. 2nd ed. edited by B. Robert. ASTM International.
- Araoyinbo, A.O., Noor, A.F.M., Sreekantan, S., Aziz, A. 2010 "Voltage Effect On Electrochemical Anodization Of Aluminium At Ambient Suhue", *International Journal Of Mechanical Dan Materials Engineering*, Vol. 5, No. 1, pp. 53-58.
- Bensalah, W., Feki, M., Wery, M., Ayedi, H.F., 2011 "Chemical Dissolution Resistance Of Anodic Oxide Layers Formed On Aluminium", *Transactions of Nonferrous Metals Society of China*, Vol. 21, pp. 1673-1679.
- BPPT. 1998. *Teknologi Pelapisan Logam Secara Listrik*. Program Penerapan IPTEK di Daerah: Jakarta
- Canning, W., 1970, *Canning Hand Book on Electroplating*, 2nd edition, pp. 695-706
- Canyook R, dkk. 2018, Influences of sealing solutions on anodized layer properties of 7075 aluminium alloy, *The 10th Thailand International Metallurgy Conference (The 10th TIMETC)*, *Materials Today, Proceedings* 5 (2018) 9483–9488
- Chaudhuri, J., Y. M. Tan, K. Patni, and A. Eftekhari. 1992. "Comparison of Corrosion-Fatigue Properties of 6013 Bare, Alclad 2024, and 2024 Bare Aluminum Alloy Sheet Materials." *JMEPEG* 1 (February):91–96.
- Chaussumier, Michel, Catherine Mabru, Rémy Chieragatti, and Majid Shahzad. 2013. "Fatigue Life Model for 7050 Chromic Anodized Aluminium Alloy." *Procedia Engineering* 66:300–312.

- Cree, A. M. and G. W. Weidmann. 1997. "Effect of anodised coatings on fatigue crack growth rates in aluminium alloy." *Surface Engineering* 1997 13(1):51–55.
- Cristian and Tileagă. 2013. "Loughborough University Institutional Repository." *Apologia*. IN: Keightley, E. and Pickering, M. (Eds.) *Research Methods for Memory Studies* 1–2.
- Veys D, Renaux, N. Chahboun, and E. Rocca, 2016 "Anodizing of multiphase aluminium alloys in sulfuric acid: in-situ electrochemical behaviour and oxide properties," *Electrochim. Acta*, vol. 211, pp. 1056–1065,.
- Davis, J. R. 2008. Aluminum and Aluminum Alloys, in *Metals Handbook Desk Edition*, 2nd ed., J.R. Davis, Ed., ASM International, 1998, p 417–505.
- Diamantino, Teresa C., Lucia Guilhermino, Elisabete Almeida, and Amadeu M. V. M. Soares. 2000. "Toxicity of Sodium Molybdate and Sodium Dichromate to *Daphnia Magna* Straus Evaluated in Acute, Chronic, and Acetylcholinesterase Inhibition Tests." *Ecotoxicology and Environmental Safety* 45(3):253–59.
- Domingues, L., J. C. S. Fernandes, M. Da Cunha, M. G. S. Ferreira, and L. Guerra-rosa. 2003. "Anodising of Al 2024-T3 in a Modified Sulphuric Acid / Boric Acid Bath for Aeronautical Applications." *Corrosion Science* 45:149–60.
- Du, Nan, Shuai Xing Wang, Qing Zhao, and Zhi Song Shao. 2012. "Effects of Boric Acid on Microstructure and Corrosion Resistance of Boric/Sulfuric Acid Anodic Film on 7050 Aluminum Alloy." *Transactions of Nonferrous Metals Society of China (English Edition)* 22(7):1655–60.
- Elabar, D., G. R. La Monica, M. Santamaria, F. Di Quarto, P. Skeldon, and G. E. Thompson. 2017. "Anodizing of Aluminium and AA 2024-T3 Alloy in Chromic Acid: Effects of Sulphate on Film Growth." *Surface and Coatings Technology* 309:480–89.
- Emregül, K. C. and A. A. Aksüt. 2003. "The Effect of Sodium Molybdate on the Pitting Corrosion of Aluminum." *Corrosion Science* 45(11):2415–33.
- Mansfeld, F. Zhang, C. Chen. *Plat. Surf. Finish.* 84 (1997) 72–81.
- Fares, C., L. Hemmouche, M. A. Belouchrani, A. Amrouche, D. Chicot, and E. S. Puchicabrera. 2015. "Coupled Effects of Substrate Microstructure and Sulphuric Acid Anodizing on Fatigue Life of a 2017A Aluminum Alloy." *JMADE* 86:723–34.
- Fontana, M.G., 1986, "*Corrosion Engineering*", McGraw-Hill, 3<sup>th</sup> edition, New York.
- Hatch, E.J., 1984 "*Aluminum Properties and Physical Metallurgy*", Ohio, American Society for Metal.

- Frankel, G. S. (1998). Pitting corrosion of metals: a review of the critical factors. *Journal of the Electrochemical Society*, 145(6), 2186-2198.
- Gabe, D.R. 2006. *Hard Anodize-What do we mean by hard*, loughborough University, U.K
- García-rubio, M., P. Ocón, A. Climent-font, R. W. Smith, M. Curioni, and G. E. Thompson. 2009. "Influence of Molybdate Species on the Tartaric Acid / Sulphuric Acid Anodic Films Grown on AA2024 T3 Aerospace Alloy." *Corrosion Science* 51:2034–42.
- Hamdy, Abdel Salam, Anna Maria Beccaria, and Pierluigi Traverso. 2005. "Corrosion Protection of AA6061 T6-10 % Al<sub>2</sub>O<sub>3</sub> Composite by Molybdate Conversion Coatings." *Journal of Applied Electrochemistry* 35(5):467–72.
- Hashimoto, Elabar T., J. Qi P. Skeldon, G. E. Thompson Pii, and Electrochimica Acta. 2016. "Effect of Low Levels of Sulphate on the Current Density and Film Morphology." *Electrochimica Acta*.
- Heller, Daimon K., William G. Fahrenholtz, and Matthew J. O'Keefe. 2010. "The Effect of Post-Treatment Time and Temperature on Cerium-Based Conversion Coatings on Al 2024-T3." *Corrosion Science* 52(2):360–68.
- Henley, V. F. 1982. *Anodic Oxidation of Aluminium and Its Alloys*. 2nd ed. edited by I. and S. I. T. B. D. W. Hopkins, University College of Swansea J. R. BARRATT, British Steel Corporation T. Bell, University of Birmingham G. E. Sheward, Ukaea, Springfields Laboratories A. J. Smith J. R. Thornton. Pergamon Press Oxford New York, Toronto, Sydney, Paris, Frankfurt.
- Polmear I, "Aluminium Alloys--A Century of Age Hardening," *Mater. forum*, vol. 28, pp. 1–14, 2004.
- Jian-hua Liu, Liang Wu, Mei Yu Song, mei Li Guo-long Wu. 2011 Effects of sealing process on corrosion resistance and roughness of anodic films of titanium alloy Ti-10V-2Fe-3Al, *Journal of Central South University of Technology* volume 18, pages 1795–1801 .
- JA Gonza´lez, V. Lo´pez, E. Otero, A. Bautista, J. Electrochem. Soc. 147 (2000) 984
- Jones, D.A., 1991, "*Principle and Prevention of Corrosion*", Mc. Millan Publishing Company, New York
- Kim, E.S.; Jeong, Y.H.; Choe, H.C.; Brantley, W.A. 2013, "Formation Of Titanium Dioxide Nanotubes On Ti030Nb-Xta Alloys By Anodisasi", *Thin Solid Films*, Vol. S49, pp. 141-146,
- Kudari, Shashidhar K. and C. M. Sharanaprabhu. 2017. "The Effect of Anodizing Process Parameters on the Fatigue Life of 2024-T-351-Aluminium Alloy." *Fatigue of*

*Aircraft Structures* 109–15.

- Zhang, L.G. E. Thompson,\* M. Curioni, and P. Skeldon., 2013, *Anodisasi of Aluminum in Sulfuric Acid/Boric Acid Mixed Electrolyte* L. *Journal of The Electrochemical Society*, 160 (4).
- Lee, Jung hoon, 2012. *Cr2O3 of sealing aluminum anodized by alloy heat treatment*. ELSEVIER.
- Hao L, B. Rachel Cheng, *Met.Finish.*, 98 (12) (2000) 8–18
- LI, Song mei, Hong rui Zhang, and Jian hua Liu. 2007. "Corrosion Behavior of Aluminum Alloy 2024-T3 by 8-Hydroxy- Quinoline and Its Derivative in 3.5% Chloride Solution." *Transactions of Nonferrous Metals Society of China (English Edition)* 17(2):318–25.
- Li, Xianghong, Shuduan Deng, and Hui Fu. 2011. "Sodium Molybdate as a Corrosion Inhibitor for Aluminium in H<sub>3</sub>PO<sub>4</sub> Solution." *Corrosion Science* 53(9):2748–53.
- Liang, Chang Sheng, Zhong Fei Lv, Ye Ling Zhu, Shi Ai Xu, and Hong Wang. 2014. "Protection of Aluminium Foil AA8021 by Molybdate-Based Conversion Coatings." *Applied Surface Science* 288:497–502.
- Lopez-Garrity, O. and G. S. Frankel. 2014. "Corrosion Inhibition of Aluminum Alloy 2024-T3 by Sodium Molybdate." *Journal of The Electrochemical Society* 161(3):C95–106.
- Stevenson Jr M.F, "Anodisasi," 2013.
- Ma, Song jiang, Peng Luo, Hai hui Zhuo, Chao peng Fu, and Ya fei kuang. 2008. "Preparation of Anodic Films on 2024 Aluminum Alloy in Boric Acid-Containing Mixed Electrolyte." *Transactions of Nonferrous Metals Society of China (English Edition)* 18(4):825–30.
- Moreto, J. A., C. E. B. Marino, W. W. Bose Filho, L. A. Rocha, and J. C. S. Fernandes. 2014. "SVET, SKP and EIS Study of the Corrosion Behaviour of High Strength Al and Al-Li Alloys Used in Aircraft Fabrication." *Corrosion Science* 84:30–41.
- Moutarlier, V., M. P. Gigandet, B. Normand, and J. Pagetti. 2005. "EIS Characterisation of Anodic Films Formed on 2024 Aluminium Alloy , in Sulphuric Acid Containing Molybdate or Permanganate Species." *Corrosion Science* 47:937–51.
- Moutarlier, V., M. P. Gigandet, J. Pagetti, and L. Ricq. 2003. "Molybdate/Sulfuric Acid Anodising of 2024-Aluminium Alloy: Influence of Inhibitor Concentration on Film Growth and on Corrosion Resistance." *Surface and Coatings Technology* 173(1):87–95.

- Moutarlier, V., M. P. Gigandet, L. Ricq, and J. Pagetti. 2001. "Electrochemical Characterisation of Anodic Oxidation Films Formed in Presence of Corrosion Inhibitors." *Applied Surface Science* 183(1–2):1–9.
- Mu, Guannan, Xianghong Li, Qing Qu, and Jun Zhou. 2006. "Molybdate and Tungstate as Corrosion Inhibitors for Cold Rolling Steel in Hydrochloric Acid Solution." *Corrosion Science* 48(2):445–59.
- Mukhurov, N.I., Zhvayi, S.P., Terekhov, S.N., 2008, "Influence of Electrolyte Composition on Photoluminescent Properties of anodic Aluminum Oxide", *Journal of Applied Spectroscopy*, Vol.75.
- Nie, Baohua, Zheng Zhang, Zihua Zhao, and Qunpeng Zhong. 2013. "Effect of Anodizing Treatment on the Very High Cycle Fatigue Behavior of 2A12-T4 Aluminum Alloy." *Materials and Design* 50:1005–10.
- Nicklen D. A. L. and Gabe, D. R. A.C. Anodizing of aluminium in sulphuric acid vol. 7, pp. 353–359, 1978.
- Parkhutik, V. P., J. M. Albella, and Experimental Procedure. 1989. "Study of Aluminium Anodization in Sulfuric and Chromic Acid Solution - I Kinetics of Growth and Composition of Oxides." *Electrochimica Acta* 35(6):955–60.
- Poinern, G.E.J., Ali, N., Fawcett, D., 2011 "Progress in Nano-Engineered Anodic Aluminum Oxide Membrane Development, *Materials*, Vol. 4, pp. 487-526.
- Pooladi, R., Rezai, H., Aezami, M., Sayyar, M.R., 2009, "Fabrication of Anodic Aluminum Oxide Nanotemplate and Investigation of Their Anodization Parameters", *Transaction of Indian Institute of Metals*, Vol. 62, Issue 3
- Pourbaix, M. (1984). Atlas of Electrochemical Equilibria in Aqueous Solutions. National Association of Corrosion Engineers.
- Roberge, P. R. 2008. *Corrosion Engineering Principles and Practice*. New York Chicago San Francisco Lisbon London Madrid Mexico City Milan New Delhi San Juan Seoul Singapore Sydney Toronto: The McGraw-Hill Companies, Inc.
- Saeedikhani, M., M. Javidi, and A. Yazdani. 2013. "Anodizing of 2024-T3 Aluminum Alloy in Sulfuric-Boric-Phosphoric Acids and Its Corrosion Behavior." *Transactions of Nonferrous Metals Society of China (English Edition)* 23(9):2551–59.
- Saeedikhani, M, M. Javidi, and A. Yazdani. 2013. "Anodizing of 2024-T3 Aluminum Alloy in Sulfuric – Boric – Phosphoric Acids and Its Corrosion Behavior." *Transactions of Nonferrous Metals Society of China* 23(9):2551–59.
- Sastri, V. S., Edward Ghali, and Mimoun Elboujdaini. 2012. *Corrosion Prevention and*

*Protection: Practical Solutions.*

- Scully, J. R. (1990). *The fundamentals of corrosion*. Pergamon Press.
- Serdechnova, Maria, Sergey A. Karpushenkov, Larisa S. Karpushenkava, Maksim Sarykevich, Mario G. S. Ferreira, Theodor Hack, Mariia H. Iuzviuk, Igor A. Zobkalo, Carsten Blawert, and Mikhail L. Zheludkevich. 2018. "The Influence of PSA Pre-Anodization of AA2024 on PEO Coating Formation : Composition ,." *Materials*.
- Shahzad, M., M. Chaussurier, R. Chieragatti, C. Mabru, and F. Rezai-Aria. 2010. "Influence of Anodizing Process on Fatigue Life of Machined Aluminium Alloy." *Procedia Engineering* 2(1):1015–24.
- Sheasby, P. G., Pinner, R. "The surface Treatment & Finishing of Aluminium Its Alloys", 6th Ed. Vol I&2, Finishing Publications Ltd, 2001
- Shen, Y. Z., H. G. Li, H. J. Tao, J. Ling, T. Wang, and J. Tao. 2015. "Effect of Anodic Films on Corrosion Resistance and Fatigue Crack Initiator of 2060-T8 Al-Li Alloy." *International Journal of Electrochemical Science* 10(1):938–46.
- Silva, J. W. J., E. N. Codaro, R. Z. Nakazato, and L. R. O. Hein. 2005. "Influence of Chromate, Molybdate and Tungstate on Pit Formation in Chloride Medium." *Applied Surface Science* 252(4):1117–22.
- Speidel, M. O. (1981). Stress corrosion cracking of aluminum alloys. *Metallurgical Transactions A*, 12(4), 779-789.
- Srinivasan, V., & Hardie, D. (1983). The effect of crack tip environment on the stress corrosion cracking of aluminium alloys. *Corrosion Science*, 23(6), 549-571.
- Starke, E. A. and J. T. Staley. 1996. "Application of modern aluminum alloys to aircraft." *Prog. Aerospace Sci* 32(95):131–72.
- Stevenson, Milton F. and Anoplate Corporation. 1994. "Anodizing." Pp. 482–93 in *ASM Handbook*. Vol. 5.
- TU, George C., Lee Teng CHEN, and Reng Yow HWANG. 1990. "The Effect on Anodizing on the Corrosion Fatigue Behavior of 2024-T3 Aluminum Alloy." *JSME International* 33(4):527–34.
- Twite, R. L. and G. P. Bierwagen. 1998. "Review of Alternatives to Chromate for Corrosion Protection of Aluminum Aerospace Alloys." *Progress in Organic Coatings* 33(2):91–100.
- Vargel, Christian. 2004. *Corrosion of Aluminium*.

- Velterop, L. 2003. "Phosphoric Sulphuric Acid Anodising: An Alternative for Chromic Acid Anodising in Aerospace Applications?" *Aluminium Surface Science and Technology* 18.
- Ventura X.V , 2004 Sealing Method fr Anodizing Aluminium and Hard Anodizing and Test For Seal Quality Of Aluminium, Laboratory of Electrochemical Research & Development, Integral Centre, Barcelona, Spain 2004 SUR/FIN® Conference ©2004 AESF 44
- Venugopal, A., Rajiv Panda, Sushant Manwatkar, K. Sreekumar, L. Rama Krishna, and G. Sundararajan. 2012. "Effect of Micro Arc Oxidation Treatment on Localized Corrosion Behaviour of AA7075 Aluminum Alloy in 3.5 NaCl Solution." *Transactions of Nonferrous Metals Society of China (English Edition)* 22(3):700–710.
- V. López, E. Otero, A. Bautista, J.A. González, *Surf. Coat. Tech.*, 124 (2000) 76–84. 14
- Verdaguer, D. S. 2015. "Alternative Surface Treatments without Chromium Content in Aeronautical Aluminium Alloys, MSc Thesis." *Thesis* (July).
- Vukasovich, M. S. and J. P. G. Farr. 1986. "Molybdate in Corrosion Inhibition - a Review." *Materials Performance* 25(5):9–18.
- Wahab ,M.A., Sakano, M., 2001, *Experimental Study of Corrosion Fatigue Behavior of Welded Steel Structure*, Journal of Materials Processing Technology, 118 pp. 117 - 122
- Wang dkk, 2015 Sealing of anodized aluminum with phytic acid solution, *Surface & Coatings Technology* .
- Wong, Y. Moji and C. 1989. "US, Patent No.4894127." 2–6.
- Yu, Z. Penghui, Z. Jingmao, *Surf. Coat. Tech.*, 166 (2003) 237–242
- Y. Zuo, P.H. Zhao, J.M. Zhao. *Surf. Coat. Technol.* 166 (2003) 237–242.
- Yan Shang, Linshan Wang, Zhaoyue Liu , Dun Niu , Yuhong Wang Changsheng Liu , The Effects of Different Sealing Techniques for Anodic Film of Al-12.7Si-0.7Mg Alloys *International Journal of ELECTROCHEMICAL SCIENCE* 11 (2016) 5234 – 5244
- Zamber, J. E. and B. M. Hillberry. 1999. "Probabilistic Approach to Predicting Fatigue Lives of Corroded 2024-T3." *AIAA Journal* 37(10):1311–17.
- Zhang, Jin sheng, Xu hui Zhao, Yu Zuo, and Jin ping Xiong. 2008. "The Bonding Strength and Corrosion Resistance of Aluminum Alloy by Anodizing Treatment in a Phosphoric Acid Modified Boric Acid/Sulfuric Acid Bath." *Surface and Coatings Technology* 202(14):3149–56.

Zhang, L., G. E. Thompson, M. Curioni, and P. Skeldon. 2013. "Anodizing of Aluminum in Sulfuric Acid/Boric Acid Mixed Electrolyte." *Journal of the Electrochemical Society* 160(4):179–84.

Zuo, Y. dkk , 2003, The influences of sealing methods on corrosion behavior of anodized aluminum alloys in NaCl solutions, *Surf. Coat. Technol.* 166,237-242.

# LAMPIRAN



## HASIL UJI KOMPOSISI

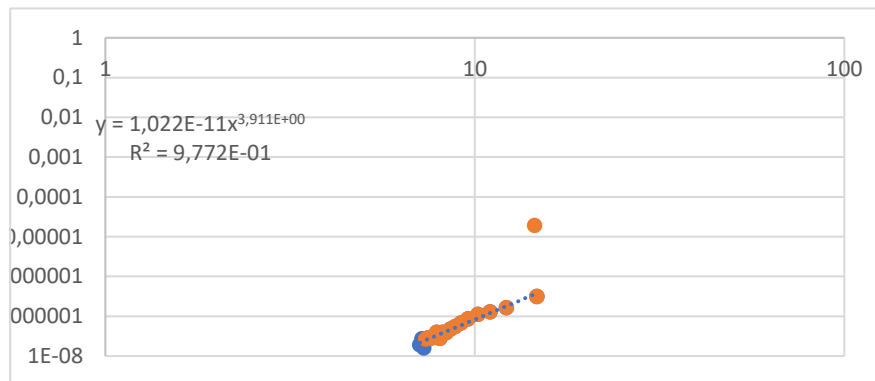
Nomor : 022/ST/VIII/2024  
Nama : M. Zuchry / UNHAS  
Tanggal Uji : 21 Agustus 2024

Element	wt%
Al	93.47
Si	0.132
Fe	0.199
Cu	4.116
Mn	0.530
Mg	1.261
Cr	0.0090
Ni	<0.0050
Zn	0.153
Ti	0.023
Pb	0.0072
Sn	0.015
V	0.011
Sr	<0.0020
Zr	0.0046
Cd	<0.0050
Co	<0.0030
B	<0.0010
Ag	0.0012
Ca	0.0046

## Raw AI 2024

Cycle	crack length (mm)	crack average (mm)	da/dN (secant method) (m/cycles)	t	sec	ft	BW <sup>0.5</sup>	delta K (Mpa.m <sup>1/2</sup> )
0	2,6152999							
2000	2,6536197	2,634459841	1,91599E-08	0,420002	1,265249	0,913405	16,47958	7,0979656
4000	2,7079219	2,680770826	2,71511E-08	0,427385	1,276807	0,925597	16,47958	7,19271
6000	2,7396536	2,723787763	1,58658E-08	0,434243	1,28789	0,937034	16,47958	7,2815878
8000	2,7929352	2,766294411	2,66408E-08	0,441019	1,299181	0,948448	16,47958	7,3702829
10000	2,8508562	2,821895709	2,89605E-08	0,449884	1,31448	0,963556	16,47958	7,4876858
12000	2,9071879	2,87902204	2,81658E-08	0,458991	1,33085	0,979302	16,47958	7,6100454
14000	2,9656098	2,936398857	2,9211E-08	0,468139	1,347989	0,99536	16,47958	7,7348311
16000	3,0448446	3,005227224	3,96174E-08	0,479112	1,369518	1,014967	16,47958	7,8871964
18000	3,0998378	3,072341188	2,74966E-08	0,489811	1,391587	1,034474	16,47958	8,0387791
20000	3,178692	3,139264881	3,94271E-08	0,500481	1,414718	1,054334	16,47958	8,1931152
22000	3,2566526	3,217672296	3,89803E-08	0,512981	1,44334	1,078164	16,47958	8,3782905
24000	3,3519164	3,304284485	4,76319E-08	0,526789	1,477011	1,105249	16,47958	8,5887641
26000	3,4610394	3,406477881	5,45615E-08	0,543081	1,519759	1,138334	16,47958	8,8458642
28000	3,5969117	3,528975527	6,79361E-08	0,562611	1,575783	1,179783	16,47958	9,1679591
30000	3,7684182	3,682664958	8,57533E-08	0,587113	1,654497	1,234934	16,47958	9,5965304
32000	3,9892953	3,878856783	1,10439E-07	0,618391	1,771232	1,311352	16,47958	10,190367
34000	4,2475915	4,118443415	1,29148E-07	0,656587	1,945159	1,416034	16,47958	11,003839

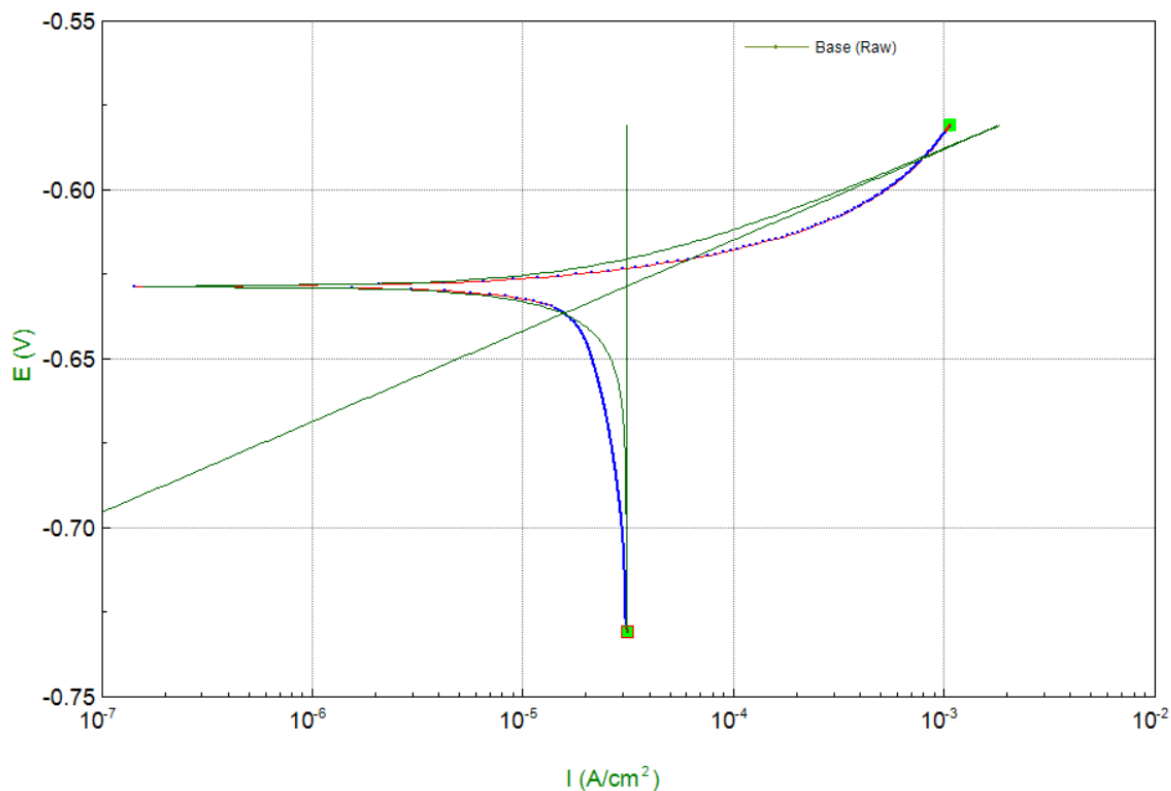
36000	4,5745666	4,411079047	1,63488E-07	0,703241	2,222475	1,566464	16,47958	12,172815
38000	5,1990113	4,886788957	3,12222E-07	0,779082	2,93532	1,894825	16,47958	14,72447
38705	4,8465497	5,022780505	-4,9995E-07	0,800762	3,24165	2,01876	16,47958	15,687558
38706	4,865563	4,85605635	1,90133E-05	0,774182	2,874386	1,869149	16,47958	14,524947
38707	4,1584798	4,512021401	-0,00070708	0,719334	2,340584	1,625838	16,47958	12,634202
38708	3,8762513	4,01736555	-0,00028223	0,640473	1,866959	1,370148	16,47958	10,647269
38709	1,9196219	2,897936631	-0,00195663	0,462007	1,336421	0,984568	16,47958	7,6509664



## TEST RESULT

No : LM-01/15/09/2022

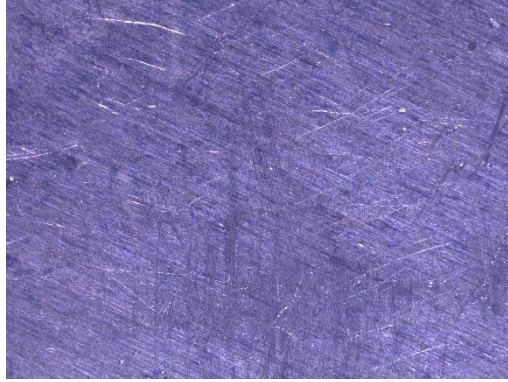
<b>Customer</b>	Zuhri	<b>Tanggal</b>	Kamis, 29 September 2022
<b>Material</b>	Aluminium 2024	<b>Pengujian</b>	<i>Corrosion Test</i>
<b>Operator</b>	Ruben Sanilo	<b>Standard</b>	ASTM G102



<b>Spesimen</b>	<b>Potensial (mV)</b>	<b>Arus (<math>\mu A/cm^2</math>)</b>	<b>Laju Korosi (mppy)</b>
Raw Material (Base)	628,69	31,055	1,0762

Laporan ini tidak boleh digandakan sebagian atau seluruhnya  
Laporan pengujian ini hanya berlaku untuk sampel yang diuji

Keterangan :



Spesimen Sebelum Uji Korosi



Spesimen Setelah Uji Korosi

**TIM PENGUJI :**

Penguji 1



Ruben Sanilo

Penguji 2



Andiyanto, ST

**Semarang, 29 September 2022**

Mengetahui

Ketua Laboratorium Material

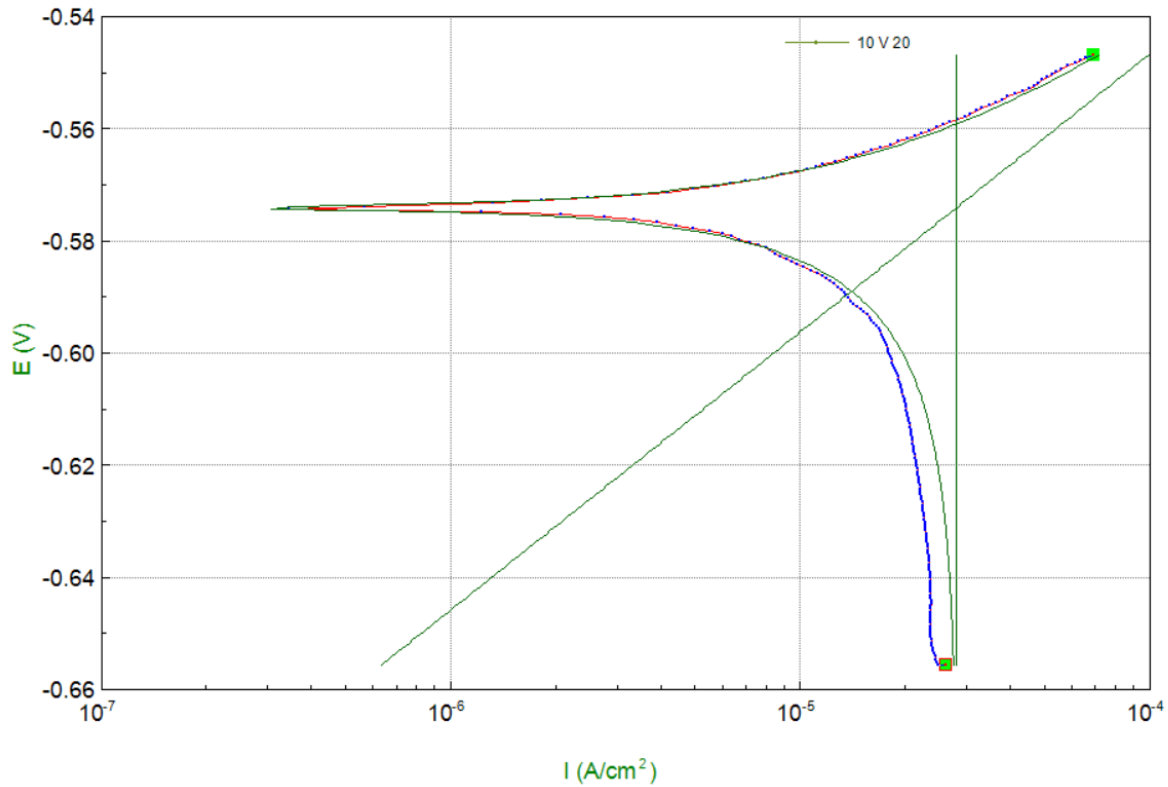


Yusuf Umardhani, ST., MT

## TEST RESULT

**No : LM-01/15/09/2022**

<b>Customer</b>	Zuhri	<b>Tanggal</b>	Kamis, 29 September 2022
<b>Material</b>	Aluminium 2024	<b>Pengujian</b>	<i>Corrosion Test</i>
<b>Operator</b>	Ruben Sanilo	<b>Standard</b>	ASTM G102



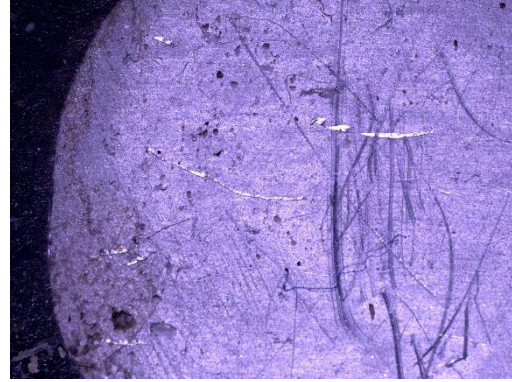
<b>Spesimen</b>	<b>Potensial (mV)</b>	<b>Arus (μA/cm<sup>2</sup>)</b>	<b>Laju Korosi (mmpy)</b>
10 V 20	574,16	28,07	0,97271

Laporan ini tidak boleh digandakan sebagian atau seluruhnya  
Laporan pengujian ini hanya berlaku untuk sampel yang diuji

Keterangan :



Spesimen Sebelum Uji Korosi



Spesimen Setelah Uji Korosi

**TIM PENGUJI :**

Penguji 1

Ruben Sanilo

**Semarang, 29 September**

**2022**

Penguji 2

Andiyanto, ST

Mengetahui

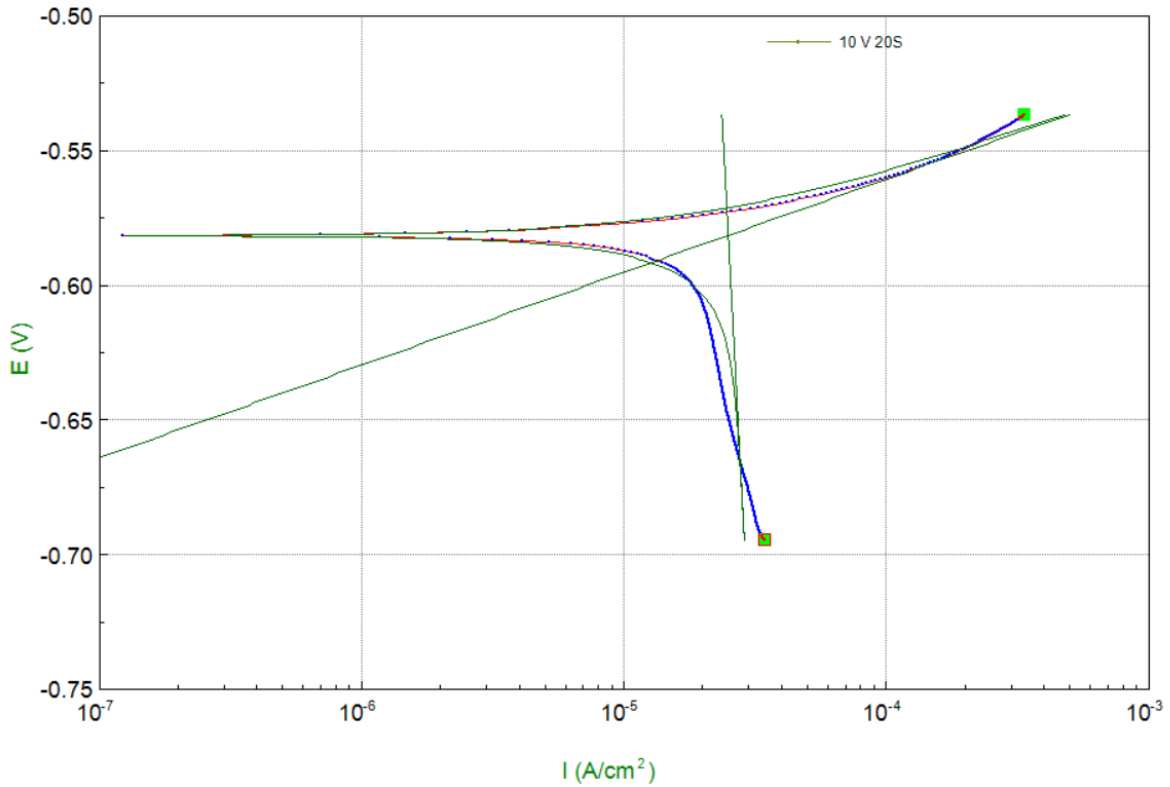
Ketua Laboratorium Material

Yusuf Umardhani, ST., MT

## TEST RESULT

**No : LM-01/15/09/2022**

<b>Customer</b>	Zuhri	<b>Tanggal</b>	Kamis, 29 September 2022
<b>Material</b>	Aluminium 2024	<b>Pengujian</b>	<i>Corrosion Test</i>
<b>Operator</b>	Ruben Sanilo	<b>Standard</b>	ASTM G102



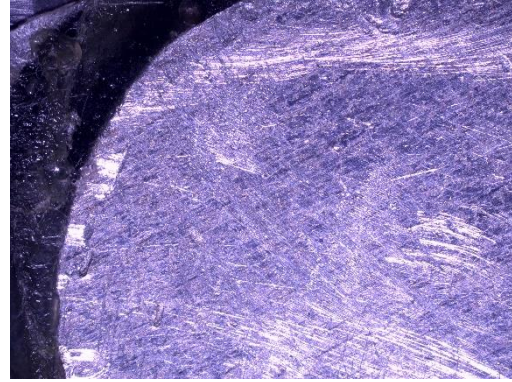
Laporan ini tidak boleh digandakan sebagian atau seluruhnya  
Laporan pengujian ini hanya berlaku untuk sampel yang diuji

<b>Spesimen</b>	<b>Potensial (mV)</b>	<b>Arus (<math>\mu A/cm^2</math>)</b>	<b>Laju Korosi (mmpy)</b>
10 V 20S	581,62	25,01	0,86668

Keterangan :



Spesimen Sebelum Uji Korosi



Spesimen Setelah Uji Korosi

**TIM PENGUJI :**

Penguji 1

Ruben Sanilo

**Semarang, 29 September**

**2022**

Penguji 2

Andiyanto, ST

Mengetahui

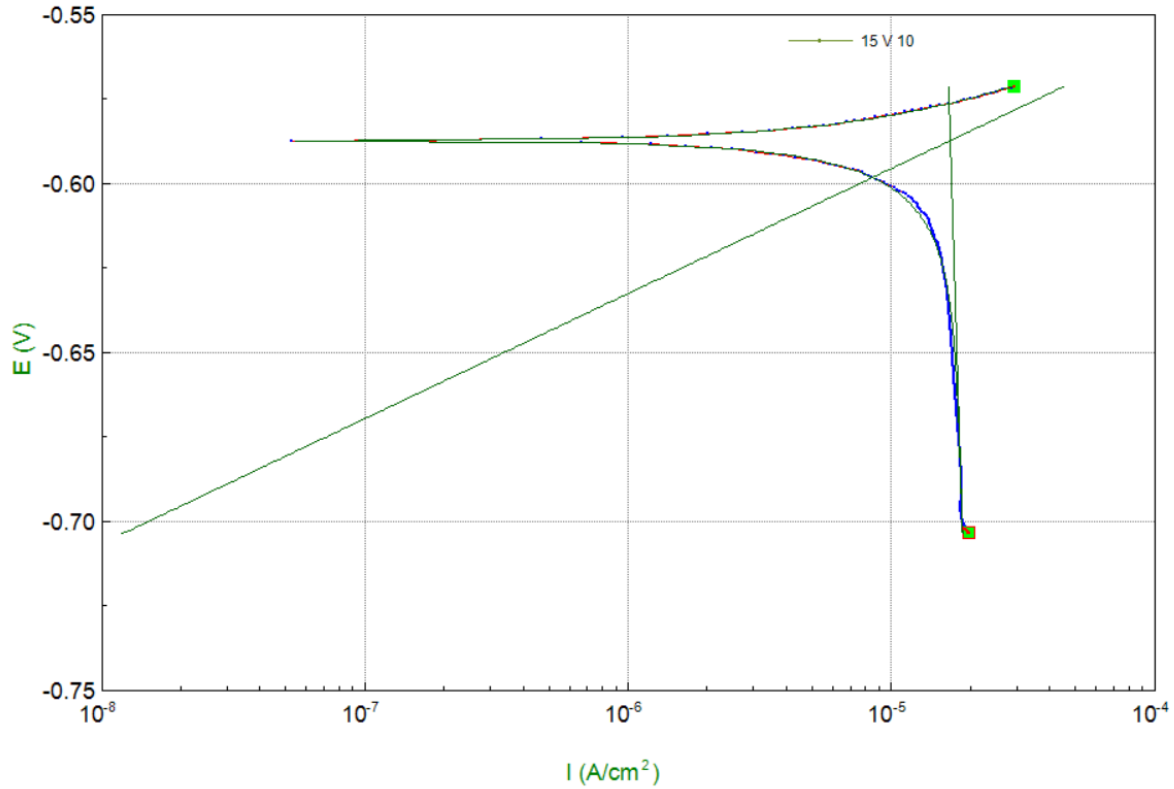
Ketua Laboratorium Material

Yusuf Umardhani, ST., MT

## TEST RESULT

**No : LM-01/15/09/2022**

<b>Customer</b>	Zuhri	<b>Tanggal</b>	Kamis, 29 September 2022
<b>Material</b>	Aluminium 2024	<b>Pengujian</b>	<i>Corrosion Test</i>
<b>Operator</b>	Ruben Sanilo	<b>Standard</b>	ASTM G102



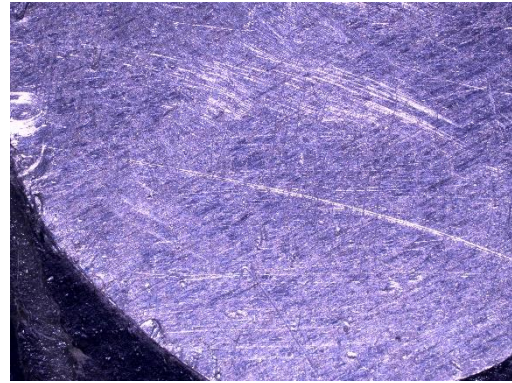
Laporan ini tidak boleh digandakan sebagian atau seluruhnya  
Laporan pengujian ini hanya berlaku untuk sampel yang diuji

<b>Spesimen</b>	<b>Potensial (mV)</b>	<b>Arus (μA/cm<sup>2</sup>)</b>	<b>Laju Korosi (mmpy)</b>
15 V 10	587,39	16,77	0,58114

Keterangan :



Spesimen Sebelum Uji Korosi



Spesimen Setelah Uji Korosi

**TIM PENGUJI :**

Penguji 1

Ruben Sanilo

**Semarang, 29 September**

**2022**

Penguji 2

Andiyanto, ST

Mengetahui

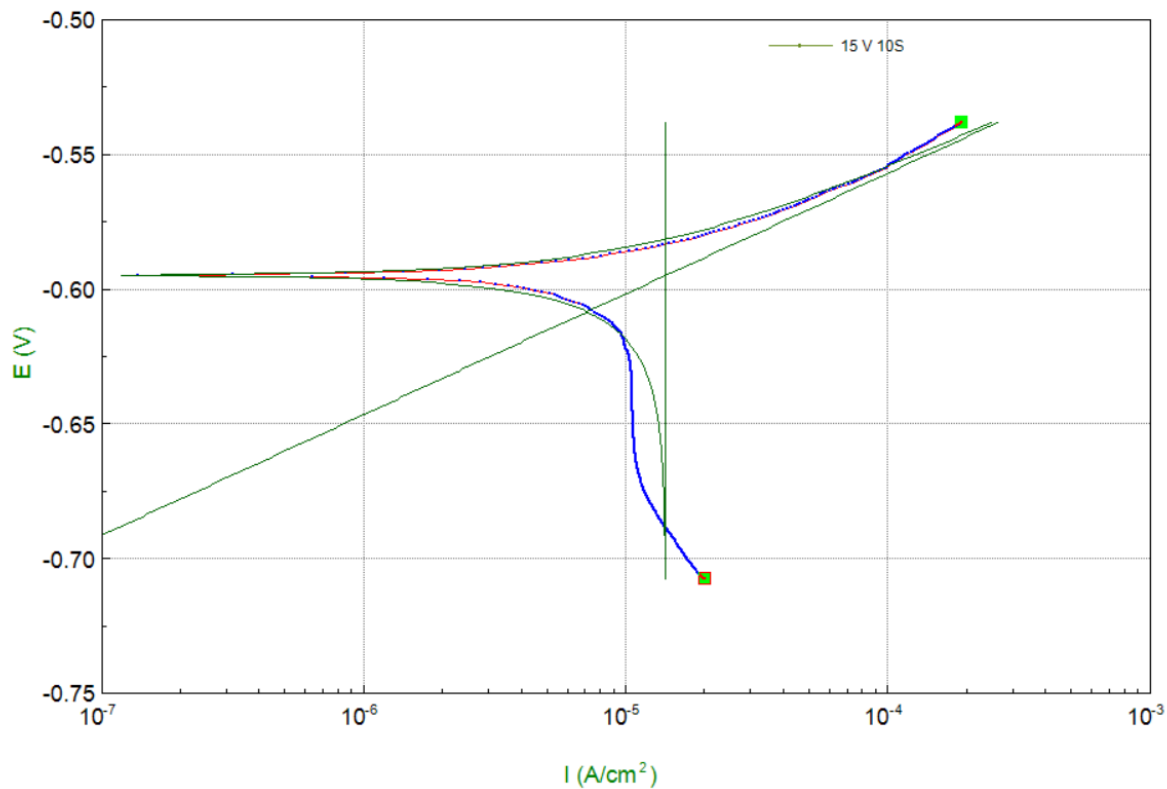
Ketua Laboratorium Material

Yusuf Umardhani, ST., MT

## TEST RESULT

**No : LM-01/15/09/2022**

<b>Customer</b>	Zuhri	<b>Tanggal</b>	Kamis, 29 September 2022
<b>Material</b>	Aluminium 2024	<b>Pengujian</b>	<i>Corrosion Test</i>
<b>Operator</b>	Ruben Sanilo	<b>Standard</b>	ASTM G102



<b>Spesimen</b>	<b>Potensial (mV)</b>	<b>Arus (<math>\mu A/cm^2</math>)</b>	<b>Laju Korosi (mmpy)</b>
15 V 10S	595,14	14,185	0,49156

Keterangan :



Spesimen Sebelum Uji Korosi



Spesimen Setelah Uji Korosi

**TIM PENGUJI :**

Penguji 1

Ruben Sanilo

**Semarang, 29 September**

**2022**

Penguji 2

Andiyanto, ST

Mengetahui

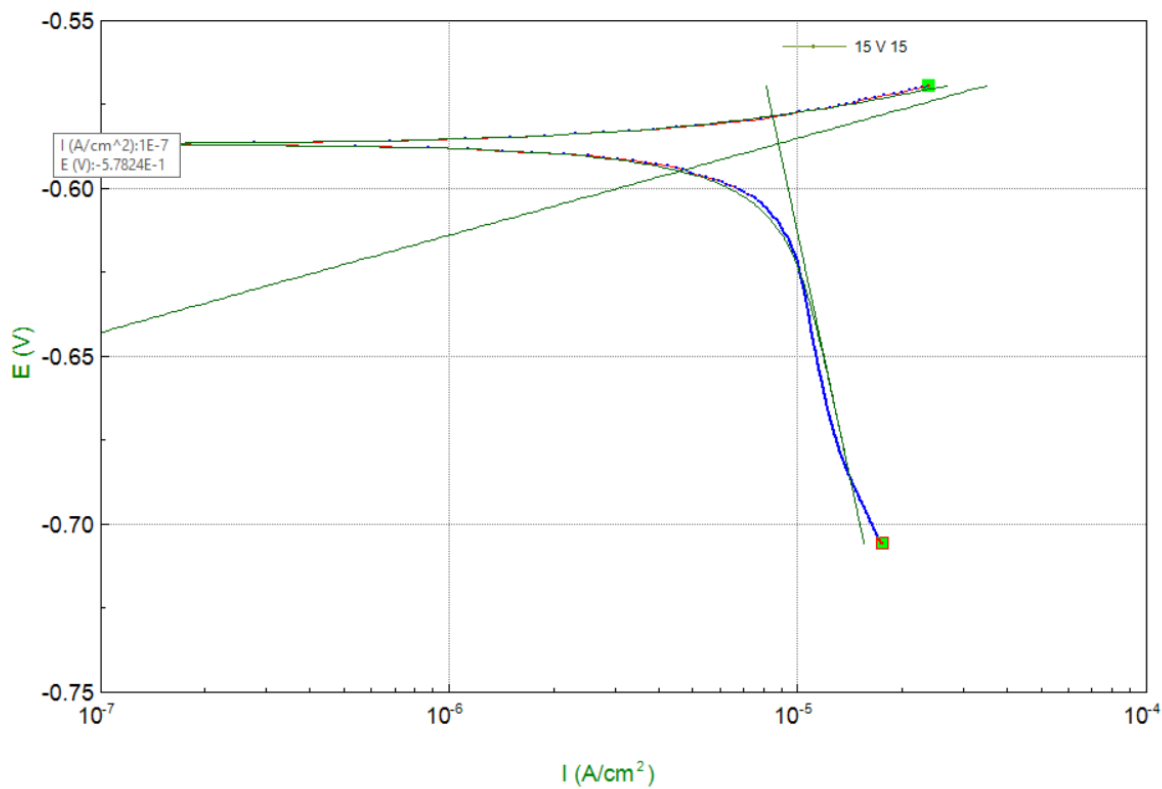
Ketua Laboratorium Material

Yusuf Umardhani, ST., MT

## TEST RESULT

**No : LM-01/15/09/2022**

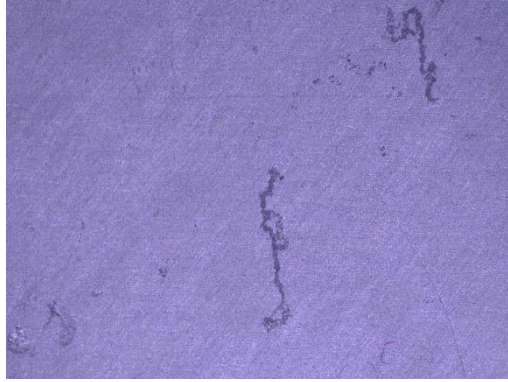
<b>Customer</b>	Zuhri	<b>Tanggal</b>	Kamis, 29 September 2022
<b>Material</b>	Aluminium 2024	<b>Pengujian</b>	Corrosion Test
<b>Operator</b>	Ruben Sanilo	<b>Standard</b>	ASTM G102



Spesimen	Potensial (mV)	Arus (μA/cm <sup>2</sup> )	Laju Korosi (mmpy)
15 V 15	586,77	8,8244	0,3058

Laporan ini tidak boleh digandakan sebagian atau seluruhnya  
Laporan pengujian ini hanya berlaku untuk sampel yang diuji

Keterangan :



Spesimen Sebelum Uji Korosi



Spesimen Setelah Uji Korosi

**TIM PENGUJI :**

Penguji 1



Ruben Sanilo

Penguji 2



Andiyanto, ST

**Semarang, 29 September 2022**

Mengetahui

Ketua Laboratorium Material

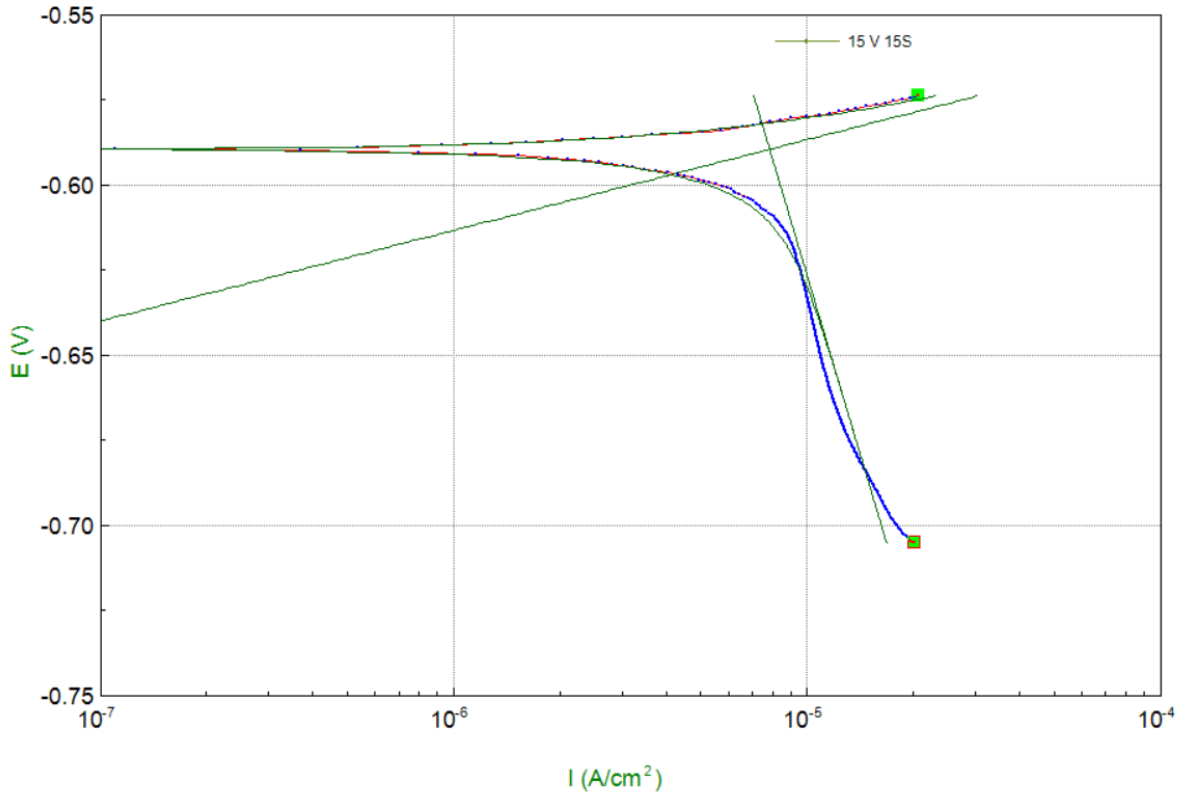


Yusuf Umardhani, ST., MT

## TEST RESULT

**No : LM-01/15/09/2022**

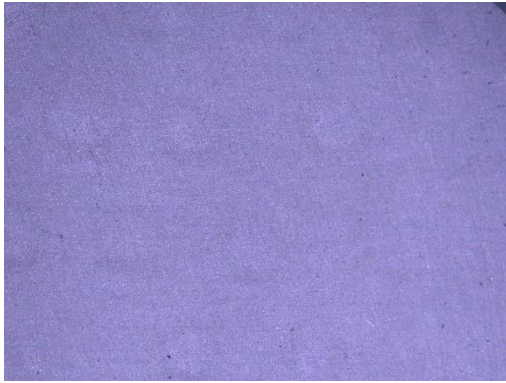
<b>Customer</b>	Zuhri	<b>Tanggal</b>	Kamis, 29 September 2022
<b>Material</b>	Aluminium 2024	<b>Pengujian</b>	<i>Corrosion Test</i>
<b>Operator</b>	Ruben Sanilo	<b>Standard</b>	ASTM G102



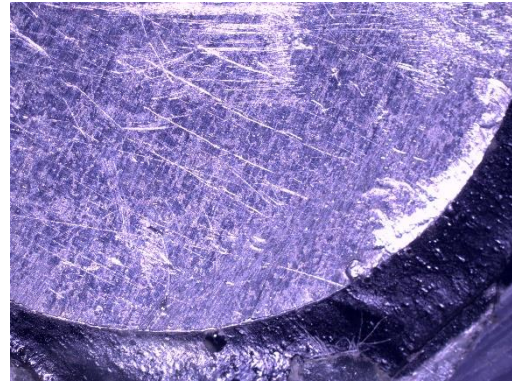
Laporan ini tidak boleh digandakan sebagian atau seluruhnya  
Laporan pengujian ini hanya berlaku untuk sampel yang diuji

<b>Spesimen</b>	<b>Potensial (mV)</b>	<b>Arus (<math>\mu\text{A}/\text{cm}^2</math>)</b>	<b>Laju Korosi (mmpy)</b>
15 V 15S	589,62	7,8407	0,27171

Keterangan :



Spesimen Sebelum Uji Korosi



Spesimen Setelah Uji Korosi

**TIM PENGUJI :**

Penguji 1



Ruben Sanilo

Penguji 2



Andiyanto, ST

**Semarang, 29 September 2022**

Mengetahui

Ketua Laboratorium Material

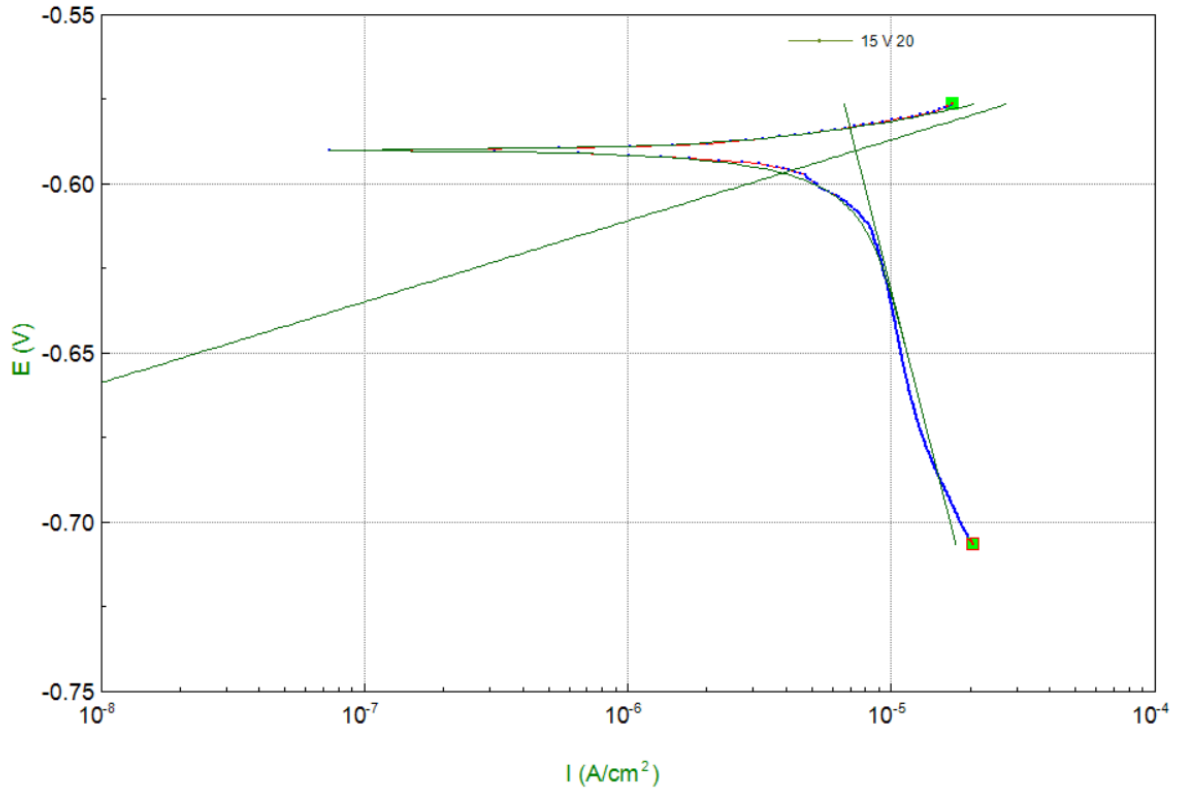


Yusuf Umardhani, ST., MT

## TEST RESULT

**No : LM-01/15/09/2022**

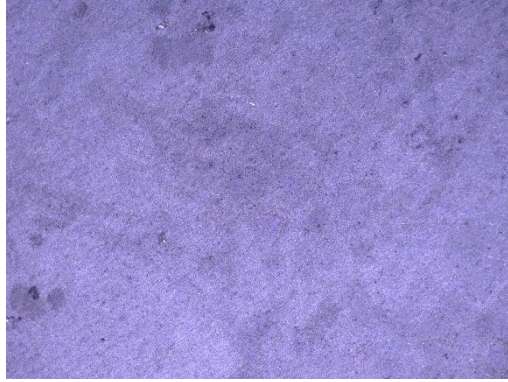
<b>Customer</b>	Zuhri	<b>Tanggal</b>	Kamis, 29 September 2022
<b>Material</b>	Aluminium 2024	<b>Pengujian</b>	<i>Corrosion Test</i>
<b>Operator</b>	Ruben Sanilo	<b>Standard</b>	ASTM G102



<b>Spesimen</b>	<b>Potensial (mV)</b>	<b>Arus (μA/cm<sup>2</sup>)</b>	<b>Laju Korosi (mmpy)</b>
15 V 20	590,28	7,346	0,25456

Laporan ini tidak boleh digandakan sebagian atau seluruhnya  
Laporan pengujian ini hanya berlaku untuk sampel yang diuji

Keterangan :



Spesimen Sebelum Uji Korosi



Spesimen Setelah Uji Korosi

**TIM PENGUJI :**

Penguji 1

Ruben Sanilo

**Semarang, 29 September 2022**

Penguji 2

Andiyanto, ST

Mengetahui

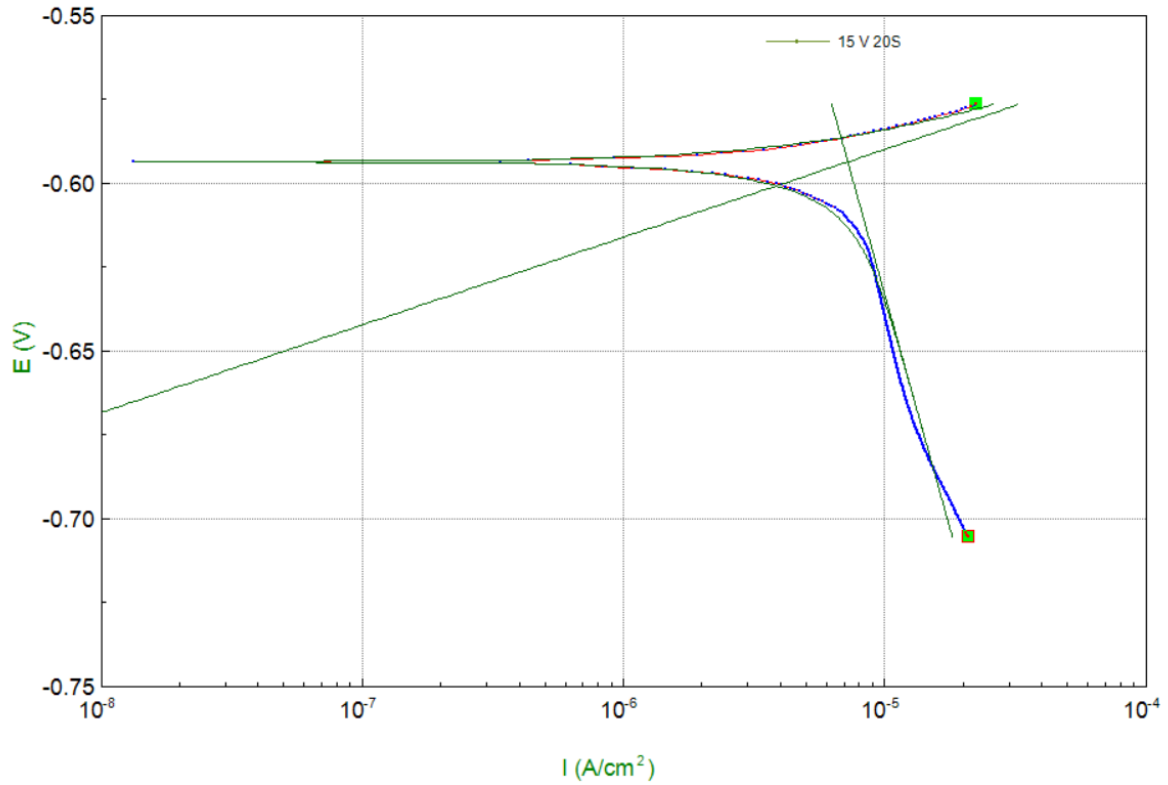
Ketua Laboratorium Material

Yusuf Umardhani, ST., MT

## TEST RESULT

**No : LM-01/15/09/2022**

<b>Customer</b>	Zuhri	<b>Tanggal</b>	Kamis, 29 September 2022
<b>Material</b>	Aluminium 2024	<b>Pengujian</b>	<i>Corrosion Test</i>
<b>Operator</b>	Ruben Sanilo	<b>Standard</b>	ASTM G102



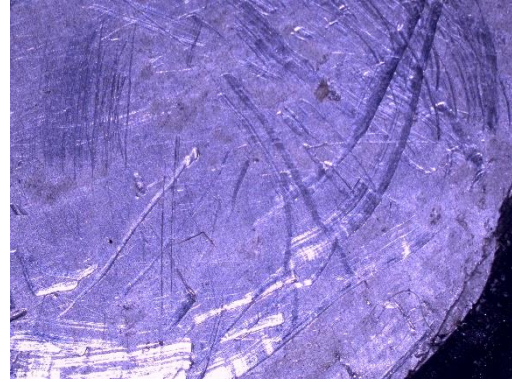
<b>Spesimen</b>	<b>Potensial (mV)</b>	<b>Arus (μA/cm<sup>2</sup>)</b>	<b>Laju Korosi (mmpy)</b>
15 V 20S	593,69	7,2285	0,25409

Laporan ini tidak boleh digandakan sebagian atau seluruhnya  
Laporan pengujian ini hanya berlaku untuk sampel yang diuji

Keterangan :



Spesimen Sebelum Uji Korosi



Spesimen Setelah Uji Korosi

**TIM PENGUJI :**

Penguji 1

Ruben Sanilo

Penguji 2

Andiyanto, ST

**Semarang, 29 September 2022**

Mengetahui

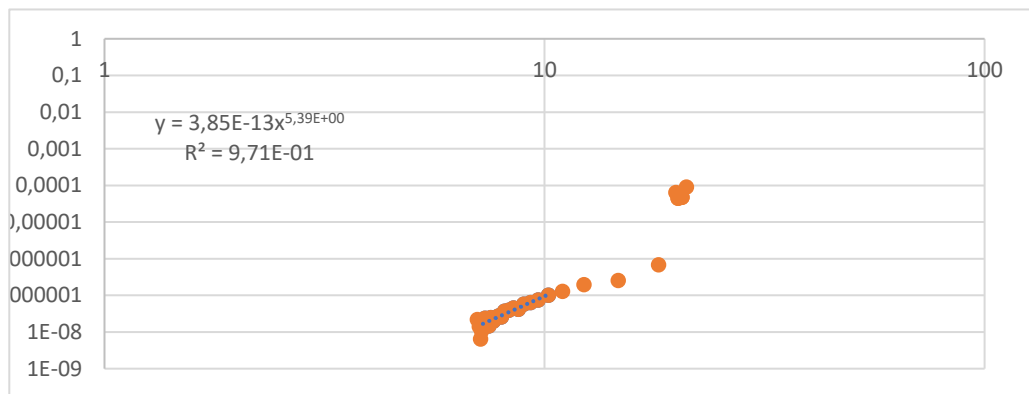
Ketua Laboratorium Material

Yusuf Umardhani, ST., MT

Non Inhibitor

Cycle	crack length (mm)	crack average (mm)	da/dN (secant method) (m/cycles)	t	sec	ft	BW <sup>0.5</sup>	delta K (Mpa.m <sup>1/2</sup> )
0	2,5814636							
2000	2,6254435	2,60345356	2,19899E-08	0,415058	1,25772	0,905308	16,47958	7,0350491
4000	2,653534	2,639488727	1,40452E-08	0,420803	1,266485	0,914723	16,47958	7,1082084
6000	2,66631	2,659921998	6,38805E-09	0,424061	1,271556	0,920093	16,47958	7,1499396
8000	2,6875377	2,676923894	1,06139E-08	0,426771	1,275832	0,924579	16,47958	7,1848035
10000	2,7205106	2,704024193	1,64864E-08	0,431092	1,282755	0,931766	16,47958	7,2406466
12000	2,767458	2,743984298	2,34737E-08	0,437463	1,293212	0,942443	16,47958	7,3236194
14000	2,79721	2,782333997	1,4876E-08	0,443577	1,303532	0,952785	16,47958	7,4039859
16000	2,8262407	2,811725391	1,45154E-08	0,448262	1,311636	0,960777	16,47958	7,4660897
18000	2,8750369	2,850638822	2,43981E-08	0,454466	1,322632	0,971449	16,47958	7,5490239
20000	2,9141332	2,89458506	1,95482E-08	0,461472	1,335429	0,983633	16,47958	7,6437002
22000	2,9624881	2,938310642	2,41774E-08	0,468443	1,348572	0,995899	16,47958	7,739023
24000	3,017155	2,989821534	2,73335E-08	0,476655	1,364604	1,010545	16,47958	7,8528291
26000	3,068087	3,042620996	2,5466E-08	0,485073	1,381679	1,025787	16,47958	7,9712725
28000	3,1416423	3,10486463	3,67776E-08	0,494996	1,402684	1,044073	16,47958	8,113372
30000	3,2203875	3,18101491	3,93726E-08	0,507137	1,429747	1,066945	16,47958	8,2911092
32000	3,3110465	3,265717024	4,53295E-08	0,52064	1,461741	1,093085	16,47958	8,4942411
34000	3,393508	3,352277227	4,12307E-08	0,53444	1,496661	1,120627	16,47958	8,7082687

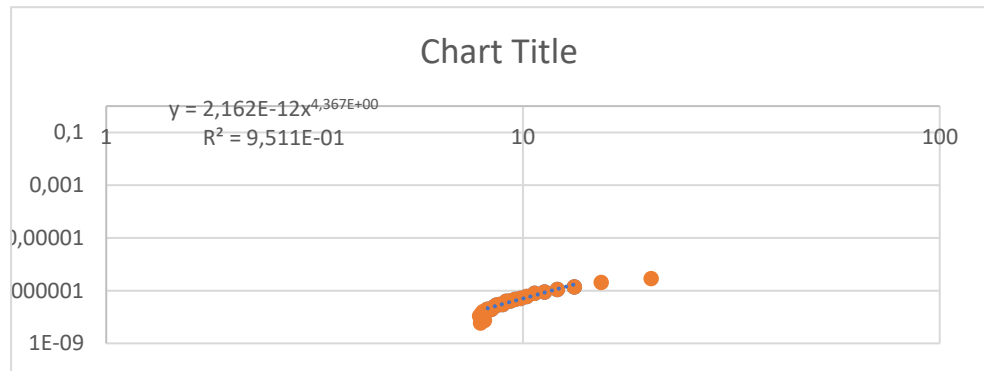
36000	3,5084884	3,45099817	5,74902E-08	0,550179	1,539486	1,153161	16,47958	8,9610817
38000	3,63587	3,572179181	6,36908E-08	0,569498	1,596906	1,194912	16,47958	9,2855247
40000	3,7835374	3,709703711	7,38337E-08	0,591423	1,669427	1,245039	16,47958	9,6750565
42000	3,9842678	3,883902602	1,00365E-07	0,619195	1,77451	1,313418	16,47958	10,206423
44000	4,2401536	4,112210684	1,27943E-07	0,655594	1,940111	1,413125	16,47958	10,981234
46000	4,6297961	4,434974858	1,94821E-07	0,707051	2,249216	1,580122	16,47958	12,278953
48000	5,1382929	4,884044482	2,54248E-07	0,778644	2,929767	1,8925	16,47958	14,706403
48463	5,4509086	5,294600731	6,75196E-07	0,844097	4,113484	2,334807	16,47958	18,143525
48464	5,5085806	5,479744583	5,7672E-05	0,873614	5,05288	2,632565	16,47958	20,45737
48465	5,4603389	5,484459746	-4,8242E-05	0,874366	5,082594	2,64143	16,47958	20,526258
48466	5,5073288	5,483833843	4,69898E-05	0,874266	5,078629	2,640249	16,47958	20,517079
48467	5,4312361	5,469282411	-7,6093E-05	0,871946	4,9882	2,613164	16,47958	20,306602
48468	5,4760538	5,453644948	4,48178E-05	0,869453	4,894615	2,584831	16,47958	20,086434
48469	5,4063695	5,441211666	-6,9684E-05	0,867471	4,822727	2,562853	16,47958	19,915642
48470	5,4702051	5,438287308	6,38356E-05	0,867005	4,806131	2,557752	16,47958	19,876002
48471	5,5606142	5,515409659	9,04091E-05	0,8793	5,286843	2,701572	16,47958	20,993616



## 0,3 % Inhibitor

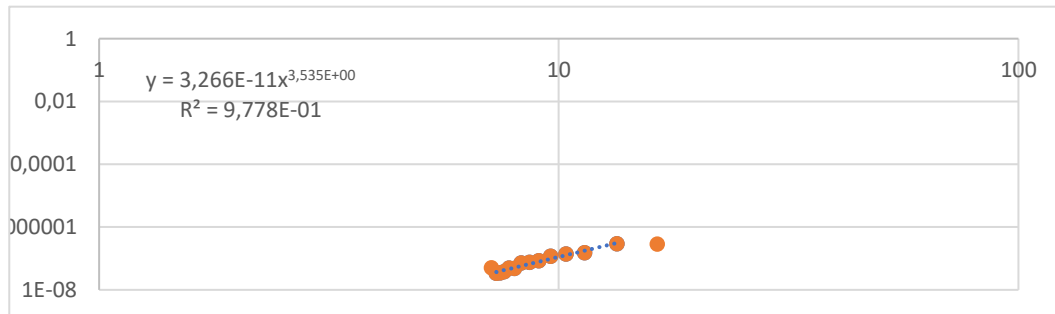
Cycle	crack length (mm)	crack average (mm)	da/dN (secant method) (m/cycles)	t	sec	ft	BW <sup>0.5</sup>	delta K (Mpa.m <sup>1/2</sup> )
0	2,9907778							
2000	3,012676	3,001726926	1,09491E-08	0,478554	1,368397	1,013961	16,47958	7,8793742
4000	3,0244266	3,018551302	5,87525E-09	0,481236	1,373813	1,018808	16,47958	7,9170464
6000	3,0516561	3,038041352	1,36148E-08	0,484343	1,380171	1,024455	16,47958	7,9609247
8000	3,0840751	3,06786561	1,62095E-08	0,489098	1,390081	1,03316	16,47958	8,0285736
10000	3,0988081	3,091441593	7,36652E-09	0,492856	1,398071	1,040099	16,47958	8,0824935
12000	3,1331469	3,115977486	1,71694E-08	0,496768	1,406538	1,047375	16,47958	8,1390362
14000	3,1720957	3,152621259	1,94744E-08	0,50261	1,419475	1,05835	16,47958	8,2243176
16000	3,2095189	3,190807294	1,87116E-08	0,508698	1,433341	1,069928	16,47958	8,3142919
18000	3,2484961	3,22900749	1,94886E-08	0,514788	1,447621	1,081662	16,47958	8,4054714
20000	3,2956382	3,272067107	2,35711E-08	0,521653	1,464224	1,095076	16,47958	8,5097141
22000	3,3525592	3,324098684	2,84605E-08	0,529948	1,485035	1,111565	16,47958	8,6378446
24000	3,412013	3,382286125	2,97269E-08	0,539225	1,509328	1,130385	16,47958	8,7840959
26000	3,4723251	3,442169077	3,0156E-08	0,548771	1,535518	1,150199	16,47958	8,9380698
28000	3,5499776	3,511151371	3,88263E-08	0,559769	1,567283	1,173621	16,47958	9,1200805
30000	3,6318753	3,590926457	4,09488E-08	0,572487	1,606308	1,201565	16,47958	9,3372251
32000	3,7258653	3,678870295	4,6995E-08	0,586508	1,652429	1,233525	16,47958	9,5855887
34000	3,8258144	3,775839878	4,99746E-08	0,601967	1,707443	1,270309	16,47958	9,87143

36000	3,9467405	3,886277499	6,04631E-08	0,619574	1,776058	1,314392	16,47958	10,213995
38000	4,1052792	4,026009891	7,92693E-08	0,641851	1,873354	1,373969	16,47958	10,676956
40000	4,2834304	4,194354832	8,90756E-08	0,668689	2,009212	1,452362	16,47958	11,286144
42000	4,5070845	4,395257466	1,11827E-07	0,700719	2,20516	1,557549	16,47958	12,103538
44000	4,7830515	4,645067984	1,37983E-07	0,740545	2,519504	1,711524	16,47958	13,300063
46000	5,1874624	4,985256913	2,02205E-07	0,79478	3,150547	1,982742	16,47958	15,407669
47974	5,7542046	5,470833503	2,87103E-07	0,872193	4,997682	2,616017	16,47958	20,328775



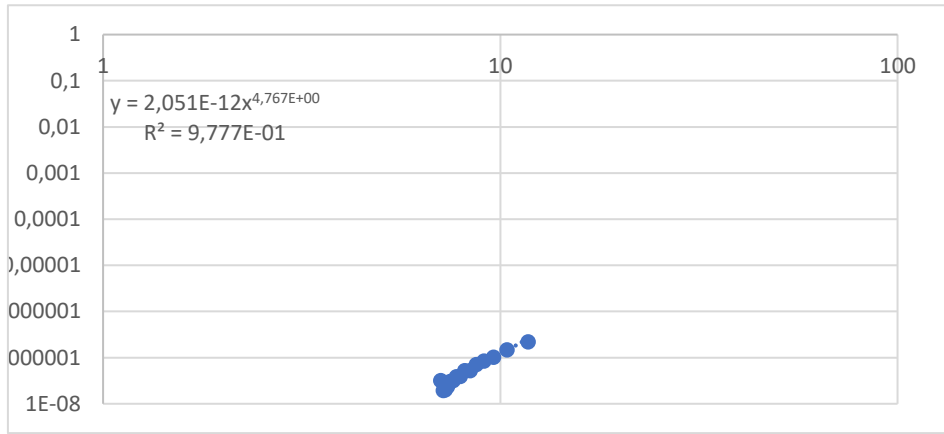
0,5 % Inhibitor

Cycle	crack length (mm)	crack average (mm)	da/dN (secant method) (m/cycles)	t	sec	ft	BW <sup>0.5</sup>	delta K (Mpa.m <sup>1/2</sup> )
0	2,6056							
2000	2,7044753	2,655037647	4,94376E-08	0,423282	1,270337	0,918807	16,47958	7,1399476
4000	2,7718453	2,73816029	3,3685E-08	0,436534	1,291669	0,940881	16,47958	7,3114785
6000	2,8398568	2,80585104	3,40058E-08	0,447326	1,310002	0,959175	16,47958	7,453641
8000	2,915832	2,8778444	3,79876E-08	0,458803	1,330506	0,978975	16,47958	7,6075044
10000	3,0123763	2,96410416	4,82722E-08	0,472555	1,356525	1,003206	16,47958	7,7958006
12000	3,1075414	3,059958878	4,75826E-08	0,487837	1,387433	1,030845	16,47958	8,0105788
14000	3,248324	3,177932733	7,03913E-08	0,506645	1,428621	1,066008	16,47958	8,2838282
16000	3,3982691	3,323296585	7,49726E-08	0,52982	1,484707	1,111308	16,47958	8,6358508
18000	3,5662945	3,482281802	8,40127E-08	0,555166	1,553774	1,163739	16,47958	9,0432823
20000	3,7967658	3,681530142	1,15236E-07	0,586932	1,653878	1,234512	16,47958	9,5932562
22000	4,0687818	3,932773795	1,36008E-07	0,626987	1,807048	1,333717	16,47958	10,364169
24000	4,3712868	4,22003426	1,51252E-07	0,672783	2,032014	1,465045	16,47958	11,384698
26000	4,9477734	4,659530053	2,88243E-07	0,742851	2,54079	1,721412	16,47958	13,376903
27143	5,2725135	5,110143409	2,84112E-07	0,81469	3,476902	2,108833	16,47958	16,387508



0,7% inhibitor

Cycle	crack length (mm)	crack average (mm)	da/dN (secant method) (m/cycles)	t	sec	ft	BW <sup>0.5</sup>	delta K (Mpa.m <sup>1/2</sup> )
0	2,5957							
2000	2,6599761	2,627838031	3,2138E-08	0,418946	1,263627	0,911671	16,47958	7,0844949
4000	2,6992268	2,679601417	1,96254E-08	0,427198	1,27651	0,925288	16,47958	7,1903058
6000	2,7395747	2,719400729	2,0174E-08	0,433543	1,286744	0,935863	16,47958	7,2724838
8000	2,7865909	2,763082777	2,35081E-08	0,440507	1,298316	0,947582	16,47958	7,3635501
10000	2,847466	2,817028411	3,04375E-08	0,449108	1,313116	0,962225	16,47958	7,4773435
12000	2,9117923	2,879629107	3,21632E-08	0,459088	1,331028	0,97947	16,47958	7,6113555
14000	2,989713	2,950752625	3,89604E-08	0,470427	1,35239	0,999417	16,47958	7,766359
16000	3,0683913	3,029052134	3,93391E-08	0,48291	1,377227	1,021847	16,47958	7,9406551
18000	3,1735476	3,120969448	5,25782E-08	0,497564	1,408279	1,048863	16,47958	8,1505945
20000	3,2787801	3,226163841	5,26162E-08	0,514335	1,446543	1,080783	16,47958	8,3986425
22000	3,4206888	3,34973443	7,09544E-08	0,534035	1,495601	1,119805	16,47958	8,7018831
24000	3,5909729	3,505830835	8,5142E-08	0,558921	1,56477	1,171791	16,47958	9,1058578
26000	3,7953667	3,693169808	1,02197E-07	0,588788	1,660257	1,238844	16,47958	9,626921
28000	4,0920242	3,943695464	1,48329E-07	0,628728	1,814521	1,338327	16,47958	10,399987
30000	4,5346998	4,313361996	2,21338E-07	0,687662	2,120195	1,512953	16,47958	11,756986
31908	4,751104	4,642901908	1,13419E-07	0,7402	2,516349	1,710054	16,47958	13,288635





# CERTIFICATE OF PRESENTER

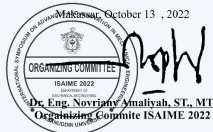
The certificate presented to:

**Muhammad Zuchry M**

Has participated with a paper entitled

**The Effect Sealing of BSAA (Boric Sulfur Acid Anodizing)  
on Roughness and Corrosion Rate Alumimium Alloys 2024**

*At The International Symposium on Advance and Innovation in Mechanical Engineering (ISAIME) 2022*  
held on October 13 , 2022 by Mechanical Engineering Departement of Universitas Hasanuddin in collaboration with  
Badan Kerja Sama Teknik Mesin Indonesia ( BKS-TM Indonesia)



The utilization of metal materials finds widespread applications in various industries, including the aircraft industry, where aluminum alloys are commonly employed. However, metal materials are prone to corrosion under specific conditions, necessitating the implementation of corrosion prevention methods to decelerate the material's corrosion rate. Corrosion is a process in which the quality of metal deteriorates due to environmental influences. An effective approach to inhibit corrosion is through anodizing, which involves applying a protective coating to the metal surface, preventing direct contact with the surrounding environment. In this research, the focus was on studying the corrosion rate of aluminum alloy 2024 using Boric Sulfate Acid Anodizing (BSAA) at 10 volts and immersion times of 10, 15, and 20 minutes, followed by sealing with acetic acid in a corrosive environment containing 3.5 % NaCl. The main goals were to evaluate the effectiveness of anodizing with and without sealing in lowering the rate of aluminum corrosion, to compare the effectiveness of anodizing with and without sealing, and to create adsorption models using Langmuir adsorption. Through the examination of the potentiodynamic approach, it was shown that anodizing had an inhibitory impact that was strengthened by sealing. The maximum efficiency of 76 % was attained after 20 minutes of anodizing and sealing at 10 volts. A correlation value of 0.7487 from the Langmuir adsorption modeling was also obtained, pointing to an advantageous adsorption behavior. This research demonstrates how effectively anodizing for aluminum alloy 2024 works with and without sealing, especially in a 3.5 % NaCl-corrosive environment

**Keywords:** Langmuir adsorption, aluminum alloy, acetic acid, inhibition efficiency, surface coverage

# EFFECT OF ANODIZING ON ALUMINUM ALLOY 2024 WITH BORIC SULFATE ACID IN MEDIUM 3.5 % NaCl

**Muhammad Zuchry**

Doctoral Student, Graduate Student\*

**Ilyas Renreng**

Corresponding Author

Doctorate, Professor\*

E-mail: ilyas.renreng@gmail.com

**Hairul Arsyad**

Doctorate, Assistant Professor\*

**Lukmanul Hakim Arma**

Doctorate, Assistant Professor\*

\*Department of Mechanical Engineering

Hasanuddin University

Malino str., Bontomarannu District, Gowa Regency, South Sulawesi, Indonesia, 92171

Received date 25.05.2023

Accepted date 15.08.2023

Published date 30.08.2023

**How to Cite:** Zuchry, M., Renreng, I., Arsyad, H., Arma, L. H. (2023). Effect of anodizing on aluminum alloy 2024 with boric sulfate acid in medium 3.5 % NaCl. *Eastern-European Journal of Enterprise Technologies*, 4 (6 (124)), 35–44. doi: <https://doi.org/10.15587/1729-4061.2023.286351>

## 1. Introduction

Aluminum AA2024 is widely used in various industries due to its excellent strength-to-weight ratio and high fatigue resistance. However, one of its major drawbacks is its susceptibility to corrosion, especially in corrosive environments such as saline solutions [1]. Corrosion can significantly compromise the structural integrity and performance of aluminum AA2024, leading to substantial economic losses and safety concerns. Researchers have explored various surface treatment techniques to mitigate the corrosion issue to enhance the material's resistance to corrosion. One promising approach is boric sulfate acid anodizing, which involves the electrochemical oxidation of the aluminum surface in a solution containing boric acid and sulfate ions [2].

Aluminum Alloy 2024 (AA2024) benefits significantly from surface treatments such as anodizing and sealing [3, 4]. The exceptional strength-to-weight ratio and strong fatigue resistance [4] of AA2024 make it a popular choice in various industries, including aerospace, automotive, and construction. However, corrosion may weaken AA2024's structure and

enhanced corrosion resistance and may be refined for further aesthetic or functional applications.

Corrosion is a multifaceted and persistent phenomenon that exposes metals' susceptibility to their environment's dynamic influences. The durability of metals is constantly tested by the relentless assaults orchestrated by the elements, resulting in a silent yet profound battle. The metal oxidation process initiates as metals react with the surrounding atmosphere, particularly with elements like oxygen, marking the beginning of a complex interaction. Water, a seemingly ordinary substance, plays a significant role in promoting chemical reactions and facilitating the movement of ions. This creates conditions that are highly conducive to corrosion [7].

Sealing is a subsequent step often performed after anodizing to enhance corrosion resistance and improve the durability of the anodized surface. Sealing involves the closure of the pores present in the anodized oxide layer, making it more resistant to penetration by corrosive agents. Common sealing methods include hot water sealing, chromate conversion coating, or proprietary sealing solutions [8, 9]. The choice of

against corrosive environments, ensuring the longevity and reliability of the aluminum alloy.

Boric sulfate acid anodizing has drawn interest as a potential strategy for slowing the rate of corrosion of aluminum AA2024. This procedure creates a shield between the alloy's surface and the corrosive environment in the form of a protective oxide layer. The material's mechanical characteristics and corrosion resistance are both improved by the anodized coating. There are various benefits to using boric sulfate acid as an anodizing electrolyte [10]. Boric acid provides buffering properties, maintaining a stable pH during the anodizing process. The presence of sulfate ions aids in the formation of a dense and adherent oxide layer. Additionally, this process can be performed at relatively low temperatures and with adjustable parameters, allowing for control over the resulting oxide layer's thickness and morphology [11, 12].

Boric sulfate acid's anodizing process may be modified to produce the required coating thicknesses and surface properties by modifying parameters such as voltage, current density, and anodizing duration [13, 14]. This allows for a greater degree of control over the final product. Because of this versatility, optimizing the anodizing process to meet specific performance criteria and achieve the required results is possible. In both scientific and commercial contexts, the boric sulfate acid anodizing AA2024 approach has garnered much interest. Numerous researches have been conducted to study the effect that anodizing parameters, surface preparation processes, and post-treatment techniques have on the overall performance of AA2024 and its corrosion resistance. According to the results [14, 15], boric sulfate acid anodizing is a successful method for lowering the corrosion rate, improving surface characteristics, and extending the amount of time AA2024 may remain in operation in settings where corrosion is present.

Current research is being conducted to explore the application of the anodizing method for surface coating in various studies. One of the objectives is to possess resistance against corrosion. Aluminum is a highly utilized material in multiple industries. The aluminum material tends to rust quickly. Therefore, it is crucial to implement a suitable coating method to protect it. Anodizing is commonly employed for applying a protective coating to aluminum materials. Different solutions are used to identify the most appropriate coating solution for aluminum. Therefore, studies devoted to developing anodizing methods for coating aluminum are relevant.

---

## 2. Literature review and problem statement

---

Numerous investigations have examined various methodologies for surface treatment aimed at mitigating the corrosion rate of Aluminum Alloy 2024 (AA2024) owing to its inherent vulnerability to corrosion. One approach that has been receiving increasing interest is Boric Sulfate Acid Anodizing. This process includes the deliberate electrochemical oxidation of the aluminum surface in an electrolyte solution that contains boric acid and sulfate ions [13, 16].

This study only used a small sample size, and data on how easily these results may be replicated is lacking. The reliability of the research might be improved with a bigger sample size and by regularly repeating the studies. The process's potential uses are limited because sulfuric acid electrolyte with organic additions is required. Increasing the anodization method's adaptability would need investigating its compatibility with alternative electrolytes or process changes.

The study conducted in the paper [13] examines the influence of the sealing process on the corrosion resistance of AA2024 aluminum alloy. The research utilizes a suitable methodology involving anodizing with boric sulfuric acid, sealing the specimens, and performing corrosion resistance tests. The study uses corrosion resistance tests, and precise weight loss measurements, to objectively evaluate the efficacy of the sealing process. The purpose of these tests is to gather quantitative data that can be used to evaluate the effectiveness of the corrosion protection provided by the anodized aluminum. The article does not thoroughly analyze the underlying mechanisms involved in the sealing process and its impact on improving the corrosion resistance of anodized aluminum. The report lacks information regarding the sample size utilized in the study, which hinders the ability to assess the statistical significance of the findings. Additionally, there is limited data on the variability of the results, making it difficult to determine the reliability and generalizability of the study's conclusions. The article lacks a comparison of the corrosion resistance of the sealing process with other commonly used corrosion protection techniques, such as different sealing agents or alternative surface treatments.

The research [18] investigated the anti-corrosion capabilities of organic-based sealants on anodized AA2024T3 metal. Organic-based sealing is compared with more traditional techniques of corrosion prevention. The potential of organic-based species as a replacement corrosion prevention method may be gauged by comparing their performance to conventional methods. There is a lack of statistical analysis to determine the significance of the data, and the article does not give information regarding the sample size utilized in the research. The validity and applicability of the results might improve with a bigger sample size and proper statistical testing. To what extent employing organic species for sealing affects the environment or is sustainable is not investigated. The study's significance would be increased if it included the environmental effects of the sealing procedure.

The paper [6] examines using a sulfuric acid-free solution for hard anodizing, which offers a distinct and unconventional alternative to the commonly used sulfuric acid-based anodizing method. The potential outcome of this could be the identification and development of novel corrosion protection methods that are both effective and environmentally sustainable. The article compares the corrosion resistance between AA2024 and hard anodizing in a sulfuric acid-free solution, as opposed to the more commonly used sulfuric acid-based anodizing method. The comparative analysis offers valuable insights into the potential benefits and drawbacks of the innovative approach. The article's exclusive focus on aluminum alloy AA2024 may restrict the applicability of the

The article [19] comprehensively analyzes the current literature on anodizing aerospace aluminum alloys for corrosion protection. The review offers an in-depth analysis of aerospace aluminum alloys, focusing on the impact of anodizing techniques on different materials frequently employed in the aerospace sector. The review primarily examines the effectiveness of anodized aerospace aluminum alloys in preventing corrosion. The review lacks a direct comparison of the efficacy of various anodizing methods and fails to analyze their respective advantages and disadvantages thoroughly. A comparative analysis can provide readers with a better understanding of the most suitable techniques for specific aerospace applications. The article lacks an in-depth analysis of the environmental consequences of different anodizing techniques.

Despite the shown effectiveness of boric sulfate acid anodizing in reducing the susceptibility of Aluminum AA2024 to corrosion, there are still unresolved issues that need remediation. The existing body of research primarily investigates the impact of anodizing and the subsequent buildup of the oxide layer on the corrosion resistance properties. However, more investigation is required to ascertain the durability and longevity of anodized coatings in varying conditions and over extended periods. Further research is needed to determine the influence of other variables, including surface preparation methodologies, post-treatment procedures, and alloying elements' impact on the corrosion behavior of boric sulfate acid anodized AA2024. In order to optimize the efficacy of the anodizing process and ensure the long-term durability of the rust-resistant properties conferred by anodized coatings, it is necessary to possess a comprehensive understanding of the following factors.

All this allows to assert that it is expedient to conduct a study on anodizing AA2024 using boric acid sulfate in 3.5 % sodium chloride. Anodizing is done to aluminum in order to strengthen its resistance to corrosion, which is one of the aims of the process. A thin coating of oxide can be produced by the anodizing process and applied to the surface of the material. When applied to aluminum material, the anodizing process, as opposed to the coating process, is the more suited option. Finding the appropriate solution to apply throughout the anodizing process and the sealing step might be difficult because of this. All of this provides us with the opportunity to underline how important it is to undertake research to evaluate the effect of anodizing using boric acid sulfate on AA2024 when it is immersed in 3.5 % NaCl medium.

---

### 3. The aim and objectives of the study

---

The aim of the study is to identifying the influence of boric sulfuric acid anodizing (BSAA) in a 3.5 % NaCl environment on corrosion resistance of AA2024.

To achieve this aim, the following objectives are accomplished:

– to investigate the impact of boric sulfate acid anodizing with sealing on the corrosion rate of AA2024 in a 3.5

---

## 4. Materials and methods of research

---

### 4. 1. Object and hypothesis of the study

The object of this study is corrosion resistance of AA2024 aluminum alloy inside a corrosive environment, including a 3.5 % sodium chloride (NaCl) solution. The subobject of this study the effects of anodization, especially using boric sulfate acid, on the corrosion resistance of alloys when subjected to a salty environment. This study examines the correlation between several anodization factors, such as voltage, anodizing time, the sealing technique, and the resultant corrosion resistance of the alloy. Furthermore, the study aims to employ scanning electron microscopy (SEM) to investigate the surface features and properties of the anodized surfaces. This will contribute to a deeper comprehension of changes in surface structure and the creation of oxide layers.

The study's primary hypothesis is that boric sulfate acid anodization increases aluminum alloy 2024's corrosion resistance in a 3.5 % sodium chloride environment. The idea states that anodization forms an oxide coating on the alloy's surface, minimizing corrosion and improving seawater resilience. Boric sulfate acid anodization creates a stable and effective oxide coating on aluminum alloy. This oxide layer will protect the material against NaCl corrosion. A sealing technique following anodization improves alloy corrosion resistance. The sealing procedure is anticipated to plug oxide layer pores and fissures, increasing its density and impermeability and preventing corrosion. The hypothesis predicts that Langmuir adsorption modeling will show a positive association between corrosion inhibition and anodized surface adsorption. A more significant correlation coefficient indicates a stronger association between the anodized layer's corrosion-inhibiting characteristics.

The study may have relied on numerous assumptions to inform the research methodology and the interpretation of findings. The analysis assumes that the aluminum alloy 2024 employed in the trials had a uniform and homogenous composition devoid of notable fluctuations in alloying components that might potentially impact the anodization process or corrosion characteristics. The research may assume that the corrosion conditions in the 3.5 % NaCl medium are in a state of equilibrium, hence enabling accurate and consistent measurements of corrosion rates within the designated periods. The study posits that the sealing procedure has the potential to efficiently occlude the pores and fissures present in the oxide layer, hence augmenting its protective characteristics without inducing any harmful consequences. The study may posit that extraneous variables or impurities that have the potential to influence the anodization process or corrosion characteristics are mitigated or regulated throughout the experimental procedures.

The research study may have employed various simplifications to streamline the experimental procedures and improve data processing. The investigation might simplify the alloy composition analysis by exclusively considering AA2024, disregarding any composition discrepancies across various alloy batches. The research may assume idealized

### 4. 2. Material

The 12 mm in diameter, 3 mm thick aluminum alloy AA2024 was the primary focus of the investigation. The anodizing procedure was carried out at a controlled temperature of between 27 and 29 degrees Celsius and a steady voltage of 10 V. The anodizing electrolyte was a solution of 45 gr/l sulfuric acid and 8 g/l boric acid, known as boric sulfuric acid anodizing (BSAA).

The anode and cathode were kept at a constant distance of 5 cm apart during the anodizing procedure. Both 10 and 15 minutes were allotted for the anodizing process. The roughness of the surface and the rate of corrosion after anodizing were two of the primary mechanical properties studied. The anodized layer's protective qualities were then improved by an additional sealing procedure. 0.5 % silicon and iron, 3.9 % copper, 0.6 % manganese, 1.5 % magnesium and titanium, 0.25 % zinc, 0.1 % chromium, and the rest 92.5 % was aluminum (in wt %) made up the AA2024 aluminum alloy utilized in the research.

To establish the basic metal's mechanical strength, its tensile strength was also assessed. The highest tensile stress ( $T_{max}$ ) measured during the tensile test was 463 MPa, the yield stress ( $Y_{max}$ ) was 360 MPa, and the elongation (E) measured at 17.8 %. These values fell within the acceptable ranges outlined in AA2024.

### 4. 3. Anodizing and sealing process

Aluminum alloy AA2024 with a diameter of 12 mm and a thickness of 3 mm was used in the testing setup. At a temperature of 27 °C, anodizing was carried out at a constant voltage of 10 V for periods of 10, 15, and 20 minutes. The BSAA electrolyte, which was composed of a combination of 45 gr/l sulfuric acid and 8 gr/l boric acid, served as the experiment's primary controlled variable. The cathode and anode were placed five centimeters apart from one another. The electrolyte mixture ratio for aluminum anodizing typically falls within the range of 30.5 to 52.0 g/l sulfuric acid and 5.2 to 10.7 g/l boric acid. However, the focus of this investigation was on employing a 45 g/l sulfuric acid/eight g/l combination [6].

The repair sequence before anodizing involved several steps. It began with degreasing and cleaning using a 10 gr/l sodium hydroxide (NaOH) solution, followed by rinsing with reverse osmosis (RO) water. Subsequently, etching was carried out using a caustic soda solution with a concentration of 100 gr/l, followed by rinsing. After that, desmutting was carried out for two minutes at a temperature between 27 and 32 degrees Celsius using a solution made up of 75 % phosphoric acid ( $H_3PO_4$ ), 15 % sulfuric acid ( $H_2SO_4$ ), and 10 % acetic acid ( $CH_3COOH$ ). After washing, an electrolyte solution containing 45 gr/l sulfuric acid and 8 gr/l boric acid was used to carry out the anodizing procedure. The sealing process was then completed using a 50 gr/l solution of acetic acid ( $CH_3COOH$ ). Fig. 1

process. Both sulfuric acid (45 gr/l) and boric acid (8 gr/l) were used in the electrolyte. The anodizing process was carried out at a constant 10 volts for 10, 15, and 20 minutes. In this configuration, one specimen (made of the aluminum alloy AA2024) was used as the anode (+) and the other as the cathode (-). The voltage source for the anodizing process was established by connecting the cathode to the power supply.

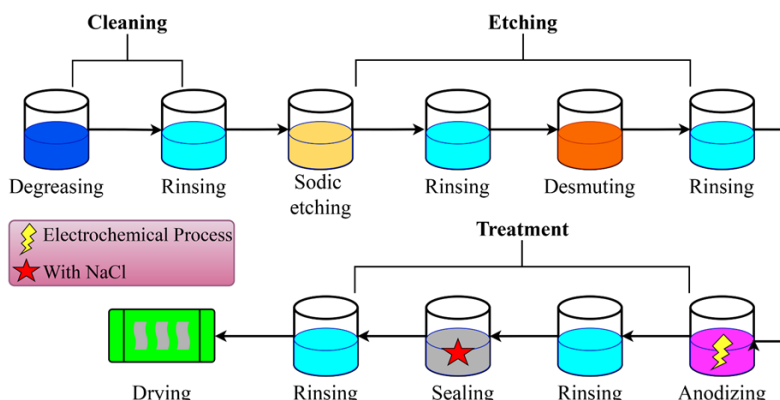


Fig. 1. Preparation scheme for anodizing process

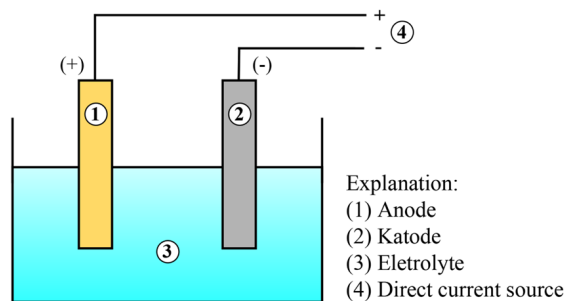


Fig. 2. Diagrammatic representation of the anodizing apparatus [1]

### 4. 4. Weight loss measurement

The experiment on weight loss adhered to the approach that was used, in which aluminum coupons were made and totally suspended in 1.4 M  $HNO_3$  solutions, either with or without varying doses of Anisaldehyde. Glass hooks were utilized to suspend the coupons at a temperature of 308 K for 3 hours. The solution volume was maintained at 100  $cm^3$ . After the 3-hour immersion period, the coupons were retrieved, rinsed with distilled water, thoroughly dried, and reweighed. The corrosion rate in  $mg/cm^2$  was then calculated based on the weight loss data obtained. The weight loss and corrosion rate of aluminum in the 1.4 M  $HNO_3$  solution were determined for the solution without Anisaldehyde and the solutions with concentrations of 0.02, 0.04, 0.06, 0.08, and 0.10 M of Anisaldehyde. These calculations were performed using the provided equation, utilizing the weight loss data obtained. (1) shows the estimate of weight loss during the anodization process [19]:

$$\text{Weight loss } (\Delta W) = W_0 - W_i \tag{1}$$

The inhibition efficiency (I.E.) is calculated using the (3) [19]:

$$\text{Inhibition efficiency} = ((W_o - W_i) / W_o) \times 100 \%, \quad (3)$$

where  $W_o$  represents the initial weight of the specimen before immersion, and  $W_i$  represents the weight of the specimen after immersion in the acidic media.

The inhibition efficiency is expressed as a percentage and represents the inhibitor's effectiveness in reducing the specimen's weight loss. These equations provide a quantitative assessment of the degree of surface coverage and the inhibitor's effectiveness in protecting the specimen against corrosion in acidic environments.

#### 4. 5. Scanning electron microscopic analysis

The surface of the aluminum sample was analyzed using a scanning electron microscope (SEM), specifically the FEI In-spect F50, to determine the thickness of the oxide layer formed after the anodization process. The SEM analysis was also conducted on aluminum samples that had undergone the sealing process. The SEM test was performed at a magnification of 20  $\mu\text{m}$ , allowing for detailed examination and measurement of the oxide layer thickness. This characterization technique provides valuable insights into the structural and morphological properties of the anodized aluminum surfaces, aiding in evaluating the effectiveness of the anodization and sealing processes.

### 5. Results of the experiment using AA2024 anodized in boric sulfuric acid in a 3.5 % NaCl environment

#### 5. 1. Corrosion rate on AA2024 in 3.5 % NaCl environment

Using the Boric Acid and Sulfuric Acid (BASA) approach, an essential quantitative examination of AA2024 was the measurement of the corrosion rate. The corrosion rate of diverse samples, including raw, unsealed, and sealed materials, is evaluated by this measurement. Additionally, the length of the anodizing procedure affects how quickly the material corrodes. The corrosion rate seen at a 10-volt anodizing voltage is shown in Fig. 3. This graphic gives a visual depiction of the data on corrosion rates and provides insightful information about how anodizing settings affect the corrosion resistance of the material.

Based on the obtained results, it is evident that incorporating a sealing process following anodization significantly reduces the corrosion rate across different anodizing time variations. The average corrosion rates for each variation were below 0.6 mmpy, indicating improved corrosion resistance. The corrosion rate actually lowered by up to 15 % after applying the sealing technique for a 10-minute anodizing period. Similar to this, after sealing, the corrosion rates for anodizing times of 15 and 20 minutes fell by 11 % and 0.2 %, respectively.

It is also interesting that, regardless of whether the samples were sealed or left unsealed, the direct anodization period alone helped to lower the corrosion rate. Unsealed samples saw a 47 % reduction in corrosion rate from their initial state. The corrosion rate was reduced by 45 % in the unsealed samples, compared to 45 % in the sealed samples. These results show how the sealing procedure and the anodization period work together to reduce corrosion and increase the durability of the aluminum samples.

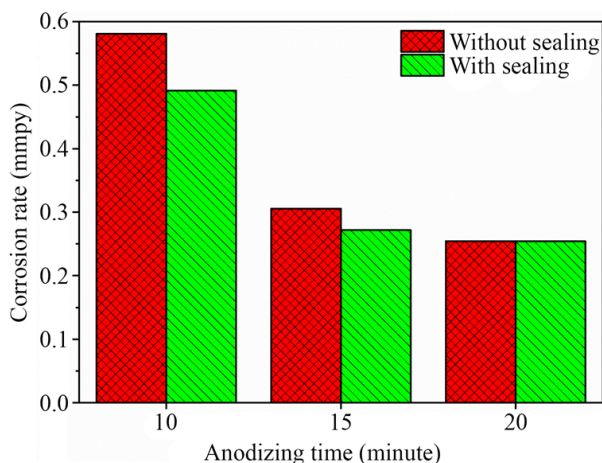


Fig. 3. Corrosion rate on anodized specimens

#### 5. 2. Inhibition efficiency on AA2024 in 3.5 % NaCl environment

The inhibition efficiency of AA2024 in a 3.5 % NaCl environment was evaluated, and the results showed significant corrosion protection. The inhibition efficiency, calculated based on weight loss measurements and other corrosion-related parameters, indicated that the surface treatment, most likely anodizing, effectively reduced the corrosion rate of AA2024 in the aggressive NaCl environment. The inhibition efficiency values obtained demonstrated that the treated AA2024 specimens exhibited improved resistance against corrosion when exposed to the 3.5 % NaCl solution compared to untreated samples (Fig. 4).

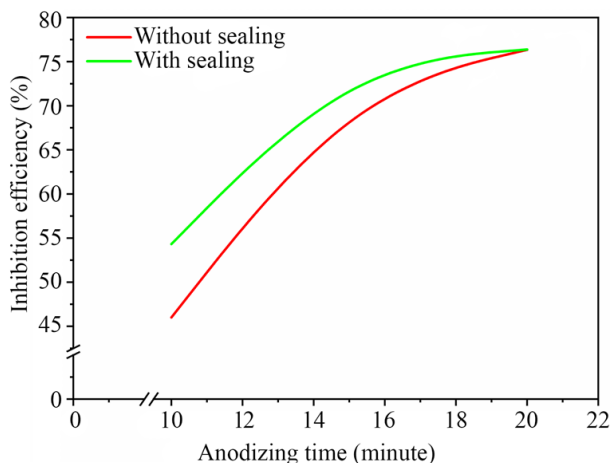


Fig. 4. The inhibition efficiency observed in anodized specimens

When examining the inhibition efficiency, a noticeable trend emerges, indicating that the efficiency increases after the sealing process is applied to the specimens. Moreover, as the anodizing time is extended, the efficiency demonstrates a positive correlation, showing a progressive improvement. The results indicate that up to a 20-minute anodizing time, the inhibition efficiency of specimens with sealing is nearly equivalent to that of samples without sealing.

The similarity in inhibition efficiency between sealed and unsealed specimens for up to 20 minutes may suggest that the anodizing process provides significant corrosion

protection. However, it is essential to note that the sealing process still contributes to enhancing the overall effectiveness of the surface treatment technique, providing additional durability and extended service life, especially in more challenging corrosive environments.

The surface coverage results on AA2024 in the 3.5 % NaCl environment demonstrate a significant improvement after the sealing process illustrated in Fig. 5. The data indicates that the specimens' surface coverage increases following the sealing step's application. As the anodizing time is extended, the surface coverage also significantly increases. Up to 20 minutes of anodizing time, the surface coverage of specimens without sealing and those with sealing show a similar trend, with both achieving substantial coverage.

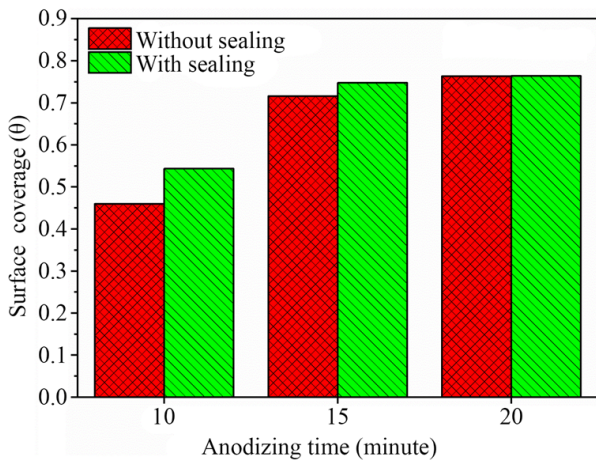


Fig. 5. The extent of surface coverage observed in anodized specimens

The surface coverage percentage rose when comparing the samples without sealing to those with the sealing process at anodizing durations of 10 minutes, 15 minutes, and 20 minutes, with increases of 18 %, 4 %, and 0.05 %, respectively. These findings suggest that the length of the anodizing time impacts the surface coverage of aluminum. Moreover, implementing a sealing process after anodizing can further enhance the surface coverage on the aluminum surface layer. In summary, both the anodizing time and the sealing process play vital roles in improving the aluminum material's surface coverage and protective properties.

Fig. 6 presents the outcomes of the Langmuir adsorption modeling, illustrating a comparison between specimens without and those with sealing. Since the adsorption process is chemical, it has been appropriately modeled using the Langmuir adsorption method. This modeling approach provides a comprehensive understanding of the adsorption behavior and valuable insights into the interaction between the inhibitors and the aluminum surface during the sealing process. By utilizing Langmuir adsorption modeling, researchers gain valuable information about the adsorption capacity and affinity of the inhibitors, further contributing to the understanding of the corrosion protection mechanisms and the effectiveness of the sealing process in enhancing the surface properties of the aluminum alloy.

The R2 values for each material under different types of isothermal adsorption conditions were obtained by analyzing the two curves presented above. The R<sup>2</sup> value represents the coefficient of determination, providing insights into the influence of the independent variable (X) on the dependent

variable (Y). Ranging from 0 to 1, a value closer to 1 indicates a stronger influence of the independent variable on the dependent variable and vice versa. In this case, the correlation coefficient results for specimens without seals and specimens with seals were found to be 0.6526 and 0.7487, respectively.

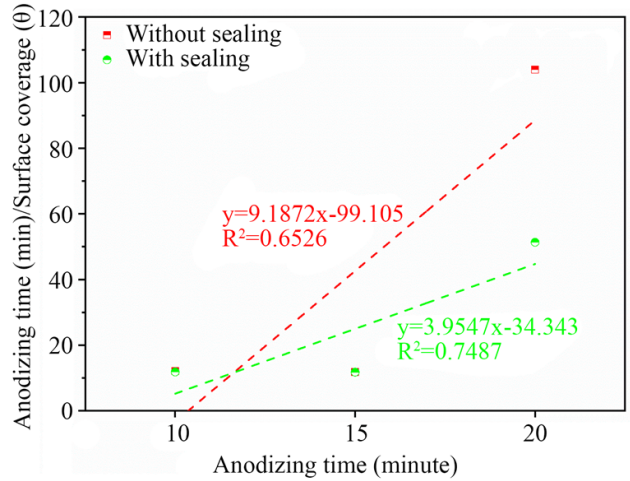


Fig. 6. The results of Langmuir adsorption modeling

The analysis of electrochemical polarization provides vital insights into the system's behavior, and these discoveries are well depicted by the Tafel curve plot illustrated in Fig. 7. The described plot functions as a graphical illustration of the correlation between current density and electrode potential. Our study focuses on two unique groups of specimens subjected to an anodizing voltage of 10 volts: one group undergoes the anodizing procedure without subsequent sealing, while the other group is sealed after anodization. The implementation of distinct treatment methods enables us to investigate the influence of sealing on the electrochemical properties of the specimens.

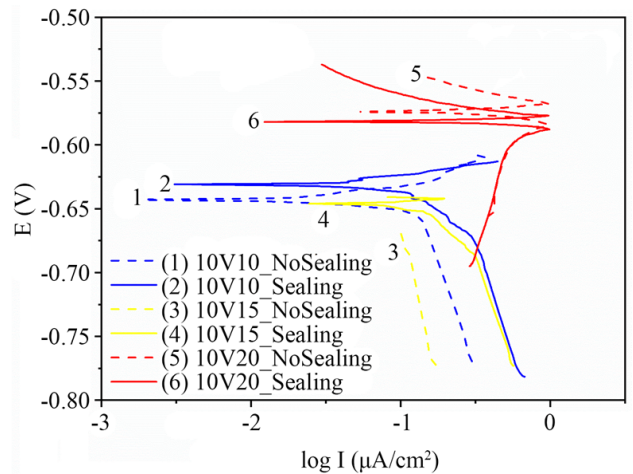


Fig. 7. The polarization curves obtained at an anodizing voltage of 10 volts

The sealed specimens demonstrate a significant increase in potential compared to the non-sealed counterparts. The observed divergence in the electrochemical behavior of the samples indicates that the sealing process has a noticeable impact on their performance. Furthermore, it is crucial

to emphasize that the corrosion potential increases as the duration of anodizing is extended. The observed correlation highlights the complex connection between the time of anodization and the changes in corrosion properties. The Tafel curve plot is a valuable tool for analyzing the relationship between anodization parameters and the electrochemical responses of aluminum alloy specimens. It visually represents these trends, providing a clear understanding of how different parameters affect the overall behavior of the samples. The visual representation enhances our comprehension of the corrosion protection mechanisms facilitated by anodization and sealing processes.

**5. 3. Thickness of anodizing and scanning electron microscopic analysis on AA2024 in 3.5 % NaCl environment**

Both specimens with and without sealing were used in the study of the thickness of the oxide layer after anodization, as shown in Fig. 8. On the aluminum's surface, the oxide layer's thickness was measured in five different places. It is crucial to remember that varied anodizing durations result in differing oxide layer thicknesses, which have a big impact on how resistant to corrosion aluminum is.

The oxide layer's thickness is a crucial determinant of the aluminum alloy's corrosion protection capabilities. A thicker oxide layer generally enhances the material's resistance to corrosion, as it acts as a more robust barrier against the detrimental effects of the surrounding environment. Consequently, anodizing processes with longer durations are expected to yield thicker oxide layers, thereby improving corrosion resistance for the aluminum material.

However, the presence of a sealing procedure following anodization might also affect how thick the oxide layer is. As a result of the sealing procedure, the oxide layer's holes and fissures are sealed off, increasing its density and boosting its protective qualities. As a result, the oxide layer on the surface of the aluminum becomes thicker and more impermeable, increasing its ability to resist corrosion. The average thickness of the oxide layer produced by the anodizing process is shown in Fig. 9. The results show that specimens without sealing have an oxide layer that is thicker than specimens with sealing. The length of the anodizing process also has a considerable impact on how thick the oxide layer is. The oxide layer thickens with longer anodizing times.

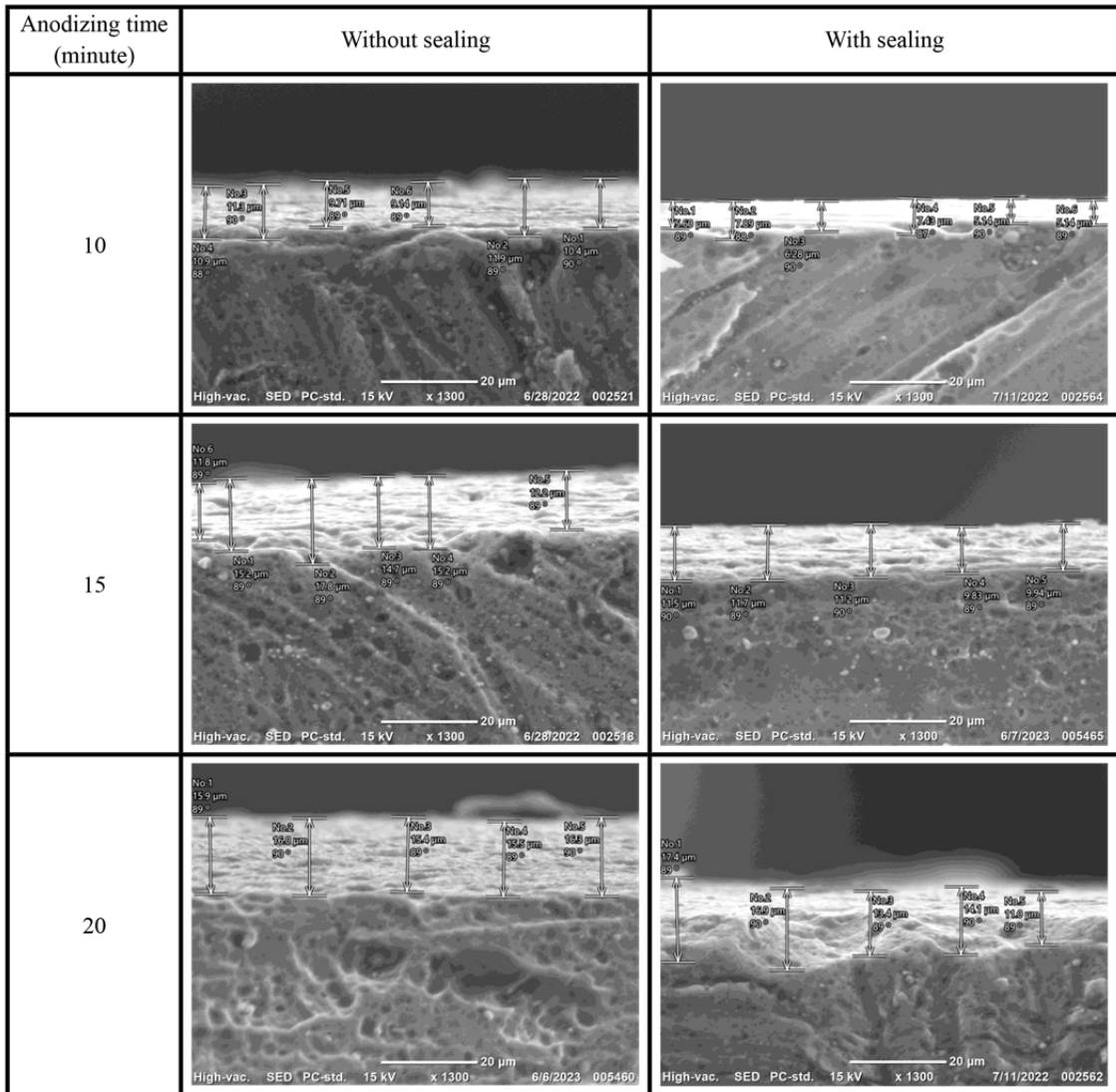


Fig. 8. The scanning electron microscopic image of the aluminum surface following the anodizing process

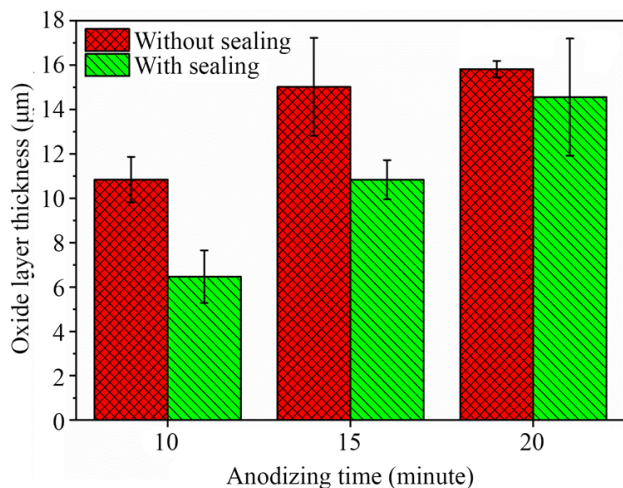


Fig. 9. The average thickness of the oxide layer for each anodization parameter

The thickness of the oxide layer observed in both specimens remains below 16 μm, indicating that the anodization process does not lead to excessively thick coatings. Instead, the oxide layer formed is within a controlled and desirable range for optimal corrosion protection. For specimens without the sealing process, the oxide layer experienced an increase of up to 46 % when subjected to an anodizing time of 20 minutes. On the other hand, specimens with the sealing process exhibited a more substantial increase of up to 125 % in the oxide layer thickness at the same anodizing time of 20 minutes.

## 6. Discussion of the experiment that involved anodizing AA2024 in a 3.5 % NaCl environment using boric sulfuric acid

The corrosion rates measured for different anodizing durations were consistently below 0.6 mmpy on average. This suggests that the specimens with varying anodizing times exhibited a greater resistance to corrosion compared to the unsealed specimens, as shown in Fig. 3. The study demonstrated that longer periods of anodizing result in more significant reductions in corrosion rates. This suggests that the sealing process becomes increasingly important as the duration of anodizing increases. The primary finding of this study indicates that the incorporation of a sealing process following anodization leads to a significant decrease in the corrosion rate observed in aluminum samples. The sealing method is an effective way to protect aluminum from corrosion. It creates a barrier that prevents direct contact between the aluminum and corrosive substances in the environment [8]. The investigation highlights that the effectiveness of the sealing procedure is influenced by the timing of anodization [13]. The correlation between the duration of anodizing and the subsequent decrease in corrosion rate becomes more evident as the duration of anodizing is increased, especially after the sealing procedure is applied. The discovery highlights the importance of modifying the duration of anodization in order to achieve the desired level of corrosion resistance that is suitable for specific applications.

The sealing procedure was successful in closing all of the holes that were present inside the anodized oxide layer,

which led to an increase in the inhibition efficiency once sealing was completed. As a direct result of this, the protective properties of the coating have been improved, which has led to an increase in its resistance to corrosive substances. As a result, sealing is of the highest significance to give greater corrosion resistance to the treated specimens, particularly in situations where the anodizing treatments are carried out over a longer period of time [20].

Fig. 6 displays the estimated values of the correlation coefficient for samples sealed and unsealed in this study. The results of this investigation support the hypothesis that isothermal adsorption is favorably affected by the post-anodization sealing procedure. A stronger association between the independent and dependent variables is shown by the higher correlation coefficient of 0.7487 found in the sealed samples compared to the unsealed specimens' value of 0.6526 (Fig. 6). The results show that the efficacy of isothermal adsorption is much improved by the sealing method [21]. According to the data, the adsorption and interaction of the adsorbate molecules with the aluminum surface are enhanced by the sealing operation, as evidenced by the higher  $R^2$  value reported for sealed specimens [22]. These findings highlight the potential benefits of employing sealed samples in real-world circumstances requiring increased resistance to corrosion, and also highlight the significance of the sealing method in boosting the overall adsorption capabilities.

The correlation coefficient value of 0.7487 obtained for specimens with seals indicates a strong relationship between the variables. This suggests that the sealing procedure significantly affects the isothermal adsorption behavior, as shown in Fig. 6. The statement suggests that the purpose of sealing is to improve the interaction between inhibitors and the aluminum surface. This enhancement is believed to enhance the adsorption properties and offer better protection against corrosion. The correlation coefficient indicates a strong positive relationship between the post-anodizing procedure and the corrosion resistance of the aluminum alloy. This suggests that implementing this procedure can be highly beneficial in improving the alloy's resistance to corrosion. The coefficient suggests that the sealing approach leads to a more advantageous and effective adsorption process [23].

The results highlight the sealing process's significant impact on the oxide layer's thickness. Applying a sealing step after anodizing increases the oxide layer's density significantly, resulting in a thicker and more effective barrier against corrosion. This phenomenon is especially prominent in specimens subjected to longer anodizing times, as the sealing process contributes to greater oxide layer growth [24]. The information obtained from these observations is valuable for understanding the relationship between anodizing conditions, sealing processes, and the resulting oxide layer characteristics. Such insights can aid in optimizing the surface treatment technique to achieve the desired corrosion protection performance for aluminum materials in various industrial applications [25].

This study has limitations, including its narrow emphasis on a single corrosive media (3.5 % NaCl). The results may not indicate the aluminum alloy's performance in other corrosive conditions, but they give valuable insights into its corrosion resistance. Corrosion processes and behaviors might change depending on the environment's aggressiveness and chemical composition. Mass loss experiments as a proxy for corrosion rate and inhibition efficiency also have limitations. Despite their popularity and the helpful information they

give, trials designed to induce weight reduction have several apparent drawbacks. Corrosion can't be monitored using weight loss studies in real time since variables like exposure duration, surface condition, and handling practices might affect the findings. The importance of localized corrosion events in certain real-world contexts may also be missed in weight-loss research.

Further investigation can be conducted to enhance the development of this research. There are several aspects that may be further explored. By utilizing sophisticated microstructural analysis techniques, such as scanning electron microscopy (SEM), transmission electron microscopy (TEM), and X-ray diffraction (XRD), it becomes possible to discern the alterations in the oxide layer's structure and gain a deeper understanding of the interface between the anodic film and the substrate. Furthermore, it is important to conduct comparative analyses using alternative corrosion protection methods, such as coatings, inhibitors, and composite materials, in order to assess the relative efficacy and constraints of anodization in various scenarios. The application of computer modeling and simulation approaches is employed to forecast and comprehend the corrosion behavior and creation of oxide layers under diverse situations, hence facilitating the development of more efficient anodization procedures.

---

## 7. Conclusions

---

1. Sealing significantly reduces corrosion across anodizing times. Average corrosion rates were below 0.6 mmpy, indicating improved resistance. Sealing reduced corrosion by 15 % at 10 minutes, 11 % at 15 minutes, and 0.2 % at 20 minutes. Direct anodization time also decreased corrosion, regardless of sealing. Unsealed samples saw a 47 % decrease, while sealed samples experienced a 45 % reduction. Both sealing and anodization time effectively enhance aluminum durability against corrosion.

2. Evaluating inhibition efficiency reveals a notable trend where sealing the specimens increases efficiency. With longer anodizing times, efficiency improves progres-

sively. Up to 20 minutes of anodizing, sealed samples show similar inhibition efficiency to unsealed ones. This suggests that anodizing alone offers significant corrosion protection. However, the sealing process further enhances the surface treatment, providing increased durability and extended service life, especially in harsh corrosive conditions.

3. The oxide layer thickness is a key component in influencing the aluminum alloy's resistance to corrosion. When the oxide layer protecting an object from the environment is made thicker, the object is better protected from corrosion. With a 20-minute sealing procedure and anodizing period, the average oxide layer thickness is below 16 microns, and there is an increase of up to 125 % on specimens.

---

## Conflict of interest

---

The authors declare that they have no conflict of interest in relation to this research, whether financial, personal, authorship or otherwise, that could affect the research and its results presented in this paper.

---

## Financing

---

The study was performed without financial support.

---

## Data availability

---

Data will be made available on reasonable request.

---

## Acknowledgments

---

This research has been made possible with the valuable support and assistance from the Mechanical Engineering Laboratory at Hasanuddin University. The dedicated contributions and resources provided by the laboratory have contributed significantly to the successful execution and completion of this study.

---

## References

- Merisalu, M., Aarik, L., Kozlova, J., Mändar, H., Tarre, A., Sammelselg, V. (2021). Effective corrosion protection of aluminum alloy AA2024-T3 with novel thin nanostructured oxide coating. *Surface and Coatings Technology*, 411, 126993. doi: <https://doi.org/10.1016/j.surfcoat.2021.126993>
- Zhang, J., Zhao, X., Zuo, Y., Xiong, J. (2008). The bonding strength and corrosion resistance of aluminum alloy by anodizing treatment in a phosphoric acid modified boric acid/sulfuric acid bath. *Surface and Coatings Technology*, 202 (14), 3149–3156. doi: <https://doi.org/10.1016/j.surfcoat.2007.10.041>
- Saeedikhani, M., Javidi, M., Yazdani, A. (2013). Anodizing of 2024-T3 aluminum alloy in sulfuric-boric-phosphoric acids and its corrosion behavior. *Transactions of Nonferrous Metals Society of China*, 23 (9), 2551–2559. doi: [https://doi.org/10.1016/s1003-6326\(13\)62767-3](https://doi.org/10.1016/s1003-6326(13)62767-3)
- Elabar, D., La Monica, G. R., Santamaria, M., Di Quarto, F., Skeldon, P., Thompson, G. E. (2017). Anodizing of aluminium and AA 2024-T3 alloy in chromic acid: Effects of sulphate on film growth. *Surface and Coatings Technology*, 309, 480–489. doi: <https://doi.org/10.1016/j.surfcoat.2016.11.108>
- Covelo, A., Rodil, S., Nóvoa, X. R., Hernández, M. (2022). Development and characterization of sealed anodizing as a corrosion

7. Schindelholz, E. J., Melia, M. A., Rodelas, J. M. (2021). Corrosion of Additively Manufactured Stainless Steels—Process, Structure, Performance: A Review. *Corrosion*, 77 (5), 484–503. doi: <https://doi.org/10.5006/3741>
8. Ofoegbu, S. U., Fernandes, F. A. O., Pereira, A. B. (2020). The Sealing Step in Aluminum Anodizing: A Focus on Sustainable Strategies for Enhancing Both Energy Efficiency and Corrosion Resistance. *Coatings*, 10 (3), 226. doi: <https://doi.org/10.3390/coatings10030226>
9. Wilcox, G. D., Walker, D. E. (2013). Chemical Conversion Coatings. *Encyclopedia of Tribology*, 359–366. doi: [https://doi.org/10.1007/978-0-387-92897-5\\_1004](https://doi.org/10.1007/978-0-387-92897-5_1004)
10. Zhang, L., Thompson, G. E., Curioni, M., Skeldon, P. (2013). Anodizing of Aluminum in Sulfuric Acid/Boric Acid Mixed Electrolyte. *Journal of The Electrochemical Society*, 160 (4), C179–C184. doi: <https://doi.org/10.1149/2.032306jes>
11. Chamidy, H. N., Ngatin, A., Rosyadi, A. F., Julviana, A., Noviyani, N. (2023). Effect of voltage on the thickness of oxide layer at aluminum alloys for structural bonding using phosphoric sulfuric acid anodizing (PSA) process. *International Journal of Mechanical Engineering Technologies and Applications*, 4 (1), 69–76. doi: <https://doi.org/10.21776/mechta.2023.004.01.8>
12. Raffin, F., Echouard, J., Volovitch, P. (2023). Influence of the Anodizing Time on the Microstructure and Immersion Stability of Tartaric-Sulfuric Acid Anodized Aluminum Alloys. *Metals*, 13 (5), 993. doi: <https://doi.org/10.3390/met13050993>
13. Zuchry, M., Renreng, I., Arsyad, H., Arma, L. H., Widianto, A. (2023). Sealing effect on corrosion resistance of boric sulfuric acid anodizing on AA2024. *Eastern-European Journal of Enterprise Technologies*, 2 (6 (122)), 43–52. doi: <https://doi.org/10.15587/1729-4061.2023.277961>
14. Naief, T. M., Rashid, K. H. (2011). Comparative Study for Anodizing Aluminum Alloy 1060 by Different Types of Electrolytes Solutions. *Engineering & Technology*. URL: [https://www.researchgate.net/publication/295911313\\_Comparative\\_Study\\_for\\_Anodizing\\_Aluminum\\_Alloy\\_1060\\_by\\_Different\\_Types\\_of\\_Electrolytes\\_Solutions](https://www.researchgate.net/publication/295911313_Comparative_Study_for_Anodizing_Aluminum_Alloy_1060_by_Different_Types_of_Electrolytes_Solutions)
15. Zarras, P., Stenger-Smith, J. D. (2015). Smart Inorganic and Organic Pretreatment Coatings for the Inhibition of Corrosion on Metals/Alloys. *Intelligent Coatings for Corrosion Control*, 59–91. doi: <https://doi.org/10.1016/b978-0-12-411467-8.00003-9>
16. Wan, Y., Wang, H., Zhang, Y., Wang, X., Li, Y. (2018). Study on Anodic Oxidation and Sealing of Aluminum Alloy. *International Journal of Electrochemical Science*, 13 (2), 2175–2185. doi: <https://doi.org/10.20964/2018.02.78>
17. Hou, F., Hu, B., Tay, S. L., Wang, Y., Xiong, C., Gao, W. (2017). A new, bright and hard aluminum surface produced by anodization. *International Journal of Modern Physics B*, 31 (16-19), 1744029. doi: <https://doi.org/10.1142/s0217979217440295>
18. Collazo, A., Ezpeleta, I., Figueroa, R., Nóvoa, X. R., Pérez, C. (2020). Corrosion protection properties of anodized AA2024T3 alloy sealing with organic-based species. *Progress in Organic Coatings*, 147, 105779. doi: <https://doi.org/10.1016/j.porgcoat.2020.105779>
19. Paz Martínez-Viademonte, M., Abrahami, S. T., Hack, T., Burchardt, M., Terryn, H. (2020). A Review on Anodizing of Aerospace Aluminum Alloys for Corrosion Protection. *Coatings*, 10 (11), 1106. doi: <https://doi.org/10.3390/coatings10111106>
20. Merino, E., Durán, A., Ceré, S., Castro, Y. (2022). Hybrid Epoxy-Alkyl Sol–Gel Coatings Reinforced with SiO<sub>2</sub> Nanoparticles for Corrosion Protection of Anodized AZ31B Mg Alloy. *Gels*, 8 (4), 242. doi: <https://doi.org/10.3390/gels8040242>
21. Aghaei, M., Anbia, M., Salehi, S. (2022). Measurements and modeling of CO<sub>2</sub> adsorption behaviors on granular zeolite 13X: Impact of temperature and time of calcination on granules properties in granulation process using organic binders. *Environmental Progress & Sustainable Energy*, 41 (5). doi: <https://doi.org/10.1002/ep.13866>
22. Hafeznezami, S., Zimmer-Faust, A. G., Dunne, A., Tran, T., Yang, C., Lam, J. R. et al. (2016). Adsorption and desorption of arsenate on sandy sediments from contaminated and uncontaminated saturated zones: Kinetic and equilibrium modeling. *Environmental Pollution*, 215, 290–301. doi: <https://doi.org/10.1016/j.envpol.2016.05.029>
23. Jedli, H., Jbara, A., Hedfi, H., Bouzgarrou, S., Slimi, K. (2017). Carbon dioxide adsorption isotherm study on various cap rocks in a batch reactor for CO<sub>2</sub> sequestration processes. *Applied Clay Science*, 136, 199–207. doi: <https://doi.org/10.1016/j.clay.2016.11.022>
24. Fedel, M., Franch, J., Rossi, S. (2021). Effect of thickness and sealing treatments on the corrosion protection properties of anodic oxide coatings on AA5005. *Surface and Coatings Technology*, 408, 126761. doi: <https://doi.org/10.1016/j.surfcoat.2020.126761>
25. Wang, R., Wang, L., He, C., Lu, M., Sun, L. (2019). Studies on the sealing processes of corrosion resistant coatings formed on 2024 aluminium alloy with tartaric-sulfuric anodizing. *Surface and Coatings Technology*, 360, 369–375. doi: <https://doi.org/10.1016/j.surfcoat.2018.12.092>

Aluminum is widely used due to its excellent properties, lightweight and thermal conductivity. However, when used in aircraft applications, it can cause corrosion and sticking, compromising safety. To address this issue, anodizing is used to improve aluminum's corrosion resistance and adhesion. In this study, the AA2024 material was anodized using the boron-sulfuric acid anodization (BSAA) process, followed by a sealing process using acetic acid. This sealing process forms an oxide layer on the aluminum's surface, which reduces the corrosion rate. The study investigated the effects of anodization voltage and time on the results of BSAA anodization through quantitative and qualitative measurements, including corrosion resistance, potentiodynamic polarization, scanning electron microscopy (SEM), and energy dispersive X-ray spectroscopy (EDS). The results showed that samples anodized with a gasket could reduce the corrosion rate by up to 85 % compared to those without a gasket and substrate. The most significant reduction in corrosion rates occurred at an anodization voltage of 10 V and an anodization time of 15 min. The potentiodynamic test results indicated that the Tafel plot during sealing lies in the cathodic region where the corrosion current density decreases with increasing voltage. SEM observations revealed that the anodizing process could provide an oxide layer on the samples' surface, while the sealing process creates a smooth surface. EDS analysis showed that an oxide compound was formed in an oxide bond state after the sample surface was subjected to the sealing treatment. Overall, the study demonstrates the effectiveness of BSAA anodization in improving corrosion resistance and highlights the importance of considering the anodization parameters

**Keywords:** corrosion resistance, acetic acid, AA2024, boric sulfuric acid anodization

# SEALING EFFECT ON CORROSION RESISTANCE OF BORIC SULFURIC ACID ANODIZING ON AA2024

**Muhammad Zuchry**

Doctoral Student, Graduate Student\*

\*Departement of Mechanical Engineering

Hasanuddin University

Jl. Poros Malino, KM. 6, Bontomarannu Gowa, Sulawesi

Selatan, Indonesia, 92171

**Ilyas Renreng**

Corresponding Author

Doctorate, Professor\*

E-mail: ilyas.renreng@gmail.com

**Hairul Arsyad**

Doctorate, Assistant Professor\*

**Lukmanul Hakim Arma**

Doctorate, Assistant Professor\*

**Agus Widjianto**

Doctorate

Department of Mechanical and Automotive Engineering

Universitas Negeri Yogyakarta

Jl. Mandung, Kec. Pengasih, Kabupaten Kulonprogo,

Daerah Istimewa Yogyakarta, Indonesia, 55652

Received date 08.02.2023

Accepted date 18.04.2023

Published date 28.04.2023

**How to Cite:** Zuchry, M., Renreng, I., Arsyad, H., Arma, L. H., Widjianto, A. (2023). Sealing effect on corrosion resistance of boric sulfuric acid anodizing on AA2024. *Eastern-European Journal of Enterprise Technologies*, 2 (6 (122)), 43–52. doi: <https://doi.org/10.15587/1729-4061.2023.277961>

## 1. Introduction

Aluminum alloys in the 2xxx series are particularly useful for their high strength-to-weight ratio, making them ideal for aircraft structures. They also have good fatigue resistance and excellent machinability, which makes them popular for aerospace applications [1]. Moreover, aluminum alloys in the 2xxx series have good weldability and formability, which allows them to be shaped into complex parts with relative ease. Additionally, they are relatively inexpensive and widely available, making them a cost-effective solution for many applications. Overall, aluminum and its alloys are an important and versatile group of materials that are widely used in industry due to their desirable properties and cost-effectiveness.

The use of the 2xxx series aluminum alloys in aircraft structures has significantly contributed to the aerospace industry's advancements. Due to their high strength-to-weight ratio and excellent resistance to fatigue crack growth [2], these alloys have enabled aircraft manufacturers to design and build lighter, more fuel-efficient, and more durable aircraft. However, the presence of copper in these alloys can negatively impact their corrosion resistance and

fatigue strength [3]. This is a significant issue since aircraft operate in harsh environments that expose them to various corrosive elements and high stress loads.

To address these issues, several methods have been developed to enhance the corrosion resistance and fatigue strength of 2xxx series aluminum alloys. One of these methods is the impressed current cathodic protection (ICCP) system [4], which involves the application of an electrical current to the metal to prevent corrosion. Coating is another effective method that can be used to protect aluminum from corrosion by forming a protective barrier between the metal and the environment [5].

Anodizing is a process that is commonly used to enhance the corrosion resistance of aluminum alloys, including the 2xxx series. This process involves immersing the metal in an acid bath and applying an electrical current to produce a protective oxide layer on the surface of the metal [6]. This coating not only provides excellent corrosion protection but also improves the metal's adhesion properties, making it more suitable for bonding with other materials [7]. The process uses oxidation to alter the chemical composition of the material's surface. The specific requirements for anodizing aluminum alloys depend on their composition, which

determines the appropriate current and voltage densities [8]. During the anodizing process, the substrate composition, current density, voltage changes, and temperature all play a role in the formation of the aluminum oxide layer [9]. Anodizing creates two different types of oxide layers: a non-porous, thin, and sturdy barrier layer called the barrier layer, and a thicker, porous oxide layer called the porous layer [10].

Boric sulfuric acid anodizing is a widely used surface treatment technique that improves the corrosion resistance and durability of aluminum and its alloys. However, the corrosion resistance of the anodized layer can be further enhanced by applying a sealing treatment to the anodized surface [11]. The sealing effect on corrosion resistance refers to the process of closing the pores and voids in the anodized layer by using various sealing agents such as hot water, nickel acetate, sodium dichromate, and others [12]. This process enhances the barrier properties of the anodized layer and protects the underlying metal from corrosive environments.

Several studies are still conducting experiments to provide a coating on metal to inhibit the corrosion rate. One coated metal type is aluminum because the material is light and easy to form. However, one of the weaknesses of aluminum is its mechanical properties, which tend to be weak. In addition, this material will easily corrode in an inappropriate environment. therefore, research on the development of the corrosion rate by sealing the material with the anodizing method is relevant.

---

## 2. Literature review and problem statement

---

Anodization is essential in automotive assembly, aircraft, and other metal products. Anodizing is done to get a thicker and uniform oxide layer on the aluminum surface. In recent years, several studies on anodization research have been carried out. First, the relationship between the forming conditions of the alumina film and the breakdown voltage is examined [13]. This study's results indicate that the breakdown voltage's magnitude during the anodizing process depends on the electrolyte solution. Furthermore, the influence of substrate composition, current density, voltage, and temperature changes during the anodizing process was investigated [9]. In addition, this study's results indicate that the electrolyte's temperature increases with increasing applied current density, while the resulting film thickness is more influenced by the magnitude of the anodizing voltage and is independent of the substrate.

The Boeing Company is developing BSAA (Boric Sulfuric Acid Anodization) anodizing and has met the technical requirements as a substitute for chromic acid anodizing [11, 14]. This anodization is environmentally friendly and also offers high corrosion resistance. Over the past two decades, researchers have conducted many experiments to optimize BSAA coatings on a wide range of aluminum alloys [15]. The paper [16] presents the effect of the composition of the electrolyte solution on the aluminum anodizing process. The results showed that the thickness of the aluminum oxide layer produced varied greatly depending on the type and composition of the electrolyte used. This research also mentions that temperature differences in the electrolyte cause the resulting viscosity.

The paper [17] highlights a study on the anodizing process of the 1100 series aluminum using variable voltage and anodizing time. The results indicate that the characteristics

of the resulting aluminum oxide layer depend on several factors, including the electrolyte temperature, current density, and the surface polishing process of the substrate. Furthermore, the paper investigates the growth mechanism of the porous aluminum oxide layer formed using an electrolytic sulfuric acid solution. The study revealed that the porosity of the coating is influenced by the substrate material rather than the level of anodizing stress. This finding is essential as it indicates that, to control the porosity of the coating, it is crucial to choose the right substrate material [18]. Additionally, this study's findings can be useful in developing improved anodizing techniques that can be used to control the porosity of the coating and, therefore, optimize the anodized aluminum's properties.

Sealing is traditionally accomplished by immersion in boiling deionized water, known as hot water sealing. However, high temperatures and slow kinetics are required, which means significant energy consumption [19]. As a result, the hot water process has been successively replaced by cold sealing since the 1980s [20]. Sealing dichromate and nickel acetate is considered the most effective for corrosion prevention, but Cr(VI) is toxic [21, 22].

Recent studies have explored various sealants to protect anodic aluminum oxide from corrosion, including nickel acetate, nickel fluoride, cerium acetate, sol-gel sealing, and a complex sealing process with PTFE. For example, one study found that cold nickel acetate and hot water sealing decreased the pore size, while hot nickel acetate filled the pores resulting in a low porosity and small mean pore radius [23]. Another study showed that boiling water and potassium dichromate sealed films provided higher corrosion resistance in acidic solutions, while nickel fluoride sealed film was better in basic solutions [24, 25]. Cerium acetate was found to be effective in protecting insulator pins in low-pH and high-corrosion-rate environments, potentially leading to the development of eco-friendly anti-corrosion coatings for power industries [12]. Sol-gel sealing was shown to delay the access of aggressive species to the barrier layer [26, 27], while a complex sealing process with PTFE had a large positive reverse pump rate but may not extend its service life before leakage [28].

The research paper referenced as [13] examined the relationship between bound water and the stability of anodic oxide films on aluminum by measuring the quantity of bound water and its stability through various experimental methods. However, it did not investigate bound water's formation mechanisms or impurities' impact on the oxide film's stability. Another paper referenced as [19] investigated the effect of different sealing processes on the corrosion resistance of coatings formed on 2024 aluminum alloy via tartaric-sulfuric anodizing. However, it did not examine the effects of other anodizing parameters on the coatings' corrosion resistance or the coatings or the microstructure and composition of the coatings and their impact on the sealing process and corrosion resistance. The effectiveness of a novel sealing process on the corrosion resistance of an anodic oxide coating was evaluated in the article [21]. However, the study did not examine the mechanical properties of the coating or how the coating affected the mechanical properties of the substrate. The article [22] investigated the effects of two sealing treatments on the corrosion behavior of Al-based amorphous/nanocrystalline coatings using electrochemical impedance spectroscopy and potentiodynamic polarization measurements. The article did not thoroughly explain the

observed corrosion behavior and recommended further research to explore the underlying mechanisms.

Previous research on the anodizing process has primarily focused on the impact of various parameters, such as temperature, time, current density, solution composition, and pre-treatment, on the thickness of the aluminum oxide layer produced. The thickness of the oxide layer is essential for determining the material's corrosion resistance. However, further research is necessary to investigate the impact of anodizing on other material properties, such as mechanical and physical properties and corrosion resistance. Such studies can help optimize the anodizing process for specific applications. Additionally, there is a need to develop new sealant methods that can improve the corrosion resistance of anodized aluminum. Based on these problems, all this allows to assert that it is expedient to conduct a study on the corrosion resistance of boric sulfuric acid anodizing on AA2024 with acetic acid sealing process.

### 3. The aim and objectives of the study

The aim of the study is to inhibit the corrosion rate of AA2024 with boric sulfuric acid anodizing (BSAA) with and without sealing process using acetic acid ( $\text{CH}_3\text{COOH}$ ) solution.

To achieve this aim, the following objectives are accomplished:

- to study the effect of sealing using boric sulfuric acid anodizing on the corrosion rate of AA2024;
- to study the effect of sealing using boric sulfuric acid anodizing on potentiodynamic polarization of AA2024;
- to study the effect of sealing using boric sulfuric acid anodizing on micrographs with SEM and changes in the compound elements of AA2024.

### 4. Materials and methods of experiment

#### 4. 1. Object and hypothesis of the study

The object of research on the sealing effect on corrosion resistance of boric sulfuric acid anodizing on AA2024 is to investigate the effect of the sealing process on the corrosion resistance of anodized AA2024 samples. The study's main hypothesis was that the sealing process using an acetic acid solution after the boric sulfuric acid anodizing process would improve the corrosion resistance and adhesion of the AA2024 material. Some of the assumptions made in this study include:

- 1) anodizing with boron-sulfuric acid improves the corrosion resistance and adhesion of AA2024;
- 2) sealing the anodized samples with acetic acid solution further enhances the corrosion resistance of the material;
- 3) anodization voltage and anodization time affect the corrosion resistance of the samples;
- 4) samples anodized with a gasket can reduce the corrosion rate compared to samples anodized without the gasket and its substrate.

In general, scientific studies often involve simplifying assumptions to make the research more manageable or to isolate specific factors of interest. Some possible simplifications that could have been adopted in this study on the sealing effect on corrosion resistance of boric sulfuric acid anodizing on AA2024 are:

- simplified sample geometry: the study may have used simple geometric shapes (e.g., flat disks) instead of more complex shapes to simplify the anodizing and sealing processes;
- controlled environmental conditions: the study may have controlled the environmental conditions (e. g., temperature, humidity, etc.) to minimize the effect of external factors on the corrosion resistance of the samples;
- homogeneous material composition: the study may have assumed that the AA2024 material used was homogeneous throughout, without any defects or impurities affecting the corrosion resistance;
- idealized sealing process: the study may have assumed an idealized sealing process that completely covers the anodized surface with a uniform layer of oxide without any defects or variations in thickness;
- single anodizing and sealing parameter: the study may have focused on a single anodizing voltage and time and a single-sealing solution and time to simplify the experimental setup and isolate the effect of sealing on the corrosion resistance.

#### 4. 2. Material

In this study, an aluminum alloy AA2024 with a diameter of 12 mm and thickness of 3 mm was used. The alloy was subjected to anodizing at room temperature with constant voltage of 10 V and 15 V using a BSAA electrolyte mixture containing 45 gr/l sulfuric acid and 8 g/l boric acid. The anodizing was performed for 10 and 15 minutes, and the selected mechanical variables were the surface roughness of the coating and the corrosion rate after anodizing and sealing. The chemical composition of aluminum AA2024 was determined using an optical emission spectrometer (OES), and it was found that AA2024 is an aluminum alloy with copper as the main alloying element. Table 1 provides details of the chemical composition of aluminum AA2024.

Table 1

Chemical composition (wt %) of aluminum AA2024

	Si	Fe	Cu	Mg
AA2024	0.5	0.5	3.9	1.5
	Zn	Cr	Ti	Al
	0.25	0.1	0.15	92.5

In addition, the base metal is also tested for tensile strength to determine the strength of the base metal. The results of the tensile test show that it still has a maximum tensile stress ( $\sigma T$ ) of 463 MPa, yield stress ( $\sigma Y$ ) of 360 MPa, and elongation ( $\epsilon$ ) of 17.8 %, which is still within the material limits of the AA2024 standard.

#### 4. 3. Anodizing process

Aluminum alloy AA2024 has a diameter of 12x3 mm thick with constant voltage, 10 V and 15 V for 10, 15, and 20 minutes at room temperature 27 °C. The controlled variable was the BSAA electrolyte used as an electrolyte mixture of 45 gr/l sulfuric acid and 8 gr/l boric acid. The distance between the anode and cathode was 5 cm. The electrolyte mixture ratio for anodizing aluminum ranges from 30.5 to 52.0 g/l sulfuric acid and 5.2 to 10.7 g/l boric acid. This study focused on a mixture of 45 gr/l of sulfuric acid and 8 gr/l and boric acid, as recommended [12].

Fig. 1 outlines the various steps involved in preparing for the anodizing process. The first step involves preparing the

material. The process involves cleaning/degreasing with alkaline solution (sodium hydroxide, potassium hydroxide, and trisodium phosphate), rinsing with RO water, etching with 100 gr/l caustic soda, rinsing, desmut with a mixture of 75 % phosphoric acid (H<sub>3</sub>PO<sub>4</sub>), 15 % sulfuric acid (H<sub>2</sub>SO<sub>4</sub>), and 10 % acetic acid (CH<sub>3</sub>COOH) at room temperature for 2 minutes, rinsing, anodizing with a mixture of 45 gr/l H<sub>2</sub>SO<sub>4</sub> and 8 gr/l boric acid, rinsing again, and finally sealing with a mixture of 50 gr/l acetic acid (CH<sub>3</sub>COOH). Acetic acid is a popular choice for filling oxide films due to its ability to dissolve in water and form a stable solution, penetrate pores of the oxide film, react with the oxide layer, and form a dense and uniform aluminum oxide layer. Moreover, acetic acid has a low boiling point and is relatively safe to handle, making it a practical choice for the anodizing process.

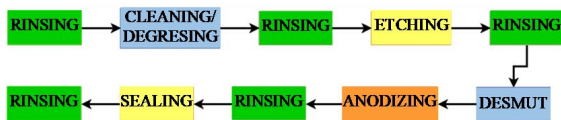


Fig. 1. Preparation scheme for anodizing process

In this anodizing tool, the anode is typically made of the material to be anodized, while the cathode is usually made of a material that doesn't react with the electrolyte. The anode and cathode are placed in the electrolyte, which is a solution that conducts electricity. The direct current source is then used to apply a voltage to the anode and cathode, which initiates the anodizing process. The voltage can be adjusted depending on the desired thickness and properties of the anodized layer. The schematic also shows other components in Fig. 2, such as the container that holds the electrolyte and the mechanism for circulating the electrolyte to ensure uniform anodizing. The anodizing tool can be designed in different shapes and sizes depending on the specific application and requirements.

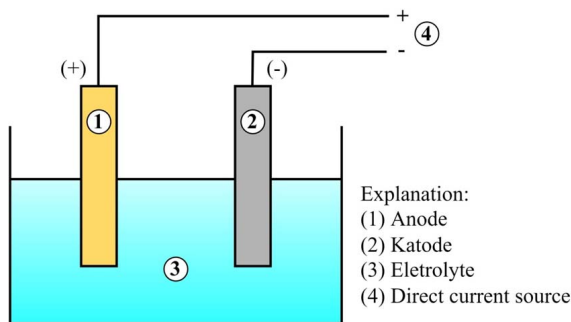


Fig. 2. Schematic illustration of anodizing tool

During the anodizing process, the two specimens of the AA2024 aluminum alloy were immersed in the electrolyte solution, with one serving as the anode (+) and the other as the cathode (-). A voltage source was connected to the cathode to supply a constant voltage of 10 volts for a duration of 10, 15, and 20 minutes. The electrolyte solution was a mixture of sulfuric acid and boric acid with concentrations of 45 gr/l sulfuric acid and 8 gr/l boric acid. The anodizing process involved the formation of a protective oxide layer on the surface of the aluminum alloy through the process of electrolysis. The duration of the process and the concentration of the electrolyte solution were varied to investigate their effect on the resulting properties of the oxide layer, such as its thickness, porosity, and corrosion resistance.

4. 4. Specimen test method

Compositional and tensile tests are performed to determine material properties. A material composition test was performed using a spectrometer to determine the type and specifications of materials used. Aluminum alloy AA2024 A tensile test to determine the strength of the base metal to obtain the following mechanical properties of the test material: Elastic limit, yield point, and tensile strength.

The process of testing corrosion with anodizing is depicted in Fig. 3. In the first step, the material is prepared as described earlier. In the second step, the corrosion test is conducted on the AA2024 specimen by utilizing the boric sulfuric acid anodizing (BSAA) process for durations of 10, 15, and 20 minutes, and the voltage utilized is either 10 or 15 volts. Finally, in the third step, the specimens are tested, and both qualitative and quantitative measurements, including corrosion rate and polarization, are conducted using Scanning Electron Microscopy (SEM) and Energy Dispersive X-Ray Spectroscopy (EDS) techniques.

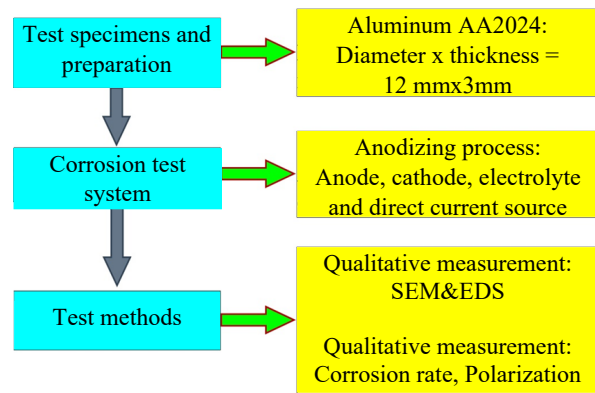


Fig. 3. Corrosion testing flow by an anodizing process

In addition to the SEM and EDS tests, the study conducted various other tests to evaluate the effectiveness of the anodizing process. The ASTM G102 standard was utilized to measure the corrosion rate and polarization of the specimen. This standard involves measuring the specimen's potential, current, and corrosion rate under specific conditions. By collecting this data, the study aimed to evaluate the corrosion resistance of the anodized aluminum samples.

The corrosion testing results were carefully analyzed to identify the optimal anodizing process parameters that could deliver the required level of corrosion resistance. By comparing the corrosion rates of samples subjected to different anodizing process parameters, the researchers could determine which process parameters produced the most effective corrosion resistance. This information can help guide the development of new anodizing processes that can deliver superior corrosion resistance in various applications.

5. Results of the experiment corrosion rate using boric sulfuric acid anodizing of AA2024

5. 1. Corrosion rate on aluminum AA2024 with boric sulfuric acid anodizing

The corrosion rate is one of the quantitative measurements carried out on AA2024 with the BASS method. This corrosion rate measurement is applied to raw materials, materials without sealing, and materials with sealing. Anodiz-

ing time also determines how fast or slow the corrosion rate is on the material. Fig. 4, *a*, *b* show the corrosion rate with an anodizing voltage of 10 and 15 volts, respectively.

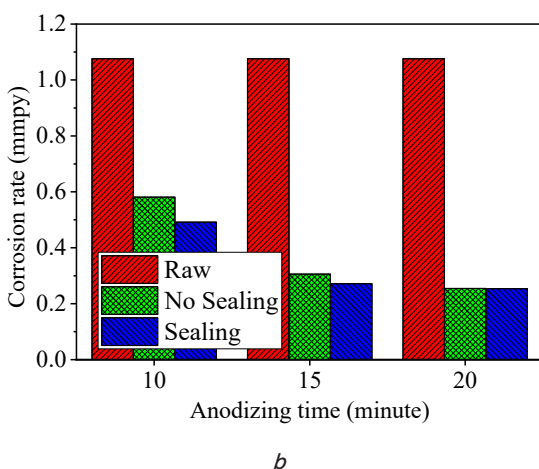
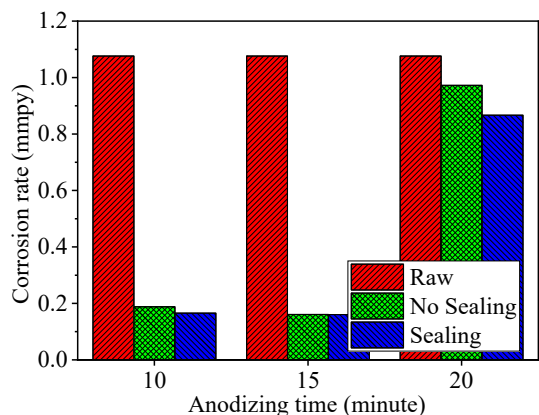


Fig. 4. Corrosion rate with anodizing voltage: *a* – 10 volts; *b* – 15 volts

The anodizing process with a voltage of 10 volts showed decreased corrosion rate on specimens without sealing and samples with sealing at each anodizing time variation. At anodizing time of 10 minutes, the corrosion rate decreased by up to 84 % of the raw material. Furthermore, at anodizing time of 15 minutes, the corrosion rate decreased by up to 85 %. Meanwhile, at anodizing time of 20 minutes, the corrosion rate only reduced by 19 %. The corrosion rate also decreased with an anodizing voltage of 15 volts and anodizing time of 10 minutes, which was 54 %. Anodizing time of 15 minutes reduced the corrosion rate by up to 74 %, while at 20 minutes, the corrosion rate decreased by 76 % compared to the raw material.

**5.2. Potentiodynamic polarization on aluminum AA2024 with boric sulfuric acid anodizing**

The results of the electrochemical polarization observations are depicted as a Tafel curve plot shown in Fig. 5. At an anodizing voltage of 10 volts (Fig. 5, *a*), there are two types of specimens: specimens without sealing and samples with sealing. Variations in the anodizing time used are 10 minutes, 15 minutes, and 20 minutes. There is an increase in potential in the sealed specimen compared to the non-sealed specimen. Meanwhile, the longer anodizing time will also increase the corrosion potential.

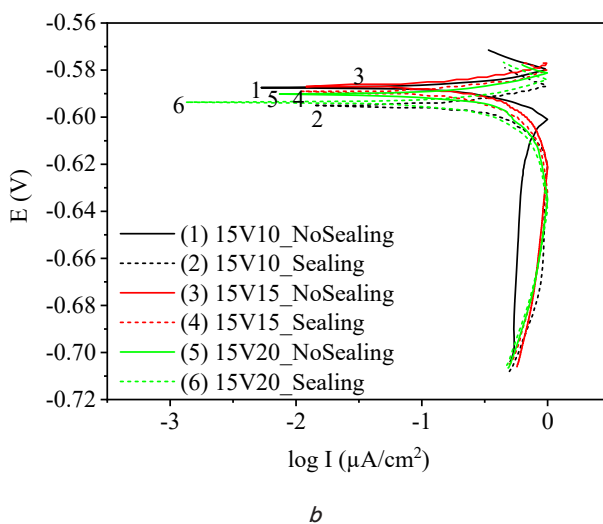
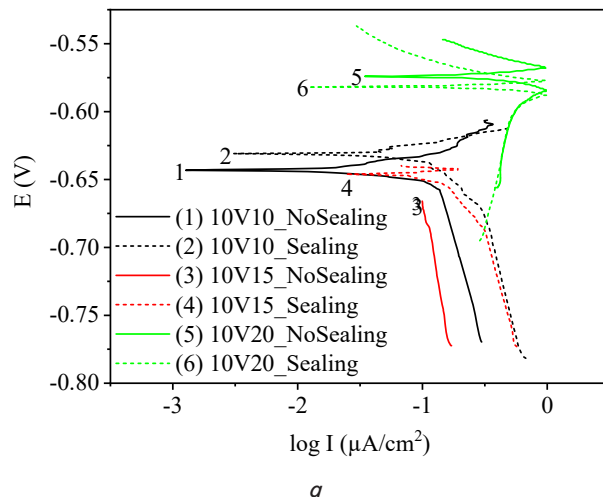


Fig. 5. Polarization curves with anodizing voltage: *a* – 10 volts; *b* – 15 volts

The graph mentioned in the text represents the corrosion rate of aluminum samples under different anodization conditions. The y-axis represents the potential corrosion (V), while the x-axis represents the current density ( $\mu\text{A}/\text{cm}^2$ ). The graph shows that the corrosion rate of the samples decreases with increasing anodization voltage and time. Based on the graph above, an odd number with a solid line on the curve indicates an anodized sample without sealing, while an even number with a dotted line is an anodized sample with sealing. The results show that sealing the samples after the anodization process can significantly reduce the corrosion rate of aluminum. The difference between the solid and dotted lines for the same anodization conditions indicates the effect of sealing on the corrosion rate.

The study involved various corrosion parameters in analyzing the effects of anodization and sealing on aluminum. The results showed that at an anodizing voltage of 15 volts, the potential for corrosion increased for each specimen parameter without sealing, and the specimen with the seal was not significantly affected. Corrosion testing yielded various parameters, including potential corrosion ( $E_{corr}$ ), current density corrosion ( $I_{corr}$ ), cathodic ( $\beta_c$ ), anodic ( $\beta_a$ ), Tafel slope, and ( $IE$ ).

The potentiodynamic test results revealed that the Tafel plot using sealing is in the cathodic region where the stress

increases, reducing the corrosion current density and indicating a decrease in the corrosion rate. The highest corrosion potential ( $E_{corr}$ ) value was  $-0.537\text{ V}$  obtained at the anodizing time of 10 minutes, while the lowest corrosion potential ( $E_{corr}$ ) value was  $-0.708\text{ V}$  with the anodizing time of 15 minutes. The highest and lowest values for the current density corrosion ( $I_{corr}$ ) were  $-8.7\text{E-}05$  and  $-2.87515$ , respectively, at 15 minutes of anodizing time. These results suggest that the anodizing and sealing processes can significantly affect the corrosion behavior of aluminum, and proper parameter selection is crucial to achieving optimal corrosion resistance.

It can be observed that the corrosion rate decreases as the anodization voltage and time increase, and the lowest corrosion rate is obtained at an anodization voltage of  $10\text{ V}$  and an anodization time of 15 minutes. Additionally, samples anodized with a gasket and substrate have a lower corrosion rate than those without the gasket and substrate. This reduction in corrosion rate is attributed to the formation of an oxide layer on the surface of the aluminum during anodization, which is further sealed by acetic acid treatment, resulting in a smooth surface and increased corrosion resistance.

### 5.3. Scanning electron microscopy and energy dispersive X-ray spectroscopy on aluminum AA2024 with boric sulfuric acid anodizing

The AA2024 aluminum alloy is characterized by a thin layer of oxide ( $\text{Al}_2\text{O}_3$ ) prior to anodizing. The SEM images depicted in Fig. 6, *a*, *b* show that the surface of the aluminum alloy without anodizing appears flat. However, after undergoing the anodizing process, the surface layer becomes uneven and porous, as evident in the SEM images. This porous surface is a characteristic feature of materials that have undergone the anodizing process.

The pores shown in the photomicrographs are larger than those typically formed on anodized aluminum because they are not proper anodic pores but rather areas where the coating is not present or incomplete due to copper, zinc, iron, or their compounds with aluminum. These areas can be more susceptible to corrosion and may impact the overall effectiveness of the anodizing process in preventing corrosion. It would require further analysis and investigation to confirm the exact cause of these larger pores.

The aluminum oxide layer significantly formed influences the corrosion resistance properties of the AA2024 aluminum alloy. However, if the resulting pores are too large or exceed their optimum size, the corrosion resistance will not be optimal or will increase again. To minimize the resulting pores, a  $50\text{ g/l}$  vinegar/acetic acid solution was used to close the open pores in the oxide layer from the anodization process to reduce the pores formed. Helpful seals are performed. The results are better where it can be seen that the surface of the specimen is smoother when sealing is done, as shown in Fig. 7, *a*. Meanwhile, if sealing is not carried out, the surface of the specimen will be rougher, as shown in Fig. 7, *b*.

The SEM-EDS test is required to determine the formation of an oxide layer in the anodizing process, where its main function is used to obtain information on topography and morphology. Topography is the surface and textural characteristics of the specimen. Meanwhile, morphology is the shape and size of the particles making up the object and composition, namely the semi-quantitative data of the elements and compounds contained in the anodizing process. Fig. 8 shows the EDS results on specimens without and with seals.

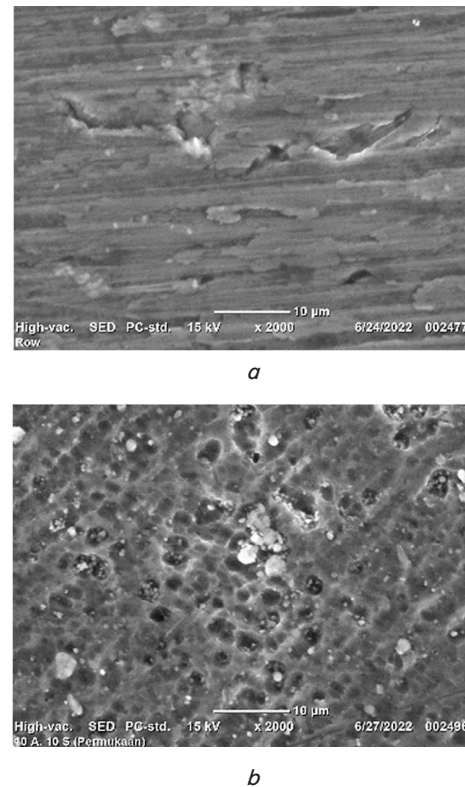


Fig. 6. Scanning electron microscopy micrography for a specimen: *a* – without anodizing; *b* – with anodizing

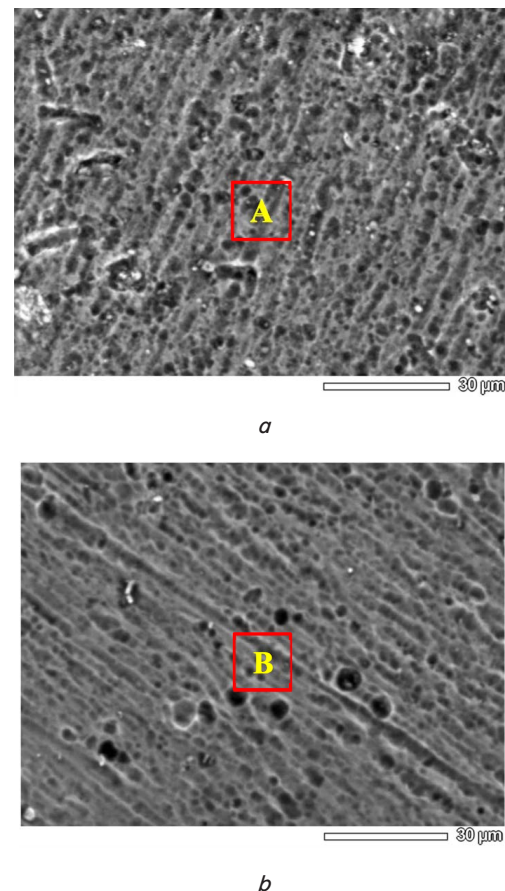


Fig. 7. Scanning electron microscopy micrography for a specimen: *a* – without sealing; *b* – with sealing

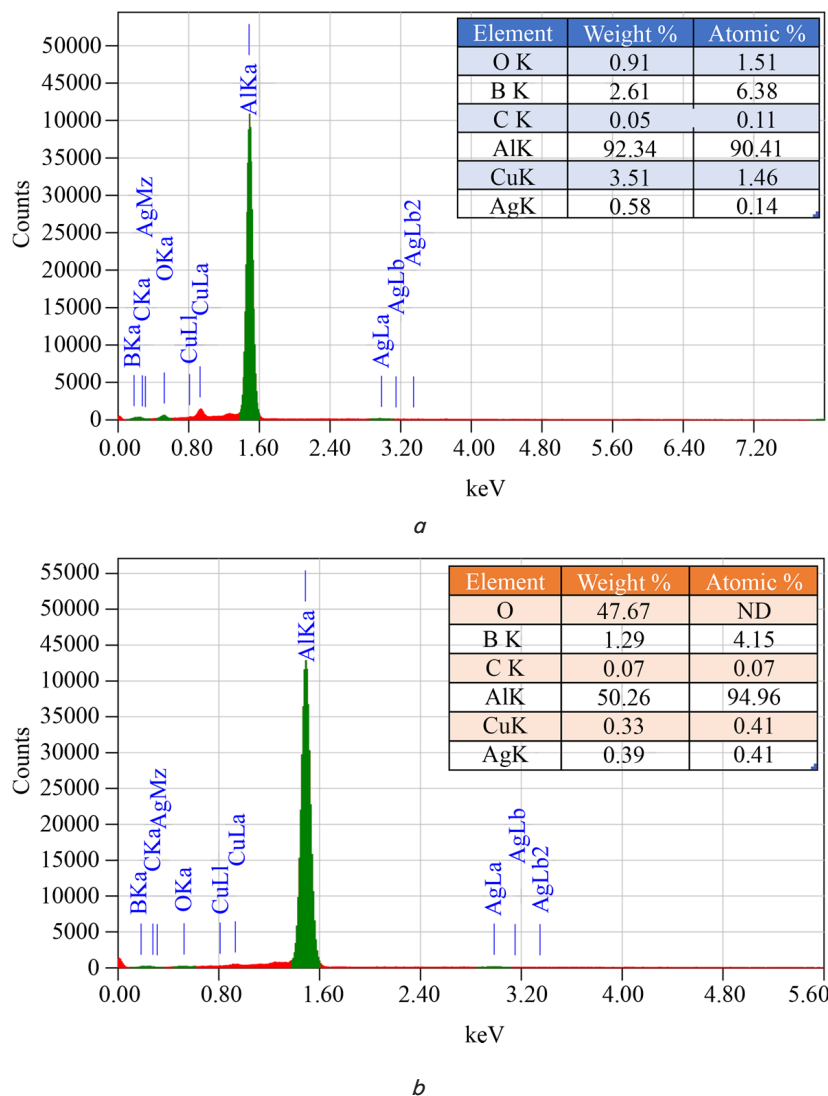


Fig. 8. Energy dispersive x-ray spectroscopy analysis of the selected area: *a* – without sealing; *b* – with sealing

The EDS test conducted on the samples provided valuable information on the composition of the aluminum oxide layer formed after the anodizing process. As expected, the results confirmed that the layer consisted of pure aluminum and oxygen. In addition, as shown in Fig. 8, *a*, the EDS spectrum revealed peaks corresponding to aluminum, oxygen, and trace amounts of other elements such as copper and zinc. These elements likely originate from the underlying aluminum alloy substrate.

Furthermore, Fig. 8, *b* shows that the elements in the oxide layer form oxide compounds, which are in an oxide bond state. This is consistent with the expected formation of a dense and uniform aluminum oxide layer during the anodizing process. The results of the EDS test support the effectiveness of the anodizing process in producing a stable and uniform oxide layer on the surface of the aluminum alloy substrate.

## 6. Discussion of the experiment corrosion rate using boric sulfuric acid anodizing of AA2024

Further analysis of the preliminary test results indicates that sealing has a significant impact on the corrosion

rate of AA2024. Corrosion rate tests were carried out on the unsealed and sealed anodized samples and the base material based on Fig. 4. The anodizing time was varied for three samples, namely 10, 15, and 20 minutes. In addition, two different anodizing voltages, namely 10 volts and 15 volts, were used. The anodizing process causes the formation of pores on the aluminum layer, resulting in a decrease in the corrosion rate of the specimen. The size of the pores is influenced by the anodizing stress and process time. The results of this study suggest that an anodizing voltage of 10 volts and an anodizing time of 10 or 15 minutes are more effective in reducing the corrosion rate than an anodizing voltage of 15 volts (Fig. 4, *a*). However, an anodizing time of 20 minutes combined with an anodizing voltage of 15 volts is more effective in reducing the corrosion rate (Fig. 4, *b*). Another study [29] found that anodizing stress affects the formation of pores in the material, with a higher anodizing stress resulting in larger pore geometry. Therefore, the decrease in the corrosion rate in this study can be attributed to the increased formation of pores with the use of a 10 V anodizing voltage. Additionally, it is likely that longer anodizing times will lead to the formation of larger pores [30].

In addition to the improvement in corrosion potential observed in the anodizing samples, the study also found that sealing the anodized specimens resulted in a slightly higher corrosion potential compared to unsealed samples based on Fig. 5. However, increasing the anodizing stress may also increase the corrosion potential of the material. Despite this, the tested parameters all demonstrated a higher corrosion potential, indicating that the addition of sealing after anodizing can effectively enhance the corrosion resistance of the material. It is worth noting that previous research has also shown that applying the BSAA process to AA2024 can lead to a lower current density in anodized samples [21], further supporting the positive effects of anodizing on the corrosion resistance of the material.

The formation of aluminum oxide layer during the anodizing process is determined by the size and number of pores present in the material (Fig. 6, *a*). However, the surface microstructure of the aluminum oxide layer formed is observed to be uneven. This unevenness is attributed to the excessive current and energy that cause decay of the aluminum oxide layer back into the electrolyte solution. This decay results in the formation of pores in the aluminum oxide layer that are too large, leading to its unevenness. As a result, the aluminum oxide layer cannot be detected on the base material using SEM or EDX. However, after the anodizing process, aluminum oxide pores are visible, which vary in size and number and are not evenly distributed, but the thickness of the oxide formed increases (Fig. 6, *b*). The presence of these pores explains how the aluminum content decreases after

the anodizing process. In addition, the quality of anodized aluminum is also affected by the potential difference provided. A significant potential difference affects the width and thickness of the aluminum oxide pores formed, leading to variations in the resulting material's properties [31].

Aluminum anodic coatings are widely used in aviation technology for various purposes, such as corrosion resistance, wear resistance, and electrical insulation. These coatings can provide a protective barrier that prevents corrosion and prolongs the lifespan of aircraft components, especially those exposed to harsh environmental conditions such as moisture and salt water. In addition, anodized aluminum can improve the adhesion of paints and other coatings, making it a popular choice for aircraft exterior and interior parts. Anodizing can also increase the hardness and durability of aluminum, making it more resistant to scratches, abrasion, and wear. Overall, using aluminum anodic coatings in aviation technology can improve the safety, reliability, and efficiency of aircraft operation.

Iron, zinc, and copper in aluminum alloys are not subject to electrochemical oxidation during anodization. To address this, a pre-treatment process is typically employed to remove these impurities from the surface of the alloy. Additionally, the anodization process can be adjusted to produce a thicker and more porous oxide layer on the surface of the alloy, which can provide increased protection against corrosion (Fig. 7, *a*). Regarding the issue of porosity, it is possible that some areas of the alloy containing phases or intermetallics of aluminum with copper are not fully anodized, leading to variations in the porosity of the surface (Fig. 7, *b*). This can result in uneven corrosion resistance across the surface of the alloy. As for the reported decrease in corrosion rate, it is important to note that anodization is not a foolproof solution for corrosion protection, and it is possible that the oxide film does not cover the entire aluminum alloy surface. Therefore, while anodization can significantly reduce the corrosion rate, it may not eliminate it completely.

In spite of the valuable insights gained from this study, it should be noted that there are still some limitations that need to be addressed. One of the main limitations is that the test samples were only taken once, whereas it is generally recommended to collect samples at least three times to ensure the accuracy of the results. This is particularly important for validating the test data. Additionally, SEM and EDS tests were only performed for one of the study parameters, which means that the SEM and EDS results are only applicable to the tested parameters. Other parameters may exhibit different properties when tested. Thus, including

SEM and EDS test results for other parameters can further enhance the discussion and results of this study.

---

## 7. Conclusions

---

1. Anodizing treatment was carried out on aluminum with the BSAA process without sealing and has been successfully carried out with sealing. The decrease in corrosion rate was more significant for specimens with sealing. With an anodizing voltage of 10 V and an anodizing time of 15 minutes, the corrosion rate decreased by up to 85 % compared to the base material.

2. Potentiodynamic polarization indicates a difference between unsealed and sealed specimens. An increase in the corrosion potential occurs in specimens with sealing. The taffel plot shows sealing in the cathodic region where the stress increases, thereby reducing the corrosion current density.

3. SEM testing showed that the specimens with anodized surface experienced a porous surface, while the sealing treatment provided an oxide layer and a smoother surface. The EDS results also indicated that oxide compounds were formed on the specimens by sealing.

---

## Conflict of interest

---

The authors declare that they have no conflict of interest in relation to this research, whether financial, personal, authorship or otherwise, that could affect the research and its results presented in this paper.

---

## Financing

---

The study was performed without financial support.

---

## Data availability

---

Data will be made available on reasonable request.

---

## Acknowledgments

---

This research is supported by the Mechanical Engineering Laboratory, Hasanuddin University.

---

## References

1. Prasad, N. E., Wanhill, R. J. H. (Eds.) (2017). *Aerospace Materials and Material Technologies*. Springer. doi: <https://doi.org/10.1007/978-981-10-2134-3>
2. Tunes, M. A., Stemper, L., Greaves, G., Uggowitzner, P. J., Pogatscher, S. (2020). Prototypic Lightweight Alloy Design for Stellar-Radiation Environments. *Advanced Science*, 7 (22), 2002397. doi: <https://doi.org/10.1002/adv.202002397>
3. Iglesias-Rubianes, L., Garcia-Vergara, S. J., Skeldon, P., Thompson, G. E., Ferguson, J., Beneke, M. (2007). Cyclic oxidation processes during anodizing of Al–Cu alloys. *Electrochimica Acta*, 52 (24), 7148–7157. doi: <https://doi.org/10.1016/j.electacta.2007.05.052>
4. Hamsir, H., Sutresman, O., Arsyad, H., Syahid, M., Widyianto, A. (2022). Suppression of corrosion on stainless steel 303 with automatic impressed current cathodic protection (a-ICCP) method in simulated seawater. *Eastern-European Journal of Enterprise Technologies*, 6 (12 (120)), 13–21. doi: <https://doi.org/10.15587/1729-4061.2022.267264>

5. Subbotina, V., Sobol, O., Belozarov, V., Subbotin, A., Smyrnova, Y. (2020). A study of the phase-structural engineering possibilities of coatings on D16 alloy during micro-arc oxidation in electrolytes of different types. *Eastern-European Journal of Enterprise Technologies*, 4 (12 (106)), 14–23. doi: <https://doi.org/10.15587/1729-4061.2020.209722>
6. Polmear, I.J. (2004). *Aluminium Alloys – A Century of Age Hardening*. Materials Forum. Available at: [https://www.researchgate.net/publication/279898292\\_Aluminium\\_Alloys\\_-\\_A\\_Century\\_of\\_Age\\_Hardening](https://www.researchgate.net/publication/279898292_Aluminium_Alloys_-_A_Century_of_Age_Hardening)
7. Bensalah, W., Feki, M., Wery, M., Ayedi, H. F. (2011). Chemical dissolution resistance of anodic oxide layers formed on aluminum. *Transactions of Nonferrous Metals Society of China*, 21 (7), 1673–1679. doi: [https://doi.org/10.1016/s1003-6326\(11\)60913-8](https://doi.org/10.1016/s1003-6326(11)60913-8)
8. Stevenson, M. F. (2013). Anodizing.
9. Fratila-Apachitei, L. E., Apachitei, I., Duszczyk, J. (2006). Thermal effects associated with hard anodizing of cast aluminum alloys. *Journal of Applied Electrochemistry*, 36 (4), 481–486. doi: <https://doi.org/10.1007/s10800-005-9102-y>
10. Poinern, G. E. J., Ali, N., Fawcett, D. (2011). Progress in Nano-Engineered Anodic Aluminum Oxide Membrane Development. *Materials*, 4 (3), 487–526. doi: <https://doi.org/10.3390/ma4030487>
11. Zhang, L., Thompson, G. E., Curioni, M., Skeldon, P. (2013). Anodizing of Aluminum in Sulfuric Acid/Boric Acid Mixed Electrolyte. *Journal of The Electrochemical Society*, 160 (4), C179–C184. doi: <https://doi.org/10.1149/2.032306jes>
12. Sanyal, S., Kim, T., Rabelo, M., Pham, D. P., Yi, J. (2022). Application of noble cerium-based anti-corrosion sealing coating approach applied on electrical insulators installed in industrial regions. *Royal Society Open Science*, 9 (4). doi: <https://doi.org/10.1098/rsos.211786>
13. Haruna, T., Ikeda, T., Miyazaki, M., Nishimoto, A., Hirohata, Y. (2015). Correlation between Bound Water and Stability of Anodic Oxide Film on Aluminum. *MATERIALS TRANSACTIONS*, 56 (12), 2000–2005. doi: <https://doi.org/10.2320/matertrans.l-m2015831>
14. Shen, Y. Z., Li, H. G., Tao, H. J., Ling, J., Wang, T., Tao, J. (2015). Effect of anodic films on corrosion resistance and fatigue crack initiator of 2060-T8 Al-Li alloy. *International Journal of Electrochemical Science*, 10 (1), 938–946. Available at: [https://www.researchgate.net/publication/281996844\\_Effect\\_of\\_anodic\\_films\\_on\\_corrosion\\_resistance\\_and\\_fatigue\\_crack\\_initiator\\_of\\_2060-T8\\_Al-Li\\_alloy](https://www.researchgate.net/publication/281996844_Effect_of_anodic_films_on_corrosion_resistance_and_fatigue_crack_initiator_of_2060-T8_Al-Li_alloy)
15. Veys-Renaux, D., Chahboun, N., Rocca, E. (2016). Anodizing of multiphase aluminium alloys in sulfuric acid: in-situ electrochemical behaviour and oxide properties. *Electrochimica Acta*, 211, 1056–1065. doi: <https://doi.org/10.1016/j.electacta.2016.06.131>
16. Mukhurov, N. I., Zhvavyi, S. P., Terekhov, S. N., Panarin, A. Yu., Kotova, I. F., Pershukevich, P. P. et al. (2008). Influence of electrolyte composition on photoluminescent properties of anodic aluminum oxide. *Journal of Applied Spectroscopy*, 75 (2), 214–218. doi: <https://doi.org/10.1007/s10812-008-9026-5>
17. Pooladi, R., Rezaei, H., Aezami, M., Sayyar, M. R. (2009). Fabrication of anodic aluminum oxide nanotemplate and investigation of their anodization parameters. *Transactions of the Indian Institute of Metals*, 62 (3), 241–244. doi: <https://doi.org/10.1007/s12666-009-0026-9>
18. Fotovvati, B., Namdari, N., Dehghanghadikolaie, A. (2019). On Coating Techniques for Surface Protection: A Review. *Journal of Manufacturing and Materials Processing*, 3 (1), 28. doi: <https://doi.org/10.3390/jmmp3010028>
19. Wang, R., Wang, L., He, C., Lu, M., Sun, L. (2019). Studies on the sealing processes of corrosion resistant coatings formed on 2024 aluminium alloy with tartaric-sulfuric anodizing. *Surface and Coatings Technology*, 360, 369–375. doi: <https://doi.org/10.1016/j.surfcoat.2018.12.092>
20. Gonzalez, J. A., Lopez, V., Otero, E., Bautista, A., Lizarbe, R., Barba, C., Baldonado, J. L. (1997). Overaging of sealed and unsealed aluminium oxide films. *Corrosion Science*, 39 (6), 1109–1118. doi: [https://doi.org/10.1016/s0010-938x\(97\)00019-x](https://doi.org/10.1016/s0010-938x(97)00019-x)
21. Yu, S., Wang, L., Wu, C., Feng, T., Cheng, Y., Bu, Z., Zhu, S. (2020). Studies on the corrosion performance of an effective and novel sealing anodic oxide coating. *Journal of Alloys and Compounds*, 817, 153257. <https://doi.org/10.1016/j.jallcom.2019.153257> doi: <https://doi.org/10.1016/j.jallcom.2019.153257>
22. Zhang, L. M., Zhang, S. D., Ma, A. L., Hu, H. X., Zheng, Y. G., Yang, B. J., Wang, J. Q. (2018). Influence of sealing treatment on the corrosion behavior of HVAF sprayed Al-based amorphous/nanocrystalline coating. *Surface and Coatings Technology*, 353, 263–273. doi: <https://doi.org/10.1016/j.surfcoat.2018.08.086>
23. Hu, N., Dong, X., He, X., Browning, J. F., Schaefer, D. W. (2015). Effect of sealing on the morphology of anodized aluminum oxide. *Corrosion Science*, 97, 17–24. doi: <https://doi.org/10.1016/j.corsci.2015.03.021>
24. Kocabaş, M., Örnek, C., Curioni, M., Cansever, N. (2019). Nickel fluoride as a surface activation agent for electroless nickel coating of anodized AA1050 aluminum alloy. *Surface and Coatings Technology*, 364, 231–238. doi: <https://doi.org/10.1016/j.surfcoat.2019.03.003>
25. Hao, X.-L., Zhao, N., Jin, H.-H., Ma, W., Zhang, D.-H. (2020). Nickel-free sealing technology for anodic oxidation film of aluminum alloy at room temperature. *Rare Metals*, 40 (4), 968–974. doi: <https://doi.org/10.1007/s12598-020-01410-8>
26. Whelan, M., Cassidy, J., Duffy, B. (2013). Sol–gel sealing characteristics for corrosion resistance of anodised aluminium. *Surface and Coatings Technology*, 235, 86–96. doi: <https://doi.org/10.1016/j.surfcoat.2013.07.018>

27. Capelossi, V. R., Poelman, M., Recloux, I., Hernandez, R. P. B., de Melo, H. G., Olivier, M. G. (2014). Corrosion protection of clad 2024 aluminum alloy anodized in tartaric-sulfuric acid bath and protected with hybrid sol-gel coating. *Electrochimica Acta*, 124, 69–79. doi: <https://doi.org/10.1016/j.electacta.2013.09.004>
28. Huang, T.-C., Lin, C.-Y., Liao, K.-C. (2022). Sealing performance assessments of PTFE rotary lip seals based on the elasto-hydrodynamic analysis with the modified archard wear model. *Tribology International*, 176, 107917. doi: <https://doi.org/10.1016/j.triboint.2022.107917>
29. Abd-Elnaiem, A. M., Abbady, G., Ali, D., Asafa, T. B. (2019). Influence of anodizing voltage and electrolyte concentration on Al-1 wt% Si thin films anodized in H<sub>2</sub>SO<sub>4</sub>. *Materials Research Express*, 6 (8), 086468. doi: <https://doi.org/10.1088/2053-1591/ab2848>
30. Park, J., Son, K., Lee, J., Kim, D., Chung, W. (2021). Effects of Anodizing Conditions on Thermal Properties of Al 20XX Alloys for Aircraft. *Symmetry*, 13 (3), 433. doi: <https://doi.org/10.3390/sym13030433>
31. Araoyinbo, A. O., Noor, A. F. M., Sreekantan, S., Aziz, A. (2010). Voltage Effect on Electrochemical Anodization of Aluminum at Ambient Temperature. *International Journal of Mechanical and Materials Engineering*, 5 (1), 53–58. Available at: [https://www.researchgate.net/publication/265811751\\_Voltage\\_effect\\_on\\_electrochemical\\_anodization\\_of\\_aluminum\\_at\\_ambient\\_temperature](https://www.researchgate.net/publication/265811751_Voltage_effect_on_electrochemical_anodization_of_aluminum_at_ambient_temperature)



# Standard Test Method for Measurement of Fatigue Crack Growth Rates<sup>1</sup>

This standard is issued under the fixed designation E 647; the number immediately following the designation indicates the year of original adoption or, in the case of revision, the year of last revision. A number in parentheses indicates the year of last reapproval. A superscript epsilon (ε) indicates an editorial change since the last revision or reapproval.

## 1. Scope

1.1 This test method<sup>2</sup> covers the determination of fatigue crack growth rates from near-threshold to  $K_{max}$  controlled instability. Results are expressed in terms of the crack-tip stress-intensity factor range ( $\Delta K$ ), defined by the theory of linear elasticity.

1.2 Several different test procedures are provided, the optimum test procedure being primarily dependent on the magnitude of the fatigue crack growth rate to be measured.

1.3 Materials that can be tested by this test method are not limited by thickness or by strength so long as specimens are of sufficient thickness to preclude buckling and of sufficient planar size to remain predominantly elastic during testing.

1.4 A range of specimen sizes with proportional planar dimensions is provided, but size is variable to be adjusted for yield strength and applied force. Specimen thickness may be varied independent of planar size.

1.5 The details of the various specimens and test configurations are shown in Annex A1-Annex A3. Specimen configurations other than those contained in this method may be used provided that well-established stress-intensity factor calibrations are available and that specimens are of sufficient planar size to remain predominantly elastic during testing.

1.6 Residual stress/crack closure may significantly influence the fatigue crack growth rate data, particularly at low stress-intensity factors and low stress ratios, although such variables are not incorporated into the computation of  $\Delta K$ .

1.7 Values stated in SI units are to be regarded as the standard. Values given in parentheses are for information only.

1.8 This test method is divided into two main parts. The first part gives general information concerning the recommendations and requirements for fatigue crack growth rate testing. The second part is composed of annexes that describe the special requirements for various specimen configurations, special requirements for testing in aqueous environments, and procedures for non-visual crack size determination. In addition, there are appendices that cover techniques for calculating

da/dN, determining fatigue crack opening force, and guidelines for measuring the growth of small fatigue cracks. General information and requirements common to all specimen types are listed as follows:

	Section
Referenced Documents	2
Terminology	3
Summary of Use	4
Significance and Use	5
Apparatus	6
Specimen Configuration, Size, and Preparation	7
Procedure	8
Calculations and Interpretation of Results	9
Report	10
Precision and Bias	11
Special Requirements for Testing in Aqueous Environments	Annex A4
Guidelines for Use of Compliance to Determine Crack Size	Annex A5
Guidelines for Electric Potential Difference Determination of Crack Size	Annex A6
Recommended Data Reduction Techniques	Appendix X1
Recommended Practice for Determination of Fatigue Crack Opening Force From Compliance	Appendix X2
Guidelines for Measuring the Growth Rates Of Small Fatigue Cracks	Appendix X3

1.9 Special requirements for the various specimen configurations appear in the following order:

The Compact Tension Specimen	Annex A1
The Middle Tension Specimen	Annex A2
The Eccentrically-Loaded Single Edge Crack Tension Specimen	Annex A3

1.10 *This standard does not purport to address all of the safety concerns, if any, associated with its use. It is the responsibility of the user of this standard to establish appropriate safety and health practices and determine the applicability of regulatory limitations prior to use.*

## 2. Referenced Documents

### 2.1 ASTM Standards:

- E 4 Practices for Force Verification of Testing Machines<sup>3</sup>
- E 6 Terminology Relating to Methods of Mechanical Testing<sup>3</sup>
- E 8 Test Methods for Tension Testing of Metallic Materials<sup>3</sup>
- E 337 Test Method for Measuring Humidity with a Psychrometer (the Measurement of Wet- and Dry-Bulb Temperatures)<sup>4</sup>
- E 338 Test Method for Sharp-Notch Tension Testing of

<sup>1</sup> This test method is under the jurisdiction of ASTM Committee E08 on Fatigue and Fracture and is the direct responsibility of Subcommittee E08.06 on Crack Growth Behavior.

Current edition approved Dec. 10, 2000. Published April 2001. Originally published as E 647 – 78 T. Last previous edition E 647 – 99.

<sup>2</sup> For additional information on this test method see RR: E 24 – 1001. Available from ASTM Headquarters, 100 Barr Harbor Drive, West Conshohocken, PA 19428.

<sup>3</sup> Annual Book of ASTM Standards, Vol 03.01.

<sup>4</sup> Annual Book of ASTM Standards, Vol 11.03.

- High-Strength Sheet Materials<sup>3</sup>  
 E 399 Test Method for Plane-Strain Fracture Toughness of Metallic Materials<sup>3</sup>  
 E 467 Practice for Verification of Constant Amplitude Dynamic Loads on Displacements in an Axial Load Fatigue Testing System<sup>3</sup>  
 E 561 Practice for R-Curve Determination<sup>3</sup>  
 E 1012 Practice for Verification of Specimen Alignment Under Tensile Loading<sup>3</sup>  
 E 1820 Test Method for Measurement of Fracture Toughness<sup>3</sup>  
 E 1823 Terminology Relating to Fatigue and Fracture Testing<sup>3</sup>

### 3. Terminology

3.1 The terms used in this test method are given in Terminology E 6, and Terminology E 1823. Wherever these terms are not in agreement with one another, use the definitions given in Terminology E 1823 which are applicable to this test method.

#### 3.2 Definitions:

3.2.1 *crack size*,  $a[L]$ ,  $n$ —a linear measure of a principal planar dimension of a crack. This measure is commonly used in the calculation of quantities descriptive of the stress and displacement fields and is often also termed crack length or depth.

3.2.1.1 *Discussion*—In fatigue testing, crack length is the physical crack size. See *physical crack size* in Terminology E 1823.

3.2.2 *cycle*—*in fatigue*, under constant amplitude loading, the force variation from the minimum to the maximum and then to the minimum force.

3.2.2.1 *Discussion*—In spectrum loading, the definition of cycle varies with the counting method used.

3.2.2.2 *Discussion*—In this test method, the symbol  $N$  is used to represent the number of cycles.

3.2.3 *fatigue-crack-growth rate*,  $da/dN$ ,  $[L]$ —crack extension per cycle of loading.

3.2.4 *fatigue cycle*—See *cycle*.

3.2.5 *force cycle*—See *cycle*.

3.2.6 *force range*,  $\Delta P$   $[F]$ —*in fatigue*, the algebraic difference between the maximum and minimum forces in a cycle expressed as:

$$\Delta P = P_{\max} - P_{\min} \quad (1)$$

3.2.7 *force ratio (also called stress ratio)*,  $R$ —*in fatigue*, the algebraic ratio of the minimum to maximum force (stress) in a cycle, that is,  $R = P_{\min}/P_{\max}$ .

3.2.8 *maximum force*,  $P_{\max}$   $[F]$ —*in fatigue*, the highest algebraic value of applied force in a cycle. Tensile forces are considered positive and compressive forces negative.

3.2.9 *maximum stress-intensity factor*,  $K_{\max}$   $[FL^{-3/2}]$ —*in fatigue*, the maximum value of the stress-intensity factor in a cycle. This value corresponds to  $P_{\max}$ .

3.2.10 *minimum force*,  $P_{\min}$   $[F]$ —*in fatigue*, the lowest algebraic value of applied force in a cycle. Tensile forces are considered positive and compressive forces negative.

3.2.11 *minimum stress-intensity factor*,  $K_{\min}$   $[FL^{-3/2}]$ —*in*

*fatigue*, the minimum value of the stress-intensity factor in a cycle. This value corresponds to  $P_{\min}$  when  $R > 0$  and is taken to be zero when  $R \leq 0$ .

3.2.12 *stress cycle*—See *cycle* in Terminology E 1823.

3.2.13 *stress-intensity factor*,  $K$ ,  $K_1$ ,  $K_2$ ,  $K_3$   $[FL^{-3/2}]$ —See Terminology E 1823.

3.2.13.1 *Discussion*—In this test method, mode 1 is assumed and the subscript 1 is everywhere implied.

3.2.14 *stress-intensity factor range*,  $\Delta K$   $[FL^{-3/2}]$ —*in fatigue*, the variation in the stress-intensity factor in a cycle, that is

$$\Delta K = K_{\max} - K_{\min} \quad (2)$$

3.2.14.1 *Discussion*—The loading variables  $R$ ,  $\Delta K$ , and  $K_{\max}$  are related in accordance with the following relationships:

$$\begin{aligned} \Delta K &= (1 - R)K_{\max} \text{ for } R \geq 0, \text{ and} \\ \Delta K &= K_{\max} \text{ for } R \leq 0. \end{aligned} \quad (3)$$

3.2.14.2 *Discussion*—These operational stress-intensity factor definitions do not include local crack-tip effects; for example, crack closure, residual stress, and blunting.

3.2.14.3 *Discussion*—While the operational definition of  $\Delta K$  states that  $\Delta K$  does not change for a constant value of  $K_{\max}$  when  $R \leq 0$ , increases in fatigue crack growth rates can be observed when  $R$  becomes more negative. Excluding the compressive forces in the calculation of  $\Delta K$  does not influence the material's response since this response ( $da/dN$ ) is independent of the operational definition of  $\Delta K$ . For predicting crack-growth lives generated under various  $R$  conditions, the life prediction methodology must be consistent with the data reporting methodology.

#### 3.3 Definitions of Terms Specific to This Standard:

3.3.1 *applied-K curve*—a curve (a fixed-force or fixed-displacement crack-extension-force curve) obtained from a fracture mechanics analysis for a specific specimen configuration. The curve relates the stress-intensity factor to crack size and either applied force or displacement.

3.3.1.1 *Discussion*—The resulting analytical expression is sometimes called a  $K$  calibration and is frequently available in handbooks for stress-intensity factors.

3.3.2 *fatigue crack growth threshold*,  $\Delta K_{th}$   $[FL^{-3/2}]$ —that asymptotic value of  $\Delta K$  at which  $da/dN$  approaches zero. For most materials an *operational*, though arbitrary, definition of  $\Delta K_{th}$  is given as that  $\Delta K$  which corresponds to a fatigue crack growth rate of  $10^{-10}$  m/cycle. The procedure for determining this *operational*  $\Delta K_{th}$  is given in 9.4.

3.3.2.1 *Discussion*—The intent of this definition is not to define a true threshold, but rather to provide a practical means of characterizing a material's fatigue crack growth resistance in the near-threshold regime. Caution is required in extending this concept to design (see 5.1.5).

3.3.3 *fatigue crack growth rate*,  $da/dN$  or  $\Delta a/\Delta N$ ,  $[L]$ —*in fatigue*, the rate of crack extension caused by fatigue loading and expressed in terms of average crack extension per cycle.

3.3.4 *normalized K-gradient*,  $C = (1/K) \cdot dK/da$   $[L^{-1}]$ —the fractional rate of change of  $K$  with increasing crack size.

3.3.4.1 *Discussion*—When  $C$  is held constant the percentage change in  $K$  is constant for equal increments of crack size. The following identity is true for the normalized  $K$ -gradient in a constant force ratio test:

$$\frac{1}{K} \cdot \frac{dK}{da} = \frac{1}{K_{\max}} \cdot \frac{dK_{\max}}{da} = \frac{1}{K_{\min}} \cdot \frac{dK_{\min}}{da} = \frac{1}{\Delta K} \cdot \frac{d\Delta K}{da} \quad (4)$$

3.3.5 *K-decreasing test*—a test in which the value of  $C$  is nominally negative. In this test method  $K$ -decreasing tests are conducted by shedding force, either continuously or by a series of decremental steps, as the crack grows.

3.3.6 *K-increasing test*—a test in which the value of  $C$  is nominally positive. For the standard specimens in this method the constant-force-amplitude test will result in a  $K$ -increasing test where the  $C$  value increases but is always positive.

## 4. Summary of Test Method

4.1 This test method involves cyclic loading of notched specimens which have been acceptably precracked in fatigue. Crack size is measured, either visually or by an equivalent method, as a function of elapsed fatigue cycles and these data are subjected to numerical analysis to establish the rate of crack growth. Crack growth rates are expressed as a function of the stress-intensity factor range,  $\Delta K$ , which is calculated from expressions based on linear elastic stress analysis.

## 5. Significance and Use

5.1 Fatigue crack growth rate expressed as a function of crack-tip stress-intensity factor range,  $da/dN$  versus  $\Delta K$ , characterizes a material's resistance to stable crack extension under cyclic loading. Background information on the rationale for employing linear elastic fracture mechanics to analyze fatigue crack growth rate data is given in Refs (1)<sup>5</sup> and (2).

5.1.1 In innocuous (inert) environments fatigue crack growth rates are primarily a function of  $\Delta K$  and force ratio,  $R$ , or  $K_{\max}$  and  $R$  (Note 1). Temperature and aggressive environments can significantly affect  $da/dN$  versus  $\Delta K$ , and in many cases accentuate  $R$ -effects and introduce effects of other loading variables such as cycle frequency and waveform. Attention needs to be given to the proper selection and control of these variables in research studies and in the generation of design data.

NOTE 1— $\Delta K$ ,  $K_{\max}$ , and  $R$  are not independent of each other. Specification of any two of these variables is sufficient to define the loading condition. It is customary to specify one of the stress-intensity parameters ( $\Delta K$  or  $K_{\max}$ ) along with the force ratio,  $R$ .

5.1.2 Expressing  $da/dN$  as a function of  $\Delta K$  provides results that are independent of planar geometry, thus enabling exchange and comparison of data obtained from a variety of specimen configurations and loading conditions. Moreover, this feature enables  $da/dN$  versus  $\Delta K$  data to be utilized in the design and evaluation of engineering structures. The concept of similitude is assumed, which implies that cracks of differing lengths subjected to the same nominal  $\Delta K$  will advance by equal increments of crack extension per cycle.

5.1.3 Fatigue crack growth rate data are not always geometry-independent in the strict sense since thickness effects sometimes occur. However, data on the influence of thickness on fatigue crack growth rate are mixed. Fatigue crack growth rates over a wide range of  $\Delta K$  have been reported to either increase, decrease, or remain unaffected as specimen thickness is increased. Thickness effects can also interact with other variables such as environment and heat treatment. For example, materials may exhibit thickness effects over the terminal range of  $da/dN$  versus  $\Delta K$ , which are associated with either nominal yielding (Note 2) or as  $K_{\max}$  approaches the material fracture toughness. The potential influence of specimen thickness should be considered when generating data for research or design.

NOTE 2—This condition should be avoided in tests that conform to the specimen size requirements listed in the appropriate specimen annex.

5.1.4 Residual stresses can have an influence on fatigue crack growth rate behavior. The effect can be significant when test specimens are removed from material in which complete stress relief is impractical, such as weldments, as-quenched materials, and complex forged or extruded shapes. Residual stresses superimposed on the applied stress can cause the localized crack-tip stress-intensity factor to be different than that computed solely from externally applied forces. Residual stresses may lead to partly compressive stress cycles, even when the nominal applied stress range is wholly tensile, or vice versa. Irregular crack growth, namely excessive crack front curvature or out-of-plane crack growth, generally indicates that residual stresses are affecting the measured  $da/dN$  versus  $\Delta K$  relationship (4).

5.1.5 The growth rate of small fatigue cracks can differ noticeably from that of long cracks at given  $\Delta K$  values. Use of long crack data to analyze small crack growth often results in non-conservative life estimates. The small crack effect may be accentuated by environmental factors. Cracks are defined as being small when 1) their length is small compared to relevant microstructural dimension (a continuum mechanics limitation), 2) their length is small compared to the scale of local plasticity (a linear elastic fracture mechanics limitation), and 3) they are merely physically small (<1 mm). Near-threshold data established according to this method should be considered as representing the materials' steady-state fatigue crack growth rate response emanating from a long crack, one that is of sufficient length such that transition from the initiation to propagation stage of fatigue is complete. Steady-state near-threshold data, when applied to service loading histories, may result in non-conservative lifetime estimates, particularly for small cracks (5-7).

5.1.6 Crack closure can have a dominant influence on fatigue crack growth rate behavior, particularly in the near-threshold regime at low stress ratios. This implies that the conditions in the wake of the crack and prior loading history can have a bearing on the current propagation rates. The understanding of the role of the closure process is essential to such phenomena as the behavior of small cracks and the transient crack growth rate behavior during variable amplitude loading. Closure provides a mechanism whereby the cyclic stress intensity near the crack tip,  $\Delta K_{\text{eff}}$ , differs from the

<sup>5</sup> The boldface numbers in parentheses refer to the list of references at the end of this standard.

nominally applied values,  $\Delta K$ . This concept is of importance to the fracture mechanics interpretation of fatigue crack growth rate data since it implies a non-unique growth rate dependence in terms of  $\Delta K$ , and  $R$  (8).<sup>6</sup>

NOTE 3—The characterization of small crack behavior may be more closely approximated in the near-threshold regime by testing at a high stress ratio where the anomalies due to crack closure are minimized.

5.2 This test method can serve the following purposes:

5.2.1 To establish the influence of fatigue crack growth on the life of components subjected to cyclic loading, provided data are generated under representative conditions and combined with appropriate fracture toughness data (for example, see Test Method E 399), defect characterization data, and stress analysis information (9, 10).

NOTE 4—Fatigue crack growth can be significantly influenced by load history. During variable amplitude loading, crack growth rates can be either enhanced or retarded (relative to steady-state, constant-amplitude growth rates at a given  $\Delta K$ ) depending on the specific loading sequence. This complicating factor needs to be considered in using constant-amplitude growth rate data to analyze variable amplitude fatigue problems (11).

5.2.2 To establish material selection criteria and inspection requirements for damage tolerant applications.

5.2.3 To establish, in quantitative terms, the individual and combined effects of metallurgical, fabrication, environmental, and loading variables on fatigue crack growth.

**6. Apparatus**

6.1 *Grips and Fixtures*—Grips and fixturing required for the specimens outlined in this method are described in the appropriate specimen annex.

6.2 *Alignment of Grips*—It is important that attention be given to achieving good alignment in the force train through careful machining of all gripping fixtures. Misalignment can cause non-symmetric cracking, particularly for critical applications such as near-threshold testing, which in turn may lead to invalid data (see Sec. 8.3.4, 8.8.3). If non-symmetric cracking occurs, the use of a strain-gaged specimen to identify and minimize misalignment might prove useful. One method to identify bending under tensile loading conditions is described in Practice E 1012. Another method which specifically addresses measurement of bending in pin-loaded specimen configurations is described in Ref (13). For tension-compression loading the length of the force train (including the hydraulic actuator) should be minimized, and rigid, non-rotating joints should be employed to reduce lateral motion in the force train.

**7. Specimen Configuration, Size, and Preparation**

7.1 *Standard Specimens*—Details of the test specimens outlined in this method are furnished as separate annexes to this method. Notch and precracking details for the specimens are given in Fig. 1.

7.1.1 For specimens removed from material for which complete stress relief is impractical (see 5.1.4), the effect of residual stresses on the crack propagation behavior can be

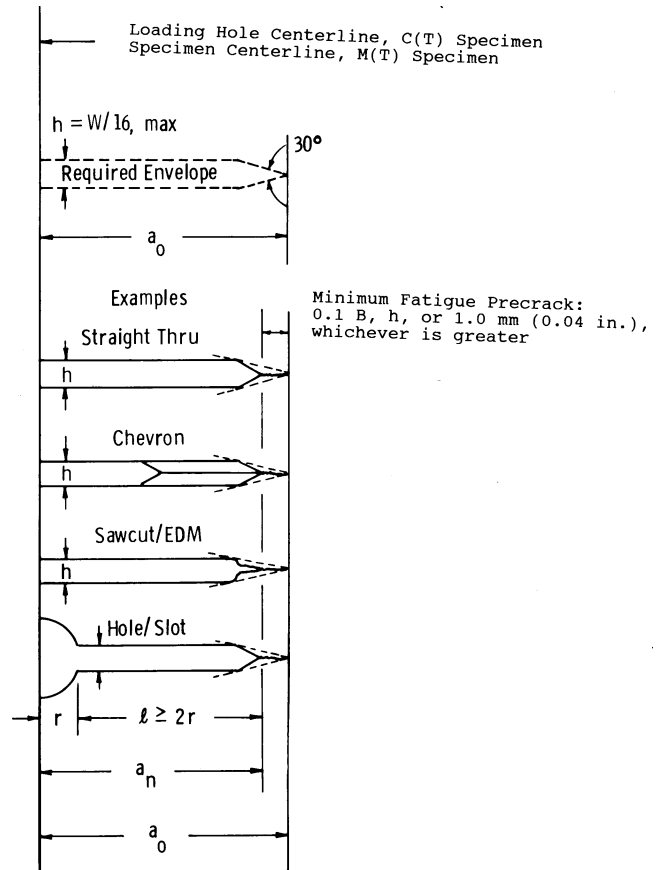


FIG. 1 Notch Details and Minimum Fatigue Precracking Requirements

minimized through the careful selection of specimen shape and size. By selecting a small ratio of specimen dimensions,  $B/W$  the effect of a through-the-thickness distribution of residual stresses acting perpendicular to the direction of crack growth can be reduced. This choice of specimen shape minimizes crack curvature or other crack front irregularities which confuse the calculation of both  $da/dN$  and  $\Delta K$ . Residual stresses acting parallel to the direction of crack growth can produce moments about the cracktip which also confound test results. These residual stresses can be minimized by selecting symmetrical specimen configurations, that is, the M(T) specimen, for the evaluation of the material's crack growth behavior.

7.2 *Specimen Size*—In order for results to be valid according to this test method it is required that the specimen be predominantly elastic at all values of applied force. The minimum in-plane specimen sizes to meet this requirement are based primarily on empirical results and are specific to the specimen configuration as furnished in the appropriate specimen annex (10).

NOTE 5—The size requirements described in the various specimen annexes are appropriate for low-strain hardening materials ( $\sigma_{ULT}/\sigma_{YS} \leq 1.3$ ) (14) and for high-strain hardening materials ( $\sigma_{ULT}/\sigma_{YS} \geq 1.3$ ) under certain conditions of force ratio and temperature (15, 16) (where  $\sigma_{ULT}$  is the ultimate tensile strength of the material). However, under other conditions of force ratio and temperature, the requirements listed in the annexes appear to be overly restrictive—that is, they require specimen sizes which are larger than necessary (17,18). Currently, the conditions giving rise to each of these two regimes of behavior are not clearly defined.

<sup>6</sup> Subcommittee E08.06 has initiated a study group activity on crack closure measurement and analysis. Reference (8) provides basic information on this subject.

7.2.1 An alternative size requirement may be employed for high-strain hardening materials as follows. The uncracked ligament requirement listed for the specific specimen geometry may be relaxed by replacing  $\sigma_{YS}$  with a higher, effective yield strength which accounts for the material strain hardening capacity. For purposes of this test method, this *effective* yield strength, termed flow strength, is defined as follows:

$$\sigma_{FS} = (\sigma_{YS} + \sigma_{ULT})/2 \quad (5)$$

However, it should be noted that the use of this alternative size requirement allows mean plastic deflections to occur in the specimen. These mean deflections under certain conditions, as noted previously, can accelerate growth rates by as much as a factor of two. Although these data will generally add conservatism to design or structural reliability computations, they can also confound the effects of primary variables such as specimen thickness (if  $B/W$  is maintained constant), force ratio, and possibly environmental effects. Thus, when the alternative size requirement is utilized, it is important to clearly distinguish between data that meet the yield strength or flow strength criteria. In this way, data will be generated that can be used to formulate a specimen size requirement of general utility.

7.3 *Notch Preparation*—The machined notch for standard specimens may be made by electrical-discharge machining (EDM), milling, broaching, or sawcutting. The following notch preparation procedures are suggested to facilitate fatigue precracking in various materials:

7.3.1 *Electric Discharge Machining*— $\rho < 0.25$  mm (0.010 in.) ( $\rho$  = notch root radius), high-strength steels ( $\sigma_{YS} \geq 1175$  MPa/170 ksi), titanium and aluminum alloys.

7.3.2 *Mill or Broach*— $\rho \leq 0.075$  mm (0.003 in.), low or medium-strength steels ( $\sigma_{YS} \leq 1175$  MPa/170 ksi), aluminum alloys.

7.3.3 *Grind*— $\rho \leq 0.25$  mm (0.010 in.), low or medium-strength steels.

7.3.4 *Mill or Broach*— $\rho \leq 0.25$  mm (0.010 in.), aluminum alloys.

7.3.5 *Sawcut*—Recommended only for aluminum alloys.

7.3.6 Examples of various machined-notch geometries and associated precracking requirements are given in Fig. 1 (see 8.3).

7.3.7 When residual stresses are suspected of being present (see 5.1.4), local displacement measurements made before and after machining the crack starter notch are useful for detecting the potential magnitude of the effect. A simple mechanical displacement gage can be used to measure distance between two hardness indentations at the mouth of the notch (4). Limited data show that for aluminum alloys when these mechanical displacement measurements change by more than 0.05 mm (0.002 in.), fatigue crack growth rates can be changed significantly.

## 8. Procedure

8.1 *Number of Tests*—At crack growth rates greater than  $10^{-8}$  m/cycle, the within-lot variability (neighboring specimens) of  $da/dN$  at a given  $\Delta K$  typically can cover about a factor of two (19). At rates below  $10^{-8}$  m/cycle, the variability in  $da/dN$  may increase to about a factor of five or more due to increased sensitivity of  $da/dN$  to small variations in  $\Delta K$ . This

scatter may be increased further by variables such as microstructural differences, residual stresses, changes in crack tip geometry (crack branching) or near tip stresses as influenced for example by crack roughness or product wedging, force precision, environmental control, and data processing techniques. These variables can take on added significance in the low crack growth rate regime ( $da/dN < 10^{-8}$  m/cycle). In view of the operational definition of the threshold stress-intensity (see 3.3.2 and 9.4), at or near threshold it is more meaningful to express variability in terms of  $\Delta K$  rather than  $da/dN$ . It is good practice to conduct replicate tests; when this is impractical, multiple tests should be planned such that regions of overlapping  $da/dN$  versus  $\Delta K$  data are obtained, particularly under both  $K$ -increasing and  $K$ -decreasing conditions. Since confidence in inferences drawn from the data increases with number of tests, the desired number of tests will depend on the end use of the data.

8.2 *Specimen Measurements*—The specimen dimensions shall be within the tolerances given in the appropriate specimen annex.

8.3 *Fatigue Precracking*—The importance of precracking is to provide a sharpened fatigue crack of adequate size and straightness (also symmetry for the M(T) specimen) which ensures that 1) the effect of the machined starter notch is removed from the specimen  $K$ -calibration, and 2) the effects on subsequent crack growth rate data caused by changing crack front shape or precrack load history are eliminated.

8.3.1 Conduct fatigue precracking with the specimen fully heat treated to the condition in which it is to be tested. The precracking equipment shall be such that the force distribution is symmetrical with respect to the machined notch and  $K_{max}$  during precracking is controlled to within  $\pm 5\%$ . Any convenient loading frequency that enables the required force accuracy to be achieved can be used for precracking. The machined notch plus the precrack must lie within the envelope, shown in Fig. 1, that has as its apex the end of the fatigue precrack. In addition the fatigue precrack shall not be less than  $0.10B$ ,  $h$ , or 1.0 mm (0.040 in.), whichever is greater (Fig. 1).

8.3.2 The final  $K_{max}$  during precracking shall not exceed the initial  $K_{max}$  for which test data are to be obtained. If necessary, forces corresponding to higher  $K_{max}$  values may be used to initiate cracking at the machined notch. In this event, the force range shall be stepped-down to meet the above requirement. Furthermore, it is suggested that reduction in  $P_{max}$  for any of these steps be no greater than 20% and that measurable crack extension occur before proceeding to the next step. To avert transient effects in the test data, apply the force range in each step over a crack size increment of at least  $(3/\pi)(K'_{max}/\sigma_{YS})^2$ , where  $K'_{max}$  is the terminal value of  $K_{max}$  from the previous forcestep. If  $P_{min}/P_{max}$  during precracking differs from that used during testing, see the precautions described in 8.5.1.

8.3.3 For the  $K$ -decreasing test procedure, prior loading history may influence near-threshold growth rates despite the precautions of 8.3.2. It is good practice to initiate fatigue cracks at the lowest stress intensity possible. Precracking growth rates less than  $10^{-8}$  m/cycle are suggested. A compressive force, less than or equal to the precracking force, may facilitate fatigue precracking and may diminish the influence of

the  $K$ -decreasing test procedure on subsequent fatigue crack growth rate behavior.

8.3.4 Measure the crack sizes on the front and back surfaces of the specimen to within 0.10 mm (0.004 in.) or  $0.002W$ , whichever is greater. For specimens where  $W > 127$  mm (5 in.), measure crack size to within 0.25 mm (0.01 in.). If crack sizes measured on front and back surfaces differ by more than  $0.25B$ , the pre-cracking operation is not suitable and subsequent testing would be invalid under this test method. In addition for the M(T) specimen, measurements referenced from the specimen centerline to the two cracks (for each crack use the average of measurements on front and back surfaces) shall not differ by more than  $0.025W$ . If the fatigue crack departs more than the allowable limit from the plane of symmetry (see 8.8.3) the specimen is not suitable for subsequent testing. If the above requirements cannot be satisfied, check for potential problems in alignment of the loading system and details of the machined notch.

8.4 *Test Equipment*—The equipment for fatigue testing shall be such that the force distribution is symmetrical to the specimen notch.

8.4.1 Verify the force cell in the test machine in accordance with Practices E 4 and E 467. Conduct testing such that both  $\Delta P$  and  $P_{\max}$  are controlled to within  $\pm 2\%$  throughout the test.

8.4.2 An accurate digital device is required for counting elapsed cycles. A timer is a desirable supplement to the counter and provides a check on the counter. Multiplication factors (for example,  $\times 10$  or  $\times 100$ ) should not be used on counting devices when obtaining data at growth rates above  $10^{-5}$  m/cycle since they can introduce significant errors in the growth rate determination.

8.5 *Constant-Force-Amplitude Test Procedure for  $da/dN > 10^{-8}$  m/cycle*—This test procedure is well suited for fatigue crack growth rates above  $10^{-8}$  m/cycle. However, it becomes increasingly difficult to use as growth rates decrease below  $10^{-8}$  m/cycle because of precracking considerations (see 8.3.3). (A  $K$ -decreasing test procedure which is better suited for rates below  $10^{-8}$  m/cycle is provided in 8.6.) When using the constant-force-amplitude procedure it is preferred that each specimen be tested at a constant force range ( $\Delta P$ ) and a fixed set of loading variables (stress ratio and frequency). However, this may not be feasible when it is necessary to generate a wide range of information with a limited number of specimens. When loading variables are changed during a test, potential problems arise from several types of transient phenomenon (20). The following test procedures should be followed to minimize or eliminate transient effects while using this  $K$ -increasing test procedure.

8.5.1 If force range is to be incrementally varied it should be done such that  $P_{\max}$  is increased rather than decreased to preclude retardation of growth rates caused by overload effects; retardation being a more pronounced effect than accelerated crack growth associated with incremental increase in  $P_{\max}$ . Transient growth rates are also known to result from changes in  $P_{\min}$  or  $R$ . Sufficient crack extension should be allowed following changes in force to enable the growth rate to establish a steady-state value. The amount of crack growth that is required depends on the magnitude of force change and on

the material. An incremental increase of 10% or less will minimize these transient growth rates.

8.5.2 When environmental effects are present, changes in force level, test frequency, or waveform can result in transient growth rates. Sufficient crack extension should be allowed between changes in these loading variables to enable the growth rate to achieve a steady-state value.

8.5.3 Transient growth rates can also occur, in the absence of loading variable changes, due to long-duration test interruptions, for example, during work stoppages. In this case, data should be discarded if the growth rates following an interruption are less than those before the interruption.

8.6 *K-Decreasing Procedure for  $da/dN < 10^{-8}$  m/cycle*—This procedure is started by cycling at a  $\Delta K$  and  $K_{\max}$  level equal to or greater than the terminal precracking values. Subsequently, forces are decreased (shed) as the crack grows, and test data are recorded until the lowest  $\Delta K$  or crack growth rate of interest is achieved. The test may then be continued at constant force limits to obtain comparison data under  $K$ -increasing conditions. The  $K$ -decreasing procedure is not recommended at fatigue crack growth rates above  $10^{-8}$  m/cycle since prior loading history at such associated  $\Delta K$  levels may influence the near-threshold fatigue crack growth rate behavior.

8.6.1 Force shedding during the  $K$ -decreasing test may be conducted as decreasing force steps at selected crack size intervals, as shown in Fig. 2. Alternatively, the force may be shed in a continuous manner by an automated technique (for example, by use of an analog computer or digital computer, or both) (21).

8.6.2 The rate of force shedding with increasing crack size shall be gradual enough to 1) preclude anomalous data resulting from reductions in the stress-intensity factor and concomitant transient growth rates, and 2) allow the establishment of about five  $da/dN$ ,  $\Delta K$  data points of approximately equal spacing per decade of crack growth rate. The above requirements can be met by limiting the normalized  $K$ -gradient,  $C = 1/K \cdot dK/da$ , to a value algebraically equal to or greater than  $-0.08 \text{ mm}^{-1}$  ( $-2 \text{ in.}^{-1}$ ). That is:

$$C = \left(\frac{1}{K}\right) \cdot \left(\frac{dK}{da}\right) > -0.08 \text{ mm}^{-1} \text{ } (-2 \text{ in.}^{-1}) \quad (6)$$

When forces are incrementally shed, the requirements on  $C$  correspond to the nominal  $K$ -gradient depicted in Fig. 2.

NOTE 6—Acceptable values of  $C$  may depend on load ratio, test material, and environment. Values of  $C$  algebraically greater than that indicated above have been demonstrated as acceptable for use in decreasing  $K$  tests of several steel alloys and aluminum alloys tested in laboratory air over a wide range of force ratios (14, 21).

8.6.3 If the normalized  $K$ -gradient  $C$  is algebraically less than that prescribed in 8.6.2, the procedure shall consist of decreasing  $K$  to the lowest growth rate of interest followed by a  $K$ -increasing test at a constant  $\Delta P$  (conducted in accordance with 8.5). Upon demonstrating that data obtained using  $K$ -increasing and  $K$ -decreasing procedures are equivalent for a given set of test conditions, the  $K$ -increasing testing may be eliminated from all replicate testing under these same test conditions.

NOTE 7—It is good practice to have  $K$ -decreasing followed by

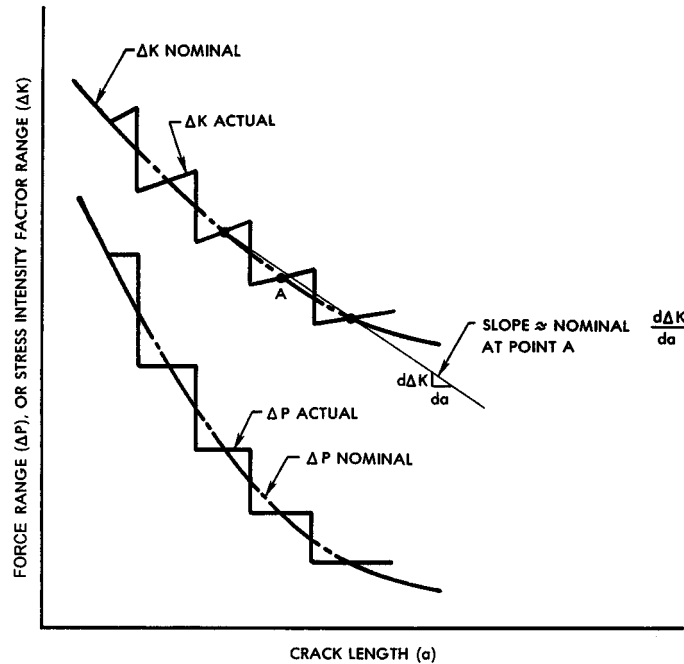


FIG. 2 Typical *K* Decreasing Test by Stepped Force Shedding

*K*-increasing data for the first test of any single material regardless of the *C* value used.

8.6.4 It is recommended that the force ratio, *R*, and *C* be maintained constant during *K*-decreasing testing (see 8.7.1 for exceptions to this recommendation).

8.6.5 The relationships between *K* and crack size and between force and crack size for a constant-*C* test are given as follows:

8.6.5.1  $\Delta K = \Delta K_o \exp[C(a - a_o)]$ , where  $\Delta K_o$  is the initial  $\Delta K$  at the start of the test, and  $a_o$  is the corresponding crack size. Because of the identities given in 5.1.1 (Note 1) and in the Definitions 3.2.14, the above relationship is also true for  $K_{max}$  and  $K_{min}$ .

8.6.5.2 The force histories for the standard specimens of this test method are obtained by substituting the appropriate *K*-calibrations given in the respective specimen annex into the above expression.

8.6.6 When employing step shedding of force, as in Fig. 2, the reduction in  $P_{max}$  of adjacent force steps shall not exceed 10 % of the previous  $P_{max}$ . Upon adjustment of maximum force from  $P_{max1}$  to a lower value,  $P_{max2}$ , a minimum crack extension of 0.50 mm (0.02 in.) is recommended.

8.6.7 When employing continuous shedding of force, the requirement of 8.6.6 is waived. Continuous force shedding is defined as  $(P_{max1} - P_{max2})/P_{max1} \leq 0.02$ .

8.7 *Alternative K-control test procedures*—Ideally, it is desirable to generate  $da/dN$ ,  $\Delta K$  data at *K*-gradients independent of the specimen geometry (22). Exercising control over this *K*-gradient allows much steeper gradients for small values of  $a/W$  without the undesirable feature of having too steep a *K*-gradient at the larger values of  $a/W$  associated with constant amplitude loading. Generating data at an appropriate *K*-gradient, using a constant and positive value of the *K*-gradient parameter, *C*, (see 8.6.2) provides numerous advantages: the test time is reduced; the  $da/dN$ - $\Delta K$  data can be

evenly distributed without using variable  $\Delta a$  increments; a wider range of data may be generated without incremental force increases; the *K*-gradient is independent of the specimen geometry.

8.7.1 Situations may arise where changing  $\Delta K$  under conditions of constant  $K_{max}$  or constant  $K_{mean}$  may be more representative than under conditions of constant *R*. The application of the test data should be considered in choosing an appropriate mode of *K*-control. For example, a more conservative estimate of near-threshold behavior may be obtained by using this test method. This process effectively measures near-threshold data at a high stress ratio.

8.8 *Measurement of Crack Size*—Make fatigue crack size measurements as a function of elapsed cycles by means of a visual, or equivalent, technique capable of resolving crack extensions of 0.10 mm (0.004 in.), or 0.002*W*, whichever is greater. For visual measurements, polishing the test area of the specimen and using indirect lighting aid in the resolution of the crack-tip. It is suggested that, prior to testing, reference marks be applied to the test specimen at predetermined locations along the direction of cracking. Crack size can then be measured using a low power (20 to 50×) traveling microscope. Using the reference marks eliminates potential errors due to accidental movement of the traveling microscope. If precision photographic grids or polyester scales are attached to the specimen, crack size can be determined directly with any magnifying device that gives the required resolution. It is preferred that measurements be made without interrupting the test.

NOTE 8—Interruption of cyclic loading for the purpose of crack size measurement can be permitted providing strict care is taken to avoid introducing any significant extraneous damage (for example, creep deformation) or transient crack extension (for example, growth under static force). The interruption time should be minimized (less than 10 min.) and if a static force is maintained for the purpose of enhanced crack tip

resolution, it should be carefully controlled. A static force equal to the fatigue mean force is probably acceptable (with high temperatures and corrosive environments, even mean levels should be questioned) but in no case should the static force exceed the maximum force applied during the fatigue test.

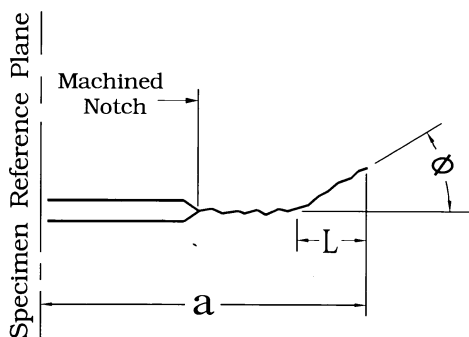
8.8.1 Make crack size measurements at intervals such that  $da/dN$  data are nearly evenly distributed with respect to  $\Delta K$ . Recommended intervals are given in the appropriate specimen annex.

8.8.1.1 A minimum  $\Delta a$  of 0.25 mm (0.01 in.) is recommended. However, situations may arise where the  $\Delta a$  needs to be reduced below 0.25 mm (0.01 in.). Such is the case for threshold testing where it is required that at least five  $da/dN$ ,  $\Delta K$  data points in the near-threshold regime (see 9.4.3). In any case, the minimum  $\Delta a$  shall be ten times the crack size measurement precision.

NOTE 9—The crack size measurement precision is herein defined as the standard deviation on the mean value of crack size determined for a set of replicate measurements.

8.8.2 As a rule, crack size measurements should be made on both sides (front and back) of a specimen to ensure that the crack symmetry requirements of 8.8.3 are met. The average value of the measurements (two crack lengths for the C(T) specimen and four crack lengths for the M(T) specimen) should be used in all calculations of growth rate and  $K$ . If crack size measurements are not made on both sides at every crack size interval, the interval of both-side measurement must be reported. Measurement on only one side is permissible only if previous experience with a particular specimen configuration, test material, testing apparatus, and growth rate regime has shown that the crack symmetry requirements are met consistently.

8.8.3 If at any point in the test the crack deviates more than  $\pm 20^\circ$  from the plane of symmetry over a distance of  $0.1W$  or greater, the data are invalid according to this test method (23). A deviation between  $\pm 10^\circ$  and  $\pm 20^\circ$  must be reported. (See Fig. 3) In addition, data are invalid if (1) crack sizes measured on front and back surfaces differ by more than  $0.25B$ . Additional validity requirements may be included in the specimen annexes.



Valid if  $\phi \leq 10^\circ$   
 Report if  $10^\circ < \phi \leq 20^\circ$   
 Invalid if  $\phi > 20^\circ$  for  $L \geq 0.1W$

FIG. 3 Out-of-Plane Cracking Limits

NOTE 10—The requirements on out-of-plane cracking are commonly violated for large-grained or single-crystal materials. In these instances, results from anisotropic, mixed-mode stress analyses may be needed to compute  $K$ ; (for example, see Ref. (24)).

NOTE 11—Crack tip branching has been noted to occur. This characteristic is not incorporated into the computation of  $\Delta K$ . As a result, crack branching, or bifurcating, may be a source of variability in measured fatigue crack growth rate data. Data recorded during branching must be noted as being for a branching crack.

8.8.3.1 If nonvisual methods for crack size measurement are used and nonsymmetric or angled cracking occurs, the nonvisual measurements derived during these periods shall be verified with visual techniques to ensure the requirements of 8.8.3 are satisfied.

9. Calculation and Interpretation of Results

9.1 Crack Curvature Correction—After completion of testing, examine the fracture surfaces, preferably at two locations (for example, at the precrack and terminal fatigue crack sizes), to determine the extent of through-thickness crack curvature (commonly termed *crack tunneling*). If a crack contour is visible, calculate a three-point, through-thickness average crack size in accordance with Test Method E 399, sections on General Procedure related to Specimen Measurement; specifically the paragraph on crack size measurement. The difference between the average through-thickness crack size and the corresponding crack size recorded during the test (for example, if visual measurements were obtained this might be the average of the surface crack size measurements) is the crack curvature correction.

9.1.1 If the crack curvature correction results in a greater than 5 % difference in calculated stress-intensity factor at any crack size, then employ this correction when analyzing the recorded test data.

9.1.2 If the magnitude of the crack curvature correction either increases or decreases with crack size, use a linear interpolation to correct intermediate data points. Determine this linear correction from two distinct crack contours separated by a minimum spacing of  $0.25W$  or  $B$ , whichever is greater. When there is no systematic variation of crack curvature with crack size, employ a uniform correction determined from an average of the crack contour measurements.

9.1.3 When employing a crack size monitoring technique other than visual, a crack curvature correction is generally incorporated in the calibration of the technique. However, since the magnitude of the correction will probably depend on specimen thickness, the preceding correction procedures may also be necessary.

9.2 Determination of Crack Growth Rate—The rate of fatigue crack growth is to be determined from the crack size versus elapsed cycles data ( $a$  versus  $N$ ). Recommended approaches which utilize the secant or incremental polynomial methods are given in Appendix X1. Either method is suitable for the  $K$ -increasing, constant  $\Delta P$  test. For the  $K$ -decreasing tests where force is shed in decremental steps, as in Fig. 2, the secant method is recommended. A crack growth rate determination shall not be made over any increment of crack extension that includes a force step. Where shedding of  $K$  is performed continuously with each cycle by automation, the incremental polynomial technique is applicable.

NOTE 12—Both recommended methods for processing  $a$  versus  $N$  data are known to give the same average  $da/dN$  response. However, the secant method often results in increased scatter in  $da/dN$  relative to the incremental polynomial method, since the latter numerically “smooths” the data (19, 25). This apparent difference in variability introduced by the two methods needs to be considered, especially in utilizing  $da/dN$  versus  $\Delta K$  data in design.

9.3 *Determination of Stress-Intensity Factor Range,  $\Delta K$* —Use the appropriate crack size values as described in the particular specimen annex to calculate the stress-intensity range corresponding to a given crack growth rate.

9.4 *Determination of a Fatigue Crack Growth Threshold*—The following procedure provides an operational definition of the threshold stress-intensity factor range for fatigue crack growth,  $\Delta K_{th}$ , which is consistent with the general definition of 3.3.2.

9.4.1 Determine the best-fit straight line from a linear regression of  $\log da/dN$  versus  $\log \Delta K$  using a minimum of five  $da/dN$ ,  $\Delta K$  data points of approximately equal spacing between growth rates of  $10^{-9}$  and  $10^{-10}$  m/cycle. Having specified the range of fit in terms of  $da/dN$  requires that  $\log \Delta K$  be the dependent variable in establishing this straight line fit.

NOTE 13—Limitations of the linear regression approach of 9.4.1 are described in Ref (28). Alternative nonlinear approaches and their advantages are also given in Ref (28).

9.4.2 Calculate the  $\Delta K$ -value that corresponds to a growth rate of  $10^{-10}$  m/cycle using the above fitted line; this value of  $\Delta K$  is defined as  $\Delta K_{th}$  according to the operational definition of this test method.

NOTE 14—In the event that lower  $da/dN$  data are generated, the above procedure can be used with the lowest decade of data. This alternative range of fit must then be specified according to 10.1.12.

## 10. Report

10.1 The report shall include the following information:

10.1.1 Specimen type, including thickness,  $B$ , and width,  $W$ . If the M(T) specimen is used, or if a specimen type not described in this test method is used shall be provided.

10.1.2 Description of the test machine and equipment used to measure crack size and the precision with which crack size measurements were made.

10.1.3 Test material characterization in terms of heat treatment, chemical composition, and mechanical properties (include at least the 0.2 % offset yield strength and either elongation or reduction in area measured in accordance with Test Methods E 8). Product size and form (for example, sheet, plate, and forging) shall also be identified. Method of stress relief, if applicable, shall be reported. For thermal methods, details of time, temperature and atmosphere. For non-thermal methods, details of forces and frequencies.

10.1.4 The crack plane orientation according to the code given in Test Method E 399. In addition, if the specimen is removed from a large product form, its location with respect to the parent product shall be given.

10.1.5 The terminal values of  $\Delta K$ ,  $R$  and crack size from fatigue precracking. If precrack forces were stepped-down, the procedure employed shall be stated and the amount of crack extension at the final force level shall be given.

10.1.6 Test loading variables, including  $\Delta P$ ,  $R$ , cyclic fre-

quency, and cyclic waveform.

10.1.7 Environmental variables, including temperature, chemical composition, pH (for liquids), and pressure (for gases and vacuum). For tests in air, the relative humidity as determined by Test Method E 337 shall be reported. For tests in inert reference environments, such as dry argon, estimates of residual levels of water and oxygen in the test environment (generally this differs from the analysis of residual impurities in the gas supply cylinder) shall be given. Nominal values for all of the above environmental variables, as well as maximum deviations throughout the duration of testing, shall be reported. Also, the material employed in the chamber used to contain the environment and steps taken to eliminate chemical/electrochemical reactions between the specimen-environment system and the chamber shall be described.

10.1.8 Analysis methods applied to the data, including the technique used to convert  $a$  versus  $N$  to  $da/dN$ , specific procedure used to correct for crack curvature, and magnitude of crack curvature correction.

10.1.9 The specimen  $K$ -calibration and size criterion to ensure predominantly elastic behavior (for specimens not described in this test method).

10.1.10  $da/dN$  as a function of  $\Delta K$  shall be plotted. (It is recommended that  $\Delta K$  be plotted on the abscissa and  $da/dN$  on the ordinate. Log-log coordinates are commonly used. For optimum data comparisons, the size of the  $\Delta K$ -log cycles should be two or three times larger than  $da/dN$ -log cycles.) All data that violate the size requirements of the appropriate specimen annex shall be identified; state whether  $\sigma_{YS}$  or  $\sigma_{FS}$  was used to determine specimen size.

NOTE 15—The definition of  $\sigma_{FS}$  is provided in 7.2.1.

10.1.11 Description of any occurrences that appear to be related to anomalous data (for example, transients following test interruptions or changes in loading variables).

10.1.12 For  $K$ -decreasing tests, report  $C$  and initial values of  $K$  and  $a$ . Indicate whether or not the  $K$ -decreasing data were verified by  $K$ -increasing data. For near-threshold growth rates, report  $\Delta K_{th}$ , the equation of the fitted line (see 9.4) used to establish  $\Delta K_{th}$ , and any procedures used to establish  $\Delta K_{th}$  which differ from the operational definition of 9.4. Also report the lowest growth rate used to establish  $\Delta K_{th}$  using the operational definition of 9.4. It is recommended that these values be reported as  $\Delta K_{th}(x)$  where  $x$  is the aforementioned lowest growth rate in m/cycle.

10.1.13 The following information shall be tabulated for each test:  $a$ ,  $N$ ,  $\Delta K$ ,  $da/dN$ , and, where applicable, the test variables of 10.1.3, 10.1.6, and 10.1.7. Also, all data determined from tests on specimens that violate the size requirements of the appropriate specimen annex shall be identified; state whether  $\sigma_{YS}$  or  $\sigma_{FS}$  was used to determine specimen size.

## 11. Precision and Bias

11.1 *Precision*—The precision of  $da/dN$  versus  $\Delta K$  is a function of inherent material variability, as well as errors in measuring crack size and applied force. The required loading precision of 8.4.1 can be readily obtained with modern closed-loop electrohydraulic test equipment and results in a  $\pm 2$  % variation in the applied  $\Delta K$ ; this translates to a  $\pm 4$  % to

$\pm 10\%$  variation in  $da/dN$ , at a given  $\Delta K$ , for growth rates above the near-threshold regime. However, in general, the crack size measurement error makes a more significant contribution to the variation in  $da/dN$ , although this contribution is difficult to isolate since it is coupled to the analysis procedure for converting  $a$  versus  $N$  to  $da/dN$ , and to the inherent material variability. Nevertheless, it is clear that the overall variation in  $da/dN$  is dependent on the ratio of crack size measurement interval to measurement error (25, 29). Furthermore, an optimum crack size measurement interval exists due to the fact that the interval should be large compared to the measurement error (or precision), but small compared to the  $K$ -gradient of the test specimen. These considerations form the basis for the recommended measurement intervals as given in the appropriate specimen annex. Recommendations are specified relative to crack size measurement precision: a quantity that must be empirically established for the specific measurement technique being employed.

11.1.1 Although it is often impossible to separate the contributions from each of the above-mentioned sources of variability, an overall measure of variability in  $da/dN$  versus  $\Delta K$  is available from results of an interlaboratory test program in which 14 laboratories participated (19).<sup>7</sup> These data, obtained on a highly homogeneous 10 Ni steel, showed the reproducibility in  $da/dN$  within a laboratory to average  $\pm 27\%$  and range from  $\pm 13$  to  $\pm 50\%$ , depending on laboratory; the repeatability between laboratories was  $\pm 32\%$ . Values cited are standard errors based on  $\pm 2$  residual standard deviations about the mean response determined from regression analysis. In computing these statistics, abnormal results from two laboratories were not considered due to improper precracking and suspected errors in force calibration. Such problems would be avoided by complying with the current requirements of this test method as they have been upgraded since the interlaboratory test program was conducted. Because a highly homogeneous

material was employed in this program, the cited variabilities in  $da/dN$  are believed to have arisen primarily from random crack size measurement errors.

11.1.2 For the near-threshold regime, a measure of the variability in  $\Delta K_{th}$  is available from the results of an interlaboratory test program in which 15 laboratories participated (30).<sup>8</sup> These data, obtained on a homogeneous 2219 T851 aluminum alloy, show a reproducibility in  $\Delta K_{th}$  within a laboratory to average  $\pm 3\%$  with the repeatability between laboratories of  $\pm 9\%$ . This observation is based on the 11 laboratories that provided valid near-threshold data. Because of the sensitivity of  $da/dN$  to small changes in  $\Delta K$ , growth rates in this near threshold regime often vary by an order of magnitude, or more, at a given  $\Delta K$  (30).<sup>7</sup>

11.1.3 It is important to recognize that for purposes of design or reliability assessment, inherent material variability often becomes the primary source of variability in  $da/dN$ . The variability associated with a given lot of material is caused by inhomogeneities in chemical composition, microstructure, or both. These same factors coupled with varying processing conditions give rise to further lot-to-lot variabilities. An assessment of inherent material variability, either within or between heats or lots, can only be determined by conducting a statistically planned test program on the material of interest. Thus, results cited above from the interlaboratory test programs on 10 Ni steel and 2219-T851 aluminum, materials selected to minimize material variability and therefore allow an assessment of measurement precision, are not generally applicable to questions regarding inherent variability in other materials.

11.2 *Bias*—There is no accepted “standard” value for  $da/dN$  versus  $\Delta K$  for any material. In the absence of such a true value, no meaningful statement can be made concerning bias of data.

## 12. Keywords

12.1 constant amplitude; crack size; fatigue crack growth rate; stress intensity factor range

<sup>7</sup> Supporting data available from ASTM Headquarters. Request RR: E-24-1001.

<sup>8</sup> Supporting data available from ASTM Headquarters. Request RR: E-24-1009.

## ANNEXES

### (Mandatory Information)

#### A1. THE COMPACT TENSION SPECIMEN

##### A1.1 Introduction

A1.1.1 The compact tension specimen, C(T), is a single edge-notch specimen loaded in tension.

A1.1.2 The C(T) specimen has the advantage over many other specimen types in that it requires the least amount of test material to evaluate crack growth behavior.

A1.1.3 The C(T) specimen is not recommended for tension-compression testing because of uncertainties introduced into the loading experienced at the crack tip.

A1.1.4 The C(T) specimen is not recommended for materials that utilize a whisker-type of discontinuous reinforcement and are anisotropic in nature; rather, the M(T) or ESE(T)

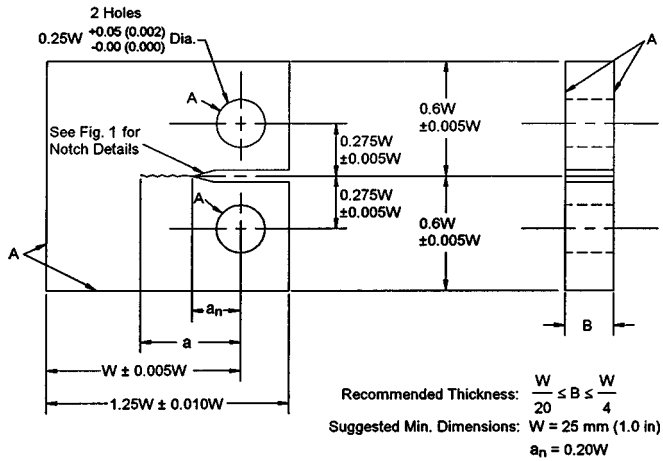
specimens should be used.<sup>9</sup>

##### A1.2 Specimen

A1.2.1 The geometry of the standard C(T) specimen is given in Fig. A1.1.

A1.2.2 The thickness,  $B$ , and width,  $W$ , may be varied independently within the following limits, which are based on specimen buckling and through-thickness crack-curvature considerations:

<sup>9</sup> Subcommittee E08.09 has performed an interlaboratory test program on a material of this type. Reference (106) provided the results of this effort.



- NOTE 1—Dimensions are in millimetres (inches).
- NOTE 2—A-surfaces shall be perpendicular and parallel as applicable to within ±0.002 W, TIR.
- NOTE 3—The intersection of the tips of the machined notch ( $a_n$ ) with the specimen faces shall be equally distant from the top and bottom edges of the specimen to within 0.005 W.
- NOTE 4—Surface finish, including holes, shall be 0.8 (32) or better.

**FIG. A1.1 Standard Compact-Tension C(T) Specimen for Fatigue Crack Growth Rate Testing**

A1.2.2.1 For C(T) specimens it is recommended that thickness be within the range  $W/20 \leq B \leq W/4$ . Specimens having thicknesses up to and including  $W/2$  may also be employed; however, data from these specimens will often require through-thickness crack curvature corrections as listed in Section 9.1 of the main body of E 647. In addition, difficulties may be encountered in meeting the through-thickness crack straightness requirements listed in Section 8 *Procedure* section of the main body of E 647.

A1.2.3 In the C(T) specimen (Fig. A1.1),  $a$  is measured from the line connecting the bearing points of force application.

A1.2.4 It is required that the machined notch,  $a_n$ , in the C(T) specimen be at least  $0.2W$  in length so that the  $K$ -calibration is not influenced by small variations in the location and dimensions of the loading-pin holes.

A1.2.5 Notch and precracking details for the C(T) specimen are given in Fig. 1 of the main body of E 647.

A1.2.6 *Specimen Size*—In order for results to be valid according to this test method it is required that the specimen be predominantly elastic at all values of applied force. The minimum in-plane specimen sizes to meet this requirement are based primarily on empirical results and are specific to specimen configuration (10).

A1.2.6.1 For the C(T) specimen the following is required:

$$(W - a) \geq (4/\pi)(K_{max}/\sigma_{YS})^2 \quad (A1.1)$$

where:

$(W - a)$  = specimen's uncracked ligament (Fig. A1.1), and

$\sigma_{YS}$  = 0.2 % offset yield strength determined at the same temperature as used when measuring the fatigue crack growth rate data.

NOTE A1.1—For high-strain hardening materials, see Note 5 of the main body of E 647.

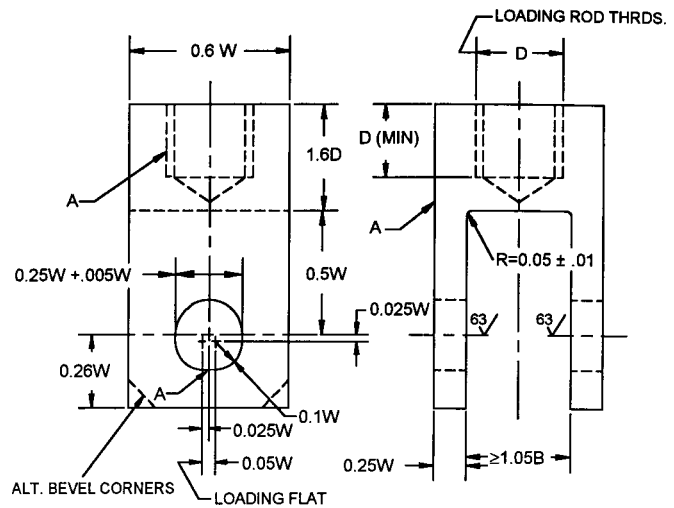
### A1.3 Apparatus

A1.3.1 *Grips and Fixtures for C(T) Specimens*—A clevis and pin assembly (Fig. A1.2) is used at both the top and bottom of the specimen to allow in-plane rotation as the specimen is loaded. This specimen and loading arrangement is to be used for tension-tension loading only.

A1.3.1.1 Suggested proportions and critical tolerances of the clevis and loading pin are given (Fig. A1.2) in terms of either the specimen width,  $W$ , or the specimen thickness,  $B$ , since these dimensions may be varied independently within certain limits.

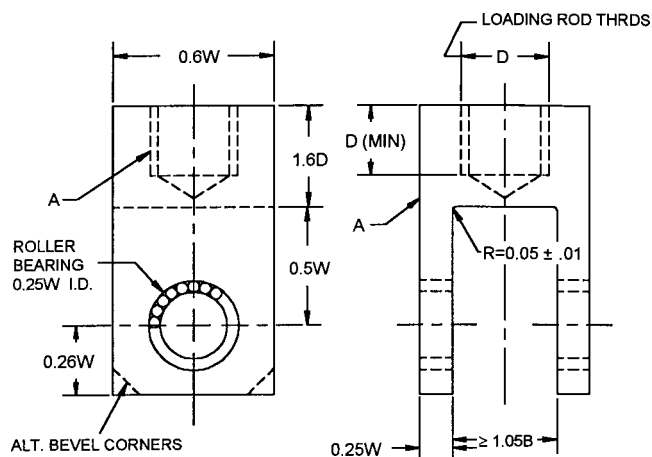
A1.3.1.2 The pin-to-hole clearances illustrated in Fig. A1.2 are designed to reduce nonlinear force vs. displacement behavior caused by rotation of the specimen and pin (12). Using this arrangement to test materials with relatively low yield strength may cause plastic deformation of the specimen hole. Similarly, when testing high strength materials or when the clevis opening exceeds  $1.05B$  (or both), a stiffer loading pin (that is,  $>0.225W$ ) may be required. In these cases, a flat bottom clevis hole or bearings may be used with the appropriate loading pins ( $D = 0.24W$ ) as indicated in Fig. A1.2. The use of high viscosity lubricants such as grease may introduce hysteresis in the force vs. displacement behavior and is not recommended.

A1.3.1.3 Using a 1000-MPa (150-ksi) yield-strength alloy (for example, AISI 4340 steel) for the clevis and pins provides adequate strength and resistance to galling and fatigue.



- NOTE 1—Pin diameter =  $0.24W - 0.005W$ .
- NOTE 2—Flat bottom hole is a modified Test Method E 399 design.
- NOTE 3—Corners of clevis may be removed if necessary to accommodate clip gage.
- A—surfaces must be flat, in-line, and perpendicular, as applicable, to within 0.05 mm.

**FIG. A1.2 Two Suggested Clevis Designs for C(T) Specimen Testing**



NOTE 1—Because of space requirements for the bearings, this grip is not practicable for small specimens.

A—surfaces must be flat, in-line, and perpendicular, as applicable, to within 0.05 mm.

FIG. A1.2 (continued)

### A1.4 Procedure

A1.4.1 Make crack size measurements at intervals such that  $da/dN$  data are nearly evenly distributed with respect to  $\Delta K$ . For the C(T) specimen, the suggested intervals are:

$$\Delta a \leq 0.04 W \text{ for } 0.25 \leq a/W \leq 0.40 \quad (\text{A1.2})$$

$$\Delta a \leq 0.02W \text{ for } 0.40 \leq a/W \leq 0.60$$

$$\Delta a \leq 0.01 W \text{ for } a/W \geq 0.60$$

If crack size is measured visually, the average value of the two surface crack lengths for the C(T) specimen should be used in all calculations of growth rate and  $K$  when using the  $K$  expression listed in A1.5.1.1. Further crack symmetry requirements are given in Section 8.3.4 of the main body of E 647. Out-of-plane cracking limits are given in Section 8.8.3 of the main body of E 647.

### A1.5 Calculation and Interpretation of Results

A1.5.1 *Determination of Stress-Intensity Factor Range,  $\Delta K$* —Use the crack size values of Section 9.1 of the main body of E 647 and Appendix X1 to calculate the stress-intensity range corresponding to a given crack growth rate from the following expressions:

A1.5.1.1 For the C(T) specimen calculate  $\Delta K$  as follows:

$$\Delta K = \frac{\Delta P}{B\sqrt{W}} \frac{(2 + \alpha)}{(1 - \alpha)^{3/2}} (0.886 + 4.64\alpha - 13.32\alpha^2 + 14.72\alpha^3 - 5.6\alpha^4) \quad (\text{A1.3})$$

where  $\alpha = a/W$ ; expression valid for  $a/W \geq 0.2$  (26, 27).

NOTE A1.2—Implicit in the above expression is the assumption that the test material is linear-elastic, isotropic, and homogeneous.

NOTE A1.3—The above operational definition does not include potential effects of residual stress or crack closure on the computed  $\Delta K$  value. Autographic force versus crack mouth opening displacement traces are useful for detecting and correcting residual stress/crack closure influences (4).

A1.5.1.2 Check for compliance with the specimen size requirements of A1.2.6.

A1.5.2 *Determination of Crack Size by Compliance*—The

crack size of a C(T) specimen can be determined by compliance procedures outlined in Annex A5.

A1.5.2.1 Theoretical compliance expressions for the specific measurement locations on the C(T) specimen are presented in Fig. A1.3 (44). Additional measurement locations are available through the use of rotation coefficients. This equation is for plane stress since this stress state is most applicable to measurements remote to the crack tip, regardless of the stress state local to the crack tip.

NOTE A1.4—For a C(T) specimen of  $W = 40$  mm, a gage located at any of the four locations shown in Fig. A1.3 and calibrated to 50  $\mu\text{m}/\text{volt}$  on a  $\pm 10$  volt range will generally provide sufficient resolution.

A1.5.2.2 Gripping techniques for specimens that undergo bending, such as the C(T) specimen, have been observed to affect compliance readings. The C(T) specimen may be loaded with grips that have either flat bottom holes or needle bearings, as shown in Fig. A1.2, to circumvent such problems.

A1.5.3 *Determination of Crack Size by Electric Potential Difference (EPD)*—The crack size of a C(T) specimen can be determined by electric potential difference (EPD) procedures outlined in Annex A6.

A1.5.3.1 *C(T) Geometry Voltage versus Crack Size Relationships*—An example of a voltage versus crack size relationship for the C(T) specimen geometry is shown in Eq A1.4. The expression was developed by Hicks and Pickard from finite element analysis and was verified through both analogue and experimental techniques for  $a/W$  ranging from 0.24 to 0.7 (62). This equation has been employed in two multi-laboratory, international co-operative testing efforts (66, 67).

$$V/V_r = A_0 + A_1(a/W) + A_2(a/W)^2 + A_3(a/W)^3 \quad (\text{A1.4})$$

for  $0.24 \leq a/W \leq 0.7$

where:

$V$  = the measured EPD voltage,

$V_r$  = the reference crack voltage corresponding to  $a/W = 0.241$ ,

$a$  = the crack size (as defined in Test Method E 647),

$W$  = the specimen width,

$A_0 = 0.5766$ ,

$A_1 = 1.9169$ ,

$A_2 = -1.0712$ , and

$A_3 = 1.6898$

or in reverse notation:

$$a/W = B_0 + B_1(V/V_r) + B_2(V/V_r)^2 + B_3(V/V_r)^3 \quad (\text{A1.5})$$

for  $0.24 \leq a/W \leq 0.7$

where:

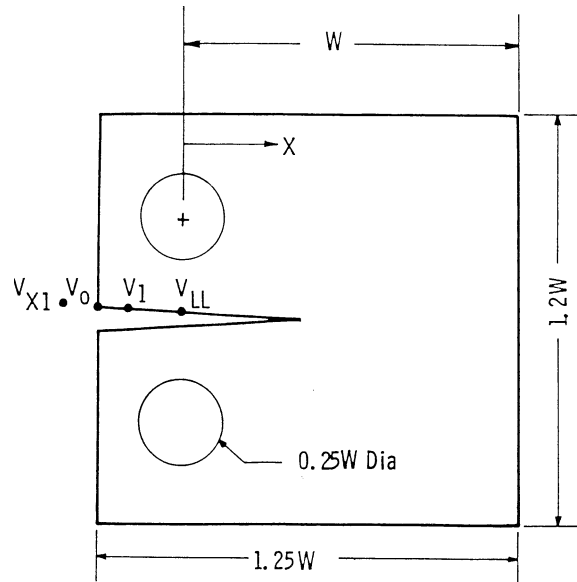
$B_0 = -0.5051$ ,

$B_1 = 0.8857$ ,

$B_2 = -0.1398$ ,

$B_3 = 0.0002398$ .

A1.5.3.2 Fig. A1.4 illustrates the C(T) geometry and specific wire placement locations for this solution. The relationship is valid only for the wire locations shown, which were determined by a compromise between sensitivity and reproducibility. If alternative wire placements (current or voltage) are used, the relationship shown is no longer valid and a new



Meas. Location	X/W	C <sub>0</sub>	C <sub>1</sub>	C <sub>2</sub>	C <sub>3</sub>	C <sub>4</sub>	C <sub>5</sub>
C(T) Specimen							
V <sub>X1</sub>	-0.345	1.0012	-4.9165	23.057	-323.91	1798.3	-3513.2
V <sub>0</sub>	-0.250	1.0010	-4.6695	18.460	-236.82	1214.9	-2143.6
V <sub>1</sub>	-0.1576	1.0008	-4.4473	15.400	-180.55	870.92	-1411.3
V <sub>LL</sub>	0	1.0002	-4.0632	11.242	-106.04	464.33	-650.68

$$\alpha = a/W = C_0 + C_1 u_x + C_2 u_x^2 + C_3 u_x^3 + C_4 u_x^4 + C_5 u_x^5$$

$$u_x = \left\{ \left[ \frac{E\nu B}{P} \right]^{\frac{1}{2}} + 1 \right\}^{-1}$$

$$0.2 \leq a/W \leq 0.975$$

FIG. A1.3 Normalized Crack Size as a Function of Plane Stress Elastic Compliance for C(T) Specimens (41).

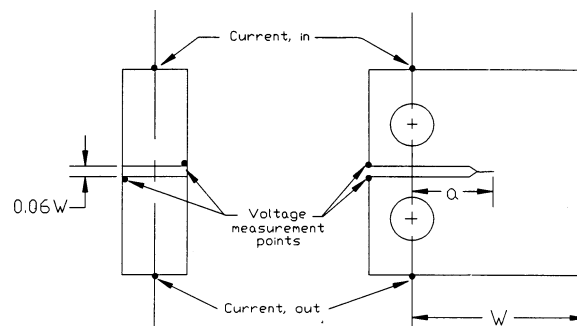


FIG. A1.4 C(T) Geometry and Electric Potential Wire Placement Locations for Eq A1.4 (52)

relationship must be developed.

A1.5.3.3 Note that the first form of the equation can be used to compute the constant  $V_r$  from any reference  $a/W$  and corresponding voltage measurement  $V$ . Computing  $V_r$  in this way accounts linearly for small changes in applied current, measured specimen dimensions, and slight errors in wire

placement from specimen to specimen. The computed reference voltage can then be used with the second form of the equation to determine the crack size for all voltage values  $V$ .

A2. THE MIDDLE TENSION SPECIMEN

A2.1 Introduction

A2.1.1 The middle tension, M(T), specimen is a center crack specimen that can be loaded in either tension-tension or tension-compression.

A2.1.2 The M(T) specimen has the advantage over many other specimen types in that it allows for fatigue loading under both positive and negative force ratios (R).

A2.1.3 In the near threshold regime (below  $10^{-8}$  m/cycle), one can experience difficulty in meeting the crack symmetry requirements listed in this method when using the M(T) specimen; the C(T) or ESE(T) specimens may be appropriate alternatives, provided that  $R \geq 0$ .

A2.2 Specimen Configuration, Size, and Preparation

A2.2.1 The general geometry of the M(T) specimen is given in Fig. A2.1, however the specific geometry depends on the method of gripping as specified in A2.3.

A2.2.2 For the M(T) specimen, the thickness,  $B$ , and width,  $W$ , may be varied independently within the following limits, which are based on specimen buckling and through-thickness crack-curvature considerations.

A2.2.2.1 For M(T) specimens it is recommended that upper limit on thickness be within the range  $W/8 \leq B \leq W/4$ . The minimum thickness necessary to avoid excessive lateral deflections or buckling is sensitive to specimen gage length, grip alignment, and stress ratio,  $R$ . It is recommended that strain gage information be obtained for the particular specimen geometry and loading condition of interest and that bending strains not exceed 5 % of the nominal strain.

A2.2.3 In the M(T) specimen (Fig. A2.1),  $a$  is measured from the perpendicular bisector of the central crack.

A2.2.3.1 The machined notch,  $2a_n$ , in the M(T) specimen shall be centered with respect to the specimen centerline to within  $\pm 0.001W$ . The length of the machined notch in the M(T) specimen will be determined by practical machining

considerations and is not restricted by limitations in the  $K$ -calibration.

A2.2.4 It is recommended that  $2a_n$  be at least  $0.2W$  when using the compliance method to monitor crack extension in the M(T) specimen so that accurate crack size determinations can be obtained.

A2.2.5 Notch and precracking details for the specimen are given in Fig. 1 of the main body of E 647.

A2.2.6 *Specimen Size*—In order for results to be valid according to this test method it is required that the specimen be predominantly elastic at all values of applied force. The minimum in-plane specimen sizes to meet this requirement are based primarily on empirical results and are specific to specimen configuration (10).

A2.2.6.1 For the M(T) specimen the following is required:

$$(W - 2a) \geq 1.25 P_{max} / (B\sigma_{YS}) \tag{A2.1}$$

where:

- ( $W - 2a$ ) = specimen's uncracked ligament (Fig. 2),
- $B$  = specimen thickness, and
- $\sigma_{YS}$  = 0.2 % offset yield strength determined at the same temperature as used when measuring the fatigue crack growth rate data.

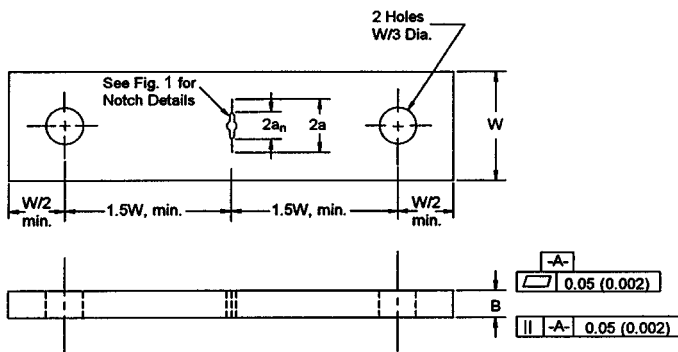
NOTE A2.1—For high-strain hardening materials, see Note 5 of the main body of E 647.

A2.3 Apparatus

A2.3.1 *Grips and Fixtures for M(T) Specimens*—The types of grips and fixtures to be used with the M(T) specimens will depend on the specimen width,  $W$ , (defined in Fig. A2.1), and the loading conditions (that is, either tension-tension or tension-compression loading). The minimum required specimen gage length varies with the type of gripping and is specified so that a uniform stress distribution is developed in the specimen gage length during testing. For testing of thin sheets, constraining plates may be necessary to minimize specimen buckling (see Practice E 561 for recommendations on buckling constraints).

A2.3.1.1 For tension-tension loading of specimens with  $W \leq 75$  mm (3 in.) a clevis and single pin arrangement is suitable for gripping provided that the specimen gage length (that is, the distance between loading pins) is at least  $3W$  (Fig. A2.1). For this arrangement it is also helpful to either use brass shims between the pin and specimen or to lubricate the pin to prevent fretting-fatigue cracks from initiating at the specimen loading hole. Additional measures which may be taken to prevent cracking at the pinhole include attaching reinforcement plates to the specimen (for example, see Test Method E 338) or employing a “dog bone” type specimen design. In either case, the gage length shall be defined as the uniform section and shall be at least  $1.7W$ .

A2.3.1.2 For tension-tension loading of specimens with  $W \geq 75$  mm (3 in.) a clevis with multiple bolts is recommended (for example, see Practice E 561). In this arrangement, the forces are applied more uniformly; thus, the minimum specimen gage length (that is, the distance between the innermost



- NOTE 1—Dimensions are in millimetres (inches).
- NOTE 2—The machined notch ( $2a_n$ ) shall be centered to within  $\pm 0.001W$ .
- NOTE 3—For specimens with  $W > 75$  mm (3 in.) a multiple pin gripping arrangement is recommended, similar to that described in Practice 561.
- NOTE 4—Surface finish, including holes, shall be 0.8 (32) or better.

FIG. A2.1 Standard Middle-Tension M(T) Specimen for Fatigue Crack Growth Rate Testing when  $W \leq 75$  mm (3 in.)

row of bolt holes) is relaxed to 1.5W.

A2.3.1.3 The M(T) specimen may also be gripped using a clamping device instead of the above arrangements. This type of gripping is necessary for tension-compression loading. An example of a specific bolt and keyway design for clamping M(T) specimens is given in Fig. A2.2. In addition, various hydraulic and mechanical-wedge systems which supply adequate clamping force are commercially available and may be used. The minimum gage length requirement for clamped specimens is relaxed to 1.2W.

**A2.4 Procedure**

A2.4.1 *Fatigue Precracking*—The importance of precracking is to provide a sharpened fatigue crack of adequate size, straightness, and symmetry for the M(T) specimen.

A2.4.1.1 In addition to the requirements listed in 8.3.4 of the main body, for the M(T) specimen, measurements referenced from the specimen centerline to the two cracks (for each crack use the average of measurements on front and back surfaces) shall not differ by more than 0.025W when using the K expression listed in A2.5.1.1.

A2.4.2 Make crack size measurements at intervals such that da/dN data are nearly evenly distributed with respect to ΔK. For the M(T) specimen, the suggested intervals are:

$$\Delta a \leq 0.03W \text{ for } 2a/W < 0.60 \tag{A2.2}$$

$$\Delta a \leq 0.02W \text{ for } 2a/W > 0.60$$

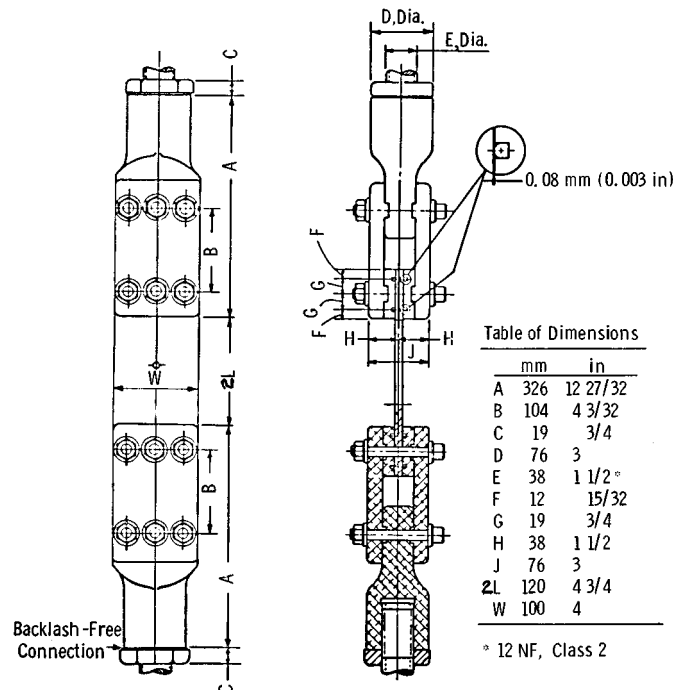


**FIG. A2.2 Example of Bolt and Keyway Assembly for Gripping 100-mm (4-in.) wide M(T) Specimen**

If crack size is measured visually, the average value of the four surface crack lengths for the M(T) specimen should be used in all calculations of growth rate and K when using the K expression listed in A2.5.1.1.

A2.4.3 In addition to the requirements listed in 8.8.3 of the main body, data are invalid if measurements referenced from the specimen centerline to the two cracks (for each crack, use the average of measurements on front and back surfaces) differ by more than 0.025W when using the K expression furnished in A2.5.1.1.

**A2.5 Calculation and Interpretation of Results**

A2.5.1 *Determination of Stress-Intensity Factor Range, ΔK*—Use the crack size values of 9.1 in the main body and Appendix X1 to calculate the stress-intensity range corresponding to a given crack growth rate from the following expression.

A2.5.1.1 For the M(T) specimen calculate ΔK consistent with the definitions of 3.2 in the main body; that is:

$$\Delta P = P_{max} - P_{min} \text{ for } R > 0 \tag{A2.3}$$

$$\Delta P = P_{max} \text{ for } R \leq 0$$

in the following expression (27):

$$\Delta K = \frac{\Delta P}{B} \sqrt{\frac{\pi \alpha}{2W} \sec \frac{\pi \alpha}{2}} \tag{A2.4}$$

where α = 2a/W; expression valid for 2a/W < 0.95.

NOTE A2.2—Implicit in the above expressions is the assumption that the test material is linear-elastic, isotropic, and homogeneous.

NOTE A2.3—The above operational definitions do not include potential effects of residual stress or crack closure on the computed ΔK value. Autographic force versus crack mouth opening displacement traces are useful for detecting and correcting residual stress/crack closure influences (4).

A2.5.1.2 Check for conformity with the specimen size requirements of A2.2.6.

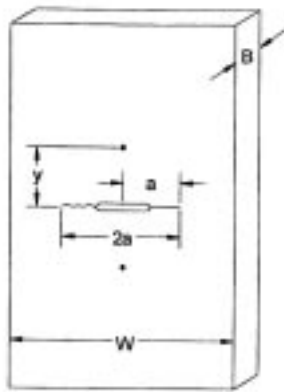
A2.5.2 *Determination of Crack Size by Compliance*—The crack size of an M(T) specimen can be determined by compliance procedures outlined in Annex A5.

A2.5.2.1 An equation for the compliance measured on the centerline of the M(T) specimen is shown in Fig. A2.3 (45). This equation is for plane stress since this stress state is most applicable to measurements remote to the crack tip, regardless of the stress state local to the crack tip.

NOTE A2.4—An M(T) specimen of W = 80 mm and 2y/W ≤ 0.4 will require a gage calibration of 15 μm/V on the same range. The increased resolution required for the M(T) specimen is caused by its greater stiffness which makes it less amenable to this form of nonvisual crack size monitoring. M(T) specimen compliance readings are also complicated by small, normally acceptable levels of bending.

A2.5.3 *Determination of Crack Size by Electric Potential Difference (EPD)*—The crack size of an M(T) specimen can be determined by electric potential difference (EPD) procedures outlined in Annex A6.

Models of Laboratory Test Specimens



Middle-Tension, M(T) Specimen

- a = crack length,
- B = specimen thickness,
- W = specimen width,
- C =  $\nu/P$  = compliance,
- E = Young's modulus,
- y = half gage length,
- $\eta = 2y/W$  = nondimensional gage length

$${}^{2a}/W = 1.06905x + 0.588106x^2 - 1.01885x^3 + 0.361691x^4$$

where:

$$x = 1 - e^{-\frac{\sqrt{(EBC + \eta)(EBC - \eta + c_1\eta + c_2\eta^3)}}{2.141}}$$

NOTE 1—This expression is valid for (1)  $0 \leq 2y/W \leq 1.0$ , and (2)  $0 \leq 2a/W \leq 1.0$ . Values of  $c_1$ ,  $c_2$ , and  $c_3$  are dependent on loading conditions and are shown below for three examples.

FIG. A2.3 Plane Stress Compliance Expression for the M(T) Specimen (45).

A2.5.3.1 M(T) Geometry Voltage versus Crack Size Relationship—A closed form analytical voltage versus crack size relationship for an infinitely long M(T) specimen (59) is shown below.

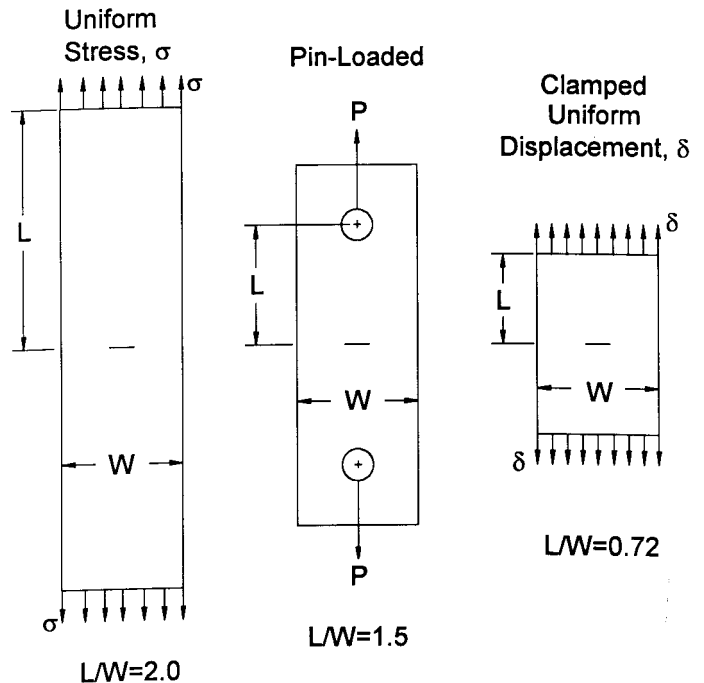
$$a = \frac{W}{\pi} \cos^{-1} \left[ \frac{\cosh\left(\frac{\pi}{W} \times Y_o\right)}{\cosh\left[\frac{V}{V_r} \times \cosh^{-1} \cdot \frac{\cosh\left(\frac{\pi}{W} \times Y_o\right)}{\cos\left(\frac{\pi}{W} \times a_r\right)}\right]} \right] \quad (A2.5)$$

for  $0 \leq \frac{2a}{W} \leq 1$

where:

- a = the crack size (as defined in Test Method E 647),
- $a_r$  = the reference crack size from some other method,
- W = the specimen width,
- V = the measured EPD voltage,
- $V_r$  = the measured voltage corresponding to  $a_r$ , and
- $Y_o$  = the voltage measurement lead spacing from the crack plane.

This relationship is valid only in cases where the current density is uniform at some cross section of the specimen remote from the crack plane and the voltage is measured on the centerline of the specimen across the crack plane. Fig. A2.4



Modification to  $x(EBC, 2y/W)$  for Different Loading Conditions

Uniform Stress	Pin-Loaded	Clamped Uniform Displacement
$c_1 = 0.0$	$c_1 = 0.005$	$c_1 = -0.03$
$c_2 = 0.0$	$c_2 = 0.0184$	$c_2 = 0.013$
$c_3 = 0.0$	$c_3 = 3.0$	$c_3 = 4.0$

FIG. A2.3 (continued)

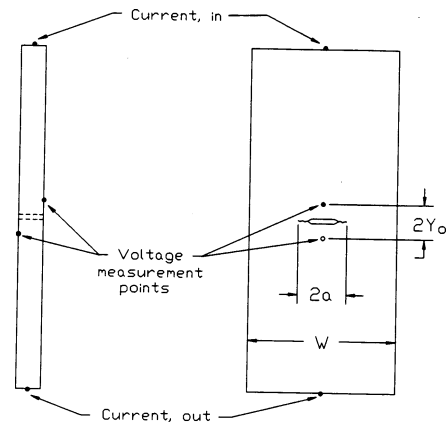


FIG. A2.4 M(T) Geometry and Electric Potential Wire Displacement Locations for Eq A2.5 (59)

illustrates the M(T) geometry and wire placement locations for this solution.

The requirement that current density be uniform at some cross section remote from the crack plane can be easily met by introducing the current through the standard M(T) specimen ends, with a distance between current input locations of approximately three times the width. Shorter current lead spacing may also be used provided that the uniform current density requirement be demonstrated. The calibration constants

$a_o$  and  $V_o$  may be any crack size and corresponding voltage measurement where the crack size has been determined using an alternate method. Optical surface measurements may be used to determine  $a_o$  provided crack front curvature is not

significant or is accounted for. If real time crack size measurements are not required during the test, post-test fracture surface measurements may be used to determine  $a_o$ .

**A3. THE ECCENTRICALLY-LOADED SINGLE EDGE CRACK TENSION SPECIMEN**

**A3.1 Introduction**

A3.1.1 The eccentrically-loaded single edge crack tension specimen ESE(T) is a single edge-cracked specimen similar to the C(T) specimen loaded in tension-tension. (71-73).

A3.1.2 The standard ESE(T) can exhibit advantages over other specimen types. The following paragraphs list possible advantages.

A3.1.2.1 The elongated (extended) design gives the experimenter additional working space compared to the standard compact tension C(T) specimen configuration. This configuration lends itself to attaching complex displacement or strain gage measurement systems and environmental cells (69).

A3.1.2.2 The specimen configuration requires lower applied forces for equivalent crack tip stress-intensity factor compared to other specimen configurations, such as the middle-crack tension M(T) specimen. This results in lower net section stress and reduces the likelihood of premature fracture of sheet materials tested in highly corrosive environments.

A3.1.2.3 The specimen design reduces the T-stress (stress parallel to crack surface) and crack fracture paths are more self-similar than in the standard C(T) specimen (70).

A3.1.2.4 The specimen design is compatible with common automated techniques for the measurement of through-the-thickness crack sizes.

**A3.2 Specimen**

A3.2.1 The general proportions of the ESE(T) specimen configuration are given in Fig. A3.1.

A3.2.2 It is recommended that the ESE(T) specimen thickness be in the range  $W/20 \leq B \leq W/4$ .

A3.2.3 *Specimen Size*—In order for results to be valid according to this test method it is required that the specimen be predominantly elastic at all values of applied force. For the ESE(T) specimen the following is required:

$$(W - a) \geq (4/\pi)(K_{max}/\sigma_{YS})^2 \tag{A3.1}$$

where:

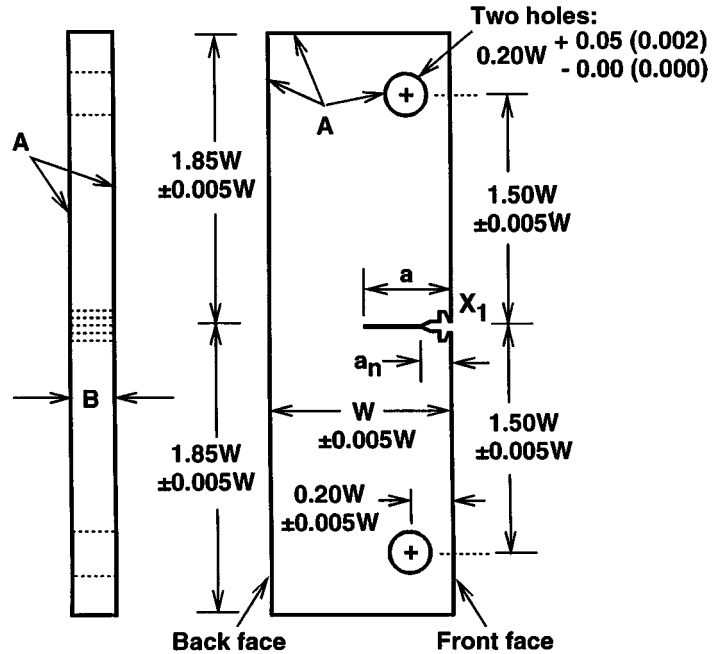
$(W - a)$  = specimen's uncracked ligament (Fig. A3.1), and  
 $\sigma_{YS}$  = 0.2 % offset yield strength determined at the same temperature as used when measuring the fatigue crack growth rate data.

NOTE A3.1—For high-strain hardening materials, see Note 5 of the main body of E 647.

**A3.3 Apparatus**

A3.3.1 Tension testing clevis and displacement gage apparatus are to be identical to that used by the C(T) specimen.

NOTE A3.2—The clevis pin is to be sized to 0.175W (+0.000, -0.025W).



NOTE 1—Dimensions are in millimeters (inches).

NOTE 2—A-surfaces perpendicular and parallel (as applicable) to within ±0.002W, TIR.

NOTE 3—Intersection of the machined notch with the specimen face shall be equi-distant from top and bottom of the specimen to within 0.005W.

NOTE 4—Surface finish, including holes, shall be 0.8(32) or better.

**FIG. A3.1 Standard Eccentrically-Loaded Single Edge Crack Tension Specimen.**

**A3.4 Procedure**

A3.4.1 *Measurement*—Measure the width,  $W$ , and the crack size,  $a$ , from the specimen front face as shown in Fig. A3.1.

A3.4.2 *ESE(T) Specimen Testing*—All testing procedures are similar to the C(T) specimen.

**A3.5 Calculations**

A3.5.1 *Determination of Stress-Intensity Factor Range, ΔK*—For the ESE(T) specimen, calculate  $\Delta K$  as follows (72).

$$\Delta K = [\Delta P/(B\sqrt{W})] F \tag{A3.2}$$

and

$$F = \alpha^{1/2} [1.4 + \alpha][1 - \alpha]^{-3/2} G \tag{A3.3}$$

where

$$G = 3.97 - 10.88\alpha + 26.25\alpha^2 - 38.9\alpha^3 + 30.15\alpha^4 - 9.27\alpha^5 \tag{A3.4}$$

$$\alpha = a/W$$

for  $0 < \alpha < 1$ .

A3.5.2 *Determination of Crack Size by Compliance*—The determination of crack size by the compliance methods outlined in Annex A5 can be conducted at the ESE(T) front-face and back-face locations.

A3.5.2.1 *Front-face compliance*—The following expressions were derived for monitoring crack size by measuring the displacement ( $v$ ) at the front face. The term  $v_0$  is the displacement at the front face knife edge location shown in Fig. A3.1 (72, 74).

$$a/W = M_0 + M_1 U + M_2 U^2 + M_3 U^3 + M_4 U^4 + M_5 U^5 \quad (A3.5)$$

where:

$$U = [(EBv_0/P)^{1/2} + 1]^{-1}$$

$$M_0 = 1.00132$$

$$M_1 = -3.58451$$

$$M_2 = 6.599541$$

$$M_3 = -19.22577$$

$$M_4 = 41.54678$$

$$M_5 = -31.75871$$

for  $0.1 \leq a/W \leq 0.84$ .

Normalized compliance in terms of crack size is given by

$$EBv_0/P = [15.52a/W - 26.38(a/W)^2 + 49.7(a/W)^3 - 40.74(a/W)^4 + 14.44(a/W)^5][1 - a/W]^2 \quad (A3.6)$$

for  $0 < a/W < 1$ .

A3.5.2.2 *Back-face compliance*—The following expression was derived for monitoring crack size by measuring strains at

the back-face. Here, back-face strain,  $\epsilon$ , is measured at a location along the crack plane similar to the C(T) specimen, shown in Fig. X2.1 of the standard.

$$a/W = N_0 + N_1 (\log A) + N_2 (\log A)^2 + N_3 (\log A)^3 + N_4 (\log A)^4 \quad (A3.7)$$

where:

$$A = -(\epsilon/P)BWE$$

$$N_0 = 0.09889$$

$$N_1 = 0.41967$$

$$N_2 = 0.06751$$

$$N_3 = -0.07018$$

$$N_4 = 0.01082$$

for  $0.1 \leq a/W \leq 0.84$ .

A3.5.3 *Determination of Crack Size by Electrical Potential Difference*—The crack size of an ESE(T) specimen can be determined by electric potential difference (EPD) procedures outlined in Annex A6. Crack size determinations may be performed using the Johnson's equation (59, 75). Typical electrical potential wire placement locations are similar to the C(T) specimen, refer to Fig. A1.4 of the C(T) specimen annex.

NOTE A3.3—The Johnson equation, based on the electrostatic analysis of a finite width plate with an infinitesimally thin central slot, has been shown to give accurate results for M(T) specimens. Its use with the ESE(T) specimen configuration, however, must be experimentally verified.

## A4. SPECIAL REQUIREMENTS FOR TESTING IN AQUEOUS ENVIRONMENTS

### A4.1 Introduction

A4.1.1 Fatigue crack growth rates in metallic materials exposed to aqueous environments can vary widely as a function of mechanical, metallurgical, and electrochemical variables. Therefore, it is essential that test results accurately reflect the effects of specific variables under study. Test methods must be chosen to represent steady state fatigue crack growth behavior which neither accentuates nor suppresses the phenomena under investigation. Only then can data be compared from one laboratory investigation to another on a valid basis, or serve as valid basis for characterizing materials and assessing structural behavior.

### A4.2 Scope

A4.2.1 This annex covers the determination of fatigue crack growth rates using the test specimens described in this test method under test conditions involving temperatures and pressures at, or near, ambient.

### A4.3 Referenced Documents

A4.3.1 *ASTM Standards*:

D 1129 Terminology Relating to Water<sup>10</sup>

E 742 Definitions of Terms Relating to Fluid Aqueous and Chemical Environmentally Affected Fatigue Testing<sup>3</sup>

G 1 Practice for Preparing, Cleaning, and Evaluating Corrosion Test Specimens<sup>11</sup>

G 3 Practice for Conventions Applicable to Electrochemical Measurements in Corrosion Testing<sup>11</sup>

G 5 Reference Test Method for Making Potentiostatic and Potentiodynamic Anodic Polarization Measurements<sup>11</sup>

G 15 Terminology Relating to Corrosion and Corrosion Testing<sup>11</sup>

### A4.4 Terminology

A4.4.1 The terms used in this annex are defined in the main body of this test method. Additional terms more specific to testing in aqueous environments can be found in Terminologies D 1129 and G 15 and Definitions E 742.

### A4.5 Significance and Use

A4.5.1 In aqueous environments, fatigue crack growth rates are a complex function of many experimental variables. These include prior force history, stress-intensity range, force ratio, cyclic frequency, force-versus-time wave-form, specimen thickness, crack geometry and size, electrolyte species and concentration, exposure time, flow rate, temperature, pH, dissolved oxygen content, and potential (free corrosion or applied). Background information on these effects can be

<sup>10</sup> Annual Book of ASTM Standards, Vol 11.01.

<sup>11</sup> Annual Book of ASTM Standards, Vol 03.02.

found in Refs. (31-38).

A4.5.2 Specimens which undergo fatigue crack growth rate testing in aqueous environments are subject to various corrosive effects which can either hasten or retard crack growth rates (see Refs. (39) and (40)). Generation of fatigue crack growth rate data on metallic materials in aqueous environments requires judicious selection, monitoring, and control of mechanical, chemical, and electrochemical test variables in order to ensure that the data are applicable to the intended use. For example, data generated in a laboratory test at a cyclic frequency of 10 Hz may not be applicable for predicting crack growth rates in a structure which is cycled at 0.1 Hz.

A4.5.3 Fatigue crack growth which occurs in the presence of an aqueous environment may be the product of both mechanical and chemical driving forces. The chemical driving force can vary with crack size, crack shape, and the degree of crack opening. Thus, fatigue crack growth rates in the presence of an aqueous environment may exhibit non-uniqueness when characterized in terms of  $da/dN$  versus  $\Delta K$ , Ref. (38).

#### A4.6 Apparatus

A4.6.1 The environmental chamber shall enclose the entire portion of the test specimen over which crack extension occurs. A circulation system to provide replenishment and aeration of the test solution may be desirable. Nonmetallic materials are recommended for the entire environmental chamber and circulation system. The environmental chamber should be designed so as to prevent galvanic contact between dissimilar test specimen and grip assembly components. If a circulation system is employed, the environmental chamber should be of sufficient size, and inlet and outlet locations should be chosen, to ensure a flow of test solution around the portion of the test specimen where crack extension occurs. A circulation system should provide for continuous aeration and filtration of the test solution in order to remove corrosion products. Exceptions to the above may occur if a quiescent solution is specifically desired.

#### A4.7 Procedure

A4.7.1 *Specimen Preparation*—It is recommended that specimens be cleaned prior to precracking and testing in accordance with Practice G 1.

A4.7.2 *Specimen Precracking*—Preliminary precracking may be conducted in an ambient laboratory air environment using a cyclic frequency and waveform which differ from the test conditions. However, a final 1.0-mm increment (0.040-in. increment) of precracking shall be conducted in the aqueous environment under full test conditions.

A4.7.3 *General Test Procedure*—Fatigue crack growth rate testing in aqueous environments provides a means of detecting and assessing the effects of localized corrosion processes involving metal surfaces at crack tips. Thus, the corrosive environment must physically reach the crack-tip region and time-dependent corrosion processes must have sufficient opportunity to proceed. If test techniques fail to adequately promote and maintain localized corrosion in crack-tip regions throughout the full test duration, nonsteady-state conditions can affect the  $da/dN$  versus  $\Delta K$  data. Therefore, testing shall be conducted in a manner which seeks to eliminate or minimize

transient or nonsteady-state effects, or both, on  $da/dN$  versus  $\Delta K$  data. Nonsteady-state or transient effects are defined as time-dependent fluctuations in  $da/dN$  values which do not directly correspond to any concomitant changes in mechanical crack driving force parameters, Ref. (20).

A4.7.3.1 It is recommended that specimens be immersed in the full test environment for a suitable period of time immediately prior to precracking or gathering crack growth rate data, or both. A minimum period of 24 h is recommended.

A4.7.3.2 It is recommended that specimens undergoing fatigue testing remain immersed in the test solution during brief periods of test interruption. If specimens are removed from the test solution for more than a brief period, it is recommended that fatigue data gathering shall not resume until the crack has extended by a 1.0-mm increment (0.040-in. increment) under test conditions.

A4.7.3.3 It is recommended that specimens be visually examined periodically during the course of testing for evidence of corrosive attack. Corrosion product accumulation which may inhibit access of the test solution to the crack-tip region may be removed. The crack-tip region of the specimen surface may also be cleaned periodically to aid in visual observation of crack size or crack-tip morphology, or both. Upon completion of fatigue testing, it is recommended that the specimen be loaded to fracture and receive a thorough visual post-mortem examination.

A4.7.3.4 It is necessary to carefully monitor tests for evidence of environmentally-induced phenomena which may affect steady state  $da/dN$  versus  $\Delta K$  data. The presence of an aqueous environment may cause numerous environmentally-induced phenomena to occur in the course of fatigue crack growth rate testing of metallic materials. Some common examples are transient changes in  $da/dN$  versus  $\Delta K$  data in response to changes or interruptions in cyclic loading, crack growth acceleration or retardation, crack arrest, crack branching, crack-front curvature or irregularity, out-of-plane crack-ing, or corrosion product build-up within cracks.

A4.7.3.5 Steady state fatigue crack growth rates in aqueous environments can be strongly affected by cyclic waveform or cyclic frequency, or both. Knowledge of these effects can be an important consideration in selecting test parameters. It is especially important to note that certain frequencies or waveforms, or both, can act to suppress the influence of aqueous environments on fatigue crack growth in metallic materials. These effects generally relate to the rise time of the loading cycle, Refs. (32) and (34). For steels and high-strength aluminum alloys, crack growth rates in aqueous environments tend to vary directly with the rise time. However, exceptions to this trend have been observed in high strength titanium alloys under cyclic loading conditions where  $K_{max} < K_{Isc}$ , Ref. (35).

A4.7.3.6 If significant transient behavior is apparent in  $da/dN$  versus  $\Delta K$  data for a particular test, it is recommended that the test be repeated. However, in assessing apparent transient behavior, particular care should be taken to ensure that the crack size measurement intervals used in the data reduction are in accordance with those recommended in 8.6.2. Improper selection of  $\Delta a$  values for data reduction can greatly magnify apparent transients in  $da/dN$  versus  $\Delta K$  data.

**A4.7.4 Crack Size Measurement**—Since the presence of an environmental chamber containing an aqueous solution may tend to obscure the crack, a nonvisual technique is recommended as the primary method, Refs. (41-43). However, optical observation of the crack tip is recommended as an auxiliary method of crack size measurement and as a means of monitoring crack morphology, specifically crack branching or out-of-plane cracking which may render the test invalid. Fatigue crack surface features revealed in a post-mortem visual examination may provide useful reference marks for calibrating *in situ* crack size measurements. If the potential drop nonvisual technique is employed, it is recommended that care be taken to assure that electrochemical effects on the  $da/dN$  versus  $\Delta K$  data are not introduced. Electrochemical effects, if sustained in duration, can either accelerate or retard crack growth rates in aqueous environments (see Refs. (33) and (40)).

**A4.7.5 Environmental Monitoring and Control**—Environmental parameters can strongly influence the results of fatigue crack growth rate tests conducted in aqueous environments. Therefore, environmental monitoring and control are recommended.

**A4.7.5.1** It is recommended that tests be initiated using unused solution which has not previously been in contact with other metallic test specimens. It is further recommended that replenishment of evaporated solution be conducted once every 24 h testing period, or more frequently if required, and the entire test solution be emptied and replaced not less than once a week.

**A4.7.5.2** It is recommended that measurements of solution temperature and specimen corrosion potential be made and recorded not less than once every 8 h testing period. Potential measurements should be made in accordance with conventions and procedures set forth in Practices G 3 and G 5. It is further recommended that measurements be made and recorded of pH, conductivity, and dissolved oxygen at similar intervals. Control of environment temperature is also recommended.

## A4.8 Report

**A4.8.1** The following information shall be reported in addition to the requirements stated in Section 11.

**A4.8.2** Descriptions of the environmental chamber and all equipment used for environmental monitoring or control, or both, shall be reported.

**A4.8.3** Environmental variables shall be reported as follows: the bulk solution chemical composition and details of its application shall be described; procedures for environmental monitoring and control shall be described; environmental monitoring data for such parameters as pH, potential, or temperature shall be expressed in terms of the normal daily range experienced throughout the duration of the test; relevant trends or transients in environmental parameters data shall be reported.

**A4.8.4** It is important to maintain a test log which records all test interruptions or force changes in terms of elapsed cycles, crack size, and time. All data shall be scrutinized for transients and anomalies. All anomalous behavior shall be reported and described in relation to recorded test events.

## A5. GUIDELINES FOR USE OF COMPLIANCE TO DETERMINE CRACK SIZE

**A5.1** The compliance method of crack size monitoring can be used during fatigue crack growth rate testing (21, 22). The optimum procedure employs the use of high speed digital data acquisition and processing systems, but low-speed autographic equipment can also be used to record the force and displacement signals. Depending on the data acquisition equipment and cyclic force frequency, it may be necessary to lower the frequency during the period of data acquisition.

**A5.2** The relationship between compliance (which is the reciprocal of the force-displacement slope normalized for elastic modulus and specimen thickness) and crack size has been analytically derived for a number of standard specimens (44). Such relationships are usually expressed in terms of the dimensionless quantities of compliance,  $\frac{EvB}{P}$  (or *ECB* where *C* is  $\nu/P$ ), and the normalized crack size,  $a/W$ , where *E* is the elastic modulus,  $\nu$  is the displacement between measurement points, *B* is specimen thickness, *P* is force, *a* is crack size, and *W* is the specimen width. All compliance-crack size relationships are applicable only for the measurement locations on the specimen for which they were developed. In lieu of an analytically derived compliance relationship, it is possible to empirically develop a compliance curve for any type of specimen used in fatigue crack growth rate testing. Such curves are not limited to displacement measurements alone and can

involve strain related quantities.

**A5.3** Specimens for fatigue crack growth rate testing covered in this standard are the compact tension, C(T), the middle tension, M(T), and the eccentrically-loaded single edge crack tension, ESE(T), specimens. Theoretical compliance expressions for these standard test specimens are presented in the respective test specimen annexes.

**A5.4** Selection of displacement measurement gages, attachment points and methods of attachment are dependent on the test conditions such as frequency, environment, stress ratio, and temperature. Gages must be linear over the range of displacement measured, and must have sufficient resolution and frequency response. Insight into these issues can be obtained from Test Method E 1820 and the relative Annex in Test Method E 399. Smaller specimens generally require higher resolution gages. Attachment points must be accurately and repetitively placed on the specimen, and must not be susceptible to wearing during the fatigue cycling.

**A5.5** Gripping techniques for specimens that undergo bending, such as the C(T) and ESE(T) specimens, have been observed to affect compliance readings. These specimens may be loaded with grips that have either flat bottom holes or needle bearings, as shown in the respective specimen annexes, to circumvent such problems.

A5.6 The force-displacement plot of one complete cycle of fatigue loading is generally not linear. The lower portion is usually nonlinear and the upper portion is linear. Compliance is calculated by fitting a straight line to the upper linear part of a force-displacement curve.

NOTE A5.1—When using a digital data acquisition system it is permissible to obtain data from a few consecutive cycles provided the growth rate is relatively small. During multiple cycle sampling the normalized crack size,  $a/W$ , cannot change by more than 0.001 ( $\Delta a/W \leq 0.001$ ).

NOTE A5.2—There are indications that near the crack growth rate threshold, the upper linear portion of the curve may be very small making the compliance method unusable.

NOTE A5.3—It is usual practice to consistently fit to either the linear portion of the loading data or the unloading data.

NOTE A5.4—It is sometimes necessary to eliminate the data close to the top force reversal point because of rounding that occurs in this area. This is predominately true for data taken at low frequencies.

A5.7 At least one visual crack size reading must be taken either at the beginning or after the test. The visual reading must

be adjusted for curvature to obtain the physical crack size using the procedures in the main section of this test method under Calculations and Interpretation of Results. Any difference between the physical and compliance crack size must be used to adjust all compliance crack sizes. Most often this is accomplished by calculating an effective modulus of elasticity,  $E'$ , and using this in the compliance equation to adjust all crack size calculations. If the effective modulus of elasticity differs from the typical elastic modulus by more than 10 %, then the test equipment is improperly set-up and data generated from such records are to be considered invalid by this method.

NOTE A5.5—Usually  $E \leq E' \leq E/(1 - \mu^2)$ , where  $\mu$  is Poisson's ratio.  $E'$  might be thought of as being proportional to  $E$ , that is,  $E' = \gamma E$ , where  $\gamma$  is an adjustment factor that accounts for parameters not controllable or measurable during a test.

NOTE A5.6—It is recommended that periodic optical readings be taken for comparison purposes during the first series of tests that use this or any other nonvisual method of crack size measurement.

## A6. GUIDELINES FOR ELECTRIC POTENTIAL DIFFERENCE DETERMINATION OF CRACK SIZE

A6.1 *Applications*—Electric potential difference (EPD) procedures for crack size determination are applicable to virtually any electrically conducting material in a wide range of testing environments. Non-conducting materials may also be tested using the electric potential method by firmly attaching a conducting foil or film and treating it as a replicate specimen. This method is acceptable provided that cracking in the film duplicates cracking in the test specimen, and the film does not alter the fatigue crack growth rate properties of the test specimen. This replicate film method may also be used with conducting specimens as well.

A6.1.1 Procedures discussed herein are those for which two-dimensional models can be used both for the specimen configuration and for the electric potential.

A6.2 *Principle*—Determining crack size from electric potential measurements relies on the principle that the electrical field in a cracked specimen with a current flowing through it is a function of the specimen geometry, and in particular the crack size. For a constant current flow, the electric potential or voltage drop across the crack plane will increase with increasing crack size due to modification of the electrical field and associated perturbation of the current streamlines. The change in voltage can be related to crack size through analytical or experimental calibration relationships.

A6.3 *Basic Methods*—Both direct current (DC) and alternating current (AC) techniques have been used to measure crack size in test specimens (46-53). For the more common DC technique, a constant current is passed through the specimen resulting in a two-dimensional electrical field which is constant through the thickness at all points. For the AC technique, a constant amplitude (normally sinusoidal) current is passed through the specimen to generate the voltage drop across the crack tip. For relatively low frequencies (less than 100 Hz with common materials), the field is approximately two-

dimensional as in the DC current case. For higher frequencies, however, a non-uniform current distribution occurs through the thickness, the degree of which is dependent on the AC frequency and magnetic permeability of the specimen. This phenomenon is commonly termed the “skin effect” because the current tends to be carried only near the surface of the specimen. For some materials, particularly ferromagnetic specimens, this skin effect can be significant at frequencies as low as 100 Hz, and below (49, 50). The AC methods can thus be subdivided into two groups: lower frequency methods where the skin effect is negligible and higher frequency methods where the skin effect must be taken into account.

A6.3.1 For many materials under test in oxidizing environments an oxide layer forms immediately upon the creation of a “fresh” fracture face, thereby insulating the two specimen halves. Under these conditions, the voltage drop across the fatigue crack should remain constant throughout a complete force cycle (assuming no crack extension). An insulating surface may not be created in a non-oxidizing environment or where high fracture surface closure forces tend to compromise such an oxide layer. In these cases, fracture surface shorting may occur at force levels above the minimum test force leading to an under-estimation of the physical fatigue crack size (54, 55). This effect is of particular concern when testing at near threshold conditions, when the force at which shorting occurs approaches the peak test force level.

A6.3.2 Unless it can be shown that electrical shorting does not occur during the entire force cycle, the voltage measurements should be taken at or near the peak tensile force. Depending on the frequency response of the AC or DC voltage measuring equipment, it may be necessary to reduce testing frequency or, in some extreme instances, even to stop the test during a voltage measurement to ensure that the measurement is taken only at peak force and without any signal attenuation. It should be noted that measurement of the electrical potential

at maximum force does not always guarantee the absence of electrical shorting errors. Shorting errors can still be present at maximum force in cases where there is electrical contact between the fracture surfaces but no mechanical force is transferred. The fracture surface shorting effect can be accounted for after the test using post-test fracture surface crack size measurements. One approach is to compute offset and scaling factors to match the initial and final crack sizes from electric potential measurements and fracture surface measurements. A simple linear interpolation technique with the scaling factor as a function of  $a/W$  is then used to correct the intermediate electric potential values. This method may not be suitable for tests in which machine control parameters are derived from the crack size (such as a constant stress intensity test). In these cases, crack size measurement errors may cause unacceptable differences between the applied forces and the desired control force.

A6.3.3 Elastic and plastic deformation can in principle affect material resistivity and, for the case of AC potential difference measurement, magnetic permeability (56). While unlikely to be an important source of error for the stress intensities typical of fatigue crack growth under small scale yielding and Test Method E 647, the user should document any force dependence of the potential for constant crack size without surface shorting and assess the importance of associated errors in calculated crack size. The correction method for shorting errors will generally account for deformation effects on the electrical and magnetic properties of the material.

A6.3.4 Changes in the specimen or instrumentation may result in proportional changes in the measured voltage. For example, a 1°C change in specimen temperature can result in a few  $\mu\text{V}$  change in EPD signal due to the change in the material's electrical resistivity. Also, some materials exhibit time-dependent conductivity changes while at elevated temperatures (54). Variations in the gain of amplifiers or calibration of voltmeters may also result in a proportional scaling of the measured voltages. To compensate for these effects, voltage measurements can be normalized using additional voltage measurements taken at a reference location. The reference location may be either on the test specimen or on an alternate specimen in the same environment. If the reference measurements are made directly on the test specimen, the location must be chosen so that the reference voltage is not affected by crack size. Since all material and instrument variations are also included in the reference measurements, the normalization process should eliminate them. Use of reference voltage measurements can significantly increase crack size resolution.

A6.3.5 DC Current Method—The DC method is an established technique which can be applied using equipment commonly found in most testing laboratories as shown in Fig. A6.1. The output voltages are typically in the 0.1 to 50.0 mV range for common current magnitudes (5 to 50 A), specimen dimensions, and materials. Precise measurements (typically  $\pm 0.1\%$ ) of these relatively small output voltages must be made to obtain accurate crack size values. To obtain sufficient voltage resolution usually requires special care in eliminating electrical noise and drift (see A6.11). Generally, tradeoffs are made

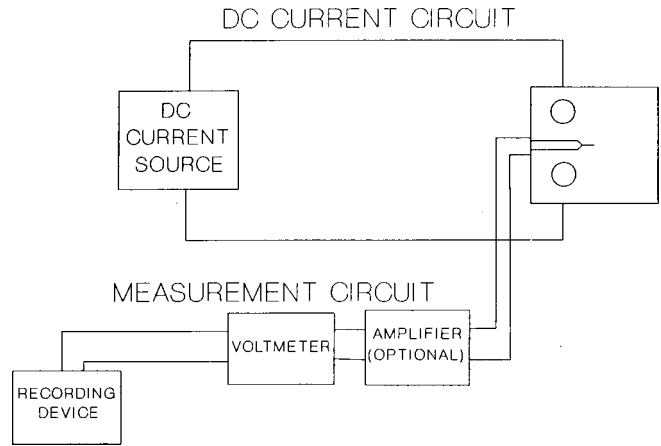


FIG. A6.1 Schematic Diagram of the DC Potential System

between measurement system response time and voltage resolution (see A6.5).

A6.3.5.1 The DC method is susceptible to thermoelectric effects (57) which produce DC potentials in addition to those due to the specimen electrical field. These thermoelectric voltages can be a substantial fraction of the total measured voltage. Since the thermoelectric effect is present even without the input current, it is possible to account for it by subtracting voltage measurements taken with the current off from the measurements made with the current on. An alternate method corrects for the thermoelectric effect by taking voltage measurements while reversing the direction of current flow. Corrected EPD measurements are then equal to one-half of the difference of the measured potential readings taken at each current polarity (58).

A6.3.6 AC Current Method—Both the low and high frequency AC methods require equipment similar to that shown in Fig. A6.2 (49). The AC equipment is more specialized than that for the DC approach (see A6.5.2). With the same specimen input current magnitude, this equipment can be used to obtain higher crack size resolution as compared to the DC method (46). This is due in part to the different amplification and filtering techniques used in the two methods in addition to the skin effect previously noted. The AC method is not influenced by thermoelectric effects which produce a DC voltage offset.

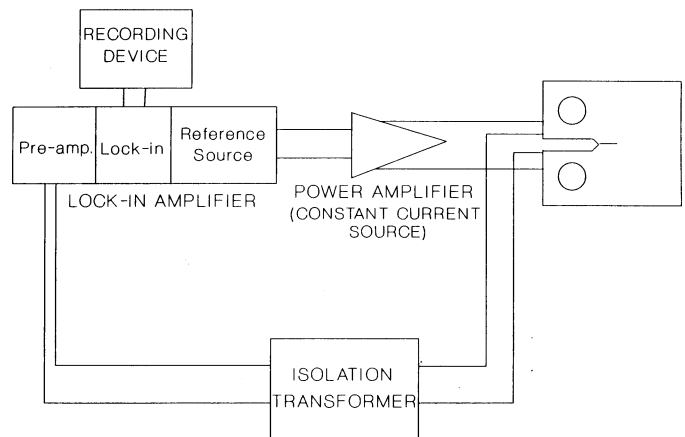


FIG. A6.2 Schematic Diagram of the AC Potential System (42)

**A6.3.6.1 Low Frequency AC Current Method**—The low frequency AC method is similar to the DC current method except that as previously noted, different equipment is required to produce the drive current and measure the output voltage. One possible problem with this type of system is that if the test force frequency is an integral multiple of the AC potential frequency, fracture surface sorting (bridging) effects may produce unwanted signal components at the AC potential frequency.

**A6.3.6.2 High Frequency AC Current Method**—An advantage of this technique over the low frequency AC method is that better crack size resolution can typically be obtained using the same input current. This is due to the skin effect previously noted which effectively reduces the specimen thickness to the surface layers (51) and the fact that the output voltage is inversely proportional to the specimen thickness.

**A6.3.6.3** At high frequencies where the skin effect becomes pronounced, only the near surface crack size will be obtained. This must be taken into account if through-the-thickness crack front curvature is significant. Other effects which may appear at high frequencies include induction and capacitance contributions from lead wires, specimen attachments, and the crack itself. These may be significant and may vary with crack size, causing difficulties in relating output voltage measurements to crack size unless precautions are taken (see A6.11.1).

**A6.4 Current Generating Equipment**—Any suitable constant current supply may be used which has sufficient short and long term stability. The required stability is a function of the resolution of the voltage measurement equipment (see A6.5) and the desired crack size resolution. For optimum conditions, the relative stability of the power supply should be equal to the effective resolution of the voltage measurements system; that is, if the voltage measurement system can effectively resolve one part in  $10^3$  of the output voltage from the specimen (including electrical noise, inherent inaccuracies such as non-linearity, and so forth), then the power supply should be stable to one part in  $10^3$ .

**A6.4.1** For AC systems, the current should be generated using an amplifier to produce an output current proportional to an input reference signal. The use of an amplifier instead of a stand-alone current generator allows the use of lock-in detection in the voltage measurement circuit (see A6.5.2). The amplifier should have suitably high input impedance ( $>10\text{ k}\Omega$ ) and should be capable of generating an output current which is stable as per the preceding discussion.

**A6.5 Voltage Measurement Equipment**—Voltage measurements may be made with any equipment which has sufficient resolution, accuracy, and stability characteristics. The following subsections deal with measurement equipment particular to the different potential drop methods.

**A6.5.1 DC Voltage Measurement Equipment**—The DC method requires equipment capable of measuring small changes in DC voltage (that is, 0.05 to 0.5  $\mu\text{V}$ ) with relatively low DC signal to AC RMS noise ratios. Although there are a variety of ways to implement the voltage measurement system, three commonly used systems are: amplifier/autographic recorder, amplifier/microcomputer analog to digital converter,

and digital voltmeter/microcomputer.

**A6.5.1.1 Autographic recorders** are commonly available with suitable sensitivity and can be used to record the output voltage directly from the specimen. A preamplifier can be used to boost the direct voltage output from the specimen before recording. Another common technique uses a preamplifier to boost the direct output from the specimen to a level that can be digitized using a conventional analog to digital (A/D) converter and microcomputer. A third method makes use of a digital voltmeter with a digital output capability. The advantage of this type of system is that all of the sensitive analog circuits are contained within a single instrument. The response time of the voltage measurement system must be sufficient to resolve changes in EPD as a function of applied force if fracture surface shorting occurs.

**A6.5.2 AC Voltage Measurement Equipment**—Both low and high frequency AC systems make use of similar voltage measurement equipment as shown in Fig. A6.2. The voltage measurement circuit and the current amplifier (see A6.4) are interconnected through the lock-in amplifier. This specialized amplifier produces a reference output signal for the current amplifier and is able to discriminate against all input signals that are not at the reference signal frequency and phase. Thus, only signals produced as a result of the current amplifier output are amplified for measurement. This method is capable of amplifying only the desired AC voltage signal at very low signal-to-noise ratios and provides excellent noise rejection (49). Note that this type of system is insensitive to DC voltages which might be produced by thermoelectric effects.

**A6.5.3** When selecting instrumentation for an AC system, care should be made to ensure proper impedance matching, since each component is designed for operation over a specific frequency domain. Input and output impedance should be matched. A check for frequency response to ensure operation in the “flat” region of the instruments’ gain should also be performed.

**A6.6 Crack Size versus Potential Difference Relationships**—Closed form solutions for the relationship between potential difference versus crack size have been analytically derived for such specimen geometries as the M(T) specimen (59) and the part-through surface crack specimen (60, 61). Additional relationships are also available based on numerical solutions for a number of other specimen geometries (62-64). Such relationships are usually expressed in terms of the normalized voltage ( $V/V_r$ ) and some reference crack size ( $a_r$ ) as shown in Eq A6.1.

$$a = f(V/V_r, a_r) \quad (\text{A6.1})$$

where:

$V$  = the measured voltage,

$V_r$  = a reference crack voltage,

$a$  = crack size, and

$a_r$  = a reference crack or notch size associated with  $V_r$ .

Alternative formulations are also used when the crack size is normalized by an in-plane characteristic dimension such as the specimen width  $W$ . When written in this form, the solutions can be made independent of specimen thickness, in-plane specimen

size, applied current, and material.

A6.6.1 In lieu of an analytically derived expression, it is possible to empirically develop relationships for virtually any type of specimen geometry used in fatigue crack growth rate testing. Such empirical relationships can be advantageous in instances when specimen geometries are complex, or wire placement must be altered. In any event, analytical or empirical relationships should be experimentally verified using alternative measurements at various crack sizes in the range of interest (optical surface measurements, compliance measurements, or post-test fracture surface measurements). Such measurements should be reported and may be used for correcting crack sizes inferred from equations of the type in Eq A6.1.

A6.6.2 Voltage wire placements are usually a compromise between good sensitivity to crack size changes and freedom from errors caused by minor variations in lead location from specimen to specimen. Near crack tip lead locations (or notch tip locations for uncracked specimens) yield better sensitivity to changes in crack size. The difficulty with this type of arrangement is that the electrical field is, in general, highly nonuniform in the near tip region. Thus, minor variations in lead placement from one specimen to the next may produce significant differences in measured voltage for the same crack size (63). In most cases those positions which give greatest sensitivity to crack size changes also have the greatest sensitivity to variations in lead wire positioning.

A6.7 *Specimen Geometries*—Specimen geometries for fatigue crack growth rate testing covered in this test method are the compact tension, C(T), the eccentrically-loaded single edge crack tension, ESE(T), and the middle tension, M(T). The equations listed in the respective specimen annexes are derived under DC conditions for sharp cracks in the respective specimen geometries. Errors in crack size measurements may arise if a blunt notch is used as the reference crack size (59, 65).

A6.7.1 One or more measurements of the crack size should be made during the test using an alternative technique such as optical measurements on the specimen surface. These values should be used for comparison to evaluate the progress of each test. This is particularly important where a parameter derived from the crack size (stress intensity, and so forth) is being controlled. If optical measurements cannot be made during the test, the final crack size, along with the initial starter crack size, should be compared to the crack sizes determined from electric potential measurements. If a difference is observed between the optical and EPD crack sizes, a linear correction factor, similar to that described for crack curvature correction in the main section (Calculation and Interpretation of Results), must be employed to “post-correct” the EPD crack size values (see also A6.3).

A6.7.2 Regardless of the EPD versus crack size expression used, the use of a reference probe is encouraged (see A6.3). This reference probe should be located on the test specimen (or another specimen at the identical test conditions) in a region unaffected by crack growth and should be equal to or greater in magnitude to the expected voltage levels measured across the crack. When employing such a reference probe, the EPD measurements made for crack size determination are divided by the ratio  $V_{\text{ref}}/V_{\text{ref}_0}$ ,

where:

$V_{\text{ref}}$  = the reference probe voltage measured at the same time as the EPD crack voltage is measured, and  
 $V_{\text{ref}_0}$  = the initial reference probe voltage.

A6.7.3 For AC potential systems, caution should be applied when using the referenced equations listed in the respective specimen annexes for crack size determination which were developed under the assumption that the measured potentials reflect only a resistive voltage component. With an AC potential system the measured EPD voltage across the crack contains both a resistive and a reactive voltage component. For materials with high conductivity at high AC frequencies the reactive component can be a substantial fraction of the measured voltage and can lead to significant errors if used with the equations cited above. If conditions are such that the reactive component is significant then a new relationship must be empirically developed for the particular test/specimen conditions.

A6.8 *Gripping Considerations*—The electric potential difference method of crack size determination relies on a current of constant magnitude passing through the specimen when the potential voltage is measured. During such potential measurements it is essential that no portion of the applied current be shunted in a parallel circuit through the test machine. For most commercially available test machines and grip assemblies the resistance through the test frame is considerably greater than that of the test specimen. However, in some situations an alternative path for the applied current may exist through the test frame. In such cases, additional steps to provide isolation between the specimen and test frame may be necessary. Users of the potential difference method should ensure that the electrical resistance measured between the grips (with no specimen in place) is several orders of magnitude higher than the resistance of the specimen between the current input locations. The specimen resistance should be determined for the range of crack sizes encountered during the test. A resistance ratio (test frame resistance divided by the specimen resistance) of  $10^4$  or greater is sufficient for most practical applications. Isolation of the specimen from the test frame is particularly important when using power supplies with non-isolated (ground referenced) outputs. Use of this type of power supply may require isolating both ends of the test specimen from the test frame to avoid ground loop problems.

A6.8.1 For specimens in which the current is introduced through the loading pins, care must be taken to ensure that good electrical contact is maintained between the pin and the specimen. Constant current power supplies can usually correct for small changes in the pin/specimen/grip resistance, however, abrupt or large changes in resistance due to oxidation or other effects may cause varying or erratic current levels, or both, during the force cycle. Poor loading pin contact may increase the percentage of an alternate current path and shunting errors.

A6.9 *Wire Selection and Attachment*—Careful selection and attachment of current input and voltage measurement wires can avoid many problems associated with the electric potential method. This is particularly important in aggressive test

environments such as elevated temperature where the strength, melting point, and oxidation resistance of the wires must be taken into account. Aggressive test environments may require special lead wire materials or coatings, or both, to avoid loss of electrical continuity caused by corrosive attack.

**A6.9.1 Current Input Wires**—Selection of current input wire should be based on current carrying ability, and ease of attachment (weldability, connector compatibility). Wires must be of sufficient gage to carry the required current under test conditions and may be mechanically fastened or welded to the specimen or gripping apparatus.

**A6.9.2 Voltage Measurement Wires**—Voltage wires should be as fine as possible to allow precise location on the specimen and minimize stress on the wire during fatigue loading which could cause detachment. Ideally, the voltage sensing wires should be resistance welded to the specimen to ensure a reliable, consistent joint. Lead wires may be fastened using mechanical fasteners for materials of low weldability (for example, certain aluminum alloys), provided that the size of the fastener is accounted for when determining location of voltage sensing leads. Voltage sensing wire should be located diagonally across the starter notch or crack tip as shown in the respective specimen annexes to average measurements of non-uniform crack fronts.

**A6.10 Resolution of Electric Potential Systems**—The effective resolution of EPD measurements depends on a number of factors including voltmeter resolution (or amplifier gain, or both), current magnitude, specimen geometry, voltage measurement and current input wire locations, and electrical conductivity of the specimen material. Herein, effective resolution is defined as the smallest change in crack size which can be distinguished in actual test operation, not simply the best resolution of the recording equipment. For common laboratory specimens, a direct current in the range of 5 to 50 A and voltage resolution of about  $\pm 0.1 \mu\text{V}$  or  $\pm 0.1\%$  of  $V_r$  will yield a resolution in crack size of better than 0.1% of the specimen width (crack size resolution must be in accordance with 8.8). For highly conductive materials (that is, aluminum, copper) or lower current levels, or both, the resolution would decrease, while for materials with a lower conductivity (that is, titanium, nickel) resolutions of better than 0.01% of the specimen width have been achieved. For a given specimen geometry, material, and instrumentation, crack size resolution shall be analyzed and reported.

NOTE A6.1—The following is an example of the magnitude of voltages as measured on a standard C(T) specimen for a direct current of 10 A:

Material	Approximate EPD Measured at 10A	Approximate Change in Crack Size for 1 $\mu\text{V}$ Change in EPD
Aluminum	0.1 mV	300 $\mu\text{m}$
Steel	0.6 mV	50 $\mu\text{m}$
Titanium	3.5 mV	9 $\mu\text{m}$

Based on  $a/W = 0.22$ ,  $B = 7.7$  mm, and  $W = 50$  mm.

**A6.11 Techniques to Reduce Voltage Measurement Scatter**—Because of the low level signals which must be measured with either the DC or AC current methods, a number

of procedures should be followed to improve voltage measurement precision.

**A6.11.1 Induced EMF**—Voltage measurement lead wires should be as short as possible and should be twisted to reduce stray voltages induced by changing magnetic fields. Holding them rigid also helps reduce the stray voltages which can be generated by moving the wires through any static magnetic fields that may exist near the test frame. In addition, routing the voltage measurement leads away from the motors, transformers, or other devices which produce strong magnetic fields is recommended.

**A6.11.1.1** For AC systems, care should be taken to keep the current wires away from the potential leads. If shielded voltage lead wire is used, the shield should be properly grounded at one end.

**A6.11.2 Electrical Groundings**—Proper grounding of all devices (current source, voltmeters, and so forth) should be made, avoiding ground loops. This is particularly important when DC procedures are used in conjunction with electrochemical polarization equipment relevant to corrosion fatigue.

**A6.11.3 Thermal Effects**—For DC systems thermal emf measurement and correction is critically important. A minimum number of connections should be used and maintained at a constant temperature to minimize thermoelectric effects (see A6.3.1).

**A6.11.3.1** All measuring devices (amplifiers/preamplifiers, voltmeters, analog-to-digital converters) and the specimen itself should be maintained at a constant temperature. Enclosures to ensure constant temperatures throughout the test are generally beneficial.

**A6.11.3.2** Some voltmeters for DC systems have built-in automatic correction for internal thermoelectric effects. These units may be of benefit in cases where it is not possible to control the laboratory environment.

**A6.11.4 Selection of Input Current Magnitude**—The choice of current magnitude is an important parameter: too low a value may not produce measurable output voltages; too high a value may cause excessive specimen heating or arcing (51).

**A6.11.4.1** To minimize these problems, current densities should be kept to the minimum value which can be used to produce the required crack size resolution. The maximum current that can be used with a particular specimen can be determined by monitoring the specimen temperature while increasing the current in steps, allowing sufficient time for the specimen to thermally stabilize. Particular care should be exercised when testing in vacuum, as convection currents are not available to help maintain the specimen at ambient temperature.

**A6.11.5 DC Current Stabilization Period**—Allow a sufficient stabilization period after turning the DC electric potential current either on or off before making a voltage measurement. Most solid-state power sources can stabilize the output current within a period of 1 or 2 s for a step change in output, however, this should be verified for each particular specimen and experimental setup.

**A6.12 Precautions**—Care must be taken to demonstrate that the applied current does not affect crack tip damage processes and crack growth rates. For example, in corrosion

fatigue, current leakage into the crack solution could alter electrochemical reaction rates and affect cracking. Results to date indicate that this is not a practical problem, presumably because of the high metal conductivity compared to even the most conductive of electrolytes (for example, NaCl). Current flow in the solution is not affected by the current in the specimen (68).

A6.12.1 Large-scale crack tip plasticity can increase measured electrical potentials due to resistivity increases without crack extension (50). Experience indicates that this potential source of error is not significant even when plastic deformation is greater than the small-scale yielding criteria of Test Method E 647 (47).

## APPENDIXES

### (Nonmandatory Information)

#### X1. RECOMMENDED DATA REDUCTION TECHNIQUES

##### X1.1 Secant Method

X1.1.1 The secant or point-to-point technique for computing the crack growth rate simply involves calculating the slope of the straight line connecting two adjacent data points on the  $a$  versus  $N$  curve. It is more formally expressed as follows:

$$(da/dN)_{\bar{a}} = (a_{i+1} - a_i)/(N_{i+1} - N_i) \quad (X1.1)$$

Since the computed  $da/dN$  is an average rate over the  $(a_{i+1} - a_i)$  increment, the average crack size,  $\bar{a} = 1/2(a_{i+1} + a_i)$ , is normally used to calculate  $\Delta K$ .

##### X1.2 Incremental Polynomial Method

X1.2.1 This method for computing  $da/dN$  involves fitting a second-order polynomial (parabola) to sets of  $(2n + 1)$  successive data points, where  $n$  is usually 1, 2, 3, or 4. The form of the equation for the local fit is as follows:

$$\hat{a}_i = b_0 + b_1 \left( \frac{N_i - C_1}{C_2} \right) + b_2 \left( \frac{N_i - C_1}{C_2} \right)^2 \quad (X1.2)$$

where:

$$-1 \leq \left( \frac{N_i - C_1}{C_2} \right) \leq +1 \quad (X1.3)$$

and  $b_0$ ,  $b_1$ , and  $b_2$  are the regression parameters that are determined by the least squares method (that is, minimization of the square of the deviations between observed and fitted values of crack size) over the range  $a_{i-n} \leq a \leq a_{i+n}$ . The value  $\hat{a}_i$  is the fitted value of crack size at  $N_i$ . The parameters  $C_1 = 1/2(N_{i-n} + N_{i+n})$  and  $C_2 = 1/2(N_{i+n} - N_{i-n})$  are used to scale

the input data, thus avoiding numerical difficulties in determining the regression parameters. The rate of crack growth at  $N_i$  is obtained from the derivative of the above parabola, which is given by the following expression:

$$(da/dN)_{\hat{a}_i} = (b_1)/(C_2) + 2b_2(N_i - C_1)/C_2^2 \quad (X1.4)$$

The value of  $\Delta K$  associated with this  $da/dN$  value is computed using the fitted crack size,  $\hat{a}_i$ , corresponding to  $N_i$ .

X1.2.2 A BASIC computer program that utilizes the above scheme for  $n = 3$ , that is, 7 successive data points, is given in Table X1.1 (see Eq X1.1). This program uses the specimen  $K$ -calibrations for the C(T) and M(T) geometries given in the respective specimen annexes and also checks the data against the size requirements listed in each annex.

X1.2.3 An example of the output from the program is given in Table X1.2. Information on the specimen, loading variables, and environment are listed in the output along with tabulated values of the raw data and processed data. A(Meas.) and A(Reg.) are values of total crack size obtained from measurement and from the regression equation (Eq X1.2), respectively. The goodness of fit of this equation is given by the multiple correlation coefficient, MCC (note that MCC = 1 represents a perfect fit). Values of Delta K ( $\Delta K$ ) and  $da/dN$  are given in the same units as the input variables (for the example problem these are ksi  $\sqrt{in.}$  and in./cycle, respectively). Values of  $da/dN$  that violate the specimen size requirement appear with an asterisk and note as shown in Table X1.2 for the final 15 data points.

TABLE X1.1 BASIC Computer Program for Data Reduction by the Seven Point Incremental Polynomial Technique

```

QuickBasic Computer Program for Data Reduction by the Seven Point Increment
' Polynomial Technique
DIM a(200), n(200), bb(3), dadn(200), delk(200), id(7), aa(10), nn(10)
OPEN "example.DAT" FOR INPUT AS #1
OPEN "result.dat" FOR OUTPUT AS #2
Input parameters as they should appear in input file:
'   ys: yield strength (ksi)
'   B: thickness (inches)
'   W: width (inches)
'   pmax: maximum load (kips)
'   pmin: minimum load (kips)
'   notch: notch length (inches)
'   freq: test frequency
'   type$: "ct" or "ccp"
'   temper$: temperature
'   labenviro$: lab environment
'   n(i), a(i): cycles, crack length (inches)- measured from notch tip

npts = 0
INPUT #1, ys, B, W, pmax, pmin, notch, freq, type$, temper$, labenviro$
DO UNTIL EOF(1)
    npts = npts + 1
    INPUT #1, n(npts), a(npts)
LOOP

k = 0
pi = 3.1416
deltap = pmax - pmin
Rratio = pmin / pmax

'Add notch length to measured crack length
FOR Inpt = 1 TO npts
    a(Inpt) = a(Inpt) + notch
NEXT Inpt

'Printing header information
PRINT #2, USING "&"; "Specimen No.:", specnumber$;
PRINT #2, USING "&"; " No. of Points: ", STR$(npts)
PRINT #2, USING "&"; "Specimen Type: ", type$, " B= ", STR$(B);
PRINT #2, USING "&"; " W= ", STR$(W), " Ao= ", STR$(notch)
PRINT #2, USING "&"; "Pmin= ", STR$(pmin), " Pmax= ", STR$(pmax);
PRINT #2, USING "&"; " R= ", STR$(Rratio), " Test Freq= ", STR$(freq)
PRINT #2, USING "&"; "Temperature= ", temper$;
PRINT #2, USING "&"; " Environment: ", labenviro$
PRINT #2,
PRINT #2, USING "&"; "No.", " Cycles", " A(Meas.)", " A(Reg.)";
PRINT #2, USING "&"; " M.C.C.", " Delta K", " da/dN"
PRINT #2,

First three data points are printed
FOR i = 1 TO 3
    PRINT #2, USING "## "; i;
    PRINT #2, USING "##### "; n(i);

```

TABLE X1.1 *Continued*

```

        PRINT #2, USING "#.#### "; a(i)
    NEXT i
    npts = npts - 6
    FOR Inpt = 1 TO npts
        l = 0
        k = k + 1
        k1 = k + 6
        FOR lindex = k TO k1
            l = l + 1
            aa(l) = a(lindex)
            nn(l) = n(lindex)
        NEXT lindex
        c1 = .5 * (nn(1) + nn(7))
        c2 = .5 * (nn(7) - nn(1))
        sx = 0
        sx2 = 0
        sx3 = 0
        sx4 = 0
        sy = 0
        syx = 0
        syx2 = 0
        FOR Inum = 1 TO 7
            x = (nn(Inum) - c1) / c2
            yy = aa(Inum)
            sx = sx + x
            sx2 = sx2 + x ^ 2
            sx3 = sx3 + x ^ 3
            sx4 = sx4 + x ^ 4
            sy = sy + yy
            syx = syx + x * yy
            syx2 = syx2 + yy * x ^ 2
        NEXT Inum
        Term1 = (sx2 * sx4 - sx3 ^ 2)
        Term2 = (sx * sx4 - sx2 * sx3)
        Term3 = (sx * sx3 - sx2 ^ 2)
        Denom = 7 * Term1 - sx * Term2 + sx2 * Term3
        Numer2 = sy * Term1 - syx * Term2 + syx2 * Term3
        bb(1) = Numer2 / Denom
        Term4 = syx * sx4 - syx2 * sx3
        Term5 = sy * sx4 - syx2 * sx2
        Term6 = sy * sx3 - syx * sx2
        Numer3 = 7 * Term4 - sx * Term5 + sx2 * Term6
        bb(2) = Numer3 / Denom
        Term7 = sx2 * syx2 - sx3 * syx
        Term8 = sx * syx2 - sx3 * sy
        Term9 = sx * syx - sx2 * sy
        Numer4 = 7 * Term7 - sx * Term8 + sx2 * Term9
        bb(3) = Numer4 / Denom
        yb = sy / 7
        rss = 0
        tss = 0
        FOR Inum = 1 TO 7
            x = (nn(Inum) - c1) / c2
            yhat = bb(1) + bb(2) * x + bb(3) * x ^ 2
            rss = rss + (aa(Inum) - yhat) ^ 2
            tss = tss + (aa(Inum) - yb) ^ 2
        NEXT Inum
    
```

TABLE X1.1 *Continued*

```

r2 = 1 - rss / tss
dadn(Inpt) = bb(2) / c2 + 2 * bb(3) * (nn(4) - c1) / c2 ^ 2
x = (nn(4) - c1) / c2
ar = bb(1) + bb(2) * x + bb(3) * x ^ 2
s = 1E+10
snet = 0
qq = Inpt + 3
IF (type$ = "ct") THEN
    t = ar / W
    num = (.886 + 4.64 * t - 13.32 * t ^ 2 + 14.72 * t ^ 3 - 5.6 * t ^ 4)
    den = (1 - t) ^ 1.5
    ft = ((2 + t) * num) / den
    s = ys * ((pi * W * (1 - t) ^ .5) / 2
ELSE
    t = 2 * ar / W
    sec = 1 / (COS(pi * t / 2))
    ft = (pi * t * sec / 2) ^ .5
    snet = pmax / (B * W * (1 - t))
END IF

delk(Inpt) = (ft * deltap) / (B * W ^ .5)
ax = delk(Inpt) / (1 - Rratio)

IF (ax >= s OR snet >= ys) THEN
    PRINT #2, USING "## "; qq;
    PRINT #2, USING "##### "; n(qq);
    PRINT #2, USING "#.#### "; a(qq), ar, r2;
    PRINT #2, USING " ##.## "; delk(Inpt);
    PRINT #2, USING "#.#### "; dadn(Inpt);
    PRINT #2, " *"
ELSE
    PRINT #2, USING "## "; qq;
    PRINT #2, USING "##### "; n(qq);
    PRINT #2, USING "#.#### "; a(qq), ar, r2;
    PRINT #2, USING " ##.## "; delk(Inpt);
    PRINT #2, USING "#.#### "; dadn(Inpt)
END IF

NEXT Inpt
j = npts + 4
k = npts + 6
FOR Iprnt = j TO k
    PRINT #2, USING "## "; Iprnt;
    PRINT #2, USING "##### "; n(Iprnt);
    PRINT #2, USING "#.#### "; a(Iprnt)
NEXT Iprnt
PRINT #2, USING "&"; "*" - Data violate specimen size requirements"

CLOSE #1
CLOSE #2
STOP
END
    
```

**TABLE X1.2 Example Output from Incremental Polynomial Computer Program**

```

Specimen No.:   No. of Points: 37
Specimen Type: ct  B= .25  W= 2  Ao= .5
Pmin= 4  Pmax= 5  R= .8  Test Freq= 5
Temperature= 75 F  Environment: lab air

```

No. Cycles	A(Meas.)	A(Reg.)	M.C.C.	Delta K	da/dN	
1	0	0.5990				
2	15480	0.6310				
3	22070	0.6560				
4	30240	0.6740	0.6772	0.9969	17.56	0.3233E-05
5	36090	0.6980	0.6977	0.9963	18.03	0.3369E-05
6	41370	0.7180	0.7156	0.9910	18.45	0.3189E-05
7	46850	0.7350	0.7345	0.9925	18.90	0.3367E-05
8	50090	0.7460	0.7439	0.9928	19.13	0.3404E-05
9	54380	0.7530	0.7579	0.9956	19.48	0.3472E-05
10	60320	0.7810	0.7794	0.9965	20.04	0.3870E-05
11	65160	0.8010	0.7998	0.9965	20.58	0.4122E-05
12	70240	0.8210	0.8225	0.9990	21.21	0.4441E-05
13	74690	0.8430	0.8416	0.9995	21.77	0.4525E-05
14	80070	0.8650	0.8665	0.9994	22.51	0.4803E-05
15	83860	0.8860	0.8853	0.9993	23.11	0.4926E-05
16	88080	0.9060	0.9061	0.9992	23.79	0.5168E-05
17	91460	0.9250	0.9240	0.9991	24.41	0.5450E-05
18	95620	0.9450	0.9465	0.9995	25.21	0.5833E-05
19	99000	0.9670	0.9669	0.9992	25.99	0.6109E-05
20	102360	0.9880	0.9883	0.9985	26.84	0.6230E-05 *
21	105110	1.0080	1.0062	0.9971	27.58	0.6677E-05 *
22	108440	1.0280	1.0283	0.9973	28.55	0.6930E-05 *
23	111660	1.0470	1.0507	0.9973	29.60	0.7411E-05 *
24	113410	1.0670	1.0636	0.9976	30.23	0.7593E-05 *
25	116810	1.0900	1.0910	0.9969	31.65	0.8432E-05 *
26	118730	1.1080	1.1079	0.9959	32.59	0.8984E-05 *
27	121220	1.1280	1.1304	0.9986	33.91	0.1049E-04 *
28	121880	1.1380	1.1372	0.9986	34.32	0.1109E-04 *
29	122830	1.1480	1.1481	0.9981	35.00	0.1140E-04 *
30	124280	1.1660	1.1663	0.9993	36.20	0.1268E-04 *
31	125820	1.1870	1.1854	0.9992	37.54	0.1342E-04 *
32	127480	1.2070	1.2076	0.9930	39.20	0.1649E-04 *
33	128700	1.2260	1.2273	0.9946	40.79	0.2015E-04 *
34	129760	1.2450	1.2494	0.9776	42.69	0.2794E-04 *
35	130790	1.2770				
36	131480	1.2980				
37	131550	1.3230				

\* - Data violate specimen size requirements

## X2. RECOMMENDED PRACTICE FOR DETERMINATION OF FATIGUE CRACK OPENING FORCE FROM COMPLIANCE

### X2.1 Introduction

X2.1.1 The term *crack closure* refers to the phenomenon whereby the fracture surfaces of a fatigue crack come into contact during the unloading portion of a force cycle and force is transferred across the crack. In many materials, crack closure can occur while the force is above the minimum force in the cycle even when the minimum force is tensile. Upon reloading from minimum force, some increment of tensile loading must be applied before the crack is again fully open. Thus, crack closure provides a mechanism whereby the effective cyclic stress intensity factor range near the crack tip ( $\Delta K_{\text{eff}}$ ) differs from the nominally applied value ( $\Delta K$ ). Therefore, information on the magnitude of the crack closure effect is essential to understand and interpret observed crack growth behavior. An estimate of  $\Delta K_{\text{eff}}$  can be obtained experimentally by determin-

ing the minimum force at which the crack is open (opening force,  $P_o$ ) and, if  $P_o > P_{\text{min}}$ , using the effective force range ( $\Delta P_{\text{eff}} = P_{\text{max}} - P_o$ ) in expressions for the stress intensity factor range instead of force range ( $\Delta P = P_{\text{max}} - P_{\text{min}}$ ).

X2.1.2 Many experimental techniques have been used to determine the opening force. These techniques have included the use of ultrasonics, potential drop, eddy current, acoustic emission, high magnification photography, and strain or displacement versus force (compliance) measurements. Due mainly to its experimental simplicity, the compliance technique has become the most widely used approach.

### X2.2 Scope

X2.2.1 This appendix covers the experimental determination of fatigue crack opening force in tests of the specimens

outlined in this test method, subjected to constant amplitude or slowly changing (similar to force shedding rates recommended in this test method for threshold tests at constant force ratio) loading.

### X2.3 Terminology

X2.3.1 Definitions of terms specific to this appendix are given in this section. Other terms used in this appendix are defined in the main body of this test method.

#### X2.3.2 Definitions:

X2.3.2.1 *crack closure*—in fatigue, the phenomenon whereby the fracture surfaces of a fatigue crack come into contact during the unloading portion of a force cycle and force is transferred across the crack.

X2.3.2.2 *effective force range*,  $\Delta P_{\text{eff}}[F]$ —in fatigue, that part of the increasing-force range of the cycle during which the crack is open. The effective force range is expressed as:

$$\Delta P_{\text{eff}} = P_{\text{max}} - P_o \quad \text{if } P_o > P_{\text{min}}, \text{ and} \quad (\text{X2.1})$$

$$\Delta P_{\text{eff}} = \Delta P = P_{\text{max}} - P_{\text{min}} \quad \text{if } P_o \leq P_{\text{min}} \quad (\text{X2.2})$$

X2.3.2.3 *effective stress intensity factor range*,  $\Delta K_{\text{eff}}[FL^{-3/2}]$ —in fatigue, the stress intensity factor range computed using the effective force range,  $\Delta P_{\text{eff}}$ .

X2.3.2.4 *opening force*,  $P_o [F]$ —in fatigue, the minimum force at which the fatigue crack is open at the tip during the increasing-force part of a cycle.

### X2.4 Significance and Use

X2.4.1 The method of determining crack opening force, and therefore of estimating  $\Delta K_{\text{eff}}$ , presented in this appendix should be useful in assessing and comparing the effects of crack closure on the crack growth behavior of various materials. The method does not define the exact portion of the applied  $\Delta K$  that is effective in growing the crack nor the exact values of the opening force at all points along the crack front, but does provide a well-defined operational approach that can be used to estimate the first-order effects of closure.

X2.4.2 Measurements of opening force made using this procedure can serve as reference or benchmark values that can be used in evaluating crack closure information from different sources and from other experimental techniques.

### X2.5 Basis for Determination of Opening Force From Compliance

X2.5.1 The determination of opening force from compliance is based on the observation that when a cracked specimen is loaded up to the force at which the crack becomes fully open, the compliance (slope of the strain or displacement against force curve) attains a characteristic value and remains essentially constant upon further force increase until the force is increased enough to cause large-scale yielding near the crack tip. Upon unloading from the maximum force in a cycle, the compliance again has the characteristic value for the fully-open crack regardless of whether large-scale yielding occurred before maximum force was achieved. Conceptually, the experimental task is very simple—determine the force at which the strain or displacement against force curve becomes linear

(analogous to the determination of proportional limit in a tensile test). However, in practice, this task is very difficult due to the gradual change in compliance as it approaches the open-crack value and to the nonlinearity and variability, or *noise*, in the compliance data. Nonlinearity and noise in the measurement system can cause significant variation in the estimates of opening force.

X2.5.2 One way to reduce scatter in opening force results due to noise and nonlinearity in the measurement system is to define opening force as the force corresponding to a compliance that is offset from (lower than) the fully-open-crack value rather than the force at which the compliance attains the fully-open value (that is, the point where the curve becomes linear). The scatter will be reduced because the offset compliance value corresponds to a position on the loading curve where a change in compliance is associated with a smaller change in force than would be the case for a position very near the start of the linear part of the curve. Of course, with the offset compliance approach, the opening forces determined will be somewhat lower than the force at which the crack becomes fully open. Selection of an appropriate compliance offset criterion then becomes a trade-off between achieving a reduction in scatter and minimizing the deviation of the compliance-offset opening force from the force at which the crack becomes fully open. Some information on this trade-off is given in Ref (76).

### X2.6 Apparatus

X2.6.1 The procedure requires a strain or displacement transducer which can be mounted on the specimen and a digital data acquisition and processing system capable of acquiring data from the testing machine force cell and the strain/displacement transducer.

X2.6.2 The requirements for the strain/displacement transducers and other experimental apparatus are, in general, the same as that specified in Annex A5 for using compliance to determine crack size. However, the requirement for high quality (good linearity and low noise) strain/displacement data is especially critical in measuring opening force using the compliance procedure. Accordingly, an accept/reject criterion for data quality is described in X2.8.

X2.6.3 The location of the strain or displacement measurement may be near the crack tip or remote from the tip. However, for tests within the scope of this appendix, remote measurements are recommended because they are experimentally simpler and are likely to be more repeatable than near-tip measurements. For the C(T) and ESE(T) specimens, the recommended measurements are: (1) displacement across the crack mouth, and (2) strain at the mid-height location on the back face. For the M(T) specimen, the recommended measurement is displacement across the crack on the longitudinal centerline (see Fig. X2.1).

### X2.7 Recommended Procedure—Determination of Opening Force by the Compliance Offset Method

X2.7.1 Background information on the rationale for using this method can be found in Refs (76) and (77). The step-by-step procedure for determining opening force from strain or displacement against force data is as follows:

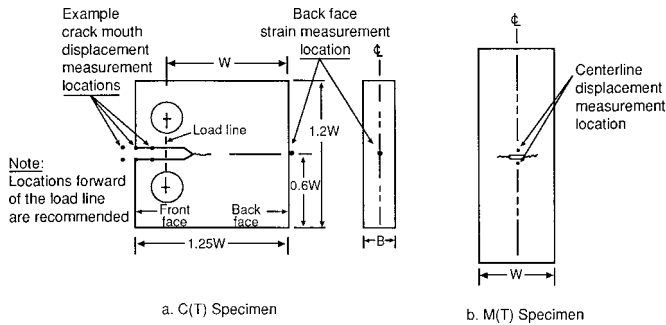


**FIG. X2.1 Recommended Displacement and Strain Measurement Locations for Determination of Fatigue Crack Opening Load on C(T) and M(T) Specimens**

X2.7.1.1 Collect digitized strain/displacement and force data for a complete force cycle. The data sampling rate should be high enough to ensure that at least one data pair (displacement and force) is taken in every 2 % interval of the cyclic force range for the entire cycle. (Different loading waveforms require different minimum sampling rates to ensure that one point is taken in every 2 % interval.)

X2.7.1.2 Starting just below maximum force (not less than 0.90 maximum force) on the unloading curve, fit a least-squares straight line to a segment of the curve that spans a range of approximately 25 % of the cyclic force range. The slope of this line is assumed to be the compliance value that corresponds to the fully-open crack configuration.

NOTE X2.1—**Caution:** For some materials and loading conditions that produce high opening forces, this assumption may not be correct. The opening force may actually lie within the fitted force range, and in that case, the computed open-crack compliance and the opening force from the analysis will be too low. The procedure in X2.7.1.6 provides a check on the reasonableness of the open-crack compliance assumption.

X2.7.1.3 Starting just below maximum force (not less than 0.95 maximum force) on the loading curve, fit least-squares straight lines to segments of the curve that span a range of approximately 10 % of the cyclic force range and that overlap each other by approximately 5 % of the cyclic force range (see Fig. X2.2). Determine the compliance (slope) and the corresponding mean force for each segment.

X2.7.1.4 Calculate the compliance offset for each segment as follows:

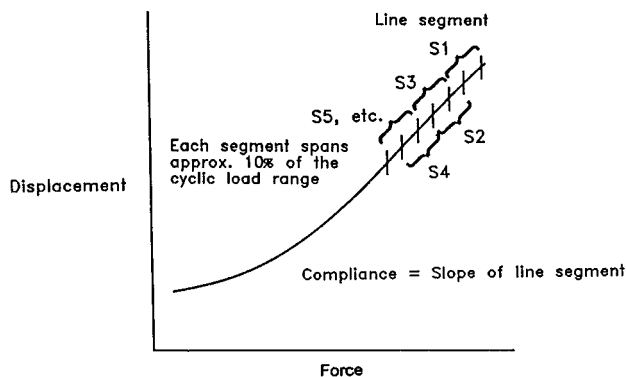


**FIG. X2.2 Evaluation of the Variation of Compliance With Load for Use in Determination of Opening Force**

$$\text{Compliance offset} = \frac{[(\text{open-crack compliance}) - (\text{compliance})](100)}{(\text{open-crack compliance})} \quad (\text{X2.3})$$

where the *open-crack* value is taken from X2.7.1.2.  
 X2.7.1.5 Plot the (compliance offset, mean force) points from the segments and connect the points with straight lines (see Fig. X2.3). Determine the opening force ( $P_o$ ) corresponding to the selected offset criterion as the lowest force at which a line connecting points has the value of compliance offset equal to the offset criterion.

NOTE X2.2—**Caution:** If more than one line connecting points crosses the offset criterion level (see Fig. X2.4), the variability of the compliance data is probably high enough to cause significant variation in the opening force results. Steps should be taken to reduce the variability. Variability can usually be reduced by electrically shielding the transducer wires and by appropriate electronic filtering of the signals before input into the data acquisition system. Matched filters must be used to prevent introduction of a phase shift between the force and displacement/strain signals.

X2.7.1.6 Check the reasonableness of the open-crack compliance value from X2.7.1.2 if an opening force above  $0.50P_{\text{max}}$  was found in X2.7.1.5. To make the check, return to X2.7.1.2 and find the slopes of lines fit to several force ranges both larger and smaller than 25 %. Plot the resulting slopes against fitted-force-range and identify the largest range below which the slope remains constant. If the identified range is smaller than 25 %, the opening force analysis should be performed again using the new, smaller-range slope value as the open-crack compliance.

X2.7.2 It is recommended that opening forces be determined and reported for offset criteria of 1, 2, and 4 % of the open-crack compliance value. As a minimum, the opening force defined by an offset criterion of 2 % of the open-crack compliance value should be reported.

X2.7.3 It is also recommended that multiple (as many as practicable) opening force determinations be made and that the mean value of the opening forces be reported. The cyclic force level must remain the same and the crack size,  $a$ , should not change more than  $0.001 W$  during the multiple determinations.

**X2.8 Data Quality Requirement**

X2.8.1 The quality of the raw strain/displacement against force data can affect the value of the opening force determined using the compliance offset method. As used here, data quality

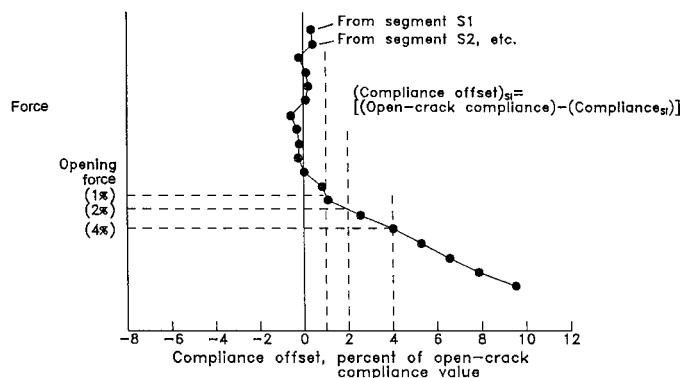
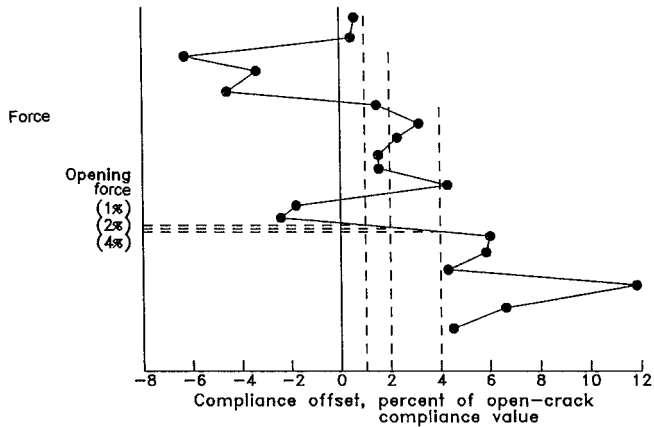


**FIG. X2.3 Determination of Opening Force Using the Compliance Offset Method**



NOTE 1—Multiple crossings of the offset criteria levels is an indication that the variation is too high.

FIG. X2.4 Example of High Variability in Compliance Offset Data

is defined in terms of two attributes of the measurement system: (1) the linearity of the system, and (2) the noise or variability in the system. Both attributes can affect the opening force results. Therefore, it is recommended that the quality of the data be checked for each test specimen.

X2.8.2 To check the quality of data for each test specimen, strain/displacement against force data should be acquired on the notched specimen before a crack is generated in the specimen. Data should be acquired for a complete force cycle at the same loading rate at which data will be acquired during the test. Analyze the data for compliance offset using the same procedure as would be used for a cracked specimen as described in X2.7.1. Using the compliance offset values for the

increasing force portion of the force cycle, compute the mean of the compliance offset values and the standard deviation of the offset values about the mean. For a perfectly linear noise-free measurement system, the mean and standard deviation of the offsets should be zero. If the absolute value of the mean of the measured offsets (expressed as percentages of the open-crack compliance) is greater than 1 % or the standard deviation of the offsets is greater than 2 %, the quality of the data is considered unacceptable for the determination of opening load using the compliance offset method. If data quality is not acceptable, the user should check for problems with transducer linearity (see A5.4), specimen flatness, force train alignment (see 6.2), gripping arrangement (see the appropriate specimen annex and A5.5), and noise on the transducer signals (see X2.7.1.5).

**X2.9 Report**

X2.9.1 The following information should be reported along with all reported measurements of opening force:

X2.9.1.1 The location of the strain or displacement measurement on the specimen and the transducer used to make the measurement.

X2.9.1.2 The value of the compliance offset criterion used in defining opening forces.

X2.9.1.3 The values of the mean and standard deviation of compliance offsets measured on the uncracked specimens.

X2.9.1.4 Typical plots of force against compliance offset for an uncracked specimen and a cracked specimen.

X2.9.1.5 Specimen thickness.

X2.9.1.6 A summary of the fatigue loading conditions prior to the opening force measurements.

**X3. GUIDELINES FOR MEASURING THE GROWTH RATES OF SMALL FATIGUE CRACKS**

**X3.1 Introduction**

X3.1.1 Fatigue cracks of relevance to many structural applications are often small or short for a significant fraction of the structural life. The growth rates of such cracks usually cannot be measured with the standard procedures described in the main body of Test Method E 647, which emphasizes the use of large, traditional fracture mechanics specimen geometries. Of greater importance, the growth behavior of these small cracks is sometimes significantly different from what would be expected based on large-crack growth rate data and standard fatigue crack growth analysis techniques. Direct measurement of small-crack growth rates may be desirable in these situations.

X3.1.2 This appendix provides general guidelines for test methods and related data analysis techniques to measure the growth rates of small fatigue cracks. Complete, detailed test procedures are not prescribed. Instead, the appendix provides general guidance on the selection of appropriate experimental and analytical techniques and identifies aspects of the testing process that are of particular importance when fatigue cracks are small.

X3.1.3 Many of the principles and procedures described in the main body of Test Method E 647 are applicable to small

fatigue cracks, and their use is encouraged unless otherwise noted here. Several aspects of Test Method E 647 that should be modified for small cracks are highlighted in this appendix.

**X3.2 Scope**

X3.2.1 This appendix describes the determination of fatigue crack growth rates in metallic materials for crack sizes that are too small to permit application of the standard methods described in the main body of Test Method E 647. A variety of possible specimen geometries and crack length measurement techniques are introduced.

**X3.3 Referenced Documents**

- E 4 Practices for Force Verification of Testing Machines<sup>3</sup>
- E 466 Practice for Conducting Constant Amplitude Axial Fatigue Tests of Metallic Materials<sup>3</sup>
- E 467 Practice for Verification of Constant Amplitude Dynamic Loads on Displacements in an Axial Load Fatigue Testing System<sup>3</sup>
- E 606 Practice for Strain-Controlled Fatigue Testing<sup>3</sup>
- E 616 Terminology Relating to Fracture Testing<sup>3</sup>
- E 1351 Practice for Production and Evaluation of Field Metallographic Replicas<sup>3</sup>

**X3.4 Terminology**

X3.4.1 The terms used in this appendix are given in the main body of Test Method E 647 and in the other terminology documents referenced in X3.3.

X3.4.2 *Descriptions of Terms Specific to This Standard:*

X3.4.2.1 *small crack*—a crack is defined as being small when all physical dimensions (in particular, both length and depth of a surface crack) are small in comparison to a relevant microstructural scale, continuum mechanics scale, or physical size scale. The specific physical dimensions that define *small* vary with the particular material, geometric configuration, and loadings of interest.

X3.4.2.2 *short crack*—a crack is defined as being short when only one physical dimension (typically, the length of a through-crack) is small according to the description of X3.4.2.1.

NOTE X3.1—Historically, the distinction between *small* and *short* cracks delineated here has not always been observed. The two terms have sometimes been used interchangeably in the literature, and some authors (especially in Europe) employ the term *short crack* to denote the meaning given here to *small crack*.

X3.4.2.3 *surface-crack length*—see Terminology E 616. In this appendix, physical surface-crack length is represented as *2c*.

X3.4.2.4 *surface-crack depth*—see **crack depth** in Terminology E 616. In this appendix, the physical surface-crack depth is represented as *a*.

**X3.5 Significance and Use**

X3.5.1 *The Small-Crack Effect:*

X3.5.1.1 Small fatigue cracks can be particularly important in structural reliability because of the so-called *small-crack effect*, the observation that small cracks sometimes grow at rates that are faster than long fatigue cracks at the same nominal crack driving force (typically expressed as  $\Delta K$ ). The reasons for this effect, the circumstances under which it will occur, and the proper means of rationalizing it analytically have been studied and discussed extensively (78-84), although full consensus has not been reached on all major issues.

X3.5.1.2 The effect is most often observed when the crack size is on the order of a characteristic microstructural dimension, such as the grain size, or a characteristic continuum mechanics dimension, such as the crack-tip or notch plastic zone size. In the former case, enhanced or reduced crack growth rates arise from interactions with the local microstructure that do not occur when total crack sizes and crack-tip

process zones are relatively large. In the latter case, the variation in growth rates may arise from a fundamental change (that is, an increase) in the crack driving force due to enhanced plastic deformation that is not reflected in the usual small-scale-yielding parameter  $\Delta K$ . Small-crack effects can also arise from other phenomena, such as alterations in localized crack chemistry and the associated kinetics of environmentally-assisted fatigue crack growth.

X3.5.1.3 It is often of practical importance to estimate the crack size below which data from small- and large-crack tests tend to differ. Different criteria (85) have been proposed for this dimension depending on the particular type of small crack, as summarized in Table X3.1. A crack which satisfies any one (or more) of these dimensional criteria may exhibit small-crack behavior.

X3.5.1.4 Another approach to identification of the small-crack regime follows from the original work of Kitagawa and Takahashi (86) which showed that threshold crack growth rate data display a dependence on crack size that is related to the material's fatigue limit ( $\Delta S_e$ ) and  $\Delta K_{th}$ . This idea, which combines fatigue crack initiation and propagation concepts, is illustrated schematically in Fig. X3.1. Considering crack initiation, and disregarding the possibility of a pre-existing crack, specimen failure should occur only if

$$\Delta S_{applied} > \Delta S_e \tag{X3.1}$$

Alternatively, considering a fracture mechanics approach, crack growth should occur only if

$$\Delta K_{applied} > \Delta K_{th} = F \Delta S \sqrt{\pi a} \tag{X3.2}$$

where *F* is a function of crack and specimen geometry and *a* is the crack length. Solving this equation for  $\Delta S$  gives

$$\Delta S = \frac{\Delta K_{th}}{F \sqrt{\pi a}} \tag{X3.3}$$

indicating that crack propagation should only occur in the region above the line of slope equal to  $-1/2$ . Thus, the utility of  $\Delta K_{th}$  as a *material property* appears to be limited to cracks of length greater than that given by the intersection of the two lines (*a*<sub>0</sub>). For many materials, *a*<sub>0</sub> appears to give a rough approximation of the crack size below which microstructural small-crack effects become potentially significant (87). Note, however, that *a*<sub>0</sub> may underestimate the importance of small-crack effects when crack wake closure or localized chemistry dominates the geometry effect on crack growth rates. Further discussion of this construction and its limitations is available in (88).

X3.5.1.5 An important manifestation of the small-crack effect is that physically small cracks may grow at  $\Delta K$  values below the measured large-crack threshold stress-intensity factor range,  $\Delta K_{th}$ , even when the small cracks are large compared to the microstructure and small-scale-yielding parameters appear to adequately describe the crack driving force. It is not entirely clear if this phenomenon indicates anomalous small-crack behavior or anomalous large-crack behavior. These small-crack growth data are often consistent with the large-crack data if the near-threshold large-crack data are neglected and if large-crack data are determined so as to minimize the

**TABLE X3.1 Classification and Size Guidelines for Small Fatigue Cracks (adapted from 84)**

NOTE 1—*a* here denotes a characteristic crack dimension (length or depth).

*r<sub>y</sub>* is plastic zone size or plastic field of notch.

*d<sub>g</sub>* is characteristic microstructural dimension, often grain size.

Type of Small Crack	Dimension
Mechanically-small	$a \sim \leq r_y$
Microstructurally-small	$a \sim \leq 5-10 d_g$
Physically-small	$a \sim \leq 1 \text{ mm}$
Chemically-small	$a \text{ up to } \sim 10 \text{ mm}$

effects of crack closure. In any case, the phenomenon is significant because predictions of small-crack growth in engineering structures based on laboratory large-crack (near-threshold) data may be extremely nonconservative. It is not clear if a measurable threshold exists for the growth of small fatigue cracks, although small cracks are sometimes observed to become nonpropagating.

X3.5.1.6 Structural applications in which small fatigue cracks are significant may involve applied stresses that approach or exceed the yield strength of the material. Characterization of the material resistance to stable cyclic crack growth under these conditions may require laboratory testing at similar applied stresses. These tests are not valid by the criteria of the main body of Test Method E 647 (see Specimen Configuration, Size, and Preparation), since the specimen is not predominantly elastic at all values of applied load. The basic techniques described in this appendix for performing the test, measuring crack length, and computing the crack growth rate are largely applicable, although a modified specimen design may be required. Alternative elastic-plastic formulations of the correlating parameter for fatigue crack growth rates, such as the range of the  $J$ -integral ( $\Delta J$ ), may be required under these conditions (89). Changes in crack closure behavior, which may further influence the crack driving force, may also be significant at larger applied stresses.

X3.5.2 Choice of a Test Method:

X3.5.2.1 Several well-established experimental techniques are available for measuring the growth rates of small fatigue cracks and for characterizing other important aspects of small-crack behavior. Some are more amenable than others for routine use, and some require significant expertise. Some require almost no financial investment, while others may require substantial expenditures. All are useful for measuring the growth of fatigue cracks sized on the order of 50  $\mu\text{m}$  or greater, and some are applicable to even smaller cracks.

X3.5.2.2 It is not the purpose of this appendix to recommend one particular measurement technique to the exclusion of the others. Each technique has unique strengths and limitations, and different techniques are optimum for different circumstances. This appendix introduces the various methods available, highlights relative advantages and disadvantages, and discusses in more detail the procedural issues that are common to all methods.

X3.5.2.3 These techniques are described in detail in an ASTM Special Technical Publication, STP 1149 (80). That publication and related references should be consulted for further information before a specific testing program is devised. Descriptions of other small fatigue crack experimental

and analytical investigations are available in (81-84).

X3.5.3 Specific Test Methods Available:

X3.5.3.1 Replication (90)—While fatigue cycling is interrupted and a static load is applied to the specimen, a small piece of thin cellulose acetate sheet is softened with acetone, gently applied to the specimen surface, and allowed to dry for a few minutes. The acetate replica forms a permanent record of the surface topography, including the crack mouth, and is subsequently viewed in an optical or (with appropriate replica processing) scanning electron microscope to measure surface crack length. See also Practice E 1351.

X3.5.3.2 Photomicroscopy (91)—To implement photomicroscopy (PM), a 35-mm camera with bulk film capability is linked to a standard metallurgical microscope and interfaced with the fatigue test frame via a microcomputer. An extensive series of high magnification photographs of the small fatigue crack is obtained during brief interruptions of cycling. Following the test, the crack photographs are projected on a computer digitizing tablet for crack length measurement.

X3.5.3.3 Potential Difference (92)—The direct current electric potential difference (dcEPD) method for continuous in-situ monitoring of crack growth (see Annex A6 to Test Method E 647) can be extended to small fatigue cracks. Closed-form analytical models are available to relate crack size to measured potential, as a function of crack shape and probe position locally spanning the crack mouth.

X3.5.3.4 Ultrasonic (93)—A surface acoustic wave (SAW) technique involves excitation of Rayleigh waves on the surface of a specimen and the automated data acquisition of the reflected echo from a small surface crack. A simple analytical model relates the echo amplitude to crack size.

X3.5.3.5 Laser Interferometry (94)—A computerized, laser-based, interferometric strain/displacement gage (ISDG) is used to monitor the relative displacement between two tiny indentations placed across small surface cracks. Estimates of crack sizes are obtained from measurements of elastic compliance.

X3.5.3.6 Scanning Electron Microscopy (95)—A small specimen is cycled on a specialized fatigue loading stage located inside the scanning electron microscope (SEM), and appropriate photographs or videotapes are taken as desired. Stereoimaging can be used to obtain high resolution displacement measurements on the specimen surface.

X3.5.3.7 Constant  $K_{\text{max}}$ -Decreasing  $\Delta K$  Method (96)—The application of a constant  $K_{\text{max}}$ -decreasing  $\Delta K$  load history to a standard (large-crack) FCG specimen has been proposed as a relatively rapid, simple means of minimizing the effects of crack closure. Based on the assumption that small cracks are distinguished from large cracks primarily in terms of reduced closure levels, it has been argued that the method generates an upper bound estimate to small-crack growth rates. This technique cannot address other aspects of the small-crack effect, such as microstructural interactions, extensive crack-tip plasticity, or near-surface residual stresses. This technique is addressed by the main body of Test Method E 647.

X3.5.4 Comparative Remarks about Test Methods:

X3.5.4.1 Crack Location—The replica technique is preferable when the location of crack initiation cannot be predicted with certainty. A chronological series of replicas can be used to

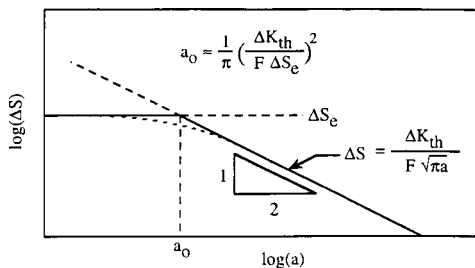


FIG. X3.1 Diagram for Estimating  $a_0$

track crack growth in reverse time from a large, easily found crack to its origins as a tiny, difficult-to-find microcrack. All other methods generally require a small crack to be located at an early stage of growth (perhaps by replication), or require the location of the crack to be fixed in advance with a micronotch.

**X3.5.4.2 Specimen and Crack Geometries**—The direct optical or imaging (PM, ISDG, SEM) and SAW techniques require specimen surfaces that are either flat or gently curved. The replica and dcEPD methods can be used on a wider variety of specimens, including cylindrical or notched geometries. Replica, PM, and SEM methods provide information on surface crack length only, while the ISDG, SAW, and dcEPD measurements give information about crack depth or cracked area. All methods require independent confirmation of crack shape to complete a crack growth analysis. The ISDG, SAW, and dcEPD information can be corrupted by the presence of multiple cracks.

**X3.5.4.3 Test Environments**—Replication is difficult to apply in any environment other than room temperature lab air unless the test is interrupted and the specimen is temporarily separated from the environment. Crack growth in high temperature or aggressive environments is probably best addressed by dcEPD. SEM, ISDG, PM, and SAW can be used, in principle, at elevated temperatures, although additional specialized equipment may be required, and some limitations may remain. The replication process has been shown to influence crack growth rates artificially in some materials, perhaps related to environmental effects. Small-crack tests in the SEM must be performed in vacuum, which may influence crack behavior if ambient environmental effects are significant.

**X3.5.4.4 Resolution**—The SEM technique gives the highest resolution of surface crack length, followed by replication with a resolution on the order of 0.1  $\mu\text{m}$ . The PM and ISDG methods both claim resolutions on the order of 1  $\mu\text{m}$ . The average crack depth resolution of dcEPD is slightly lower, and the SAW technique perhaps the lowest (on the order of several microns). These are only general, comparative guidelines. The specific resolution attained can be influenced by the quality of the equipment, the experience of the investigators, and the material under investigation. The values given above are based on the work of specialists for each technique. Also note that “resolution” can have different meanings in different applications: for example, direct resolution of surface crack length vs. average resolution of crack depth from model calculations of some measured quantity.

**X3.5.4.5 Cost**—The replica technique involves minimal equipment cost but is extremely labor-intensive and time-consuming. The SEM and ISDG approaches require expensive and highly specialized equipment and relatively highly trained operators. PM, dcEPD, and SAW techniques require some specialized but relatively inexpensive equipment and may be automated to reduce labor and clock time.

**X3.6 Apparatus**

**X3.6.1** Specimens used to measure the growth rates of small fatigue cracks (X3.7.1) are usually different from standard geometries established for long fatigue crack testing or other fatigue and fracture studies addressed by ASTM standard practices. Because nonstandard specimens and test practices

are employed, it is especially important to ensure that basic concerns about specimen fixturing and test frame preparation are given appropriate attention. Specimen fixtures should grip the ends securely, minimize backlash if negative stress ratios are imposed, transmit force to the specimen uniformly, and prevent crack formation at the grips. The test frame should be properly aligned and the force cell properly calibrated. Specific recommendations on some of these issues are contained in the main body of Test Method E 647 and in Practices E 4, E 466, E 467, and E 606.

**X3.6.2** Some small-crack specimen geometries become asymmetric as the crack grows (for example, the corner crack specimen in X3.7.1.4), and the resulting bending moment imposed on the specimen depends on the nature and rigidity of the fixturing. Special caution should be taken to minimize and/or characterize the rotation of the fixturing.

**X3.6.3** Nearly all small-crack size measurement techniques (X3.5.3) require additional specialized apparatus such as advanced electronic instrumentation, microscopes, or other devices. This apparatus must be recognized as the source of potential measurement error or artificial influence on crack growth rates. Careful attention must be given to appropriate equipment calibration and verification of proper operation before commencing small-crack testing. The sensitivity or precision of any equipment that directly influences the quantitative measurement of crack size should be determined and reported.

**X3.7 Specimen Configuration and Preparation**

**X3.7.1 Specimen Design:**

**X3.7.1.1** The study of small fatigue cracks requires detection of crack initiation and growth while physical crack sizes are extremely small, and this requirement influences specimen design. Several different small- or short-crack test specimens have been developed to obtain fatigue crack growth rate data. Some of the early specimens were prepared by growing large cracks, interrupting the test, and machining away some of the specimen material to obtain a physically short crack. However, the preferred (and most widely used) specimens promote the initiation of naturally small surface or corner cracks. The early detection of these cracks can be facilitated by using specimens with very small machined starter notches or specimens with mild stress concentrations. Some recommended small-crack specimens are shown schematically in Fig. X3.2.

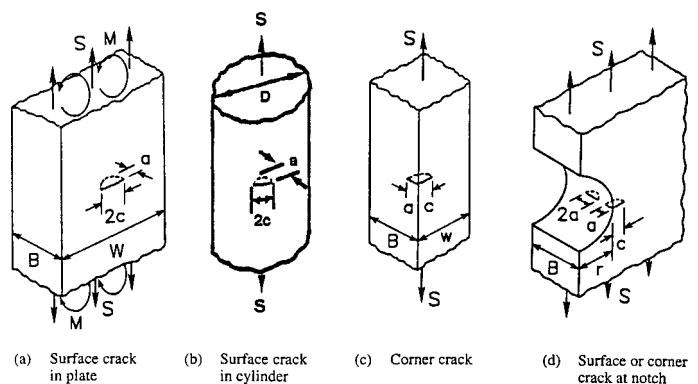


**FIG. X3.2 Schematic of Commonly Used Small Crack Specimens**

X3.7.1.2 The rectangular surface-crack specimen, Fig. X3.2(a), is subjected to either remote tension or bending forces. To localize the crack initiation site(s) for the convenience of crack monitoring, three-point bending can be used to confine the maximum outer fiber stress to a small region. Alternatively, a reduced section with a mild radius can be used to localize initiation sites under remote tension (91). Note that although localization by either means is convenient, it may also influence the behavior of naturally initiated cracks due to sampling effects (for example, worst-case effects may not be observed due to biasing of the initiation location).

X3.7.1.3 The cylindrical surface-crack specimen, Fig. X3.2(b), may be identical to a traditional axial fatigue specimen. This geometry may be particularly useful to avoid crack formation at specimen corners or for testing at large stress ranges. Cracks may be initiated naturally or from a small notch machined on the surface.

X3.7.1.4 The corner-crack specimen, Fig. X3.2(c), was developed to simulate geometries encountered in critical locations in engine discs (66, 97). The small corner crack is introduced into the specimen by electrical-discharge machining a small corner notch into one edge. This specimen has the advantage that both crack length ( $c$ ) and crack depth ( $a$ ) can be monitored by either visual or photographic means.

X3.7.1.5 The specimen with a surface or corner crack at a semi-circular edge notch, Fig. X3.2(d), was developed to produce naturally-occurring cracks at material defects and to propagate cracks through a three-dimensional stress field similar to that encountered at bolt holes in structures (98).

#### X3.7.2 Crack Initiation Sites:

X3.7.2.1 Small artificial flaws can be introduced into a specimen through methods such as electrical discharge machining or thin wafer cutoff wheels. These methods may disturb the material ahead of the resulting notch, and require precracking past the distressed zone before the onset of data acquisition. In order to eliminate mechanical notch effects, the size of the precrack region, as measured from the notch root, should be at least two times the notch tip radius.

X3.7.2.2 The specimen geometries used for naturally occurring small fatigue cracks (X3.7.1.2) are designed to localize the crack initiation region within a small area, which allows for crack monitoring methods such as replication or microphotography to be used. These natural small cracks will typically initiate at inclusion particles, voids, scratches, or deformation bands. To ensure that cracks initiate in these intended regions, it is recommended that the corners of the specimens be deburred to suppress corner initiation. This type of specimen permits the acquisition of meaningful fatigue crack growth data immediately after first crack detection.

#### X3.7.3 Surface Preparation:

X3.7.3.1 Near-surface residual stresses and surface roughness induced by specimen machining can artificially influence small-crack growth behavior and should be eliminated prior to testing. However, it should be recognized that the growth rates of small surface cracks in engineering components may be influenced by residual stress fields arising from fabrication of the component, and this may have implications for the application of the laboratory small-crack data.

X3.7.3.2 Electrical discharge machining and low stress grinding are the preferred machining methods since they have been found to produce significantly lower residual stresses than mechanical milling (91). If mechanical milling is employed, it should be followed by a low stress grinding operation.

X3.7.3.3 Surface polishing techniques are used to remove the residual stresses and surface roughness induced by the machining process, and to provide a reflective finish adequate for accurate surface crack size measurements if visual techniques are employed. The two recommended techniques for surface polishing are electropolishing and chemical polishing (90, 91). Both methods typically require a surface finish equivalent to 500 grit SiC or better before polishing is initiated. Hand polishing with abrasive media until a desired surface finish is achieved may also be used, but this procedure produces residual stresses and should be followed by either a chemical etching or electro-etching procedure to remove the affected material.

X3.7.3.4 Chemical or ion etching of the specimen surface prior to testing may facilitate identification of microstructural influences on crack behavior when optical or imaging methods are employed to measure the surface crack size. In some materials, however, an etch may confound clear identification of the crack tip location or even remove key microstructural features from which small cracks naturally initiate. Etching after a naturally-initiated crack has been located may be preferable in some cases, although chemical etching in this case may influence subsequent crack growth.

### X3.8 Procedure

X3.8.1 The detailed procedure for conducting small-crack experiments is test method-specific, and extended discussion of suggested practices for the methods discussed in X3.5.3 is found in (80). Procedural issues of general applicability are outlined below.

X3.8.2 *Crack Size and Geometry*—Because the initiation and growth of small fatigue cracks are often dominated by local microstructural and geometric features, it is important that small-crack test specimens simulate actual applications in terms of microstructure, heat treatment, surface finish, and residual stress state, as well as crack size and geometry. The range of crack sizes to be investigated and the crack geometry of interest may have a significant impact on the selection of a test method. For example, the smallest of cracks must be naturally initiated, which precludes the use of artificial crack starters that predetermine the point of crack initiation. Although the absolute minimum detectable crack size may be of scientific interest, data to be used in life predictions of engineering structures may have a practical minimum crack size that is dictated by the limits of available, or foreseeable, methods of nondestructive inspection. Crack sizes in this range tend to be more amenable to study by a variety of experimental techniques.

X3.8.3 *Stress Level and Stress Ratio*—Selection of the stress level and stress ratio for testing are important considerations, and have numerous ramifications, both experimentally and analytically. For many materials, nominal maximum stresses of the order of 0.6 times the material yield strength ( $\sigma_{YS}$ ) will facilitate natural initiation of a small number of

cracks in a relatively short time, and the nominally elastic stress state permits a traditional fracture mechanics analysis to be used. Maximum stress levels approaching or exceeding  $\sigma_{YS}$  tend to produce multiple cracks, and the associated analysis must deal with the accompanying extended plastic deformation. Moreover, the stress ratio chosen may dramatically influence the time required to naturally initiate cracks. Ultimately, decisions regarding stress level and stress ratio may be dictated by the intended application for the data.

#### X3.8.4 Crack Size Measurements:

X3.8.4.1 To document crack growth events adequately at the smallest crack sizes, it is desirable to measure crack size at frequent intervals. In addition, real-time assessment of crack size may not be practical using some techniques, requiring that frequent measurements be made to capture unexpected events. This is particularly true for the smallest crack sizes. Recommended analysis procedures for dealing with such data are discussed in X3.9.2.

X3.8.4.2 In addition to measurement of surface crack length (2c), calculations of crack driving force require knowledge of crack shape. Normally a semielliptical crack shape is assumed, but some measurement of crack depth (a) must be made. Given a knowledge of surface crack length, some measurement techniques provide approaches for deducing crack depth, but direct, nondestructive measurement of crack shape is not currently possible. For some materials, it is possible to use fractographic measurements to develop a relationship of crack aspect ratio as a function of crack size that is representative of all small cracks in the material (90). This relationship may then be used in crack driving force calculations.

X3.8.5 *Controlled- $\Delta K$  Testing*—It may be useful to monitor small-crack growth under computer-automated applied  $\Delta K$ -control. The major requirement for such experiments is continuous input of small-crack size and aspect ratio for calculation of  $\Delta K$  (or other correlating parameter), along with computer control of force (and therefore  $\Delta K$ ). The dcEPD and ISDG methods are well suited for  $\Delta K$ -controlled small-crack growth from artificial initiation sites (92, 99). Other methods such as SAW could be similarly automated.  $\Delta K$ -controlled experiments are particularly useful for characterizing growth rate changes at constant  $\Delta K$  in response to crack wake morphology evolution, crack tip-microstructure interactions, and crack size-sensitive occluded chemistry changes. The application of  $\Delta K$ -decreasing methods with small or short cracks provides an expeditious means of characterizing low growth rate cracking, often at low testing frequencies where large-crack methods are not feasible.

### X3.9 Calculation and Interpretation

#### X3.9.1 Calculation of $\Delta K$ :

X3.9.1.1 Many of the available small-crack test methods address cracks that are assumed to be approximately semielliptical in shape. Accepted stress intensity factor solutions for a variety of embedded, surface, and corner crack geometries in plates and rods are given in (100-102). The general form of these solutions is

$$\Delta K = F_j \Delta S_i \sqrt{\pi a/Q} \quad (X3.4)$$

where  $\Delta S_i$  is the remote uniform tensile stress range ( $i = t$ ) or

outer fiber bending stress range ( $i = b$ ),  $Q$  is the elliptical crack shape factor, and  $F_j$  is the boundary-correction factor which accounts for the influence of the various free-boundary conditions. Note that  $F_j$  changes around the perimeter of the crack, and this dependence may influence the crack growth process. It is customary to characterize fatigue crack growth for a stable, semicircular crack shape on the basis of  $\Delta K$  calculated at the deepest point of the crack. Note also that some  $K$  solutions in the literature are presented using notations that differ from the notations in Fig. X3.2 (for example, plate half-width  $w$  versus full plate width  $W = 2w$ ).

X3.9.1.2 For fine-grain, isotropic materials the assumption of a semielliptical shape appears reasonable. Although the shapes of very small cracks may be dramatically affected by local microstructural features, as the cracks grow they tend to assume a semielliptical shape and, in many instances, become nearly semicircular. Cracks in materials having coarse microstructures and/or exhibiting crystallographic texture and anisotropy may never assume a semielliptical shape. As stated in X3.8.4.2, crack shape must be documented for accurate calculation of  $\Delta K$ . Simple approximation techniques have been presented to estimate the stress intensity factor for surface or corner cracks of non-elliptical shape (103). Typically, non-elliptical crack shapes depend on local microstructural features and, as such, their shapes tend to be inherently variable. Recognizing the stochastic nature of these cracks, it is often reasonable, or necessary, to approximate their shapes as semielliptical.

X3.9.1.3 Another problem involves the initiation of multiple cracks within a small region. These cracks may coalesce to form a single long, shallow surface crack. Criteria have been proposed (90) for defining the point at which the stress fields of closely spaced crack tips begin to interact.

X3.9.1.4 Under tension-compression loading,  $R \leq 0$ , it is conventional to use only the positive portion of the stress range to calculate the crack driving force; that is,  $\Delta K = K_{\max}$  (see Terminology in the main body of Test Method E 647). When crack closure is considered, however, the issue becomes significantly more complex, and the conventional definition of  $\Delta K = K_{\max}$  may be inappropriate. Numerous investigators have demonstrated that the level of crack closure depends on many factors, including crack size (for example, see (104)). In particular, crack opening stresses are thought to be lower for small cracks, even opening at nominally compressive stresses under some conditions. This factor raises important questions regarding the applicability of large-crack data, particularly in the near- $\Delta K_{th}$  region, to the prediction of the growth of small cracks. Some of the crack size measurement techniques described in X3.5.3 also may be used to measure crack closure levels, particularly ISDG and SEM.

#### X3.9.2 Calculation of Crack Growth Rate:

X3.9.2.1 Analysis of crack-size data to determine crack growth rates requires special consideration. The minimum interval between successive crack size measurements for large-crack tests (see Procedure in the main body of Test Method E 647) is stipulated as ten times the measurement precision. This may require that crack growth data be acquired at specified intervals of crack length, or that the  $a-N$  data be

edited to remove data to achieve the desired interval,  $\Delta a$ . The inherent difficulty in this process is selecting the data points for removal. Small-crack measurement techniques often have measurement precision that is of the order of microstructural dimensions. As a result, discontinuities in the  $a-N$  (or  $2c-N$ ) data arise due to crack interactions with microstructure, as well as from inherent errors in the measurements. If a minimum level of  $\Delta a$  is used as a criterion for editing the data, then the selected data points will often be the first point after the crack has broken through a local microstructural obstacle, and the data exhibiting the crack retardation in the microstructure will be lost. While the large-crack measurement intervals are recommended where possible, some uses of small-crack data may require smaller measurement intervals in order to capture key microstructural effects.

X3.9.2.2 Much of the small-crack growth rate data in the literature has not been reduced following the above guidance, and in many cases the  $da/dN$  calculations appear to demonstrate variability that is significantly influenced by measurement error. The basic problem may be outlined as follows. As the crack size interval,  $\Delta a$ , between successive measurements decreases, the relative contribution of the measurement error to the calculated value of  $da/dN$  increases. For example, assume that a single crack size measurement is given by  $\hat{a} = a + \epsilon$ , where  $\hat{a}$  is the measured crack size,  $a$  is the true crack size, and  $\epsilon$  is the error inherent in the crack size measurement, normally distributed about zero. A direct-secant calculation of crack growth rate between two successive crack size measurements ( $a_1$  and  $a_2$ ) is given by

$$\frac{\Delta \hat{a}}{\Delta N} = \frac{(a_2 + \epsilon_2) - (a_1 + \epsilon_1)}{\Delta N} = \frac{\Delta a}{\Delta N} + \frac{\Delta \epsilon}{\Delta N} \quad (\text{X3.5})$$

Thus, as  $\Delta a/\Delta N$  approaches zero, the error term  $\Delta \epsilon/\Delta N$  dominates the calculated value of  $\Delta \hat{a}/\Delta N$ . Since small-crack data are often acquired at low growth rates, the crack extension

between successive measurements tends to be small, and the growth rate data may exhibit an unusually large variability due to measurement error. It is recommended that the small-crack data be edited to remove this variability, or one may use a modified version (for example, (91)) of the standard incremental polynomial regression used for large cracks. The reader is cautioned that different data analysis procedures can also significantly influence the apparent scatter in growth rate (105).

### X3.10 Reporting

X3.10.1 The reporting guidelines prescribed in the main body of Test Method E 647 apply to the suggested procedure for small-crack tests. In addition, it is often useful to provide a record of the degree of crack deflection and tortuosity, the degree of asymmetric crack growth, and the crack shape for use in calculations of crack driving force. It is customary to report crack size in terms of its projection on a plane normal to the axis of loading, but significant deviations of the crack path from this plane should be noted in the report. Since the method of crack initiation can have a significant influence on subsequent crack growth, the test conditions and number of cycles required for crack initiation should be reported, along with the measured size of the crack at this number of cycles. The estimated resolution of the crack size measurement technique, the specific data analysis method used to calculate crack growth rates, and the specific  $K$  solution employed should also be recorded.

### X3.11 Precision and Bias

X3.11.1 The general guidelines in the main body of Test Method E 647 apply. Specific emphasis should be given to the concerns described in X3.9.2 of this appendix, as a significant component of the variability exhibited by small-crack data can often be attributed to errors inherent in the crack size measurements.

## REFERENCES

- (1) Hudak, Jr., S. J., and Bucci, R. J., *Fatigue Crack Growth Measurement and Data Analysis*, ASTM STP 738, ASTM, 1981.
- (2) Paris, P. C., "The Fracture Mechanics Approach to Fatigue," *Proceedings of the Tenth Sagamore Army Materials Research Conference*, Syracuse University Press, 1964, pp. 107–132.
- (3) Beevers, C. J., *The Measurement of Crack Length and Shape During Fracture and Fatigue*, Engineering Materials Advisory Services LTD, West Middlelands, U.K., 1981.
- (4) Bucci, R. J., "Effect of Residual Stress on Fatigue Crack Growth Rate Measurement," *Fracture Mechanics (13<sup>th</sup> Conference)*, ASTM STP 743, 1981, pp. 28–47.
- (5) Suresh, S., and Ritchie, R. O., "Propagation of Short Fatigue Cracks," *International Metals Review*, Vol 29, #6, December 1984, pp. 445–476.
- (6) Hudak, Jr., S. J., "Small Crack Behavior and the Prediction of Fatigue Life," *Journal of Engineering Materials and Technology*, Vol 103, Jan. 1981, pp. 26–35.
- (7) Herman, W. A., Hertzberg, R. W., and Jaccard, R., "A Simplified Laboratory Approach for the Prediction of Short Crack Behavior in Engineering Structures," *Fatigue and Fracture of Engineering Materials and Structures*, Vol II, No. 4, 1988.
- (8) Suresh, S., and Ritchie, R. O., "Near-Threshold Fatigue Crack Propagation: A Perspective on the Role of Crack Closure," *Fatigue Crack Growth Threshold Concepts* TMS-AIME D. L. Davidson, S. Suresh, editors; Warrendale, PA, 1984, pp. 227–261.
- (9) Clark, Jr., W. G., "Fracture Mechanics in Fatigue," *Experimental Mechanics*, September 1971, pp. 1–8.
- (10) Hoepfner, D. W., and Krupp, W. E., "Prediction of Component Life by Application of Fatigue Crack Growth Knowledge," *Engineering Fracture Mechanics*, Vol 6, 1974, pp. 47–70.
- (11) *Fatigue Crack Growth Under Spectrum Loads*, ASTM STP 595, ASTM, 1976.
- (12) Hartman, G. A., and Ashbaugh, N. E., "Load Pin Size Effects in the C(T) Geometry," ASTM Research Report RR: E24-1016, Oct 1991.
- (13) Scarone, D. W., "Development of an Instrumented Device to Measure Fixture-Induced Bending in Pin-Loaded Specimen Trains," *Factors That Affect the Precision of Mechanical Test*, ASTM STP 1025, Papirno, R. and Weiss, H. C. Eds., ASTM, 1989, pp. 160–173.
- (14) Hudak, Jr., S. J., Saxena, A., Bucci, R. J., and Malcolm, R. C., "Development of Standard Methods of Testing and Analyzing Fatigue Crack Growth Rate Data—Final Report," AFML TR 78-40, Air Force Materials Laboratory, Wright Patterson Air Force Base, OH, 1978.
- (15) Brose, W. R., and Dowling, N. E., "Size Effects on the Fatigue Crack

- Growth Rate of Type 304 Stainless Steel," *Elastic-Plastic Fracture, ASTM STP 668*, 1979, pp. 720–735.
- (16) Hudak, Jr., S. J., "Defining the Limits of Linear Elastic Fracture Mechanics in Fatigue Crack Growth," *Fatigue Crack Growth Measurement and Data Analysis, ASTM STP 738*, ASTM, Oct. 29–30, 1980.
  - (17) Dowling, N. E., "Fatigue Crack Growth Rate Testing at High Stress Intensities," *Flaw Growth and Fracture, ASTM STP 631*, ASTM, 1977, pp. 139–158.
  - (18) James, L. A., "Specimen Size Considerations in Fatigue-Crack Growth Rate Testing," *Fatigue Crack Growth Measurement and Data Analysis, ASTM STP 738*, ASTM, 1981, pp. 45–57.
  - (19) Clark, Jr., W. G., and Hudak, Jr., S. J., "Variability in Fatigue Crack Growth Rate Testing," *Journal of Testing and Evaluation*, Vol 3, No. 6, 1975, pp. 454–476.
  - (20) Hudak, Jr., S. J., and Wei, R. P., "Consideration of Nonsteady State Crack Growth in Materials Evaluation and Design," *International Journal of Pressure Vessels and Piping*, Vol 9, 1981, pp. 63–74.
  - (21) Saxena, A., Hudak, Jr., S. J., Donald, J. K., and Schmidt, D. W., "Computer-Controlled Decreasing Stress Intensity Technique for Low Rate Fatigue Crack Growth Testing," *Journal of Testing and Evaluation*, Vol 6, No. 3, 1978, pp. 167–174.
  - (22) Donald, J. K., and Schmidt, D. W., "Computer-Controlled Stress Intensity Gradient Technique for High Rate Fatigue Crack Growth Testing," *Journal of Testing and Evaluation*, Vol 8, No. 1, Jan. 1980, pp. 19–24.
  - (23) Donald, J. K., "The Effect of Out-of-Plane Cracking on FCGR Behavior," ASTM Research Report #E8-1001, December 12, 1995.
  - (24) Chan, K. S., and Cruse, T. A., "Stress Intensity Factors for Anisotropic Compact Tension Specimens With Inclined Cracks," *Engineering Fracture Mechanics*, Vol 23, No. 5, pp. 863–874.
  - (25) Clark, Jr., W. G., and Hudak, Jr., S. J., "The Analysis of Fatigue Crack Growth Rate Data," *Application of Fracture Mechanics to Design*, Burke, J. J. and Weiss, V., Eds, Vol 22, Plenum, 1979, pp. 67–81.
  - (26) Newman, Jr., J. C., "Stress Analysis of the Compact Specimen Including the Effects of Pin Loading" *Fracture Analysis (8<sup>th</sup> Conference)*, ASTM STP 560, ASTM, 1974, pp. 105–121.
  - (27) Srawley, J. E., "Wide Range Stress Intensity Factor Expressions for ASTM Method E 399 Standard Fracture Toughness Specimens," *International Journal of Fracture*, Vol 12, June 1976, pp. 475–476.
  - (28) Bucci, R. J., in *Fatigue Crack Growth Measurement and Data Analysis, ASTM STP 738*, ASTM, 1981, pp. 5–28.
  - (29) Wei, R. P., Wei, W., and Miller, G. A., "Effect of Measurement Precision and Data-Processing Procedure on Variability in Fatigue Crack Growth-Rate Data," *Journal of Testing and Evaluation*, Vol 7, No. 2, March 1979, pp. 90–95.
  - (30) Donald, J. K., "Preliminary Results of the ASTM E24.04.03 Round-Robin Test Program on Low Delta-K Fatigue Crack Growth Rates," ASTM E24.04.03 Task Group Document, December 1982.
  - (31) Wei, R. P., and Shim, G., "Fracture Mechanics and Corrosion Fatigue," *Corrosion Fatigue: Mechanics, Metallurgy, Electrochemistry and Engineering, ASTM STP 801*, ASTM, 1983, pp. 5–25.
  - (32) Barsom, J. M., "Effects of Cyclic Stress Form on Corrosion Fatigue Crack Propagation Below  $K_{Isc}$  in a High Yield Strength Steel," *Corrosion Fatigue: Chemistry, Mechanics and Microstructure*, NACE-2, National Association of Corrosion Engineers, 1972, pp. 424–433.
  - (33) Vosikovskiy, O., "Effects of Mechanical and Environmental Variables on Fatigue Crack Growth Rates in Steel. A Summary of Work Done At CANMET," *Canadian Metallurgical Quarterly*, Vol 19, 1980, pp. 87–97.
  - (34) Selines, R. J., and Pelloux, R. M., "Effect of Cyclic Stress Wave Form on Corrosion Fatigue Crack Propagation in Al-Zn-Mg Alloys," *Metallurgical Transactions*, Vol 3, 1972, pp. 2525–2531.
  - (35) Dawson, D. B., and Pelloux, R. M., "Corrosion Fatigue Crack Growth in Titanium Alloys in Aqueous Environments," *Metallurgical Transactions*, Vol 5, 1974, pp. 723–731.
  - (36) Bogar, F. D., and Crooker, T. W., "The Influence of Bulk-Solution-Chemistry Conditions on Marine Corrosion Fatigue Crack Growth Rate," *Journal of Testing and Evaluation*, Vol 7, 1979, pp. 155–159.
  - (37) Vosikovskiy, O., Neill, W. R., Carlyle, D. A., and Rivard, A., "The Effect of Sea Water Temperature on Corrosion Fatigue Crack Growth in Structural Steels," *CANMET Physical Metallurgy Research Laboratories Report ERP/PMRL 83-27 (OP-J)*, Ottawa, Canada, April 1983.
  - (38) Gangloff, R. P., "The Criticality of Crack Size in Aqueous Corrosion Fatigue," *Res Mechanica Letters*, Vol 1, 1981, pp. 299–306.
  - (39) van der Velden, R., Ewalds, H. L., Schultze, W. A., and Punter, A., "Anomalous Fatigue Crack Growth Retardation in Steels for Off-shore Applications," *Corrosion Fatigue: Mechanics, Metallurgy, Electrochemistry and Engineering, ASTM STP 180*, ASTM, 1983, pp. 64–80.
  - (40) Bogar, F. D., and Crooker, T. W., "Effects of Natural Seawater and Electrochemical Potential on Fatigue-Crack Growth in 5086 and 5456 Aluminum Alloys," *NRL Report 8153*, Naval Research Laboratory, Washington, DC, October 7, 1977.
  - (41) Yoder, G. R., Cooley, L. A., and Crooker, T. W., "Procedures for Precision Measurement of Fatigue Crack Growth Rate Using Crack-Opening Displacement Techniques," *Fatigue Crack Growth Measurements and Data Analysis, ASTM STP 738*, ASTM, 1981, pp. 85–102.
  - (42) Wei, R. P., and Brazill, R. L., "An Assessment of A-C and D-C Potential Systems for Monitoring Fatigue Crack Growth," *Fatigue Crack Growth Measurement and Data Analysis, ASTM STP 738*, ASTM, 1981, pp. 103–119.
  - (43) Liaw, P. K., Hartmann, H. R., and Helm, E. J., "Corrosion Fatigue Crack Propagation Testing with the KRAK-GAGE® in Salt Water," *Engineering Fracture Mechanics*, Vol 18, 1983, pp. 121–131.
  - (44) Saxena, A., and Hudak, Jr., S. J., "Review and Extension of Compliance Information for Common Crack Growth Specimens," *International Journal of Fracture*, Vol 14, No. 5, Oct 1978.
  - (45) Ashbaugh, N. E., and Johnson, D. A., "Determination of Crack Length as a Function of Compliance and Gage Length for an M(T) Specimen," ASTM Research Report (RR: E24-1017, April 1992).
  - (46) Watt, K. R., "Consideration of an a.c. Potential Drop Method for Crack Length Measurement," from *The Measurement of Crack Length and Shape During Fracture and Fatigue*, Beevers, C. J., Ed., EMAS, Cradley Heath, UK, 1980, pp. 202–201.
  - (47) Bakker, A., "A DC Drop Procedure for Crack Initiation and R-Curve Measurements During Fracture Tests," *Elastic-Plastic Fracture Test Methods: The User Experience, ASTM STP 856*, Wessel, E. T. and Loss, F. J., Eds., ASTM, 1985, pp. 394–410.
  - (48) Richards, C. E., "Some Guidelines to the Selection of Techniques," *The Measurement of Crack Length and Shape During Fracture and Fatigue*, Beevers, C. J., Ed., EMAS, Cradley Heath, UK, 1980, pp. 461–468.
  - (49) Wei, R. P., and Brazill, R. L., "An a.c. Potential System for Crack Length Measurement" from *The Measurement of Crack Length and Shape During Fracture and Fatigue*, Beevers, C. J., Ed., EMAS, Cradley Heath, UK, 1980, pp. 190–201.
  - (50) Wilkowski, G. M., and Maxey, W. A., "Review and Applications of the Electric Potential Method for Measuring Crack Growth in Specimens, Flawed Pipes, and Pressure Vessels," *Fracture Mechanics: Fourteenth Symposium-Volume II: Testing and Applications, ASTM STP 791*, Lewis, J. C. and Sines, G., Eds., ASTM, 1983, pp. II-266–II-294.
  - (51) Dover, W. D., et al., "a.c. Field Measurement—Theory and Practice," from *The Measurement of Crack Length and Shape During Fracture and Fatigue*, Beevers, C. J., Ed., EMAS, Cradley Heath, UK, 1980, pp. 222–260.
  - (52) Metals Handbook, Vol 8, Published under the direction of the American Society for Metals, 9th Edition, Metals Park, OH, 1987, pp. 386–391.
  - (53) Gangloff, R. P., "Electrical Potential Monitoring of the Formation and

- Growth of Small Fatigue Cracks in Embrittling Environments,” from *Advances in Crack Length Measurement*, Beevers, C. J., Ed., EMAS, Cradley Heath, UK, 1982, pp. 175–229.
- (54) Hartman, G. A., and Johnson, D. A., “D-C Electric Potential Method Applied to Thermal/Mechanical Fatigue Crack Growth,” *Experimental Mechanics*, March 1987, pp. 106–112.
- (55) Bachman, V., and Munz, D., “Fatigue Crack Closure Evaluation with the Potential Method,” *Engineering Fracture Mechanics*, Vol 11, No. 1, 1979, pp. 61–71.
- (56) Okumra, N., Venkatasubramanian, T. V., Unvala, B. A., and Baker, T. J., “Application of the AC Potential Drop Technique to the Determination of R-Curves of Tough Ferritic Steels,” *Engineering Fracture Mechanics*, Vol 14, 1981, pp. 617–625.
- (57) Pollock, D. D., “Thermoelectricity, Theory, Thermometry, Tool,” *ASTM STP 852*, ASTM, 1985.
- (58) Catlin, W. R., Lord, D. C., Prater, T. A., and Coffin, L. F., “The Reversing D-C Electrical Potential Method,” *Automated Test Methods for Fracture and Fatigue Crack Growth*, ASTM STP 877, Cullen, W. H., Landgraf, R. W., Kaisand, L. R., and Underwood, J. H., Eds., ASTM, 1985, pp. 67–85.
- (59) Johnson, H. H., “Calibrating the Electric Potential Method for Studying Slow Crack Growth,” *Materials Research and Standards*, Vol 5, No. 9, Sept. 1965, pp. 442–445.
- (60) Van Stone, R. H., and Richardson, T. L., “Potential Drop Monitoring of Cracks in Surface Flawed Specimens,” *Automated Test Methods for Fracture and Fatigue Crack Growth*, ASTM STP 877, W. H. Cullen, R. W. Landgraf, L. R. Kaisand, and J. H. Underwood, Eds., ASTM, 1985, pp. 148–166.
- (61) Gangloff, R. P., “Electrical Potential Monitoring of Crack Formation and Subcritical Growth from Small Defects,” *Fatigue of Engineering Materials and Structures*, Vol 4, 1981, pp. 15–33.
- (62) Hicks, M. A., and Pickard, A. C., “A Comparison of Theoretical and Experimental Methods of Calibrating the Electrical Potential Drop Technique for Crack Length Determination,” *Int. Journal of Fracture*, No. 20, 1982, pp. 91–101.
- (63) Aronson, G. H., and Ritchie, R. O., “Optimization of the Electrical Potential Technique for Crack Monitoring in Compact Test Pieces Using Finite Element Analysis,” *Journal of Testing and Evaluation*, JTEVA, Vol 7, No. 4, July 1979, pp. 208–215.
- (64) Ritchie, R. O., and Bathe, K. J., “On the Calibration of the Electrical Potential Technique for Monitoring Crack Growth Using Finite Element Methods,” *International Journal of Fracture*, Vol 15, No. 1, February 1979, pp. 47–55.
- (65) Li, Che-Yu, and Wei, R. P., “Calibrating the Electrical Potential Method for Studying Slow Crack Growth,” *Materials Research & Standards*, Vol 6, No. 8, August 1966, pp. 392–394.
- (66) Mom, A., and Raizenne, M. D., “AGARD Engine Disk Cooperative Test Programme,” AGARD report number 766, Aug., 1988.
- (67) Raizenne, M. D., “AGARD TX114 Test Procedures for Supplemental Engine Disc Test Programme,” National Research Council Canada, LTR-ST-1671, June 1988.
- (68) Piascik, R. S., “Mechanisms of Intrinsic Damage Localization During Corrosion Fatigue: Al-Li-Cu System,” Ph.D. Dissertation, University of Virginia, 1989.
- (69) Piascik, R. S. and Willard, S. A., “The Growth of Small Corrosion Fatigue Cracks in Alloy 2024,” *Fatigue Fract. Engng. Mater. Struct.*, Vol. 17, No. 11, 1994, pp. 1247–1259.
- (70) Richardson, D. E. and Goree, J. G., “Experimental Verification of a New Two-Parameter Fracture Model,” *ASTM STP 1189*, R. Chona, ed., 1993, pp. 738–750.
- (71) Sullivan, A.M., “New Specimen Design for Plane-Strain Fracture Toughness Tests,” *Materials Research and Standard*, Vol. 4, No. 1, 1964, pp. 20–24.
- (72) Piascik, R.S., Newman, J.C., Jr., and Underwood, J.H., “The Extended Compact Tension Specimen,” *Fatigue and Fract. Engng. Mater. Struct.*, Vol. 20, No. 4, 1997, pp. 559–563.
- (73) John, R., “Stress Intensity Factor and Compliance Solutions for an Eccentrically Loaded Single Edge Cracked Geometry,” *Engineering Fracture Mechanics*, Vol. 58, No. 1/2, 1997, pp. 87–96.
- (74) Piascik, R.S. and Newman, J.C., Jr., “An Extended Compact Tension Specimen for Fatigue Crack Growth and Fracture Testing,” *International Journal of Fracture*, Vol. 76, No. 3, 1995, pp. R43–R48.
- (75) Schwalbe, K. H. and Hellmann, “Applications of the Electrical Potential Method to Crack Length Measurements Using Johnson’s Formula,” *Journal of Testing and Evaluation*, Vol. 9, No. 3, 1981, pp. 218–221.
- (76) Phillips, Edward P., “Results of the Second Round Robin on Opening-Load Measurement Conducted by ASTM Task Group E24.04.04 on Crack Closure Measurement and Analysis,” NASA Technical Memorandum 109032, November 1993.
- (77) Donald, J. Keith, “A Procedure for Standardizing Crack Closure Levels,” *Mechanics of Fatigue Crack Closure*, ASTM STP 982, ASTM, 1988, pp. 222–229.
- (78) Suresh, S., and Ritchie, R. O., “Propagation of Short Fatigue Cracks,” *International Metals Review*, Vol 29, 1984, pp. 445–476.
- (79) Hudak, S. J., Jr., “Small Crack Behavior and the Prediction of Fatigue Life,” *ASME Journal of Engineering Materials and Technology*, Vol 103, 1981, pp. 26–35.
- (80) *Small-Crack Test Methods*, ASTM STP 1149, Larsen, J. M., and Allison, J. E., Eds., ASTM, 1992.
- (81) *Current Research on Fatigue Cracks*, Tanaka, T., Jono, M., and Komai, K., Eds., The Society of Materials Science, Japan, 1985.
- (82) *Small Fatigue Cracks*, Ritchie, R. O., and Lankford, J., Eds., The Metallurgical Society, Warrendale, PA, 1986.
- (83) *The Behaviour of Short Fatigue Cracks*, EGF 1, Miller, K. J., and de los Rios, E. R., Eds., Mechanical Engineering Publications, London, 1986.
- (84) *Short Fatigue Cracks*, ESIS 13, Miller, K. J., and de los Rios, E. R., Eds., Mechanical Engineering Publications, London, 1992.
- (85) Ritchie, R. O., and Lankford, J., “Overview of the Small Crack Problem,” *Small Fatigue Cracks*, Ritchie, R. O., and Lankford, J., Eds., The Metallurgical Society, Warrendale, PA, 1986, pp. 1–5.
- (86) Kitagawa, H., and Takahashi, S., “Applicability of Fracture Mechanics to Very Small Cracks or the Cracks in the Early Stage,” Proc. Second International Conference on Mechanical Behavior of Materials, Boston, MA, 1976, pp. 627–631.
- (87) Tanaka, K., Nakai, Y., and Yamashita, M., “Fatigue Growth Threshold of Small Cracks,” *International Journal of Fracture*, Vol 17, 1981, pp. 519–533.
- (88) Miller, K. J., “Materials Science Perspective of Metal Fatigue Resistance,” *Materials Science and Technology*, Vol 9, 1993, pp. 453–462.
- (89) McClung, R. C., and Sehitoglu, H., “Characterization of Fatigue Crack Growth in Intermediate and Large Scale Yielding,” *ASME Journal of Engineering Materials and Technology*, Vol 113, 1991, pp. 15–22.
- (90) Swain, M. H., “Monitoring Small-Crack Growth by the Replication Method,” *ASTM STP 1149*, ASTM, pp. 34–56.
- (91) Larsen, J. M., Jira, J. R., and Ravichandran, K. S., “Measurement of Small Cracks by Photomicroscopy: Experiments and Analysis,” *ASTM STP 1149*, ASTM, pp. 57–80.
- (92) Gangloff, R. P., Slavik, D. C., Piascik, R. S., and Van Stone, R. H., “Direct Current Electrical Potential Measurement of the Growth of Small Cracks,” *ASTM STP 1149*, ASTM, pp. 116–168.
- (93) Resch, M. T., and Nelson, D. V., “An Ultrasonic Method for Measurement of Size and Opening Behavior of Small Fatigue Cracks,” *ASTM STP 1149*, ASTM, pp. 169–196.
- (94) Sharpe, W. N., Jr., Jira, J. R., and Larsen, J. M., “Real-Time Measurement of Small-Crack Opening Behavior Using an Interferometric Strain/Displacement Gage,” *ASTM STP 1149*, ASTM, pp. 92–115.
- (95) Davidson, D. L., “The Experimental Mechanics of Microcracks,” *ASTM STP 1149*, ASTM, pp. 81–91.
- (96) Hertzberg, R., Herman, W. A., Clark, T., and Jaccard, R., “Simulation

- of Short Crack and Other Low Closure Loading Conditions Utilizing Constant  $K_{max}$   $\Delta K$ -Decreasing Fatigue Crack Growth Procedures," *ASTM STP 1149*, ASTM, pp. 197–220.
- (97) Pickard, A. C., Brown, C. W., and Hicks, M. A., "The Development of Advanced Specimen Testing and Analysis Techniques Applied to Fracture Mechanics Lifting of Gas Turbine Components," *Advances in Life Prediction Methods*, Woodford, D. A. and Whitehead, J. R., Eds., ASME, New York, 1983, pp. 173–178.
- (98) Newman, J. C., Jr., and Edwards, P. R., "Short-Crack Growth Behaviour in an Aluminum Alloy—an AGARD Cooperative Test Programme," AGARD Report No. 732, 1988 (available NTIS).
- (99) Jira, J. R., Nagy, D., and Nicholas, T., "Influences of Crack Closure and Load History on Near-Threshold Crack Growth Behavior in Surface Flaws," *Surface-Crack Growth: Models, Experiments, and Structures*, ASTM STP 1060, Reuter, W. G., Underwood, J. H., and Newman, J. C., Jr., Eds., ASTM, 1990, pp. 303–314.
- (100) Newman, J. C., Jr., and Raju, I. S., "Stress-Intensity Factor Equations for Cracks in Three-Dimensional Finite Bodies," *Fracture Mechanics: Fourteenth Symposium—Volume I: Theory and Analysis*, ASTM STP 791, Lewis, J. C. and Sines, G., Eds., ASTM, 1983, pp. I-238–I-265.
- (101) Raju, I. S., and Newman, J. C., Jr., "Stress-Intensity Factors for Circumferential Surface Cracks in Pipes and Rods under Tension and Bending Loads," *Fracture Mechanics: Seventeenth Volume*, ASTM STP 905, Underwood, J. H., Chait, R., Smith, C. W., Wilhem, D. P., Andrews, W. A., and Newman, J. C., Jr., Eds., ASTM, 1986, pp. 789–805.
- (102) Newman, J. C., Jr., "Fracture Mechanics Parameters for Small Fatigue Cracks," *ASTM STP 1149*, ASTM, pp. 6–33.
- (103) Tada, H., and Paris, P., "Discussion on Stress-Intensity Factors for Cracks," *Part-Through Crack Fatigue Life Prediction*, ASTM STP 687, Chang, J. B., Ed., ASTM, 1979, pp. 43–46.
- (104) *Mechanics of Fatigue Crack Closure*, ASTM STP 982, Newman, J. C., Jr., and Elber, W., Eds., ASTM, 1988.
- (105) Kendall, J. M., and King, J. E., "Short Fatigue Crack Growth Behaviour: Data Analysis Effects," *International Journal of Fatigue*, Vol 10, 1988, pp. 163–170.
- (106) Saliver, G.C. and Goree, J.G., "The Applicability of ASTM Standard Test Specimens to Fracture and Fatigue Crack Growth of Discontinuous-Fiber Composites," *Journal of Testing and Evaluation*, JTEVA, Vol. 26, No. 4, July 1998, pp. 336-345.

*The American Society for Testing and Materials takes no position respecting the validity of any patent rights asserted in connection with any item mentioned in this standard. Users of this standard are expressly advised that determination of the validity of any such patent rights, and the risk of infringement of such rights, are entirely their own responsibility.*

*This standard is subject to revision at any time by the responsible technical committee and must be reviewed every five years and if not revised, either reapproved or withdrawn. Your comments are invited either for revision of this standard or for additional standards and should be addressed to ASTM Headquarters. Your comments will receive careful consideration at a meeting of the responsible technical committee, which you may attend. If you feel that your comments have not received a fair hearing you should make your views known to the ASTM Committee on Standards, at the address shown below.*

*This standard is copyrighted by ASTM, 100 Barr Harbor Drive, PO Box C700, West Conshohocken, PA 19428-2959, United States. Individual reprints (single or multiple copies) of this standard may be obtained by contacting ASTM at the above address or at 610-832-9585 (phone), 610-832-9555 (fax), or service@astm.org (e-mail); or through the ASTM website (www.astm.org).*



# Standard Test Methods for Tension Testing of Metallic Materials<sup>1</sup>

This standard is issued under the fixed designation E8/E8M; the number immediately following the designation indicates the year of original adoption or, in the case of revision, the year of last revision. A number in parentheses indicates the year of last reapproval. A superscript epsilon ( $\epsilon$ ) indicates an editorial change since the last revision or reapproval.

*This standard has been approved for use by agencies of the Department of Defense.*

## 1. Scope\*

1.1 These test methods cover the tension testing of metallic materials in any form at room temperature, specifically, the methods of determination of yield strength, yield point elongation, tensile strength, elongation, and reduction of area.

1.2 The gauge lengths for most round specimens are required to be 4D for E8 and 5D for E8M. The gauge length is the most significant difference between E8 and E8M test specimens. Test specimens made from powder metallurgy (P/M) materials are exempt from this requirement by industry-wide agreement to keep the pressing of the material to a specific projected area and density.

1.3 Exceptions to the provisions of these test methods may need to be made in individual specifications or test methods for a particular material. For examples, see Test Methods and Definitions [A370](#) and Test Methods [B557](#), and [B557M](#).

1.4 Room temperature shall be considered to be 10 to 38°C [50 to 100°F] unless otherwise specified.

1.5 The values stated in SI units are to be regarded as separate from inch/pound units. The values stated in each system are not exact equivalents; therefore each system must be used independently of the other. Combining values from the two systems may result in non-conformance with the standard.

1.6 *This standard does not purport to address all of the safety concerns, if any, associated with its use. It is the responsibility of the user of this standard to establish appropriate safety and health practices and determine the applicability of regulatory limitations prior to use.*

<sup>1</sup> These test methods are under the jurisdiction of ASTM Committee [E28](#) on Mechanical Testing and are the direct responsibility of Subcommittee [E28.04](#) on Uniaxial Testing.

Current edition approved July 1, 2013. Published August 2013. Originally approved in 1924. Last previous edition approved 2013 as E8/E8M – 13. DOI: 10.1520/E0008\_E0008M-13A.

## 2. Referenced Documents

### 2.1 ASTM Standards:<sup>2</sup>

- [A356/A356M](#) Specification for Steel Castings, Carbon, Low Alloy, and Stainless Steel, Heavy-Walled for Steam Turbines
- [A370](#) Test Methods and Definitions for Mechanical Testing of Steel Products
- [B557](#) Test Methods for Tension Testing Wrought and Cast Aluminum- and Magnesium-Alloy Products
- [B557M](#) Test Methods for Tension Testing Wrought and Cast Aluminum- and Magnesium-Alloy Products (Metric)
- [E4](#) Practices for Force Verification of Testing Machines
- [E6](#) Terminology Relating to Methods of Mechanical Testing
- [E29](#) Practice for Using Significant Digits in Test Data to Determine Conformance with Specifications
- [E83](#) Practice for Verification and Classification of Extensometer Systems
- [E345](#) Test Methods of Tension Testing of Metallic Foil
- [E691](#) Practice for Conducting an Interlaboratory Study to Determine the Precision of a Test Method
- [E1012](#) Practice for Verification of Testing Frame and Specimen Alignment Under Tensile and Compressive Axial Force Application
- [D1566](#) Terminology Relating to Rubber
- [E1856](#) Guide for Evaluating Computerized Data Acquisition Systems Used to Acquire Data from Universal Testing Machines

## 3. Terminology

### 3.1 Definitions of Terms Common to Mechanical Testing—

3.1.1 The definitions of mechanical testing terms that appear in the Terminology [E6](#) apply to this test method.

<sup>2</sup> For referenced ASTM standards, visit the ASTM website, [www.astm.org](http://www.astm.org), or contact ASTM Customer Service at [service@astm.org](mailto:service@astm.org). For *Annual Book of ASTM Standards* volume information, refer to the standard's Document Summary page on the ASTM website.

\*A Summary of Changes section appears at the end of this standard

3.1.1.1 These terms include bending strain, constraint, elongation, extensometer, force, gauge length, necking, reduced section, stress-strain diagram, testing machine, and modulus of elasticity.

3.1.2 In addition, the following common terms from Terminology E6 are defined:

3.1.3 *discontinuous yielding, n—in a uniaxial test*, a hesitation or fluctuation of force observed at the onset of plastic deformation, due to localized yielding.

3.1.3.1 *Discussion*—The stress-strain curve need not appear to be discontinuous.

3.1.4 *elongation after fracture, n*—the elongation measured by fitting the two halves of the broken specimen together.

3.1.5 *elongation at fracture, n*—the elongation measured just prior to the sudden decrease in force associated with fracture.

3.1.6 *lower yield strength, LYS [FL<sup>-2</sup>]*—in a uniaxial test, the minimum stress recorded during discontinuous yielding, ignoring transient effects.

3.1.7 *reduction of area, n*—the difference between the original cross-sectional area of a tension test specimen and the area of its smallest cross section.

3.1.7.1 *Discussion*—The reduction of area is usually expressed as a percentage of the original cross-sectional area of the specimen.

3.1.7.2 *Discussion*—The smallest cross section may be measured at or after fracture as specified for the material under test.

3.1.7.3 *Discussion*—The term reduction of area when applied to metals generally means measurement after fracture; when applied to plastics and elastomers, measurement at fracture. Such interpretation is usually applicable to values for reduction of area reported in the literature when no further qualification is given. **(E28.04)**

3.1.8 *tensile strength, S<sub>u</sub> [FL<sup>-2</sup>]*, *n*—the maximum tensile stress that a material is capable of sustaining.

3.1.8.1 *Discussion*—Tensile strength is calculated from the maximum force during a tension test carried to rupture and the original cross-sectional area of the specimen.

3.1.9 *uniform elongation, El<sub>w</sub> [%]*—the elongation determined at the maximum force sustained by the test piece just prior to necking or fracture, or both.

3.1.9.1 *Discussion*—Uniform elongation includes both elastic and plastic elongation.

3.1.10 *upper yield strength, UYS [FL<sup>-2</sup>]*—in a uniaxial test, the first stress maximum (stress at first zero slope) associated with discontinuous yielding at or near the onset of plastic deformation.

3.1.11 *yield point elongation, YPE, n—in a uniaxial test*, the strain (expressed in percent) separating the stress-strain curve's first point of zero slope from the point of transition from discontinuous yielding to uniform strain hardening.

3.1.11.1 *Discussion*— If the transition occurs over a range of strain, the YPE end point is the intersection between (a) a horizontal line drawn tangent to the curve at the last zero slope and (b) a line drawn tangent to the strain hardening portion of the stress-strain curve at the point of inflection. If there is no

point at or near the onset of yielding at which the slope reaches zero, the material has 0 % YPE.

3.1.12 *yield strength, YS or S<sub>y</sub> [FL<sup>-2</sup>]*, *n*—the engineering stress at which, by convention, it is considered that plastic elongation of the material has commenced.

3.1.12.1 *Discussion*—This stress may be specified in terms of (a) a specified deviation from a linear stress-strain relationship, (b) a specified total extension attained, or (c) maximum or minimum engineering stresses measured during discontinuous yielding.

### 3.2 Definitions of Terms Specific to This Standard:

3.2.1 *referee test, n*—test made to settle a disagreement as to the conformance to specified requirements, or conducted by a third party to arbitrate between conflicting results. **D1566, D11.08**

## 4. Significance and Use

4.1 Tension tests provide information on the strength and ductility of materials under uniaxial tensile stresses. This information may be useful in comparisons of materials, alloy development, quality control, and design under certain circumstances.

4.2 The results of tension tests of specimens machined to standardized dimensions from selected portions of a part or material may not totally represent the strength and ductility properties of the entire end product or its in-service behavior in different environments.

4.3 These test methods are considered satisfactory for acceptance testing of commercial shipments. The test methods have been used extensively in the trade for this purpose.

## 5. Apparatus

5.1 *Testing Machines*—Machines used for tension testing shall conform to the requirements of Practices E4. The forces used in determining tensile strength and yield strength shall be within the verified force application range of the testing machine as defined in Practices E4.

### 5.2 Gripping Devices:

5.2.1 *General*—Various types of gripping devices may be used to transmit the measured force applied by the testing machine to the test specimens. To ensure axial tensile stress within the gauge length, the axis of the test specimen should coincide with the center line of the heads of the testing machine. Any departure from this requirement may introduce bending stresses that are not included in the usual stress computation (force divided by cross-sectional area).

NOTE 1—The effect of this eccentric force application may be illustrated by calculating the bending moment and stress thus added. For a standard 12.5-mm [0.500-in.] diameter specimen, the stress increase is 1.5 percentage points for each 0.025 mm [0.001 in.] of eccentricity. This error increases to 2.5 percentage points/0.025 mm [0.001 in.] for a 9 mm [0.350-in.] diameter specimen and to 3.2 percentage points/0.025 mm [0.001 in.] for a 6-mm [0.250-in.] diameter specimen.

NOTE 2—Alignment methods are given in Practice E1012.

5.2.2 *Wedge Grips*—Testing machines usually are equipped with wedge grips. These wedge grips generally furnish a satisfactory means of gripping long specimens of ductile metal

and flat plate test specimens such as those shown in Fig. 1. If, however, for any reason, one grip of a pair advances farther than the other as the grips tighten, an undesirable bending stress may be introduced. When liners are used behind the wedges, they must be of the same thickness and their faces must be flat and parallel. For best results, the wedges should be supported over their entire lengths by the heads of the testing machine. This requires that liners of several thicknesses be available to cover the range of specimen thickness. For proper gripping, it is desirable that the entire length of the serrated face of each wedge be in contact with the specimen. Proper alignment of wedge grips and liners is illustrated in Fig. 2. For short specimens and for specimens of many materials it is generally necessary to use machined test specimens and to use a special means of gripping to ensure that the specimens, when under load, shall be as nearly as possible in uniformly distributed pure axial tension (see 5.2.3, 5.2.4, and 5.2.5).

**5.2.3 Grips for Threaded and Shouldered Specimens and Brittle Materials**—A schematic diagram of a gripping device for threaded-end specimens is shown in Fig. 3, while Fig. 4 shows a device for gripping specimens with shouldered ends. Both of these gripping devices should be attached to the heads of the testing machine through properly lubricated spherical-seated bearings. The distance between spherical bearings should be as great as feasible.

**5.2.4 Grips for Sheet Materials**—The self-adjusting grips shown in Fig. 5 have proven satisfactory for testing sheet materials that cannot be tested satisfactorily in the usual type of wedge grips.

**5.2.5 Grips for Wire**—Grips of either the wedge or snubbing types as shown in Fig. 5 and Fig. 6 or flat wedge grips may be used.

**5.3 Dimension-Measuring Devices**—Micrometers and other devices used for measuring linear dimensions shall be accurate and precise to at least one half the smallest unit to which the individual dimension is required to be measured.

**5.4 Extensometers**—Extensometers used in tension testing shall conform to the requirements of Practice E83 for the classifications specified by the procedure section of this test method. Extensometers shall be used and verified to include the strains corresponding to the yield strength and elongation at fracture (if determined).

**5.4.1** Extensometers with gauge lengths equal to or shorter than the nominal gauge length of the specimen (dimension shown as “G-Gauge Length” in the accompanying figures) may be used to determine the yield behavior. For specimens without a reduced section (for example, full cross sectional area specimens of wire, rod, or bar), the extensometer gauge length for the determination of yield behavior shall not exceed 80 % of the distance between grips. For measuring elongation at fracture with an appropriate extensometer, the gauge length of the extensometer shall be equal to the nominal gauge length required for the specimen being tested.

## 6. Test Specimens

### 6.1 General:

**6.1.1 Specimen Size**—Test specimens shall be either substantially full size or machined, as prescribed in the product specifications for the material being tested.

**6.1.2 Location**—Unless otherwise specified, the axis of the test specimen shall be located within the parent material as follows:

**6.1.2.1** At the center for products 40 mm [1.500 in.] or less in thickness, diameter, or distance between flats.

**6.1.2.2** Midway from the center to the surface for products over 40 mm [1.500 in.] in thickness, diameter, or distance between flats.

**6.1.3 Specimen Machining**—Improperly prepared test specimens often are the reason for unsatisfactory and incorrect test results. It is important, therefore, that care be exercised in the preparation of specimens, particularly in the machining, to maximize precision and minimize bias in test results.

**6.1.3.1** The reduced sections of prepared specimens should be free of cold work, notches, chatter marks, grooves, gouges, burrs, rough surfaces or edges, overheating, or any other condition which can deleteriously affect the properties to be measured.

**NOTE 3**—Punching or blanking of the reduced section may produce significant cold work or shear burrs, or both, along the edges which should be removed by machining.

**6.1.3.2** Within the reduced section of rectangular specimens, edges or corners should not be ground or abraded in a manner which could cause the actual cross-sectional area of the specimen to be significantly different from the calculated area.

**6.1.3.3** For brittle materials, large radius fillets at the ends of the gauge length should be used.

**6.1.3.4** The cross-sectional area of the specimen should be smallest at the center of the reduced section to ensure fracture within the gauge length. For this reason, a small taper is permitted in the reduced section of each of the specimens described in the following sections.

**6.1.4 Specimen Surface Finish**—When materials are tested with surface conditions other than as manufactured, the surface finish of the test specimens should be as provided in the applicable product specifications.

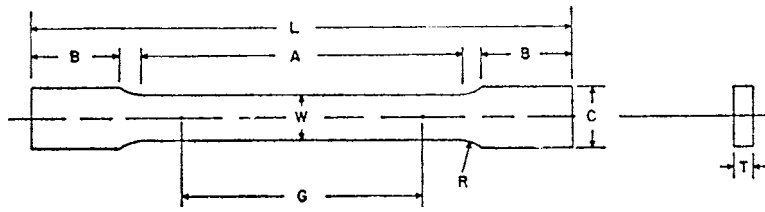
**NOTE 4**—Particular attention should be given to the uniformity and quality of surface finish of specimens for high strength and very low ductility materials since this has been shown to be a factor in the variability of test results.

**6.2 Plate-Type Specimens**—The standard plate-type test specimen is shown in Fig. 1. This specimen is used for testing metallic materials in the form of plate, shapes, and flat material having a nominal thickness of 5 mm [0.188 in.] or over. When product specifications so permit, other types of specimens may be used, as provided in 6.3, 6.4, and 6.5.

### 6.3 Sheet-Type Specimens:

**6.3.1** The standard sheet-type test specimen is shown in Fig. 1. This specimen is used for testing metallic materials in the form of sheet, plate, flat wire, strip, band, hoop, rectangles, and shapes ranging in nominal thickness from 0.13 to 19 mm [0.005 to 0.750 in.]. When product specifications so permit, other types of specimens may be used, as provided in 6.2, 6.4, and 6.5.

 **E8/E8M – 13a**



	Dimensions		
	Standard Specimens		Subsize Specimen
	Plate-Type, 40 mm [1.500 in.] Wide	Sheet-Type, 12.5 mm [0.500 in.] Wide	6 mm [0.250 in.] Wide
	mm [in.]	mm [in.]	mm [in.]
G—Gauge length (Note 1 and Note 2)	200.0 ± 0.2 [8.00 ± 0.01]	50.0 ± 0.1 [2.000 ± 0.005]	25.0 ± 0.1 [1.000 ± 0.003]
W—Width (Note 3 and Note 4)	40.0 ± 2.0 [1.500 ± 0.125, -0.250]	12.5 ± 0.2 [0.500 ± 0.010]	6.0 ± 0.1 [0.250 ± 0.005]
T—Thickness (Note 5)		thickness of material	
R—Radius of fillet, min (Note 6)	25 [1]	12.5 [0.500]	6 [0.250]
L—Overall length, min (Note 2, Note 7, and Note 8)	450 [18]	200 [8]	100 [4]
A—Length of reduced section, min	225 [9]	57 [2.25]	32 [1.25]
B—Length of grip section, min (Note 9)	75 [3]	50 [2]	30 [1.25]
C—Width of grip section, approximate (Note 4 and Note 9)	50 [2]	20 [0.750]	10 [0.375]

NOTE 1—For the 40 mm [1.500 in.] wide specimen, punch marks for measuring elongation after fracture shall be made on the flat or on the edge of the specimen and within the reduced section. Either a set of nine or more punch marks 25 mm [1 in.] apart, or one or more pairs of punch marks 200 mm [8 in.] apart may be used.

NOTE 2—When elongation measurements of 40 mm [1.500 in.] wide specimens are not required, a minimum length of reduced section (A) of 75 mm [2.25 in.] may be used with all other dimensions similar to those of the plate-type specimen.

NOTE 3—For the three sizes of specimens, the ends of the reduced section shall not differ in width by more than 0.10, 0.05 or 0.02 mm [0.004, 0.002 or 0.001 in.], respectively. Also, there may be a gradual decrease in width from the ends to the center, but the width at each end shall not be more than 1 % larger than the width at the center.

NOTE 4—For each of the three sizes of specimens, narrower widths (W and C) may be used when necessary. In such cases the width of the reduced section should be as large as the width of the material being tested permits; however, unless stated specifically, the requirements for elongation in a product specification shall not apply when these narrower specimens are used.

NOTE 5—The dimension T is the thickness of the test specimen as provided for in the applicable material specifications. Minimum thickness of 40 mm [1.500 in.] wide specimens shall be 5 mm [0.188 in.]. Maximum thickness of 12.5 and 6 mm [0.500 and 0.250 in.] wide specimens shall be 19 and 6 mm [0.750 and 0.250 in.], respectively.

NOTE 6—For the 40 mm [1.500 in.] wide specimen, a 13 mm [0.500 in.] minimum radius at the ends of the reduced section is permitted for steel specimens under 690 MPa [100 000 psi] in tensile strength when a profile cutter is used to machine the reduced section.

NOTE 7—The dimension shown is suggested as a minimum. In determining the minimum length, the grips must not extend in to the transition section between Dimensions A and B, see Note 9.

NOTE 8—To aid in obtaining axial force application during testing of 6-mm [0.250-in.] wide specimens, the overall length should be as large as the material will permit, up to 200 mm [8.00 in.].

NOTE 9—It is desirable, if possible, to make the length of the grip section large enough to allow the specimen to extend into the grips a distance equal to two thirds or more of the length of the grips. If the thickness of 12.5 mm [0.500-in.] wide specimens is over 10 mm [0.375 in.], longer grips and correspondingly longer grip sections of the specimen may be necessary to prevent failure in the grip section.

NOTE 10—For the three sizes of specimens, the ends of the specimen shall be symmetrical in width with the center line of the reduced section within 2.5, 1.25 and 0.13 mm [0.10, 0.05 and 0.005 in.], respectively. However, for referee testing and when required by product specifications, the ends of the 12.5 mm [0.500 in.] wide specimen shall be symmetrical within 0.2 mm [0.01 in.].

NOTE 11—For each specimen type, the radii of all fillets shall be equal to each other within a tolerance of 1.25 mm [0.05 in.], and the centers of curvature of the two fillets at a particular end shall be located across from each other (on a line perpendicular to the centerline) within a tolerance of 2.5 mm [0.10 in.].

NOTE 12—Specimens with sides parallel throughout their length are permitted, except for referee testing, provided: (a) the above tolerances are used; (b) an adequate number of marks are provided for determination of elongation; and (c) when yield strength is determined, a suitable extensometer is used. If the fracture occurs at a distance of less than 2 W from the edge of the gripping device, the tensile properties determined may not be representative of the material. In acceptance testing, if the properties meet the minimum requirements specified, no further testing is required, but if they are less than the minimum requirements, discard the test and retest.

**FIG. 1 Rectangular Tension Test Specimens**

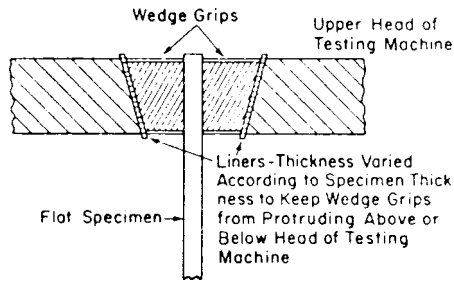


FIG. 2 Wedge Grips with Liners for Flat Specimens

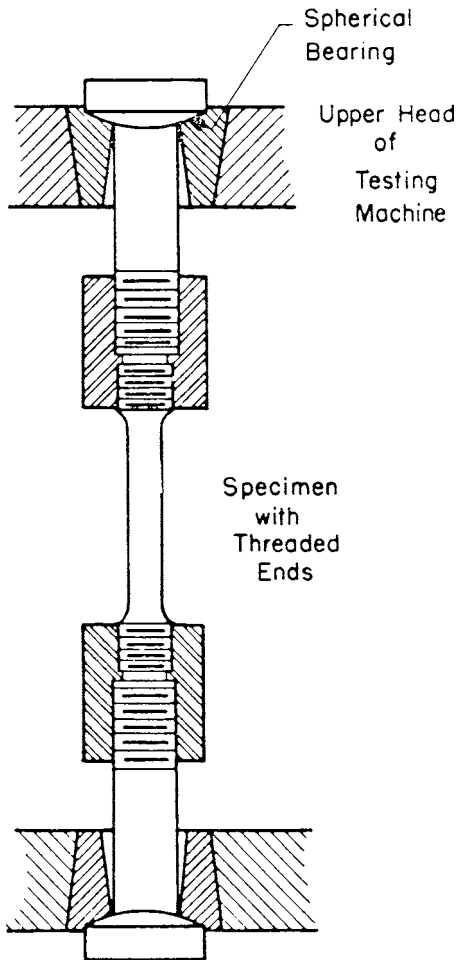


FIG. 3 Gripping Device for Threaded-End Specimens

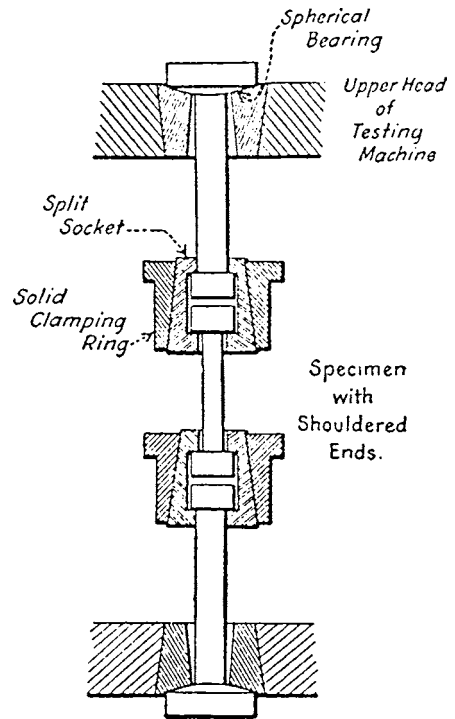


FIG. 4 Gripping Device for Shouldered-End Specimens

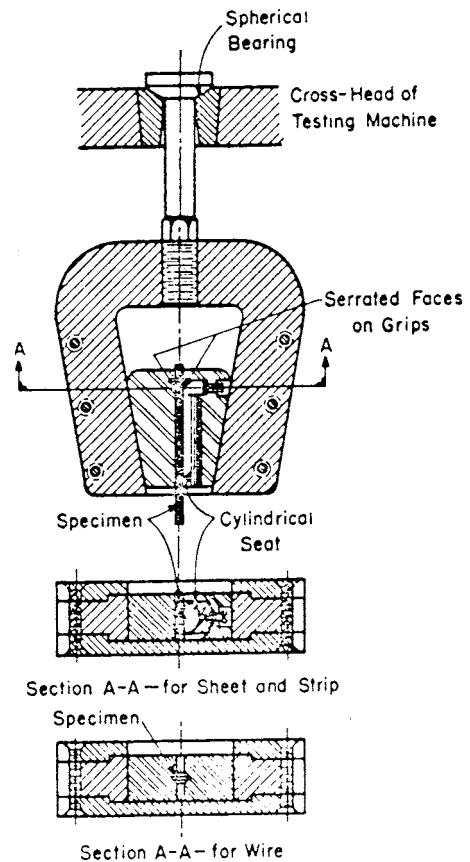


FIG. 5 Gripping Devices for Sheet and Wire Specimens

NOTE 5—Test Methods E345 may be used for tension testing of materials in thicknesses up to 0.15 mm [0.0059 in.].

6.3.2 Pin ends as shown in Fig. 7 may be used. In order to avoid buckling in tests of thin and high-strength materials, it may be necessary to use stiffening plates at the grip ends.

#### 6.4 Round Specimens:

6.4.1 The standard 12.5-mm [0.500-in.] diameter round test specimen shown in Fig. 8 is used quite generally for testing metallic materials, both cast and wrought.

6.4.2 Fig. 8 also shows small-size specimens proportional to the standard specimen. These may be used when it is necessary to test material from which the standard specimen or specimens shown in Fig. 1 cannot be prepared. Other sizes of small round

specimens may be used. In any such small-size specimen it is important that the gauge length for measurement of elongation

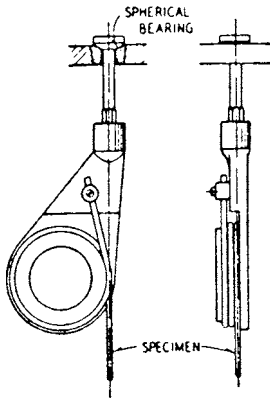


**FIG. 6 Snubbing Device for Testing Wire**

be four times the diameter of the specimen when following E8 and five times the diameter of the specimen when following E8M.

6.4.3 The shape of the ends of the specimen outside of the gauge length shall be suitable to the material and of a shape to fit the holders or grips of the testing machine so that the forces may be applied axially. Fig. 9 shows specimens with various types of ends that have given satisfactory results.

6.5 *Specimens for Sheet, Strip, Flat Wire, and Plate*—In testing sheet, strip, flat wire, and plate, use a specimen type appropriate for the nominal thickness of the material, as described in the following:

6.5.1 For material with a nominal thickness of 0.13 to 5 mm [0.005 to 0.1875 in.], use the sheet-type specimen described in 6.3.

6.5.2 For material with a nominal thickness of 5 to 12.5 mm [0.1875 to 0.500 in.], use either the sheet-type specimen of 6.3 or the plate-type specimen of 6.2.

6.5.3 For material with a nominal thickness of 12.5 to 19 mm [0.500 to 0.750 in.], use either the sheet-type specimen of 6.3, the plate-type specimen of 6.2, or the largest practical size of round specimen described in 6.4.

6.5.4 For material with a nominal thickness of 19 mm [0.750 in.], or greater, use the plate-type specimen of 6.2 or the largest practical size of round specimen described in 6.4.

6.5.4.1 If the product specifications permit, material of a thickness of 19 mm [0.750 in.], or greater may be tested using a modified sheet-type specimen conforming to the configuration shown by Fig. 1. The thickness of this modified specimen must be machined to  $10 \pm 0.5$  mm [ $0.400 \pm 0.020$  in.], and must be uniform within 0.1 mm [0.004 in.] throughout the reduced section. In the event of disagreement, a round specimen shall be used as the referee test (comparison) specimen.

6.6 *Specimens for Wire, Rod, and Bar*:

6.6.1 For round wire, rod, and bar, test specimens having the full cross-sectional area of the wire, rod, or bar shall be used wherever practicable. The gauge length for the measurement of elongation of wire less than 4 mm [0.125 in.] in diameter shall be as prescribed in product specifications. When testing wire, rod, or bar having a diameter of 4 mm [0.125 in.] or larger, a gauge length equal to four times the diameter shall be used when following E8 and a gauge length equal to five times the

diameter shall be used when following E8M unless otherwise specified. The total length of the specimens shall be at least equal to the gauge length plus the length of material required for the full use of the grips employed.

6.6.2 For wire of octagonal, hexagonal, or square cross section, for rod or bar of round cross section where the specimen required in 6.6.1 is not practicable, and for rod or bar of octagonal, hexagonal, or square cross section, one of the following types of specimens shall be used:

6.6.2.1 *Full Cross Section* (Note 6)—It is permissible to reduce the test section slightly with abrasive cloth or paper, or machine it sufficiently to ensure fracture within the gauge marks. For material not exceeding 5 mm [0.188 in.] in diameter or distance between flats, the cross-sectional area may be reduced to not less than 90 % of the original area without changing the shape of the cross section. For material over 5 mm [0.188 in.] in diameter or distance between flats, the diameter or distance between flats may be reduced by not more than 0.25 mm [0.010 in.] without changing the shape of the cross section. Square, hexagonal, or octagonal wire or rod not exceeding 5 mm [0.188 in.] between flats may be turned to a round having a cross-sectional area not smaller than 90 % of the area of the maximum inscribed circle. Fillets, preferably with a radius of 10 mm [0.375 in.], but not less than 3 mm [0.125 in.], shall be used at the ends of the reduced sections. Square, hexagonal, or octagonal rod over 5 mm [0.188 in.] between flats may be turned to a round having a diameter no smaller than 0.25 mm [0.010 in.] less than the original distance between flats.

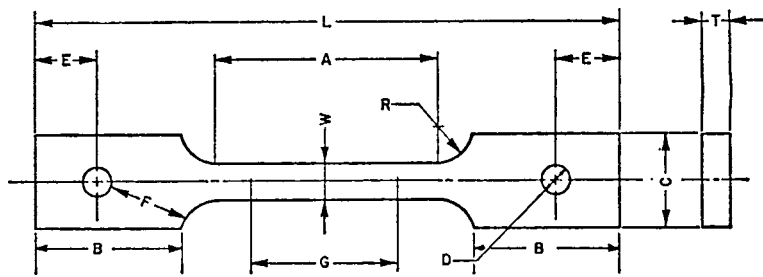
NOTE 6—The ends of copper or copper alloy specimens may be flattened 10 to 50 % from the original dimension in a jig similar to that shown in Fig. 10, to facilitate fracture within the gauge marks. In flattening the opposite ends of the test specimen, care shall be taken to ensure that the four flattened surfaces are parallel and that the two parallel surfaces on the same side of the axis of the test specimen lie in the same plane.

6.6.2.2 For rod and bar, the largest practical size of round specimen as described in 6.4 may be used in place of a test specimen of full cross section. Unless otherwise specified in the product specification, specimens shall be parallel to the direction of rolling or extrusion.

6.7 *Specimens for Rectangular Bar*—In testing rectangular bar one of the following types of specimens shall be used:

6.7.1 *Full Cross Section*—It is permissible to reduce the width of the specimen throughout the test section with abrasive cloth or paper, or by machining sufficiently to facilitate fracture within the gauge marks, but in no case shall the reduced width be less than 90 % of the original. The edges of the midlength of the reduced section not less than 20 mm [ $\frac{3}{4}$  in.] in length shall be parallel to each other and to the longitudinal axis of the specimen within 0.05 mm [0.002 in.]. Fillets, preferably with a radius of 10 mm [ $\frac{3}{8}$  in.] but not less than 3 mm [ $\frac{1}{8}$  in.] shall be used at the ends of the reduced sections.

6.7.2 Rectangular bar of thickness small enough to fit the grips of the testing machine but of too great width may be reduced in width by cutting to fit the grips, after which the cut surfaces shall be machined or cut and smoothed to ensure failure within the desired section. The reduced width shall not



Dimensions, mm [in.]

G—Gauge length	50.0 ± 0.1 [2.000 ± 0.005]
W—Width (Note 1)	12.5 ± 0.2 [0.500 ± 0.010]
T—Thickness, max (Note 2)	16 [0.625]
R—Radius of fillet, min (Note 3)	13 [0.5]
L—Overall length, min	200 [8]
A—Length of reduced section, min	57 [2.25]
B—Length of grip section, min	50 [2]
C—Width of grip section, approximate	50 [2]
D—Diameter of hole for pin, min (Note 4)	13 [0.5]
E—Edge distance from pin, approximate	40 [1.5]
F—Distance from hole to fillet, min	13 [0.5]

NOTE 1—The ends of the reduced section shall differ in width by not more than 0.1 mm [0.002 in.]. There may be a gradual taper in width from the ends to the center, but the width at each end shall be not more than 1 % greater than the width at the center.

NOTE 2—The dimension *T* is the thickness of the test specimen as stated in the applicable product specifications.

NOTE 3—For some materials, a fillet radius *R* larger than 13 mm [0.500 in.] may be needed.

NOTE 4—Holes must be on center line of reduced section within ± 0.05mm [0.002 in.].

NOTE 5—Variations of dimensions *C*, *D*, *E*, *F*, and *L* may be used that will permit failure within the gauge length.

FIG. 7 Pin-Loaded Tension Test Specimen with 50-mm [2-in.] Gauge Length

be less than the original bar thickness. Also, one of the types of specimens described in 6.2, 6.3, and 6.4 may be used.

6.8 *Shapes, Structural and Other*—In testing shapes other than those covered by the preceding sections, one of the types of specimens described in 6.2, 6.3, and 6.4 shall be used.

#### 6.9 *Specimens for Pipe and Tube* (Note 7):

6.9.1 For all small tube (Note 7), particularly sizes 25 mm [1 in.] and under in nominal outside diameter, and frequently for larger sizes, except as limited by the testing equipment, it is standard practice to use tension test specimens of full-size tubular sections. Snug-fitting metal plugs shall be inserted far enough into the ends of such tubular specimens to permit the testing machine jaws to grip the specimens properly. The plugs shall not extend into that part of the specimen on which the elongation is measured. Elongation is measured over a length of four times the diameter when following E8 or five times the diameter when following E8M unless otherwise stated in the product specification. Fig. 11 shows a suitable form of plug, the location of the plugs in the specimen, and the location of the specimen in the grips of the testing machine.

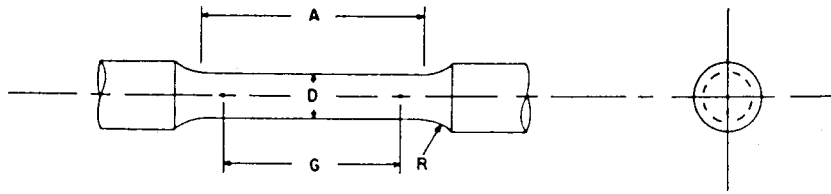
NOTE 7—The term “tube” is used to indicate tubular products in general, and includes pipe, tube, and tubing.

6.9.2 For large-diameter tube that cannot be tested in full section, longitudinal tension test specimens shall be cut as indicated in Fig. 12. Specimens from welded tube shall be located approximately 90° from the weld. If the tube-wall thickness is under 20 mm [0.750 in.], either a specimen of the form and dimensions shown in Fig. 13 or one of the small-size

specimens proportional to the standard 12.5-mm [0.500-in.] specimen, as mentioned in 6.4.2 and shown in Fig. 8, shall be used. Specimens of the type shown in Fig. 13 may be tested with grips having a surface contour corresponding to the curvature of the tube. When grips with curved faces are not available, the ends of the specimens may be flattened without heating. If the tube-wall thickness is 20 mm [0.750 in.] or over, the standard specimen shown in Fig. 8 shall be used.

NOTE 8—In clamping of specimens from pipe and tube (as may be done during machining) or in flattening specimen ends (for gripping), care must be taken so as not to subject the reduced section to any deformation or cold work, as this would alter the mechanical properties.

6.9.3 Transverse tension test specimens for tube may be taken from rings cut from the ends of the tube as shown in Fig. 14. Flattening of the specimen may be either after separating as in *A*, or before separating as in *B*. Transverse tension test specimens for large tube under 20 mm [0.750 in.] in wall thickness shall be either of the small-size specimens shown in Fig. 8 or of the form and dimensions shown for Specimen 2 in Fig. 13. When using the latter specimen, either or both surfaces of the specimen may be machined to secure a uniform thickness, provided not more than 15 % of the normal wall thickness is removed from each surface. For large tube 20 mm [0.750 in.] and over in wall thickness, the standard specimen shown in Fig. 8 shall be used for transverse tension tests. Specimens for transverse tension tests on large welded tube to determine the strength of welds shall be located perpendicular to the welded seams, with the welds at about the middle of their lengths.



Dimensions, mm [in.]

**For Test Specimens with Gauge Length Four times the Diameter [E8]**

	Standard Specimen		Small-Size Specimens Proportional to Standard		
	Specimen 1	Specimen 2	Specimen 3	Specimen 4	Specimen 5
G—Gauge length	50.0 ± 0.1 [2.000 ± 0.005]	36.0 ± 0.1 [1.400 ± 0.005]	24.0 ± 0.1 [1.000 ± 0.005]	16.0 ± 0.1 [0.640 ± 0.005]	10.0 ± 0.1 [0.450 ± 0.005]
D—Diameter (Note 1)	12.5 ± 0.2 [0.500 ± 0.010]	9.0 ± 0.1 [0.350 ± 0.007]	6.0 ± 0.1 [0.250 ± 0.005]	4.0 ± 0.1 [0.160 ± 0.003]	2.5 ± 0.1 [0.113 ± 0.002]
R—Radius of fillet, min	10 [0.375]	8 [0.25]	6 [0.188]	4 [0.156]	2 [0.094]
A—Length of reduced section, min (Note 2)	56 [2.25]	45 [1.75]	30 [1.25]	20 [0.75]	16 [0.625]

Dimensions, mm [in.]

**For Test Specimens with Gauge Length Five times the Diameter [E8M]**

	Standard Specimen		Small-Size Specimens Proportional to Standard		
	Specimen 1	Specimen 2	Specimen 3	Specimen 4	Specimen 5
G—Gauge length	62.5 ± 0.1 [2.500 ± 0.005]	45.0 ± 0.1 [1.750 ± 0.005]	30.0 ± 0.1 [1.250 ± 0.005]	20.0 ± 0.1 [0.800 ± 0.005]	12.5 ± 0.1 [0.565 ± 0.005]
D—Diameter (Note 1)	12.5 ± 0.2 [0.500 ± 0.010]	9.0 ± 0.1 [0.350 ± 0.007]	6.0 ± 0.1 [0.250 ± 0.005]	4.0 ± 0.1 [0.160 ± 0.003]	2.5 ± 0.1 [0.113 ± 0.002]
R—Radius of fillet, min	10 [0.375]	8 [0.25]	6 [0.188]	4 [0.156]	2 [0.094]
A—Length of reduced section, min (Note 2)	75 [3.0]	54 [2.0]	36 [1.4]	24 [1.0]	20 [0.75]

NOTE 1—The reduced section may have a gradual taper from the ends toward the center, with the ends not more than 1 % larger in diameter than the center (controlling dimension).

NOTE 2—If desired, the length of the reduced section may be increased to accommodate an extensometer of any convenient gauge length. Reference marks for the measurement of elongation should, nevertheless, be spaced at the indicated gauge length.

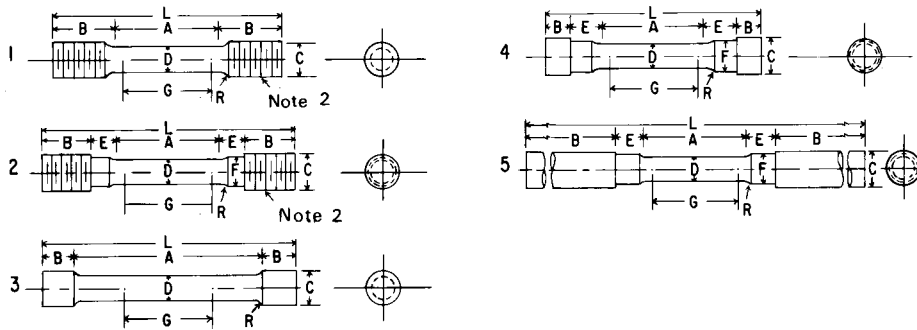
NOTE 3—The gauge length and fillets may be as shown, but the ends may be of any form to fit the holders of the testing machine in such a way that the force shall be axial (see Fig. 9). If the ends are to be held in wedge grips it is desirable, if possible, to make the length of the grip section great enough to allow the specimen to extend into the grips a distance equal to two thirds or more of the length of the grips.

NOTE 4—On the round specimens in Figs. 8 and 9, the gauge lengths are equal to four [E8] or five times [E8M] the nominal diameter. In some product specifications other specimens may be provided for, but unless the 4-to-1 [E8] or 5-to-1 [E8M] ratio is maintained within dimensional tolerances, the elongation values may not be comparable with those obtained from the standard test specimen.

NOTE 5—The use of specimens smaller than 6-mm [0.250-in.] diameter shall be restricted to cases when the material to be tested is of insufficient size to obtain larger specimens or when all parties agree to their use for acceptance testing. Smaller specimens require suitable equipment and greater skill in both machining and testing.

NOTE 6—For inch/pound units only: Five sizes of specimens often used have diameters of approximately 0.505, 0.357, 0.252, 0.160, and 0.113 in., the reason being to permit easy calculations of stress from loads, since the corresponding cross-sectional areas are equal or close to 0.200, 0.100, 0.0500, 0.0200, and 0.0100 in.<sup>2</sup>, respectively. Thus, when the actual diameters agree with these values, the stresses (or strengths) may be computed using the simple multiplying factors 5, 10, 20, 50, and 100, respectively. (The metric equivalents of these five diameters do not result in correspondingly convenient cross-sectional areas and multiplying factors.)

**FIG. 8 Standard 12.5-mm [0.500-in.] Round Tension Test Specimen and Examples of Small-Size Specimens Proportional to the Standard Specimen**



Dimensions, mm [in.]

For Test Specimens with Gauge Length Four times the Diameter [E8]

	Specimen 1	Specimen 2	Specimen 3	Specimen 4	Specimen 5
G—Gauge length	50 ± 0.1	50 ± 0.1	50 ± 0.1	50 ± 0.1	50 ± 0.1
D—Diameter (Note 1)	[2.000 ± 0.005]	[2.000 ± 0.005]	[2.000 ± 0.005]	[2.000 ± 0.005]	[2.000 ± 0.005]
R—Radius of fillet, min	12.5 ± 0.2	12.5 ± 0.2	12.5 ± 0.2	12.5 ± 0.2	12.5 ± 0.2
A—Length of reduced section	[0.500 ± 0.010]	[0.500 ± 0.010]	[0.500 ± 0.010]	[0.500 ± 0.010]	[0.500 ± 0.010]
L—Overall length, approximate	10 [0.375]	10 [0.375]	2 [0.0625]	10 [0.375]	10 [0.375]
B—Length of end section (Note 3)	56 [2.25]	56 [2.25]	100 [4]	56 [2.25]	56 [2.25]
	min	min	approximate	min	min
L—Overall length, approximate	145 [5]	155 [5.5]	155 [5.5]	140 [4.75]	255 [9.5]
B—Length of end section (Note 3)	35 [1.375]	25 [1]	20 [0.75]	15 [0.5]	75 [3]
	approximate	approximate	approximate	approximate	min
C—Diameter of end section	20 [0.75]	20 [0.75]	20 [0.75]	22 [0.875]	20 [0.75]
E—Length of shoulder and fillet section, approximate		15 [0.625]		20 [0.75]	15 [0.625]
F—Diameter of shoulder		15 [0.625]		15 [0.625]	15 [0.625]

Dimensions, mm [in.]

For Test Specimens with Gauge Length Five times the Diameter [E8M]

	Specimen 1	Specimen 2	Specimen 3	Specimen 4	Specimen 5
G—Gauge length	62.5 ± 0.1	62.5 ± 0.1	62.5 ± 0.1	62.5 ± 0.1	62.5 ± 0.1
D—Diameter (Note 1)	[2.500 ± 0.005]	[2.500 ± 0.005]	[2.500 ± 0.005]	[2.500 ± 0.005]	[2.500 ± 0.005]
R—Radius of fillet, min	12.5 ± 0.2	12.5 ± 0.2	12.5 ± 0.2	12.5 ± 0.2	12.5 ± 0.2
A—Length of reduced section	[0.500 ± 0.010]	[0.500 ± 0.010]	[0.500 ± 0.010]	[0.500 ± 0.010]	[0.500 ± 0.010]
L—Overall length, approximate	10 [0.375]	10 [0.375]	2 [0.0625]	10 [0.375]	10 [0.375]
B—Length of end section (Note 3)	75 [3]	75 [3]	75 [3]	75 [3]	75 [3]
	min	min	approximate	min	min
L—Overall length, approximate	145 [5]	155 [5.5]	155 [5.5]	140 [4.75]	255 [9.5]
B—Length of end section (Note 3)	35 [1.375]	25 [1]	20 [0.75]	15 [0.5]	75 [3]
	approximate	approximate	approximate	approximate	min
C—Diameter of end section	20 [0.75]	20 [0.75]	20 [0.75]	22 [0.875]	20 [0.75]
E—Length of shoulder and fillet section, approximate		15 [0.625]		20 [0.75]	15 [0.625]
F—Diameter of shoulder		15 [0.625]		15 [0.625]	15 [0.625]

NOTE 1—The reduced section may have a gradual taper from the ends toward the center with the ends not more than 1 % larger in diameter than the center.

NOTE 2—On Specimens 1 and 2, any standard thread is permissible that provides for proper alignment and aids in assuring that the specimen will break within the reduced section.

NOTE 3—On Specimen 5 it is desirable, if possible, to make the length of the grip section great enough to allow the specimen to extend into the grips a distance equal to two thirds or more of the length of the grips.

NOTE 4—The values stated in SI units in the table for Fig. 9 are to be regarded as separate from the inch/pound units. The values stated in each system are not exact equivalents; therefore each system must be used independently of the other.

FIG. 9 Various Types of Ends for Standard Round Tension Test Specimens

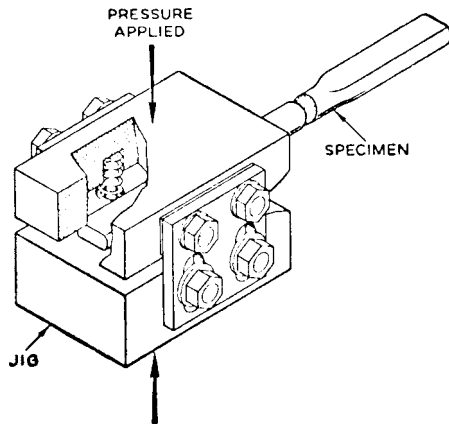
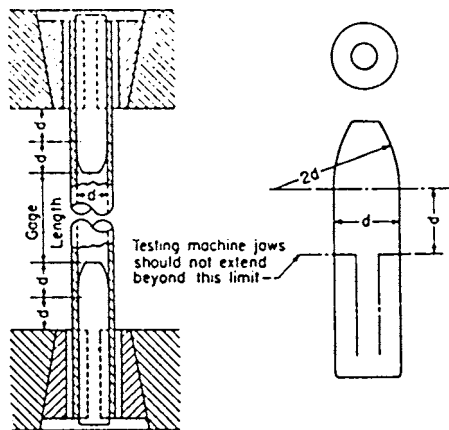
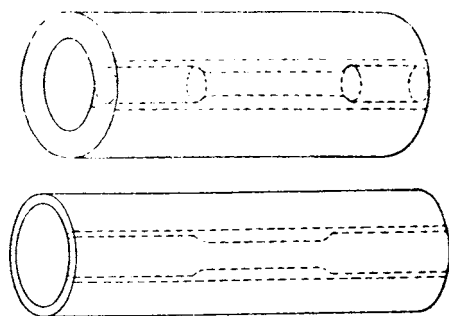


FIG. 10 Squeezing Jig for Flattening Ends of Full-Size Tension Test Specimens



NOTE 1—The diameter of the plug shall have a slight taper from the line limiting the test machine jaws to the curved section.

FIG. 11 Metal Plugs for Testing Tubular Specimens, Proper Location of Plugs in Specimen and of Specimen in Heads of Testing Machine



NOTE 1—The edges of the blank for the specimen shall be cut parallel to each other.

FIG. 12 Location from Which Longitudinal Tension Test Specimens Are to be Cut from Large-Diameter Tube

6.10 *Specimens for Forgings*—For testing forgings, the largest round specimen described in 6.4 shall be used. If round specimens are not feasible, then the largest specimen described in 6.5 shall be used.

6.10.1 For forgings, specimens shall be taken as provided in the applicable product specifications, either from the predominant or thickest part of the forging from which a coupon can be

obtained, or from a prolongation of the forging, or from separately forged coupons representative of the forging. When not otherwise specified, the axis of the specimen shall be parallel to the direction of grain flow.

6.11 *Specimens for Castings*—In testing castings either the standard specimen shown in Fig. 8 or the specimen shown in Fig. 15 shall be used unless otherwise provided in the product specifications.

6.11.1 Test coupons for castings shall be made as shown in Fig. 16 and Table 1.

6.12 *Specimen for Malleable Iron*—For testing malleable iron the test specimen shown in Fig. 17 shall be used, unless otherwise provided in the product specifications.

6.13 *Specimen for Die Castings*—For testing die castings the test specimen shown in Fig. 18 shall be used unless otherwise provided in the product specifications.

6.14 *Specimens for Powder Metallurgy (P/M) Materials*—For testing powder metallurgy (P/M) materials the test specimens shown in Figs. 19 and 20 shall be used, unless otherwise provided in the product specifications. When making test specimens in accordance with Fig. 19, shallow transverse grooves, or ridges, may be pressed in the ends to allow gripping by jaws machined to fit the grooves or ridges. Because of shape and other factors, the flat unmachined tensile test specimen (Fig. 19) in the heat treated condition will have an ultimate tensile strength of 50 % to 85 % of that determined in a machined round tensile test specimen (Fig. 20) of like composition and processing.

## 7. Procedures

7.1 *Preparation of the Test Machine*—Upon startup, or following a prolonged period of machine inactivity, the test machine should be exercised or warmed up to normal operating temperatures to minimize errors that may result from transient conditions.

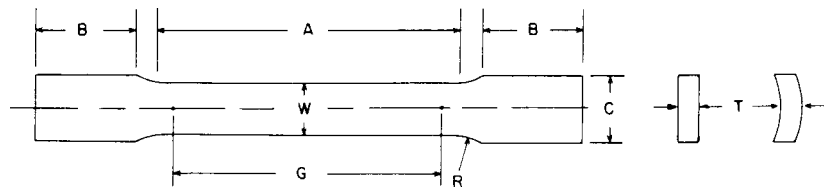
### 7.2 Measurement of Dimensions of Test Specimens:

7.2.1 To determine the cross-sectional area of a test specimen, measure the dimensions of the cross section at the center of the reduced section. For referee testing of specimens less than 5 mm [0.188 in.] in their least dimension, measure the dimensions where the least cross-sectional area is found. Measure and record the cross-sectional dimensions of tension test specimens as follows:

- (1) Specimen dimension  $\geq 5$  mm [0.200 in.] to the nearest 0.02 mm [0.001 in.].
- (2)  $2.5$  mm [0.100 in.]  $\leq$  Specimen dimension  $< 5$  mm [0.200 in.] to the nearest 0.01 mm [0.0005 in.].
- (3)  $0.5$  mm [0.020 in.]  $\leq$  specimen dimension  $< 2.5$  mm [0.100 in.] to the nearest 0.002 mm [0.0001 in.].
- (4) Specimen dimensions  $< 0.5$  mm [0.020 in.], to at least the nearest 1 % when practical but in all cases to at least the nearest 0.002 mm [0.0001 in.].

NOTE 9—Accurate and precise measurement of specimen dimensions can be one of the most critical aspects of tension testing, depending on specimen geometry. See Appendix X2 for additional information.

NOTE 10—Rough surfaces due to the manufacturing process such as hot rolling, metallic coating, etc., may lead to inaccuracy of the computed



	Dimensions						
	Specimen 1	Specimen 2	Specimen 3	Specimen 4	Specimen 5	Specimen 6	Specimen 7
	mm [in.]	mm [in.]	mm [in.]	mm [in.]	mm [in.]	mm [in.]	mm [in.]
G—Gauge length	50.0 ± 0.1 [2.000 ± 0.005]	50.0 ± 0.1 [2.000 ± 0.005]	200.0 ± 0.2 [8.00 ± 0.01]	50.0 ± 0.1 [2.000 ± 0.005]	100.0 ± 0.1 [4.000 ± 0.005]	50.0 ± 0.1 [2.000 ± 0.005]	100.0 ± 0.1 [4.000 ± 0.005]
W—Width (Note 1)	12.5 ± 0.2 [0.500 ± 0.010]	40.0 ± 2.0 [1.5 ± 0.125-0.25]	40.0 ± 0.2 [1.5 ± 0.125-0.25]	20.0 ± 0.7 [0.750 ± 0.031]	20.0 ± 0.7 [0.750 ± 0.031]	25.0 ± 1.5 [1.000 ± 0.062]	25.0 ± 1.5 [1.000 ± 0.062]
T—Thickness	measured thickness of specimen						
R—Radius of fillet, min	12.5 [0.5]	25 [1]	25 [1]	25 [1]	25 [1]	25 [1]	25 [1]
A—Length of reduced section, min	60 [2.25]	60 [2.25]	230 [9]	60 [2.25]	120 [4.5]	60 [2.25]	120 [4.5]
B—Length of grip section, min (Note 2)	75 [3]	75 [3]	75 [3]	75 [3]	75 [3]	75 [3]	75 [3]
C—Width of grip section, approximate (Note 3)	20 [0.75]	50 [2]	50 [2]	25 [1]	25 [1]	40 [1.5]	40 [1.5]

NOTE 1—The ends of the reduced section shall differ from each other in width by not more than 0.5 %. There may be a gradual taper in width from the ends to the center, but the width at each end shall be not more than 1 % greater than the width at the center.

NOTE 2—It is desirable, if possible, to make the length of the grip section great enough to allow the specimen to extend into the grips a distance equal to two thirds or more of the length of the grips.

NOTE 3—The ends of the specimen shall be symmetrical with the center line of the reduced section within 1 mm [0.05 in.] for specimens 1, 4, and 5, and 2.5 mm [0.10 in.] for specimens 2, 3, 6, and 7.

NOTE 4—For each specimen type, the radii of all fillets shall be equal to each other within a tolerance of 1.25 mm [0.05 in.], and the centers of curvature of the two fillets at a particular end shall be located across from each other (on a line perpendicular to the centerline) within a tolerance of 2.5 mm [0.10 in.].

NOTE 5—For circular segments, the cross-sectional area may be calculated by multiplying  $W$  and  $T$ . If the ratio of the dimension  $W$  to the diameter of the tubular section is larger than about  $\frac{1}{6}$ , the error in using this method to calculate the cross-sectional area may be appreciable. In this case, the exact equation (see 7.2.3) must be used to determine the area.

NOTE 6—Specimens with  $G/W$  less than 4 should not be used for determination of elongation.

NOTE 7—Specimens with sides parallel throughout their length are permitted, except for referee testing, provided: (a) the above tolerances are used; (b) an adequate number of marks are provided for determination of elongation; and (c) when yield strength is determined, a suitable extensometer is used. If the fracture occurs at a distance of less than  $2W$  from the edge of the gripping device, the tensile properties determined may not be representative of the material. If the properties meet the minimum requirements specified, no further testing is required, but if they are less than the minimum requirements, discard the test and retest.

FIG. 13 Tension Test Specimens for Large-Diameter Tubular Products

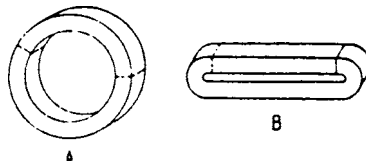


FIG. 14 Location of Transverse Tension Test Specimen in Ring Cut from Tubular Products

areas greater than the measured dimensions would indicate. Therefore, cross-sectional dimensions of test specimens with rough surfaces due to processing may be measured and recorded to the nearest 0.02 mm [0.001 in.]

NOTE 11—See X2.9 for cautionary information on measurements taken from coated metal products.

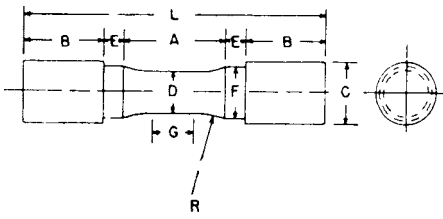
7.2.2 Determine the cross-sectional area of a full-size test specimen of uniform but nonsymmetrical cross section by determining the mass of a length not less than 20 times longer than the largest cross-sectional dimension.

7.2.2.1 Determine the weight to the nearest 0.5 % or less.

7.2.2.2 The cross-sectional area is equal to the mass of the specimen divided by the length and divided by the density of the material.

7.2.3 When using specimens of the type shown in Fig. 13 taken from tubes, the cross-sectional area shall be determined as follows:

If  $D/W \leq 6$ :



material being tested. Gauge marks shall be stamped lightly with a punch, scribed lightly with dividers or drawn with ink as preferred. For material that is sensitive to the effect of slight notches and for small specimens, the use of layout ink will aid in locating the original gauge marks after fracture.

7.3.2 For materials where the specified elongation is 3 % or less, measure the original gauge length to the nearest 0.05 mm [0.002 in.] prior to testing.

7.4 Zeroing of the Testing Machine:

7.4.1 The testing machine shall be set up in such a manner that zero force indication signifies a state of zero force on the specimen. Any force (or preload) imparted by the gripping of the specimen (see Note 13) must be indicated by the force measuring system unless the preload is physically removed prior to testing. Artificial methods of removing the preload on the specimen, such as taring it out by a zero adjust pot or removing it mathematically by software, are prohibited because these would affect the accuracy of the test results.

NOTE 13—Preloads generated by gripping of specimens may be either tensile or compressive in nature and may be the result of such things as:

- grip design
- malfunction of gripping apparatus (sticking, binding, etc.)
- excessive gripping force
- sensitivity of the control loop

NOTE 14—It is the operator’s responsibility to verify that an observed preload is acceptable and to ensure that grips operate in a smooth manner. Unless otherwise specified, it is recommended that momentary (dynamic) forces due to gripping not exceed 20 % of the material’s nominal yield strength and that static preloads not exceed 10 % of the material’s nominal yield strength.

7.5 Gripping of the Test Specimen:

7.5.1 For specimens with reduced sections, gripping of the specimen shall be restricted to the grip section, because gripping in the reduced section or in the fillet can significantly affect test results.

7.6 Speed of Testing:

7.6.1 Speed of testing may be defined in terms of (a) rate of straining of the specimen, (b) rate of stressing of the specimen, (c) crosshead speed, (d) the elapsed time for completing part or all of the test, or (e) free-running crosshead speed (rate of movement of the crosshead of the testing machine when not under load).

7.6.2 Specifying suitable numerical limits for speed and selection of the method are the responsibilities of the product committees. Suitable limits for speed of testing should be specified for materials for which the differences resulting from the use of different speeds are of such magnitude that the test results are unsatisfactory for determining the acceptability of the material. In such instances, depending upon the material and the use for which the test results are intended, one or more of the methods described in the following paragraphs is recommended for specifying speed of testing.

NOTE 15—Speed of testing can affect test values because of the rate sensitivity of materials and the temperature-time effects.

7.6.2.1 Rate of Straining—The allowable limits for rate of straining shall be specified in mm/mm/min [in./in./min]. Some testing machines are equipped with pacing or indicating devices for the measurement and control of rate of straining,

	Dimensions		
	Specimen 1	Specimen 2	Specimen 3
	mm [in.]	mm [in.]	mm [in.]
G—Length of parallel section	Shall be equal to or greater than diameter <i>D</i>		
<i>D</i> —Diameter	12.5 ± 0.2 [0.500 ± 0.010]	20 ± 0.4 [0.750 ± 0.015]	36.0 ± 0.6 [1.25 ± 0.02]
<i>R</i> —Radius of fillet, min	25 [1]	25 [1]	50 [2]
<i>A</i> —Length of reduced section, min	32 [1.25]	38 [1.5]	60 [2.25]
<i>L</i> —Overall length, min	95 [3.75]	100 [4]	160 [6.375]
<i>B</i> —Length of end section, approximate	25 [1]	25 [1]	45 [1.75]
<i>C</i> —Diameter of end section, approximate	20 [0.75]	30 [1.125]	48 [1.875]
<i>E</i> —Length of shoulder, min	6 [0.25]	6 [0.25]	8 [0.312]
<i>F</i> —Diameter of shoulder	16.0 ± 0.4 [0.625 ± 0.016]	24.0 ± 0.4 [0.94 ± 0.016]	36.5 ± 0.4 [1.438 ± 0.016]

NOTE 1—The reduced section and shoulders (dimensions *A*, *D*, *E*, *F*, *G*, and *R*) shall be as shown, but the ends may be of any form to fit the holders of the testing machine in such a way that the force can be axial. Commonly the ends are threaded and have the dimensions *B* and *C* given above.

FIG. 15 Standard Tension Test Specimen for Cast Iron

$$A = \left[ \left( \frac{W}{4} \right) \times \sqrt{D^2 - W^2} \right] + \left[ \left( \frac{D^2}{4} \right) \times \arcsin \left( \frac{W}{D} \right) \right] - \left[ \left( \frac{W}{4} \right) \times \sqrt{(D - 2T)^2 - W^2} \right] - \left[ \left( \frac{D - 2T}{2} \right)^2 \times \arcsin \left( \frac{W}{D - 2T} \right) \right] \quad (1)$$

where:

- A* = exact cross-sectional area, mm<sup>2</sup> [in.<sup>2</sup>],
- W* = width of the specimen in the reduced section, mm [in.],
- D* = measured outside diameter of the tube, mm [in.], and
- T* = measured wall thickness of the specimen, mm [in.].

arcsin values to be in radians

If *D/W* > 6, the exact equation or the following equation may be used:

$$A = W \times T \quad (2)$$

where:

- A* = approximate cross-sectional area, mm<sup>2</sup> [in.<sup>2</sup>],
- W* = width of the specimen in the reduced section, mm [in.], and
- T* = measured wall thickness of the specimen, mm [in.].

NOTE 12—See X2.8 for cautionary information on measurements and calculations for specimens taken from large-diameter tubing.

7.3 Gauge Length Marking of Test Specimens:

7.3.1 The gauge length for the determination of elongation shall be in accordance with the product specifications for the

**TABLE 1 Details of Test Coupon Design for Castings (see Fig. 16)**

NOTE 1—*Test Coupons for Large and Heavy Steel Castings*: The test coupons in Fig. 16A and B are to be used for large and heavy steel castings. However, at the option of the foundry the cross-sectional area and length of the standard coupon may be increased as desired. This provision does not apply to Specification A356/A356M.

NOTE 2—*Bend Bar*: If a bend bar is required, an alternate design (as shown by dotted lines in Fig. 16) is indicated.

	Leg Design, 125 mm [5 in.]		Riser Design
1. <i>L</i> (length)	A 125mm [5-in.] minimum length will be used. This length may be increased at the option of the foundry to accommodate additional test bars (see Note 1).	1. <i>L</i> (length)	The length of the riser at the base will be the same as the top length of the leg. The length of the riser at the top therefore depends on the amount of taper added to the riser. The width of the riser at the base of a multiple-leg coupon shall be $n(57\text{ mm}) - 16\text{ mm}$ [ $n(2.25\text{ in.}) - 0.625\text{ in.}$ ] where $n$ equals the number of legs attached to the coupon. The width of the riser at the top is therefore dependent on the amount of taper added to the riser.
2. End taper	Use of and size of end taper is at the option of the foundry.	2. Width	
3. Height	32 mm [1.25 in.]		
4. Width (at top)	32 mm [1.25 in.] (see Note 1)		
5. Radius (at bottom)	13 mm [0.5 in.] max		
6. Spacing between legs	A 13 mm [0.5 in.] radius will be used between the legs.		
7. Location of test bars	The tensile, bend, and impact bars will be taken from the lower portion of the leg (see Note 2).		
8. Number of legs	The number of legs attached to the coupon is at the option of the foundry providing they are equispaced according to Item 6.	3. <i>T</i> (riser taper) Height	Use of and size is at the option of the foundry. The minimum height of the riser shall be 51 mm [2 in.]. The maximum height is at the option of the foundry for the following reasons: (a) many risers are cast open, (b) different compositions may require variation in risering for soundness, or (c) different pouring temperatures may require variation in risering for soundness.
9. $R_x$	Radius from 0 to approximately 2 mm [0.062 in.]		

but in the absence of such a device the average rate of straining can be determined with a timing device by observing the time required to effect a known increment of strain.

7.6.2.2 *Rate of Stressing*—The allowable limits for rate of stressing shall be specified in megapascals per second [pounds per square inch per minute]. Many testing machines are equipped with pacing or indicating devices for the measurement and control of the rate of stressing, but in the absence of such a device the average rate of stressing can be determined with a timing device by observing the time required to apply a known increment of stress.

7.6.2.3 *Crosshead Speed*—The allowable limits for crosshead speed, during a test, may be specified in mm/min [in./min]; in this case, the limits for the crosshead speed should be further qualified by specifying different limits for various types and sizes of specimens. In cases where different length specimens may be used, it is often more practical to specify the crosshead speed in terms of mm [in.] per mm [in.] of length of the original reduced section of the specimen (or distance between grips for specimens not having reduced sections) per minute. Many testing machines are equipped with pacing or indicating devices for the measurement and control of the crosshead speed during a test, but in the absence of such devices the average crosshead speed can be experimentally determined by using suitable length-measuring and timing devices.

NOTE 16—This method of specifying speed of testing, “Crosshead Speed”, was previously called “Rate of Separation of Heads During Tests.”

NOTE 17—For machines not having crossheads or having stationary

crossheads, the phrase “crosshead speed” may be interpreted to mean the rate of grip separation.

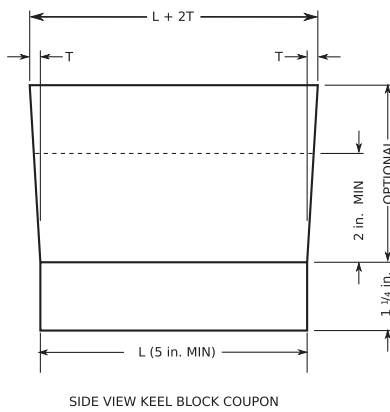
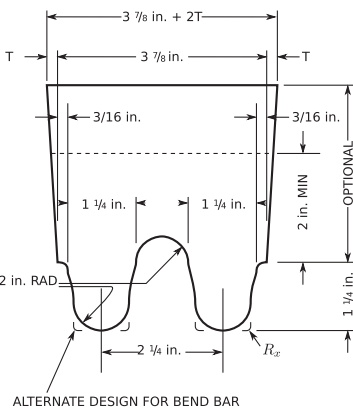
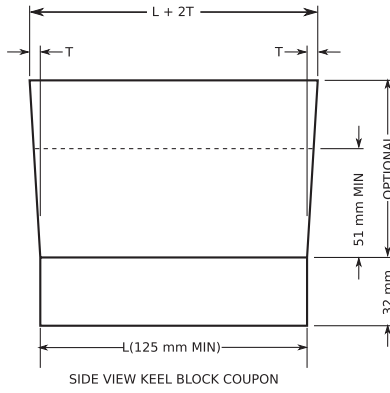
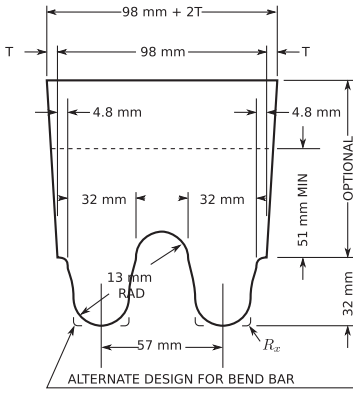
7.6.2.4 *Elapsed Time*—The allowable limits for the elapsed time from the beginning of force application (or from some specified stress) to the instant of fracture, to the maximum force, or to some other stated stress, shall be specified in minutes or seconds. The elapsed time can be determined with a timing device.

7.6.2.5 *Free-Running Crosshead Speed*—The allowable limits for the rate of movement of the crosshead of the testing machine, with no force applied by the testing machine, shall be specified in mm per mm [inches per inch] of length of reduced section (or distance between grips for specimens not having reduced sections) per second [minute]. The limits for the crosshead speed may be further qualified by specifying different limits for various types and sizes of specimens. The average crosshead speed can be experimentally determined by using suitable length-measuring and timing devices.

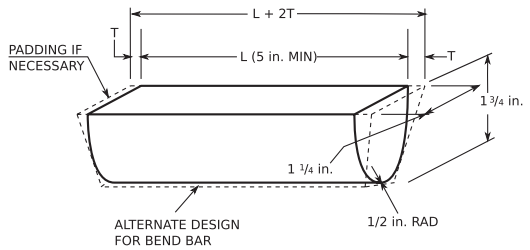
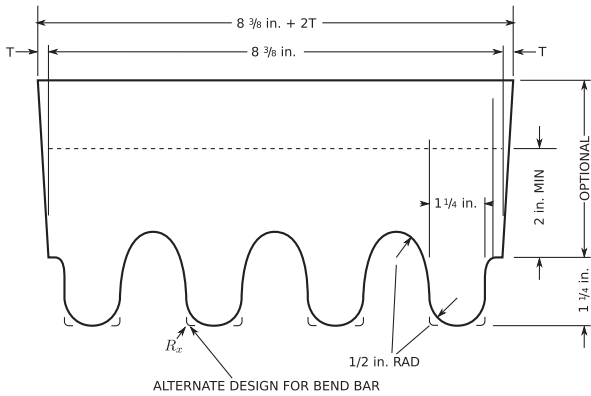
NOTE 18—For machines not having crossheads or having stationary crossheads, the phrase “free-running crosshead speed” may be interpreted to mean the free-running rate of grip separation.

7.6.3 *Speed of Testing When Determining Yield Properties*—Unless otherwise specified, any convenient speed of testing may be used up to one half the specified minimum yield strength or up to one quarter of the specified minimum tensile strength, whichever is smaller. The speed above this point shall be within the specified limits. If different speed limitations are required for use in determining yield strength, yield point elongation, tensile strength, elongation, and reduction of area,

 E8/E8M - 13a



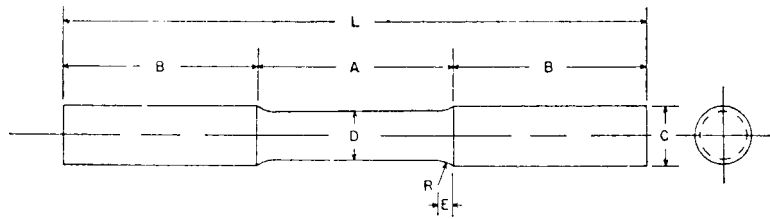
**Design for Double Keel Block Coupon**



**Design for "Attached" Coupon**

**Design for Multiple Keel Block Coupon (4 legs)**

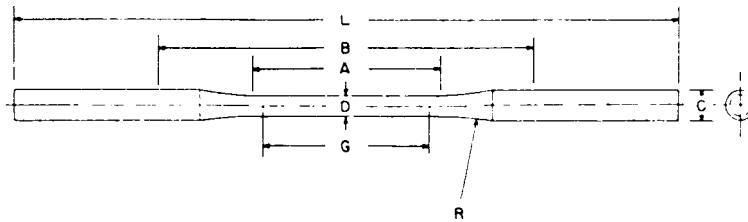
**FIG. 16 Test Coupons for Castings**



Dimensions, mm [in.]

D—Diameter	16 [0.625]
R—Radius of fillet	8 [0.312]
A—Length of reduced section	64 [2.5]
L—Overall length	190 [7.5]
B—Length of end section	64 [2.5]
C—Diameter of end section	20 [0.75]
E—Length of fillet	5 [0.188]

FIG. 17 Standard Tension Test Specimen for Malleable Iron



Dimensions, mm [in.]

G—Gauge length	50 ± 0.1 [2.000 ± 0.005]
D—Diameter (see Note)	6.4 ± 0.1 [0.250 ± 0.005]
R—Radius of fillet, min	75 [3]
A—Length of reduced section, min	60 [2.25]
L—Overall length, min	230 [9]
B—Distance between grips, min	115 [4.5]
C—Diameter of end section, approximate	10 [0.375]

NOTE 1—The reduced section may have a gradual taper from the end toward the center, with the ends not more than 0.1 mm [0.005 in.] larger in diameter than the center.

FIG. 18 Standard Tension Test Specimens for Die Castings

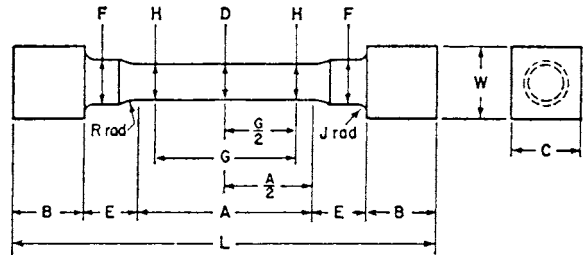
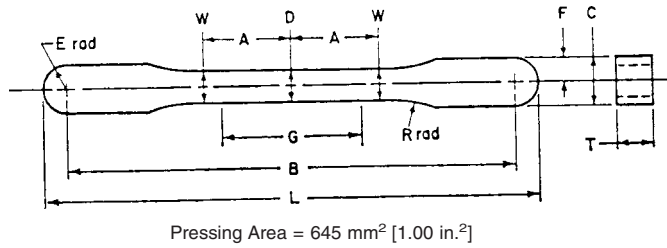
they should be stated in the product specifications. In all cases, the speed of testing shall be such that the forces and strains used in obtaining the test results are accurately indicated. Determination of mechanical properties for comparison of product properties against a specification value should be run using the same control method and rate used to determine the specification value unless it can be shown that another method yields equivalent or conservative results. In the absence of any specified limitations, one of the following control methods shall be used. Appendix X4 provides additional guidance on selecting the control method.

NOTE 19—In the previous and following paragraphs, the yield properties referred to include yield strength, yield point, and yield point elongation.

7.6.3.1 Control Method A—Rate of Stressing Method for Determining Yield Properties - In this method, the testing machine shall be operated such that the rate of stress application in the linear elastic region is between 1.15 and 11.5 MPa/s [10 000 and 100 000 psi/min]. The speed of the testing machine

testing machine be operated in closed-loop control using the force signal through yield; however closed-loop control of the force signal can be used in the linear-elastic portion of the test.

NOTE 20—It is not the intent of this method to maintain constant stress rate or to control stress rate with closed loop force control while determining yield properties, but only to set the crosshead speed to achieve the target stress rate in the elastic region. When a specimen being tested begins to yield, the stressing rate decreases and may even become negative in the case of a specimen with discontinuous yielding. To maintain a constant stressing rate through the yielding process requires the testing machine to operate at extremely high speeds and, in most cases, this is neither practical nor desirable. In practice, it is simpler to use either a strain rate, crosshead speed, or a free-running crosshead speed that approximates the desired stressing rate in the linear-elastic portion of the test. As an example, use a strain rate that is between 1.15 and 11.5 MPa/s divided by the nominal Young's Modulus of the material being tested. As another example, find a crosshead speed through experimentation that approximates the desired stressing rate prior to the onset of yielding, and maintain that crosshead speed through the region that yield properties are determined. While both of these methods will provide similar rates of stressing and straining prior to the onset of yielding, the rates of stressing and straining are generally quite different in the region where yield



Approximate Pressing Area of Unmachined Compact = 752 mm<sup>2</sup> [1.166 in.<sup>2</sup>] Machining Recommendations

1. Rough machine reduced section to 6.35-mm [0.25-in.] diameter
2. Finish turn 4.75/4.85-mm [0.187/0.191-in.] diameter with radii and taper
3. Polish with 00 emery cloth
4. Lap with crocus cloth

Dimensions, mm [in.]	
G—Gauge length	25.4 ± 0.08 [1.000 ± 0.003]
D—Width at center	5.72 ± 0.03 [0.225 ± 0.001]
W—Width at end of reduced section	5.97 ± 0.03 [0.235 ± 0.001]
T—Compact to this thickness	3.56 to 6.35 [0.140 to 0.250]
R—Radius of fillet	25.4 [1]
A—Half-length of reduced section	15.9 [0.625]
B—Grip length	80.95 ± 0.03 [3.187 ± 0.001]
L—Overall length	89.64 ± 0.03 [3.529 ± 0.001]
C—Width of grip section	8.71 ± 0.03 [0.343 ± 0.001]
F—Half-width of grip section	4.34 ± 0.03 [0.171 ± 0.001]
E—End radius	4.34 ± 0.03 [0.171 ± 0.001]

Dimensions, mm [in.]	
G—Gauge length	25.4 ± 0.08 [1.000 ± 0.003]
D—Diameter at center of reduced section	4.75 ± 0.03 [0.187 ± 0.001]
H—Diameter at ends of gauge length	4.85 ± 0.03 [0.191 ± 0.001]
R—Radius of gauge fillet	6.35 ± 0.13 [0.250 ± 0.005]
A—Length of reduced section	47.63 ± 0.13 [1.875 ± 0.003]
L—Overall length (die cavity length)	75 [3], nominal
B—Length of end section	7.88 ± 0.13 [0.310 ± 0.005]
C—Compact to this end thickness	10.03 ± 0.13 [0.395 ± 0.005]
W—Die cavity width	10.03 ± 0.08 [0.395 ± 0.003]
E—Length of shoulder	6.35 ± 0.13 [0.250 ± 0.005]
F—Diameter of shoulder	7.88 ± 0.03 [0.310 ± 0.001]
J—End fillet radius	1.27 ± 0.13 [0.050 ± 0.005]

NOTE 1—Dimensions Specified, except G and T, are those of the die.

**FIG. 19 Standard Flat Unmachined Tension Test Specimens for Powder Metallurgy (P/M) Products**

testing materials that exhibit low strain rate sensitivity such as some steels and aluminum.

**7.6.3.2 Control Method B - Rate of Straining Control Method for Determining Yield Properties**—In this method, the testing machine shall be operated in closed-loop control using the extensometer signal. The rate of straining shall be set and maintained at  $0.015 \pm 0.006$  mm/mm/min [in./in./min].

NOTE 22—Proper precautions must be observed when operating a machine in closed-loop strain control because unexpected crosshead movement may occur if the control parameters are not set properly, if proper safety limits are not set, or if the extensometer slips.

NOTE 23—A Rate of Straining at 0.005 mm/mm/min [in./in./min] is often required for aerospace, high-temperature alloys, and titanium applications and when specified, must be followed rather than the requirement above.

**7.6.3.3 Control Method C—Crosshead Speed Control Method for Determining Yield Properties**—The testing machine shall be set to a crosshead speed equal to  $0.015 \pm 0.003$  mm/mm/min [in./in./min] of the original reduced section (dimension A in Fig. 1, Fig. 7, Fig. 8, Fig. 9, Fig. 13, Fig. 15, Fig. 17, Fig. 18, and Fig. 20, and 2 times dimension A in Fig. 19) or distance between grips for specimens without reduced sections.

NOTE 24—It is recommended that crosshead speed be used for control in regions of discontinuous yielding.

NOTE 25—Using different Control Methods may produce different yield results especially if the material being tested is strain-rate sensitive. To achieve the best reproducibility in cases where the material may be strain-rate sensitive, the same control method should be used. Methods described in 7.6.3.2 or 7.6.3.3 will tend to give similar results in the case of a strain-rate sensitive material. The control method described in 7.6.3.1 should be avoided for strain rate sensitive materials if it is desirable to reproduce similar test results on other testing machines or in other laboratories.

NOTE 1—The gauge length and fillets of the specimen shall be as shown. The ends as shown are designed to provide a practical minimum pressing area. Other end designs are acceptable, and in some cases are required for high-strength sintered materials.

NOTE 2—It is recommended that the test specimen be gripped with a split collet and supported under the shoulders. The radius of the collet support circular edge is to be not less than the end fillet radius of the test specimen.

NOTE 3—Diameters D and H are to be concentric within 0.03 mm [0.001 in.] total indicator runout (T.I.R.), and free of scratches and tool marks.

**FIG. 20 Standard Round Machined Tension Test Specimen for Powder Metallurgy (P/M) Products**

of testing, the following general rules shall apply for materials with expected elongations greater than 5%. When determining only the tensile strength, or after the yield behavior has been recorded, the speed of the testing machine shall be set between 0.05 and 0.5 mm/mm [or in./in.] of the length of the reduced section (or distance between the grips for specimens not having a reduced section) per minute. Alternatively, an extensometer and strain rate indicator may be used to set the strain rate between 0.05 and 0.5 mm/mm/min [or in./in./min].

NOTE 26—For materials with expected elongations less than or equal to 5%, the speed of the testing machine may be maintained throughout the test at the speed used to determine yield properties.

NOTE 27—Tensile strength and elongation are sensitive to test speed for many materials (see Appendix X1) to the extent that variations within the range of test speeds given above can significantly affect results.

Where extensometers are employed, use only those that are verified over a strain range in which the yield strength will be determined (see 5.4).

NOTE 28—For example, a verified strain range of 0.2 % to 2.0 % is appropriate for use in determining the yield strengths of many metals.

NOTE 29—Determination of yield behavior on materials which cannot support an appropriate extensometer (thin wire, for example) is problematic and outside the scope of this standard.

7.7.1 *Offset Method*—To determine the yield strength by the offset method, it is necessary to secure data (autographic or numerical) from which a stress-strain diagram may be drawn. Then on the stress-strain diagram (Fig. 21) lay off  $Om$  equal to the specified value of the offset, draw  $mn$  parallel to  $OA$ , and thus locate  $r$ , the intersection of  $mn$  with the stress-strain diagram (Note 36). In reporting values of yield strength obtained by this method, the specified value of offset used should be stated in parentheses after the term yield strength. Thus:

$$\text{Yield strength (offset = 0.2\%)} = 360 \text{ MPa [52 000 psi]} \quad (3)$$

In using this method, a Class B2 or better extensometer (see Practice E83) shall be used.

NOTE 30—There are two general types of extensometers, averaging and non-averaging, the use of which is dependent on the product tested. For most machined specimens, there are minimal differences. However, for some forgings and tube sections, significant differences in measured yield strength can occur. For these cases, it is recommended that the averaging type be used.

NOTE 31—When there is a disagreement over yield properties, the offset method for determining yield strength is recommended as the referee test method.

NOTE 32—In practice, for a number of reasons, the straight-line portion of the stress-strain curve (line  $OA$  shown in Fig. 21) may not go through the origin of the stress-strain diagram. In these cases, Point  $O$  in Figs. 21-27 is not the origin of the stress-strain diagram, but rather where the straight-line portion of the stress-strain curve,  $OA$ , intersects the strain axis, see Fig. 26 and Fig. 27. All offsets and extensions are calculated from the intersection of the straight-line portion of the stress-strain curve,  $OA$ , with the strain axis, and not necessarily from the origin of the stress-strain diagram.

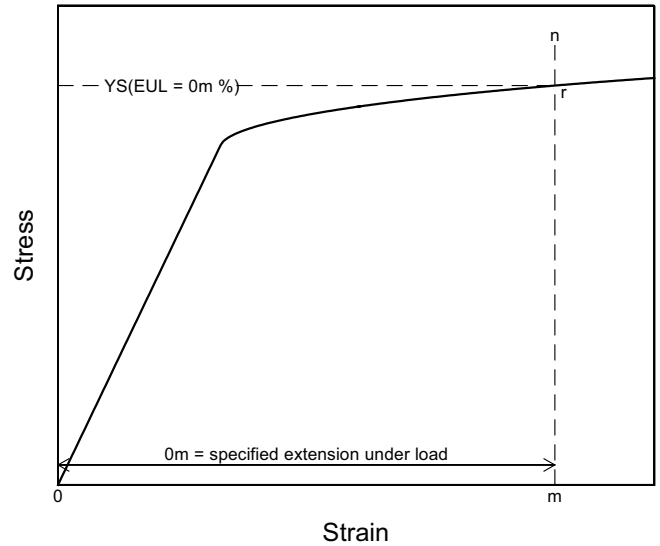
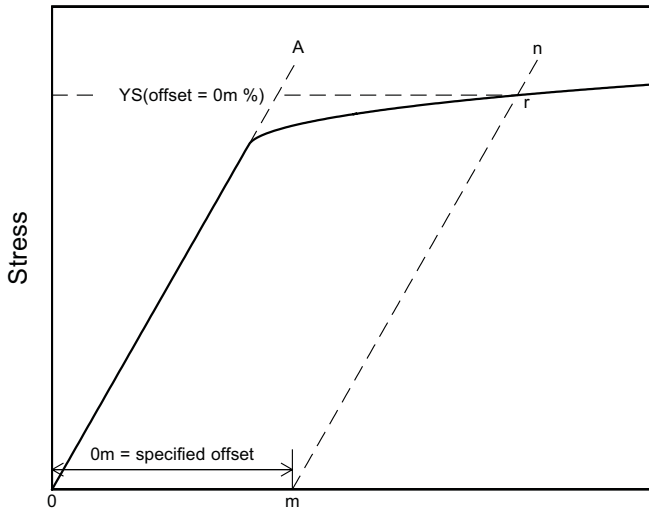


FIG. 22 Stress-Strain Diagram for Determination of Yield Strength by the Extension-Under-Load Method

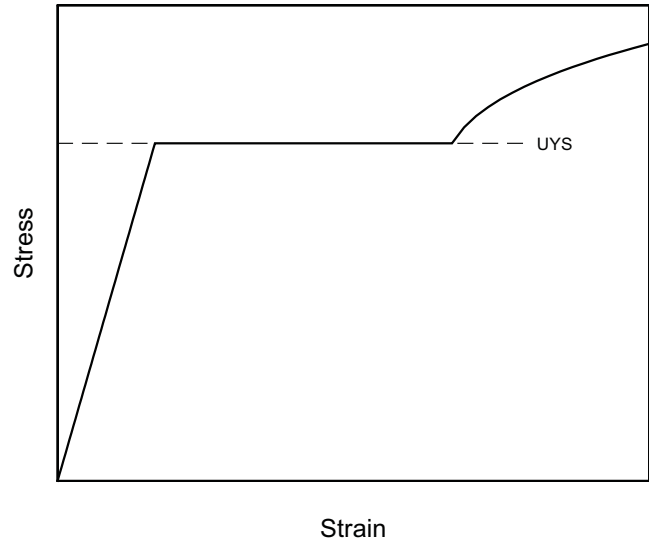


FIG. 23 Stress-Strain Diagram Showing Upper Yield Strength Corresponding with Top of Knee

7.7.2 *Extension-Under-Load (EUL) Method*—Yield strength by the extension-under-load method may be determined by: (1) using autographic or numerical devices to secure stress-strain data, and then analyzing this data (graphically or using automated methods) to determine the stress value at the specified value of extension, or (2) using devices that indicate when the specified extension occurs, so that the stress then occurring may be ascertained (Note 34). Any of these devices may be automatic. This method is illustrated in Fig. 22. The stress at the specified extension shall be reported as follows:

$$\text{Yield strength (EUL = 0.5\%)} = 52\,000 \text{ psi} \quad (4)$$

Extensometers and other devices used in determination of

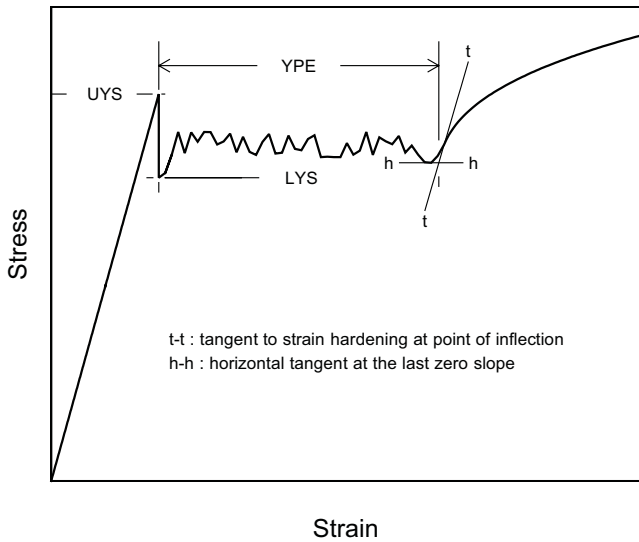


FIG. 24 Stress-Strain Diagram Showing Yield Point Elongation (YPE) and Upper (UYS) and Lower (LYS) Yield Strengths

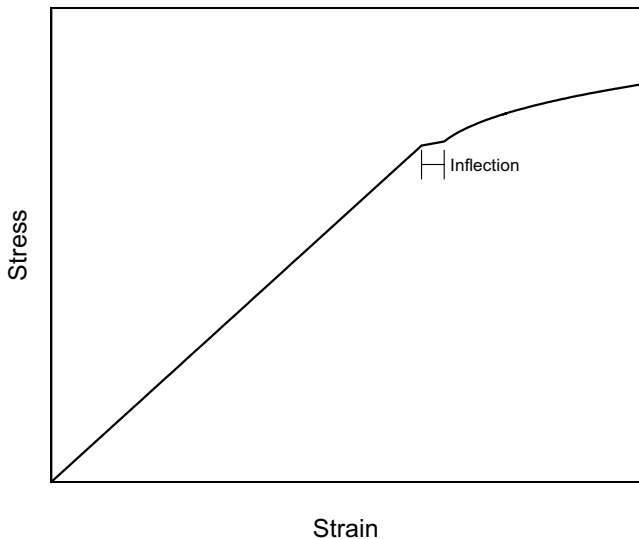


FIG. 25 Stress-Strain Diagram With an Inflection, But No YPE

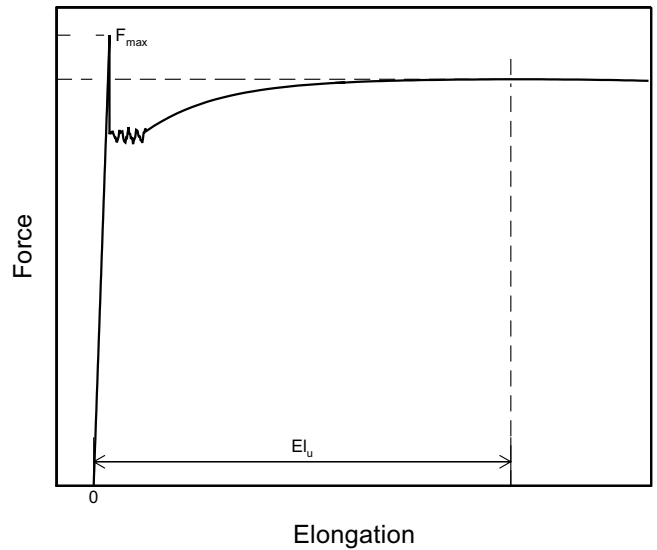


FIG. 26 Stress-Strain Diagram in Which the Upper Yield Strength is the Maximum Stress Recorded Method

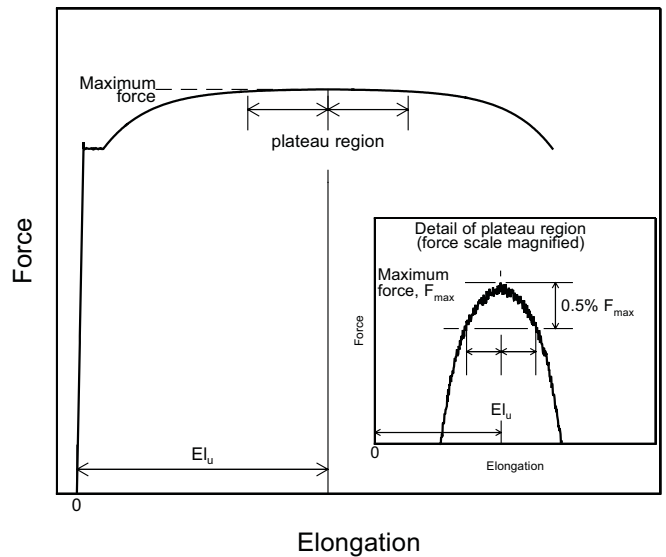


FIG. 27 Force-Elongation Diagram for Determination of Uniform Elongation of Steel Sheet Materials Exhibiting a Plateau at Maximum Force

facilitating measurement of YPE, if observed. If Class C devices are used, this must be reported along with the results.

NOTE 33—The appropriate value of the total extension must be specified. For steels with nominal yield strengths of less than 550 MPa [80 000 psi], an appropriate value is 0.005 mm/mm [or in./in.] (0.5 %) of the gauge length. For higher strength steels, a greater extension or the offset method should be used.

NOTE 34—When no other means of measuring elongation are available, a pair of dividers or similar device can be used to determine a point of detectable elongation between two gauge marks on the specimen. The gauge length shall be 50 mm [2 in.]. The stress corresponding to the load at the instant of detectable elongation may be recorded as the approximate extension-under-load yield strength.

7.7.3 Autographic Diagram Method (for materials exhibiting discontinuous yielding)—Obtain stress-strain (or force-elongation) data or construct a stress-strain (or force-

7.7.3.1 Record the stress corresponding to the maximum force at the onset of discontinuous yielding as the upper yield strength. This is illustrated in Figs. 23 and 24.

NOTE 35—If multiple peaks are observed at the onset of discontinuous yielding, the first is considered the upper yield strength. (See Fig. 24.)

7.7.3.2 Record the minimum stress observed during discontinuous yielding (ignoring transient effects) as the lower yield strength. This is illustrated in Fig. 24.

NOTE 36—Yield properties of materials exhibiting yield point elongation are often less repeatable and less reproducible than those of similar materials having no YPE. Offset and EUL yield strengths may be significantly affected by stress fluctuations occurring in the region where the offset or extension intersects the stress-strain curve. Determination of

as test machine stiffness and alignment. Speed of testing may also have a significant effect, regardless of the method employed.

**NOTE 37**—Where low-magnification autographic recordings are needed to facilitate measurement of yield point elongation for materials which may exhibit discontinuous yielding, Class C extensometers may be employed. When this is done but the material exhibits no discontinuous yielding, the extension-under-load yield strength may be determined instead, using the autographic recording (see Extension-Under-Load Method).

**7.7.4 Halt-of-the-Force Method (for materials exhibiting discontinuous yielding)**—Apply an increasing force to the specimen at a uniform deformation rate. When the force hesitates, record the corresponding stress as the upper yield strength.

**NOTE 38**—The Halt-of-the-Force Method was formerly known as the Halt-of-the-Pointer Method, the Drop-of-the-Beam Method, and the Halt-of-the-Load Method.

**7.8 Yield Point Elongation**—Calculate the yield point elongation from the stress-strain diagram or data by determining the difference in strain between the upper yield strength (first zero slope) and the onset of uniform strain hardening (see definition of YPE in Terminology E6 and Fig. 24).

**NOTE 39**—The stress-strain curve of a material exhibiting only a hint of the behavior causing YPE may have an inflection at the onset of yielding with no point where the slope reaches zero (Fig. 25). Such a material has no YPE, but may be characterized as exhibiting an inflection. Materials exhibiting inflections, like those with measurable YPE, may in certain applications acquire an unacceptable surface appearance during forming.

**7.9 Uniform Elongation (if required):**

**7.9.1** Uniform elongation shall include both plastic and elastic elongation.

**7.9.2** Uniform elongation shall be determined using autographic methods with extensometers conforming to Practice E83. Use a class B2 or better extensometer for materials having a uniform elongation less than 5 %. Use a class C or better extensometer for materials having a uniform elongation greater than or equal to 5 % but less than 50 %. Use a class D or better extensometer for materials having a uniform elongation of 50 % or greater.

**7.9.3** Determine the uniform elongation as the elongation at the point of maximum force from the force elongation data collected during a test.

**7.9.3.1** Some materials exhibit a yield point followed by considerable elongation where the yield point is the maximum force achieved during the test. In this case, uniform elongation is not determined at the yield point, but instead at the highest force occurring just prior to necking (see Fig. 26).

**7.9.3.2** Stress-strain curves for some materials exhibit a lengthy, plateau-like region in the vicinity of the maximum force. For such materials, determine the uniform elongation at the center of the plateau as indicated in Fig. 27 (see also Note 40 below).

**NOTE 40**—When uniform elongation is being determined digitally, noise in the stress-strain data generally causes many small, local peaks and valleys to be recorded in the plateau region. To accommodate this, the following procedure is recommended:

— Determine the maximum force recorded (after discontinuous yield-

ing) — Digitally define the “plateau” as consisting of all consecutive data points wherein the force value is within 0.5 % of the magnitude of the peak force value.

— Determine the uniform elongation as the strain at the mid-point of the “plateau.”

**7.9.3.3 Discussion**—The 0.5 % value of Note 40 has been selected arbitrarily. In actual practice, the value should be selected so as to be the minimum figure that is large enough to effectively define the force plateau. This may require that the percentage be about five times the amplitude of the force fluctuations occurring due to noise. Values ranging from 0.1 % to 1.0 % may be found to work acceptably.

**7.10 Tensile Strength (also known as Ultimate Tensile Strength)**—Calculate the tensile strength by dividing the maximum force carried by the specimen during the tension test by the original cross-sectional area of the specimen.

**NOTE 41**—If the upper yield strength is the maximum stress recorded, and if the stress-strain curve resembles that of Fig. 26, it is recommended that the maximum stress after discontinuous yielding be reported as the tensile strength. Where this may occur, determination of the tensile strength should be in accordance with the agreement between the parties involved.

**7.11 Elongation:**

**7.11.1** In reporting values of elongation, give both the original gauge length and the percentage increase. If any device other than an extensometer is placed in contact with the specimen’s reduced section during the test, this also shall be noted.

*Example:* Elongation = 30 % increase (50 – mm [2 – in.] gauge length) (5)

**NOTE 42**—Elongation results are very sensitive to variables such as: (a) speed of testing, (b) specimen geometry (gauge length, diameter, width, and thickness), (c) heat dissipation (through grips, extensometers, or other devices in contact with the reduced section), (d) surface finish in reduced section (especially burrs or notches), (e) alignment, and (f) fillets and tapers. Parties involved in comparison or conformance testing should standardize the above items, and it is recommended that use of ancillary devices (such as extensometer supports) which may remove heat from specimens be avoided. See Appendix X1 for additional information on the effects of these variables.

**7.11.2** When the specified elongation is greater than 3 %, fit ends of the fractured specimen together carefully and measure the distance between the gage marks to the nearest 0.25 mm [0.01 in.] for gauge lengths of 50 mm [2 in.] and under, and to at least the nearest 0.5 % of the gauge length for gauge lengths over 50 mm [2 in.]. A percentage scale reading to 0.5 % of the gauge length may be used.

**7.11.3** When the *specified* elongation is 3 % or less, determine the elongation of the specimen using the following procedure, except that the procedure given in 7.11.2 may be used instead when the *measured* elongation is greater than 3 %.

**7.11.3.1** Prior to testing, measure the original gauge length of the specimen to the nearest 0.05 mm [0.002 in.].

**7.11.3.2** Remove partly torn fragments that will interfere

7.11.3.3 Fit the fractured ends together with matched surfaces and apply a force along the axis of the specimen sufficient to close the fractured ends together. If desired, this force may then be removed carefully, provided the specimen remains intact.

NOTE 43—The use of a force generating a stress of approximately 15 MPa [2000 psi] has been found to give satisfactory results on test specimens of aluminum alloy.

7.11.3.4 Measure the final gauge length to the nearest 0.05 mm [0.002 in.] and report the elongation to the nearest 0.2 %.

7.11.4 Elongation measured per paragraph 7.11.2 or 7.11.3 may be affected by location of the fracture, relative to the marked gauge length. If any part of the fracture occurs outside the gauge marks or is located less than 25 % of the elongated gauge length from either gauge mark, the elongation value obtained using that pair of gauge marks may be abnormally low and non-representative of the material. If such an elongation measure is obtained in acceptance testing involving only a minimum requirement and meets the requirement, no further testing need be done. Otherwise, discard the test and retest the material.

#### 7.11.5 *Elongation at Fracture:*

7.11.5.1 Elongation at fracture shall include elastic and plastic elongation and may be determined with autographic or automated methods using extensometers verified over the strain range of interest (see 5.4). Use a class B2 or better extensometer for materials having less than 5 % elongation, a class C or better extensometer for materials having elongation greater than or equal to 5 % but less than 50 %, and a class D or better extensometer for materials having 50 % or greater elongation. In all cases, the extensometer gauge length shall be the nominal gauge length required for the specimen being tested. Due to the lack of precision in fitting fractured ends together, the elongation after fracture using the manual methods of the preceding paragraphs may differ from the elongation at fracture determined with extensometers.

7.11.5.2 Percent elongation at fracture may be calculated directly from elongation at fracture data and be reported instead of percent elongation as calculated in 7.11.2 to 7.11.3. However, these two parameters are not interchangeable. Use of the elongation at fracture method generally provides more repeatable results.

NOTE 44—When disagreements arise over the percent elongation results, agreement must be reached on which method to use to obtain the results.

#### 7.12 *Reduction of Area:*

7.12.1 The reduced area used to calculate reduction of area (see 7.11.2 and 7.11.3) shall be the minimum cross section at the location of fracture.

7.12.2 *Specimens with Originally Circular Cross Sections*—Fit the ends of the fractured specimen together and measure the reduced diameter to the same accuracy as the original measurement.

NOTE 45—Because of anisotropy, circular cross sections often do not remain circular during straining in tension. The shape is usually elliptical.

7.12.3 *Specimens with Original Rectangular Cross Sections*—Fit the ends of the fractured specimen together and measure the thickness and width at the minimum cross section to the same accuracy as the original measurements.

NOTE 46—Because of the constraint to deformation that occurs at the corners of rectangular specimens, the dimensions at the center of the original flat surfaces are less than those at the corners. The shapes of these surfaces are often assumed to be parabolic. When this assumption is made, an effective thickness,  $t_e$ , may be calculated as follows:  $(t_1 + 4t_2 + t_3)/6$ , where  $t_1$  and  $t_3$  are the thicknesses at the corners, and  $t_2$  is the thickness at mid-width. An effective width may be similarly calculated.

7.12.4 Calculate the reduced area based upon the dimensions determined in 7.12.2 or 7.12.3. The difference between the area thus found and the area of the original cross section expressed as a percentage of the original area is the reduction of area.

7.12.5 If any part of the fracture takes place outside the middle half of the reduced section or in a punched or scribed gauge mark within the reduced section, the reduction of area value obtained may not be representative of the material. In acceptance testing, if the reduction of area so calculated meets the minimum requirements specified, no further testing is required, but if the reduction of area is less than the minimum requirements, discard the test results and retest.

7.12.6 Results of measurements of reduction of area shall be rounded using the procedures of Practice E29 and any specific procedures in the product specifications. In the absence of a specified procedure, it is recommended that reduction of area test values in the range from 0 to 10 % be rounded to the nearest 0.5 % and test values of 10 % and greater to the nearest 1 %.

7.13 *Rounding Reported Test Data for Yield Strength and Tensile Strength*—Test data should be rounded using the procedures of Practice E29 and the specific procedures in the product specifications. In the absence of a specified procedure for rounding the test data, one of the procedures described in the following paragraphs is recommended.

7.13.1 For test values up to 500 MPa [50 000 psi], round to the nearest 1 MPa [100 psi]; for test values of 500 MPa [50 000 psi] and up to 1000 MPa [100 000 psi], round to the nearest 5 MPa [500 psi]; for test values of 1000 MPa [100 000 psi] and greater, round to the nearest 10 MPa [1000 psi].

NOTE 47—For steel products, see Test Methods and Definitions A370.

7.13.2 For all test values, round to the nearest 1 MPa [100 psi].

NOTE 48—For aluminum- and magnesium-alloy products, see Methods B557.

7.13.3 For all test values, round to the nearest 5 MPa [500 psi].

7.14 *Replacement of Specimens*—A test specimen may be discarded and a replacement specimen selected from the same lot of material in the following cases:

7.14.1 The original specimen had a poorly machined surface,

7.14.2 The original specimen had the wrong dimensions,

- 7.14.4 The test procedure was incorrect,
- 7.14.5 The fracture was outside the gauge length,
- 7.14.6 For elongation determinations, the fracture was outside the middle half of the gauge length, or
- 7.14.7 There was a malfunction of the testing equipment.

NOTE 49—The tension specimen is inappropriate for assessing some types of imperfections in a material. Other methods and specimens employing ultrasonics, dye penetrants, radiography, etc., may be considered when flaws such as cracks, flakes, porosity, etc., are revealed during a test and soundness is a condition of acceptance.

## 8. Report

8.1 Test information on materials not covered by a product specification should be reported in accordance with 8.2 or both 8.2 and 8.3.

8.2 Test information to be reported shall include the following when applicable:

- 8.2.1 Reference to the standard used, i.e. E8 or E8M.
- 8.2.2 Material and sample identification.
- 8.2.3 Specimen type (see Section 6).
- 8.2.4 Yield strength and the method used to determine yield strength (see 7.7).
- 8.2.5 Yield point elongation (see 7.8).
- 8.2.6 Tensile Strength (also known as Ultimate Tensile Strength) (see 7.10).
- 8.2.7 Elongation (report original gauge length, percentage increase, and method used to determine elongation; i.e. at fracture or after fracture) (see 7.11).
- 8.2.8 Uniform Elongation, if required (see 7.9).
- 8.2.9 Reduction of area, if required (see 7.12).

8.3 Test information to be available on request shall include:

- 8.3.1 Specimen test section dimension(s).
- 8.3.2 Equation used to calculate cross-sectional area of rectangular specimens taken from large-diameter tubular products.
- 8.3.3 Speed and method used to determine speed of testing (see 7.6).
- 8.3.4 Method used for rounding of test results (see 7.13).
- 8.3.5 Reasons for replacement specimens (see 7.14).

## 9. Precision and Bias

9.1 *Precision*—An interlaboratory test program<sup>3</sup> gave the following values for coefficients of variation for the most commonly measured tensile properties:

	Coefficient of Variation, %				
	Tensile Strength	Yield Strength Offset = 0.02 %	Yield Strength Offset = 0.2 %	Elongation Gauge Length = 4 Diameter	Reduction of Area
CV % <sub>r</sub>	0.9	2.7	1.4	2.8	2.8
CV % <sub>R</sub>	1.3	4.5	2.3	5.4	4.6

CV %<sub>r</sub> = repeatability coefficient of variation in percent within a laboratory  
 CV %<sub>R</sub> = repeatability coefficient of variation in percent between laboratories

9.1.1 The values shown are the averages from tests on six frequently tested metals, selected to include most of the normal range for each property listed above. When these materials are compared, a large difference in coefficient of variation is found. Therefore, the values above should not be used to judge whether the difference between duplicate tests of a specific material is larger than expected. The values are provided to allow potential users of this test method to assess, in general terms, its usefulness for a proposed application.

9.2 *Bias*—The procedures in Test Methods E8/E8M for measuring tensile properties have no bias because these properties can be defined only in terms of a test method.

## 10. Keywords

10.1 accuracy; bending stress; discontinuous yielding; drop-of-the-beam; eccentric force application; elastic extension; elongation; extension-under-load; extensometer; force; free-running crosshead speed; gauge length; halt-of-the force; percent elongation; plastic extension; preload; rate of stressing; rate of straining; reduced section; reduction of area; sensitivity; strain; stress; taring; tensile strength; tension testing; yield point elongation; yield strength

<sup>3</sup> Supporting data can be found in Appendix X1 and additional data are available from ASTM Headquarters. Request RR:E28-1004.

## APPENDIXES

### (Nonmandatory Information)

#### X1. FACTORS AFFECTING TENSION TEST RESULTS

X1.1 The precision and bias of tension test strength and ductility measurements depend on strict adherence to the stated test procedure and are influenced by instrumental and material factors, specimen preparation, and measurement/testing errors.

X1.2 The consistency of agreement for repeated tests of the same material is dependent on the homogeneity of the material, and the repeatability of specimen preparation, test conditions, and measurements of the tension test parameters.

X1.3 Instrumental factors that can affect test results include: the stiffness, damping capacity, natural frequency, and mass of moving parts of the tensile test machine; accuracy of force indication and use of forces within the verified range of the machine; rate of force application, alignment of the test specimen with the applied force, parallelness of the grips, grip pressure, nature of the force control used, appropriateness and calibration of extensometers, heat dissipation (by grips, extensometers, or ancillary devices), and so forth.

X1.4 Material factors that can affect test results include: representativeness and homogeneity of the test material, sampling scheme, and specimen preparation (surface finish, dimensional accuracy, fillets at the ends of the gauge length, taper in the gauge length, bent specimens, thread quality, and so forth).

X1.4.1 Some materials are very sensitive to the quality of the surface finish of the test specimen (see **Note 4**) and must be ground to a fine finish, or polished to obtain correct results.

X1.4.2 Test results for specimens with as-cast, as-rolled, as-forged, or other non-machined surface conditions can be affected by the nature of the surface (see **Note 10**).

X1.4.3 Test specimens taken from appendages to the part or component, such as prolongs or risers, or from separately produced castings (for example, keel blocks) may produce test results that are not representative of the part or component.

X1.4.4 Test specimen dimensions can influence test results. For cylindrical or rectangular specimens, changing the test specimen size generally has a negligible effect on the yield and tensile strength but may influence the upper yield strength, if one is present, and elongation and reduction of area values. Comparison of elongation values determined using different specimens requires that the following ratio be controlled:

$$L_o/(A_o)^{1/2} \quad (X1.1)$$

where:

$L_o$  = original gauge length of specimen, and  
 $A_o$  = original cross-sectional area of specimen.

X1.4.4.1 Specimens with smaller  $L_o/(A_o)^{1/2}$  ratios generally give greater elongation and reduction in area values. This is the case for example, when the width or thickness of a rectangular tensile test specimen is increased.

X1.4.4.2 Holding the  $L_o/(A_o)^{1/2}$  ratio constant minimizes, but does not necessarily eliminate, differences. Depending on material and test conditions, increasing the size of the proportional specimen of **Fig. 8** may be found to increase or decrease elongation and reduction in area values somewhat.

X1.4.5 Use of a taper in the gauge length, up to the allowed 1 % limit, can result in lower elongation values. Reductions of as much as 15 % have been reported for a 1 % taper.

X1.4.6 Changes in the strain rate can affect the yield strength, tensile strength, and elongation values, especially for materials which are highly strain rate sensitive. In general, the yield strength and tensile strength will increase with increasing strain rate, although the effect on tensile strength is generally less pronounced. Elongation values generally decrease as the strain rate increases.

X1.4.7 Brittle materials require careful specimen preparation, high quality surface finishes, large fillets at the ends of the gauge length, oversize threaded grip sections, and cannot tolerate punch or scribe marks as gauge length indicators.

X1.4.8 Flattening of tubular products to permit testing does alter the material properties, generally nonuniformly, in the flattened region which may affect test results.

dividers, and other measurement devices, alignment and zeroing of chart recording devices, and so forth.

X1.5.1 Measurement of the dimensions of as-cast, as-rolled, as-forged, and other test specimens with non-machined surfaces may be imprecise due to the irregularity of the surface flatness.

X1.5.2 Materials with anisotropic flow characteristics may exhibit non-circular cross sections after fracture and measurement precision may be affected, as a result (see **Note 41**).

X1.5.3 The corners of rectangular test specimens are subject to constraint during deformation and the originally flat surfaces may be parabolic in shape after testing which will affect the precision of final cross-sectional area measurements (see **Note 46**).

X1.5.4 If any portion of the fracture occurs outside of the middle of the gauge length, or in a punch or scribe mark within the gauge length, the elongation and reduction of area values may not be representative of the material. Wire specimens that break at or within the grips may not produce test results representative of the material.

X1.5.5 Use of specimens with shouldered ends (“button-head” tensiles) will produce lower 0.02 % offset yield strength values than threaded specimens.

X1.6 Because standard reference materials with certified tensile property values are not available, it is not possible to rigorously define the bias of tension tests. However, by the use of carefully designed and controlled interlaboratory studies, a reasonable definition of the precision of tension test results can be obtained.

X1.6.1 An interlaboratory test program<sup>3</sup> was conducted in which six specimens each, of six different materials were prepared and tested by each of six different laboratories. **Tables X1.1-X1.6** present the precision statistics, as defined in **Practice E691**, for: tensile strength, 0.02 % yield strength, 0.2 % yield strength, % elongation in 4D, % elongation in 5D, and % reduction in area. In each table, the first column lists the six materials tested, the second column lists the average of the average results obtained by the laboratories, the third and fifth columns list the repeatability and reproducibility standard deviations, the fourth and sixth columns list the coefficients of variation for these standard deviations, and the seventh and eighth columns list the 95 % repeatability and reproducibility limits.

X1.6.2 The averages (below columns four and six in each table) of the coefficients of variation permit a relative comparison of the repeatability (within-laboratory precision) and reproducibility (between-laboratory precision) of the tension test parameters. This shows that the ductility measurements exhibit less repeatability and reproducibility than the strength measurements. The overall ranking from the least to the most repeatable and reproducible is: % elongation in 4D, % elongation in 5D, % reduction in area, 0.02 % offset yield strength, 0.2 % offset yield strength, and tensile strength. Note that the

reproducibility (between-laboratory precision) is poorer than the repeatability (within-laboratory precision) as would be expected.

X1.6.3 No comments about bias can be made for the interlaboratory study due to the lack of certified test results for these specimens. However, examination of the test results

showed that one laboratory consistently exhibited higher than average strength values and lower than average ductility values for most of the specimens. One other laboratory had consistently lower than average tensile strength results for all specimens.

**TABLE X1.1 Precision Statistics—Tensile Strength, MPa [ksi]**

NOTE 1— $\bar{X}$  is the average of the cell averages, that is, the grand mean for the test parameter,

$s_r$  is the repeatability standard deviation (within-laboratory precision) in MPa [ksi],

$s_r/\bar{X}$  is the coefficient of variation in %,

$s_R$  is the reproducibility standard deviation (between-laboratory precision) in MPa [ksi],

$s_R/\bar{X}$  is the coefficient of variation, %,

$r$  is the 95 % repeatability limits in MPa [ksi],

$R$  is the 95 % reproducibility limits in MPa [ksi].

Material	$\bar{X}$	$s_r$	$s_r/\bar{X}$ , %	$s_R$	$s_R/\bar{X}$ , %	$r$	$R$
EC-H19	176.9 [25.66]	4.3 [0.63]	2.45	4.3 [0.63]	2.45	12.1 [1.76]	12.1 [1.76]
2024-T351	491.3 [71.26]	6.1 [0.88]	1.24	6.6 [0.96]	1.34	17.0 [2.47]	18.5 [2.68]
ASTM A105	596.9 [86.57]	4.1 [0.60]	0.69	8.7 [1.27]	1.47	11.6 [1.68]	24.5 [3.55]
AISI 316	694.6 [100.75]	2.7 [0.39]	0.39	8.4 [1.22]	1.21	7.5 [1.09]	23.4 [3.39]
Inconel 600	685.9 [99.48]	2.9 [0.42]	0.43	5.0 [0.72]	0.72	8.2 [1.19]	13.9 [2.02]
SAE 51410	1253.0 [181.73]	0.25 [0.46]	0.25	7.9 [1.14]	0.63	8.9 [1.29]	22.1 [3.20]
		Averages:	0.91		1.30		

**TABLE X1.2 Precision Statistics—0.02 % Yield Strength, MPa [ksi]**

Material	$\bar{X}$	$s_r$	$s_r/\bar{X}$ , %	$s_R$	$s_R/\bar{X}$ , %	$r$	$R$
EC-H19	111.4 [16.16]	4.5 [0.65]	4.00	8.2 [1.19]	7.37	12.5 [1.81]	23.0 [3.33]
2024-T351	354.2 [51.38]	5.8 [0.84]	1.64	6.1 [0.89]	1.73	16.3 [2.36]	17.2 [2.49]
ASTM A105	411.1 [59.66]	8.3 [1.20]	2.02	13.1 [1.90]	3.18	23.2 [3.37]	36.6 [5.31]
AISI 316	336.1 [48.75]	16.7 [2.42]	4.97	31.9 [4.63]	9.49	46.1 [6.68]	89.0 [12.91]
Inconel 600	267.1 [38.74]	3.2 [0.46]	1.18	5.2 [0.76]	1.96	8.8 [1.28]	14.7 [2.13]
SAE 51410	723.2 [104.90]	16.6 [2.40]	2.29	21.9 [3.17]	3.02	46.4 [6.73]	61.2 [8.88]
		Averages:	2.68		4.46		

**TABLE X1.3 Precision Statistics—0.2 % Yield Strength, MPa [ksi]**

Material	$\bar{X}$	$s_r$	$s_r/\bar{X}$ , %	$s_R$	$s_R/\bar{X}$ , %	$r$	$R$
EC-H19	158.4 [22.98]	3.3 [0.47]	2.06	3.3 [0.48]	2.07	9.2 [1.33]	9.2 [1.33]
2024-T351	362.9 [52.64]	5.1 [0.74]	1.41	5.4 [0.79]	1.49	14.3 [2.08]	15.2 [2.20]
ASTM A105	402.4 [58.36]	5.7 [0.83]	1.42	9.9 [1.44]	2.47	15.9 [2.31]	27.8 [4.03]
AISI 316	481.1 [69.78]	6.6 [0.95]	1.36	19.5 [2.83]	4.06	18.1 [2.63]	54.7 [7.93]
Inconel 600	268.3 [38.91]	2.5 [0.36]	0.93	5.8 [0.85]	2.17	7.0 [1.01]	16.3 [2.37]
SAE 51410	967.5 [140.33]	8.9 [1.29]	0.92	15.9 [2.30]	1.64	24.8 [3.60]	44.5 [6.45]
		Averages:	1.35		2.32		

**TABLE X1.4 Precision Statistics—% Elongation in 4D for E8 Specimens**

NOTE 1—Length of reduced section = 6D.

Material	$\bar{X}$	$s_r$	$s_r/\bar{X}$ , %	$s_R$	$s_R/\bar{X}$ , %	$r$	$R$
EC-H19	17.42	0.64	3.69	0.92	5.30	1.80	2.59
2024-T351	19.76	0.58	2.94	1.58	7.99	1.65	4.43
ASTM A105	29.10	0.76	2.62	0.98	3.38	2.13	2.76
AISI 316	40.07	1.10	2.75	2.14	5.35	3.09	6.00
Inconel 600	44.28	0.66	1.50	1.54	3.48	1.86	4.31

**TABLE X1.5 Precision Statistics—% Elongation in 5D for E8M Specimens**

NOTE 1—Length of reduced section = 6D.

Material	$X$	$s_r$	$s_r/X, \%$	$s_R$	$s_R/X, \%$	$r$	$R$
EC-H19	14.60	0.59	4.07	0.66	4.54	1.65	1.85
2024-T351	17.99	0.63	3.48	1.71	9.51	1.81	4.81
ASTM A105	25.63	0.77	2.99	1.30	5.06	2.15	3.63
AISI 316	35.93	0.71	1.98	2.68	7.45	2.00	7.49
Inconel 600	41.58	0.67	1.61	1.60	3.86	1.88	4.49
SAE 51410	13.39	0.45	3.61	0.96	7.75	1.25	2.89
Averages:			2.96		6.36		

## X2. MEASUREMENT OF SPECIMEN DIMENSIONS

**TABLE X1.6 Precision Statistics—% Reduction in Area**

Material	$X$	$s_r$	$s_r/X, \%$	$s_R$	$s_R/X, \%$	$r$	$R$
EC-H19	79.15	1.93	2.43	2.01	2.54	5.44	5.67
2024-T351	30.41	2.09	6.87	3.59	11.79	5.79	10.01
ASTM A105	65.59	0.84	1.28	1.26	1.92	2.35	3.53
AISI 316	71.49	0.99	1.39	1.60	2.25	2.78	4.50
Inconel 600	59.34	0.67	1.14	0.70	1.18	1.89	1.97
SAE 51410	50.49	1.86	3.69	3.95	7.81	5.21	11.05
Averages:			2.80		4.58		

X2.1 Measurement of specimen dimensions is critical in tension testing, and it becomes more critical with decreasing specimen size, as a given absolute error becomes a larger relative (percent) error. Measuring devices and procedures should be selected carefully, so as to minimize measurement error and provide good repeatability and reproducibility.

X2.2 Relative measurement error should be kept at or below 1 %, where possible. Ideally, this 1 % error should include not only the resolution of the measuring device but also the variability commonly referred to as repeatability and reproducibility. (Repeatability is the ability of any operator to obtain similar measurements in repeated trials. Reproducibility is the ability of multiple operators to obtain similar measurements.)

X2.3 Formal evaluation of gage repeatability and reproducibility (GR and R) by way of a GR and R study is highly recommended. A GR and R study involves having multiple operators each take two or three measurements of a number of parts—in this case, test specimens. Analysis, usually done by computer, involves comparing the observed measurement variations to a tolerance the procedure is to determine conformance to. High GR and R percentages (more than 20 %) indicate much variability relative to the tolerance, whereas low percentages (10 % or lower) indicate the opposite. The analysis also estimates, independently, the repeatability and reproducibility.

X2.4 GR and R studies in which nontechnical personnel used different brands and models of hand-held micrometers have given results varying from about 10 % (excellent) to nearly 100 % (essentially useless), relative to a dimensional

measurement procedures, and training personnel.

X2.5 With a 0.075 mm [0.003 in.] tolerance, a 10 % GR and R result (exceptionally good, even for digital hand-held micrometers reading to 0.001 mm [0.00005 in.]) indicates that the total variation due to repeatability and reproducibility is around 0.0075 [0.0003 in.]. This is less than or equal to 1 % only if all dimensions to be measured are greater than or equal to 0.75 mm [0.03 in.]. The relative error in using this device to measure thickness of a 0.25 mm [0.01 in.] flat tensile specimen would be 3 %—which is considerably more than that allowed for force or strain measurement.

X2.6 Dimensional measurement errors can be identified as the cause of many *out-of-control* signals, as indicated by statistical process control (SPC) charts used to monitor tension testing procedures. This has been the experience of a production laboratory employing SPC methodology and the best hand-held micrometers available (from a GR and R standpoint) in testing of 0.45 to 6.35 mm [0.018 to 0.25 in.] flat rolled steel products.

X2.7 Factors which affect GR and R, sometimes dramatically, and which should be considered in the selection and evaluation of hardware and procedures include:

X2.7.1 Resolution,

X2.7.2 Verification,

X2.7.3 Zeroing,

X2.7.4 Type of anvil (flat, rounded, or pointed),

X2.7.5 Cleanliness of part and anvil surfaces

X2.7.7 Stability/temperature variations,

X2.7.8 Coating removal,

X2.7.9 Operator technique, and

X2.7.10 Ratchets or other features used to regulate the clamping force.

X2.8 Flat anvils are generally preferred for measuring the dimensions of round or flat specimens which have relatively smooth surfaces. One exception is that rounded or pointed anvils must be used in measuring the thickness of curved specimens taken from large-diameter tubing (see Fig. 13), to prevent overstating the thickness. (Another concern for these curved specimens is the error that can be introduced through use of the equation  $A = W \times T$ ; see 7.2.3.)

X2.9 Heavy coatings should generally be removed from at least one grip end of flat specimens taken from coated products to permit accurate measurement of base metal thickness, assuming (a) the base metal properties are what are desired, (b) the coating does not contribute significantly to the strength of the product, and (c) coating removal can be easily accomplished (some coatings may be easily removed by chemical

stripping). Otherwise, it may be advisable to leave the coating intact and determine the base metal thickness by an alternate method. Where this issue may arise, all parties involved in comparison or conformance testing should agree as to whether or not coatings are to be removed before measurement.

X2.10 As an example of how the considerations identified above affect dimensional measurement procedures, consider the case of measuring the thickness of 0.40 mm [0.015 in.] painted, flat rolled steel specimens. The paint should be removed prior to measurement, if possible. The measurement device used should have flat anvils, must read to 0.0025 mm [0.0001 in.] or better, and must have excellent repeatability and reproducibility. Since GR and R is a significant concern, it will be best to use a device which has a feature for regulating the clamping force used, and devices without digital displays should be avoided to prevent reading errors. Before use of the device, and periodically during use, the anvils should be cleaned, and the device should be verified or zeroed (if an electronic display is used) or both. Finally, personnel should be trained and audited periodically to ensure that the measuring device is being used correctly and consistently by all.

### X3. SUGGESTED ACCREDITATION CRITERIA FOR LABORATORIES PERFORMING TENSILE TESTS

#### X3.1 Scope

X3.1.1 The following are specific features that an assessor may check to assess a laboratory's technical competence, if the laboratory is performing tests in accordance with Test Methods E8/E8M.

#### X3.2 Preparation

X3.2.1 The laboratory should follow documented procedures to ensure that machining or other preparation generates specimens conforming to applicable tolerances and requirements of Test Methods E8/E8M. Particularly important are those requirements that pertain to the dimensions and finish of reduced sections, as found in the text and in applicable figures.

X3.2.2 Where gauge marks are used, the laboratory should employ documented gauge marking procedures to ensure that the marks and gauge lengths comply with the tolerances and guidelines of Test Methods E8/E8M.

X3.2.2.1 The gauge marking procedure used should not deleteriously affect the test results.

NOTE X3.1—Frequent occurrence of fracturing at the gauge marks may indicate that gage marks have excessive depth or sharpness and may be affecting test results.

#### X3.3 Test Equipment

X3.3.1 As specified in the Apparatus sections of Test Methods E8/E8M, the axis of the test specimen should coincide with the center line of the heads of the testing machine, in order to minimize bending stresses which could affect the results.

X3.3.2 Equipment verification requirements of Practices E4 and E83 shall be met. Documentation showing the verification work to have been thorough and technically correct should be available.

X3.3.2.1 Verification reports shall demonstrate that force and extension readings have been taken at the prescribed intervals and that the prescribed runs have been completed.

X3.3.3 Extensometers used shall meet all requirements of Test Methods E8/E8M as to the classification of device to be used for the results determined. For example, an extensometer not meeting the Class B2 requirements of Practice E83 may not be used in determination of offset yield strengths.

X3.3.4 Before computerized or automated test equipment is put into routine service, or following a software revision, it is recommended that measures be taken to verify proper operation and result interpretation. Guide E1856 addresses this concern.

X3.3.5 Micrometers and other devices used in measurement of specimen dimensions should be selected, maintained and used in such a manner as to comply with the appendixes of Test Methods E8/E8M on measurement. Traceability to national standards should be established for these devices, and reasonable effort should be employed to prevent errors greater than 1 % from being generated as a result of measurement error, resolution, and rounding practice.

#### X3.4 Procedures

X3.4.1 The test machine shall be set up and zeroed in such a manner that zero force indication signifies a state of zero force on the specimen, as indicated in the Zeroing of the Test Machine sections of Test Methods E8/E8M.

NOTE X3.2—Provisions should be made to ensure that zero readings are properly maintained, from test to test. These may include, for example, zeroing after a predetermined number of tests or each time, under zero force conditions, the indicator exceeds a predetermined value.

X3.4.2 Upon request, the laboratory should be capable of demonstrating (perhaps through time, force, displacement or extensometer measurements, or both) that the test speeds used conform to the requirements of Test Methods E8/E8M, or other standards which take precedence.

X3.4.3 Upon request, the laboratory should be capable of demonstrating that the offsets and extensions used in determining yield strengths conform to the requirements of Test Methods E8/E8M and are constructed so as to indicate the forces corresponding to the desired offset strain or total strain.

NOTE X3.3—Use caution when performing calculations with extensometer magnification, because the manufacturer may report strain magnification, which relates the strain (not the elongation) to the x-axis displacement on the stress strain diagram. A user or assessor interested in an extensometer's magnification may use calibration equipment to determine the ratio between elongation and chart travel or may verify a reported magnification by calculating the Young's modulus from tests of specimens of a known nominal modulus.

X3.4.4 Measurement of elongation shall conform to requirements of Test Methods E8/E8M.

NOTE X3.4—Test Methods E8/E8M permit the measurement and reporting of elongation at fracture in place of elongation, as is often done in automated testing.

X3.4.5 Reduction of area, when required, shall be determined in accordance with the requirements of Test Methods E8/E8M.

X3.4.6 Procedures for recording, calculating, and reporting data and test results shall conform to all applicable requirements of Test Methods E8/E8M. In addition, wherever practical, the procedures should also be in accordance with widely accepted provisions of good laboratory practice, such as those detailed below.

X3.4.6.1 When recording data, personnel should record all figures that are definite, plus the best estimate of the first figure which is uncertain. (If a result is known to be approximately midway between 26 and 27, 26.5 should be the result recorded (not 26, 27, or 26.475).

X3.4.6.2 When performing calculations, personnel should avoid compounding of rounding errors. This may be accomplished by performing one large calculation, rather than several calculations using individual results. Alternatively, if multi-step calculations are done, intermediate results should not be rounded before use in subsequent calculations.

X3.4.6.3 In rounding, no final result should retain more significant figures than the least-significant-figure measurement or data point used in the calculation.

### **X3.5 Retention**

X3.5.1 A retention program appropriate for the nature and frequency of testing done in the laboratory should be maintained. Items that may warrant retention for defined time periods include:

X3.5.1.1 Raw data and forms,

X3.5.1.2 Force-elongation or stress-strain charts,

X3.5.1.3 Computer printouts of curves and test results,

X3.5.1.4 Data and results stored on computer discs or hard drives,

X3.5.1.5 Broken specimens,

X3.5.1.6 Excess material,

X3.5.1.7 Test reports, and

X3.5.1.8 Verification reports and certifications.

### **X3.6 Environment**

X3.6.1 All test equipment should be located and connected to power sources in such a manner as to minimize the effects of vibrations and electrical disturbances on raw data collected, stress-strain charts, and operation of equipment.

### **X3.7 Controls**

X3.7.1 Controlled procedures and work instructions should cover all aspects of specimen preparation, tensile testing, and result reporting. These documents should be readily available to all involved in the documented tasks.

X3.7.2 Clear, concise, operating instructions should be maintained for equipment used in specimen preparation and tensile testing. These instructions should be readily available to all qualified operators.

X3.7.3 All applicable verification requirements shall be met, as detailed in [X3.3.2](#).

X3.7.4 It is recommended that special studies and programs be employed to monitor and control tensile testing, because tensile test results are easily affected by operators, measuring devices, and test equipment. Examples of such programs include but are not limited to:

X3.7.4.1 Round-robin studies, proficiency tests, or other cross-checks,

X3.7.4.2 Repeatability and reproducibility (R and R) studies,

X3.7.4.3 Control charting, and

X3.7.4.4 Determination of typical lab uncertainties for each result typically reported.

NOTE X3.5—For nondestructive testing, repeatability and reproducibility are often measured by conducting gage R and R studies, as discussed in [Appendix X2](#) of Test Methods E8/E8M. These studies involve repeated determination of a test result, using a single part or specimen, so gage R and Rs are not directly applicable to mechanical properties, which are obtained through destructive testing. (True differences between even the best duplicate specimens manifest themselves in the form of poorer R and R results than would be obtained for perfect duplicates.) Nevertheless, quasi-R and R studies conducted with these limitations taken into consideration may be helpful in analyzing sources of error and improving reliability of test results.

## X4. ADDITIONAL INFORMATION ON SPEED OF TESTING AND EXAMPLES

X4.1 Many materials are strain-rate sensitive that is, the yield strength or tensile strength of the material is a function of the rate at which the material is being deformed. The yield strength of some materials can change by more than ten percent when tested with the slowest and then the highest speeds permitted by Test Methods E8/E8M. In order to reproduce yield test results, for strain-rate sensitive materials, it is important that strain rates during the determination of yield are similar.

X4.2 The following paragraphs further explain the various Control Methods required to be used by Test Methods E8/E8M when other guidance is not given. When other test speed requirements are specified, those speeds must be followed to comply with this test method. For example, aerospace specifications often require a test speed when determining yield strength to be a strain rate equal to  $0.005 \pm 0.002$  mm/mm/min [in./in./min]; when specified, that speed must be followed in order to comply with this standard.

X4.2.1 *Control Method A - Rate of Stressing Method for Determining Yield Properties* – This method has been the default method of control in Test Methods E8/E8M for many years. In this method, the crosshead speed of the machine is adjusted during the linear elastic portion of the curve to achieve the desired stress rate (or the speed is set to a predetermined value known to achieve the desired stress rate). The crosshead speed is not adjusted when the material begins to yield. The advantage of this control method is that it does not require any transducers other than the load indicator itself, although, load pacers and stress-rate indicators can be helpful. This method of control has a limitation in that the strain rate of the specimen at yield depends on the slope of the stress-strain curve (tangent modulus) and the testing machine stiffness. Because of this, the strain rate of the specimen when yield is determined can be different for different specimen sizes, different specimen configurations, different gripping configurations, and different testing machines. This difference in strain rate can affect the reproducibility of yield strength in strain-rate-sensitive materials.

X4.2.1.1 It is not the intent of this method to run the testing machine in closed-loop force control, because as the material begins to yield the testing machine will speed up, possibly to its maximum speed. However, using closed-loop force control during the elastic region of the test and switching to an equivalent crosshead speed prior to yield is an acceptable method.

X4.2.2 *Control Method B —Rate of Straining Control Method for Determining Yield Properties* - This method is usually performed with a testing machine that has a closed-loop control system that uses feedback from an extensometer to

automatically adjust the speed of the testing machine. However, some skilled operators can monitor a strain rate indicator attached to the extensometer and adjust the speed of the testing machine manually to maintain the required strain rate test speed. To maintain constant strain rate control during a test, the crosshead speed of the testing machine must slow down drastically when the specimen begins to yield. This method has three advantages. (1) The time to achieve yield results is short (about 20 to 40 s). (2) The reproducibility of yield strength test results from machine to machine and laboratory to laboratory is good. (3) The agreement with the results of Control Method C is good, because the strain rates are similar when the specimen's yield strength is determined. This method has three disadvantages. (1) The testing equipment is generally more expensive. (2) Proper control and safety depend on the control parameters to be properly set and that the extensometer integrity be maintained (accidental slippage of the extensometer can result in unexpected movement of the crosshead). Proper safety limits must be set to ensure safety of personnel and equipment. (3) When materials have yield points or yield discontinuously, a machine under closed-loop strain-rate control can behave erratically. This control method is not recommended for materials that yield discontinuously.

X4.2.3 *Control Method C - Crosshead Speed Control Method for Determining Yield Properties*—This method can be performed on any testing machine that has reasonably good crosshead speed control. This method has three advantages. (1) The reproducibility from machine to machine and laboratory to laboratory is good. (2) The agreement with Control Method B is good, because the strain rates are similar when the specimen's yield strength is determined. (3) This method of controlling a testing machine is excellent for materials that yield discontinuously. The disadvantage of this method of control is that the test time to yield can be more than three minutes, depending on the material being tested and the compliance of the testing machine including its grip assemblies.

X4.2.3.1 *An example using SI metric units of how to apply Control Method C to testing Specimen 1 in Fig. 13* is as follows. The length of the reduced section, that is, dimension A in Fig. 13, is equal to 60 mm. The crosshead speed is determined per Control Method C by multiplying 60 mm by 0.015 mm/mm/min to arrive at a crosshead speed of 0.9 mm/min.

X4.2.3.2 *An example using U.S. customary units of how to apply Control Method C to testing Specimen 1 in Fig. 13* is as follows. The length of the reduced section, that is, dimension A in Fig. 13 is equal to 2.25 in. The crosshead speed is determined per Control Method C by multiplying 2.25 in. by 0.015 in./in./min to arrive at a crosshead speed of 0.034 in./min.



## SUMMARY OF CHANGES

Committee E28 has identified the location of selected changes to this standard since the last issue (E8/E8M-13) that may impact the use of this standard. (Approved July 1, 2013.)

(1) 3.1.4 was revised.

(2) 3.1.5 was added.

Committee E28 has identified the location of selected changes to this standard since the last issue (E8/E8M-11) that may impact the use of this standard. (Approved June. 1, 2013.)

(1) Replaced 3.1.

(2) Added 3.1.2.

(3) Reformatted 3.1.3.

(4) Reformatted 3.1.4.

(5) Added 3.1.7, 3.1.8, and 3.1.12.

(6) Reformatted 3.1.11.

(7) Added 3.2.1.

(8) Added Note 32.

*ASTM International takes no position respecting the validity of any patent rights asserted in connection with any item mentioned in this standard. Users of this standard are expressly advised that determination of the validity of any such patent rights, and the risk of infringement of such rights, are entirely their own responsibility.*

*This standard is subject to revision at any time by the responsible technical committee and must be reviewed every five years and if not revised, either reapproved or withdrawn. Your comments are invited either for revision of this standard or for additional standards and should be addressed to ASTM International Headquarters. Your comments will receive careful consideration at a meeting of the responsible technical committee, which you may attend. If you feel that your comments have not received a fair hearing you should make your views known to the ASTM Committee on Standards, at the address shown below.*

*This standard is copyrighted by ASTM International, 100 Barr Harbor Drive, PO Box C700, West Conshohocken, PA 19428-2959, United States. Individual reprints (single or multiple copies) of this standard may be obtained by contacting ASTM at the above address or at 610-832-9585 (phone), 610-832-9555 (fax), or [service@astm.org](mailto:service@astm.org) (e-mail); or through the ASTM website ([www.astm.org](http://www.astm.org)). Permission rights to photocopy the standard may also be secured from the ASTM website ([www.astm.org/COPYRIGHT/](http://www.astm.org/COPYRIGHT/)).*

